

AD-759 534

SUMMARY OF DESIGN STUDIES AND RESULTS
OF MODEL TESTS OF THE FOLDING-PROPROTOR
AIRCRAFT CONCEPT

J. A. DeTore, et al

Bell Helicopter Company

Prepared for:

Air Force Flight Dynamics Laboratory

July 1972

DISTRIBUTED BY:

NTIS

National Technical Information Service
U. S. DEPARTMENT OF COMMERCE
5285 Port Royal Road, Springfield Va. 22151

VH
AFFDL-TR-72-81

**SUMMARY OF DESIGN STUDIES AND RESULTS OF
MODEL TESTS OF THE FOLDING-PROPROTOR
AIRCRAFT CONCEPT**

AD 759534

J. A. DETORE

E. L. BROWN

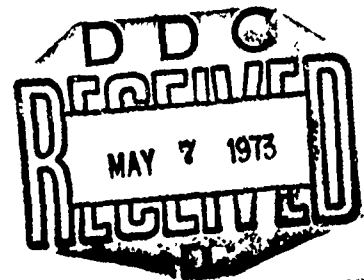
BELL HELICOPTER COMPANY

A TEXTRON COMPANY

FORT WORTH, TEXAS

TECHNICAL REPORT AFFDL-TR-72-81

JULY 1972



Approved for public release; distribution unlimited.

Reproduced by
NATIONAL TECHNICAL
INFORMATION SERVICE
U S Department of Commerce
Springfield VA 22151

AIR FORCE AVIONICS LABORATORY
AIR FORCE SYSTEMS COMMAND
WRIGHT-PATTERSON AIR FORCE BASE, OHIO

224

NOTICE

When Government drawings, specifications, or other data are used for any purpose other than in connection with a definitely related Government procurement operation, the United States Government thereby incurs no responsibility nor any obligation whatsoever; and the fact that the government may have formulated, furnished, or in any way supplied the said drawings, specifications, or other data, is not to be regarded by implication or otherwise as in any manner licensing the holder or any other person or corporation, or conveying any rights or permission to manufacture, use, or sell any patented invention that may in any way be related thereto.

Copies of this report should not be returned unless return is required by security considerations, contractual obligations, or notice on a specific document.

AIR FORCE/56780/23 April 1973 -- 150

Unclassified

Security Classification

DOCUMENT CONTROL DATA - R & D		
(Security classification of title, body of abstract and indexing annotation must be entered when the overall report is classified)		
1. ORIGINATING ACTIVITY (Corporate author) Bell Helicopter Company Fort Worth, Texas		2a. REPORT SECURITY CLASSIFICATION
		2b. GROUP
3. REPORT TITLE SUMMARY OF DESIGN STUDIES AND RESULTS OF MODEL TESTS OF THE FOLDING-PROPROTOR AIRCRAFT CONCEPT		
4. DESCRIPTIVE NOTES (Type of report and inclusive dates)		
5. AUTHOR(S) (First name, middle initial, last name) J. A. DeTore E. L. Brown		
6. REPORT DATE July 1972	7a. TOTAL NO. OF PAGES 306 224	7b. NO. OF REFS 27
8a. CONTRACT OR GRANT NO. F33615-69-C-157 8	8b. ORIGINATOR'S REPORT NUMBER(S) AFFDL-TR-72-81	
8c. PROJECT NO. 643A	8d. OTHER REPORT NO(S) (Any other numbers that may be assigned this report) D270-099-003	
10. DISTRIBUTION STATEMENT Approved for public release; distribution unlimited		
11. SUPPLEMENTARY NOTES Details of illustrations in this document may be better studied on microfiche.	12. SPONSORING MILITARY ACTIVITY AFSC Prototype Div. Air Force Flight Dynamics Laboratory Wright-Patterson Air Force Base, Ohio	
13. ABSTRACT Design studies and wind-tunnel test investigations were conducted to define preliminary designs of folding-proprotor VTOL aircraft for USAF rescue and transport missions and to identify and investigate technical risk areas. The aircraft had gross weights of 66,000 pounds and extended hover capability to 7000 feet. Convertible fan-jet engines provided forward flight speeds to 452 knots with blades folded. Technical risk areas associated with the aircraft designs were found to be in areas of mechanisms, aerodynamics, stability and control, and dynamics. A dynamic wind-tunnel investigation, conducted with a semispan aeroelastic model, demonstrated successful continuous stop/fold/unfold/start sequences, and freedom from proprorator pylon stability and blade flutter. Loads were measured for the range of stop-start rates. The angle of attack envelope at typical aircraft speed for stopping-starting of the rotor was found to be approximately six degrees based on blade loads. Aerodynamic tests showed that the folded blades decreased pitch and yaw stability, and that their drag in cruise is the smaller part of the wingtip pod contribution to total aircraft drag. A full-span, twin-rotor, powered force model of the rescue aircraft was fabricated, and tested under separate contract to investigate stability and aerodynamics throughout the pylon tilt range. The designs satisfied the requirements of the missions specified and were found to be possible VTOL design solutions for high-speed, high-hover-time missions. Recommendations include updating of folding-proprorator mechanism designs and proceeding with tilt-rotor aircraft flight investigations to validate criteria and analytical methods.		

DD FORM 1473

REPLACES DD FORM 1473, 1 JAN 64, WHICH IS OBSOLETE FOR ARMY USE.

Unclassified

Security Classification

Unclassified

Security Classification

14. KEY WORDS	LINK A		LINK B		LINK C	
	ROLE	WT	ROLE	WT	ROLE	WT
Folding Proprotor						
Test Rotor						
Aeroelastic Model						
Aerodynamic Model						
Powered Force Model						
Model Tests						
Design Studies						
VTOL						
V/STOL						
Rescue Mission						
Transport Mission						
Convertible Fan-Shaft Engine						

Unclassified

Security Classification

ia

**SUMMARY OF DESIGN STUDIES AND RESULTS OF
MODEL TESTS OF THE FOLDING-PROPROPOTOR
AIRCRAFT CONCEPT**

*J. A. DETORE
E. L. BROWN*

Approved for public release; distribution unlimited.

FOREWORD

This report was prepared by Bell Helicopter Company of Fort Worth, Texas for the Prototype Division of the Air Force Flight Dynamics Laboratory, Wright-Patterson Air Force Base, Ohio under Contract F33615-69-C-1578. The research is part of the investigation of folding-proprotor aircraft version of the tilt-rotor aircraft concept having application to potential Air Force missions. This report covers Phase I, "Design Studies," and Phase II, "Model Tests" of the subject contract. Mr. D. Fraga, AFFDL/PTA, was the Project Engineer for the Phase I effort and Mr. R. Hirt, AFFDL/PTC, was the Project Engineer for the Phase II effort.

This final report is presented in one volume and the wind-tunnel test data reports containing reduced tabulated and plotted force and moment data prepared by the Vought Aeronautics Low-Speed Wind-Tunnel personnel are available at the Flight Dynamics Laboratory.

Mr. J. DeTore was the Bell Helicopter Project Engineer for Phase I of the contract and Mr. E. L. Brown was the Bell Helicopter Project Engineer for the Phase II effort. The authors acknowledge the assistance of Dr. J. Yen and Mr. T. Gaffey of Bell Helicopter for support of the dynamics portion of the technical effort and Mr. L. Kemp of Bell Helicopter for support for the aerodynamics portion.

This report has been reviewed and is approved.



Ernest J. Cross, Jr.
LTCOL, USAF
Chief, Prototype Division

TABLE OF CONTENTS

	<u>Page</u>
I. SUMMARY	I-1
II. INTRODUCTION	II-1
A. THE FOLDING-PROPROTOR CONCEPT	II-1
B. PRIOR AND RELATED WORK	II-3
1. Basic Tilt Rotor	II-3
2. Folding Proprotor	II-4
C. PURPOSE OF DESIGN STUDIES AND MODEL TESTS	II-5
1. Phase I Design Studies	II-6
2. Phase II Model Tests	II-6
III. DESIGN STUDY SUMMARY	III-1
A. OBJECTIVES	III-1
B. APPROACH	III-1
C. POINT DESIGN SUMMARY	III-2
D. RECOMMENDED DESIGN REFINEMENT	III-4
E. REFINED DESIGNS	III-4
1. D270A	III-5
2. D270B	III-6
3. Dimensions and Parameters	III-6
4. Weight and Performance	III-7
5. Stability and Control	III-9
6. Dynamics	III-13
F. DESIGN STUDY CONCLUSIONS	III-16
IV. SEMISPAN AEROELASTIC MODEL TEST	IV-1
A. OBJECTIVES	IV-1
B. MODEL DESCRIPTION	IV-1
1. Wing	IV-1
2. Pylon	IV-4
3. Proprotors	IV-4
4. Model Instrumentation	IV-6
5. Model Control Panel	IV-6

TABLE OF CONTENTS - Continued

	<u>Page</u>
C. CONFIGURATIONS TESTED	IV-6
1. Check Dynamic Stability	IV-8
2. Determine Optimum Stop/Start Rates	IV-8
3. Define Stop/Start Envelope	IV-9
4. Investigate Folding Sequence	IV-9
5. Investigate Pylon Tilt Mode Dynamics	IV-9
D. TEST RESULTS AND ANALYSIS	
1. Dynamic Test Data	IV-10
2. Wind-Tunnel Balance Test Data	IV-22
3. Model Incident	IV-22
E. CONCLUSIONS	IV-24
V. GENERAL AERODYNAMIC FORCE MODEL TEST	V-1
A. OBJECTIVES	V-1
B. MODEL DESCRIPTION	V-1
1. General	V-1
2. Dimensions	V-2
C. CONFIGURATIONS TESTED	V-5
D. TEST RESULTS AND ANALYSIS	V-16
1. Aerodynamic Characteristics and Stability Derivatives of Complete Aircraft with Blades Folded	V-16
2. Component Lift, Drag, and Pitching Moment	V-16
3. Component Contributions to Lateral Stability	V-23
4. Blade Opening Effects	V-28
5. Aileron Effectiveness	V-29
6. Elevator and Rudder Effectiveness	V-30
7. Conclusions	V-31
VI. POWERED FULL-SPAN FORCE MODEL	VI-1
A. OBJECTIVES	VI-1
B. GENERAL	VI-1

TABLE OF CONTENTS - Continued

	<u>Page</u>
C. MODEL DESCRIPTION	VI-2
1. Model Installation	VI-3
2. Fuselage	VI-3
3. Empennage	VI-3
4. Wing	VI-4
5. Drive System	VI-4
6. Proprotors and Controls	VI-5
7. Instrumentation and Wiring Items	VI-8
8. Rotor Balances	VI-9
D. TEST PROGRAM	VI-9
1. Hover Flight	VI-9
2. Helicopter Flight	VI-10
3. Helicopter Slow-Speed Flight	VI-12
4. Conversion Flight	VI-13
5. Airplane Flight	VI-13
6. Rotor-Off Data	VI-13
VII. REFERENCES	VII-1

LIST OF TABLES

<u>Table</u>	<u>Page</u>
III-I Point Design Summary	III-3
III-II Proprotor Design Conditions	III-5
III-III Characteristics Data Summary	III-6
III-IV Weight Empty Summary	III-7
III-V Weight Summary	III-10
III-VI Performance Summary	III-11
IV-I Summary of Model C300-A1C Scale Factors	IV-2
IV-II Model C300-A1C Primary Dimensional Data	IV-3
IV-III Model C300-A1C Shake Test Results	IV-5
IV-IV Model C300-A1C Instrumentation	IV-7
IV-V Actual Run Schedule, Semispan Aeroelastic Test	IV-11
V-I Model Dimensional Data	V-3
V-II Run Schedule	V-6
V-III Nomenclature	V-13
V-IV Summary of Configurations and Variable Settings Tested - Folding Proprotor Configuration - AF Pod No. 1 and 2	V-14
V-V Characteristics of Complete Aircraft, Flaps Up, Model Clean	V-17
V-VI Characteristics of Complete Aircraft, Flaps Up, Vortex Generators On	V-18
V-VII Characteristics of Complete Aircraft, Flaps Down, Air Force Pod No. 1	V-19
V-IX Change in Longitudinal and Lateral Characteristics Due to Folded Blades	V-20
V-X Comparison of Measured and Predicted Values of Lift Curve Slope and Flap Effectiveness for the Wing	V-22

LIST OF TABLES - Concluded

<u>Table</u>		<u>Page</u>
V-XI	Comparison Between Measured and Predicted Cruise Drag Data	V-23
V-XII	Baseline Data, Basic Airframe	V-24
V-XIII	Summary of Component Effects on Aircraft Yaw Stability	V-26
VI-I	Full-Scale and Model Parameters	VI-5

ILLUSTRATIONS

<u>Figure</u>		<u>Page</u>
II-1	Folding Proprotor Conversion	II-8
II-2	Schematic of Folding Proprotor Conversion Process	II-9
III-1	D270A Three View	III-18
III-2	D270B Three View	III-19
IV-1	Installation of Semispan Aeroelastic Powered Folding Proprotor Model (C300-A1C) in the LTV Wind Tunnel, February 1971	IV-26
IV-2	Control Console for Semispan Powered Aeroelastic Folding Proprotor Model	IV-27
IV-3	Model C300-A1C Predicted Boundaries for Stability with Flapping Free and Flapping Locked Out	IV-28
IV-4	Wing Beam Frequency and Damping Versus Airspeed	IV-29
IV-5	Wing Chord Frequency and Damping Versus Airspeed	IV-30
IV-6	Wing Beam Frequency and Damping Versus Airspeed	IV-31
IV-7	Wing Chord Frequencies and Damping Versus Airspeed	IV-32
IV-8	Wing Beam and Chord Frequency and Damping at 0-Degree Mast Angle 60-Degrees Fold	IV-33
IV-9	Correlation Between Theory and Measured Frequency and Damping Versus Fold Angle	IV-34
IV-10	Correlation Between Theory and Measured Frequency and Damping Versus Fold Angle	IV-35
IV-11	Wing Beam and Chord Frequency and Damping at 0-Degrees Mast Angle of Attack.	IV-36
IV-12	Correlation Between Theory and Measured Response at Wing Beam, Chord, and Torsional Natural Frequencies	IV-37
IV-13	Conversion Axis Vibration at 0-Degree Mast Angle of Attack During Starting	IV-38
IV-14	Correlation Between Theory and Measured Wing Chord Bending Response During Stopping	VI-39

ILLUSTRATIONS - Continued

<u>Figure</u>		<u>Page</u>
IV-15	Wing Chord Bending Response During Starting	IV-40
IV-16	Conversion Axis Vibration During Stopping at $\Delta t = 2.46$ Seconds	IV-41
IV-17	Conversion Axis Vibration During Feathering at $\Delta t = 3.56$ Seconds	IV-42
IV-18	Maximum Blade Beam Oscillatory Moments at 35 Percent Radius	IV-43
IV-19	Blade Chord Oscillatory Moment at 25 Percent Radius	IV-44
IV-20	Correlation Between Theory and Measured Blade Beam Loads at 35-Percent Radius	IV-45
IV-21	Transient Blade Beam Oscillatory Loads at 35-Percent Radius	IV-46
IV-22	Correlation of Blade Beam and Chord Bending at 35-Percent Radius versus Fold Angle	IV-47
IV-23	Correlation of Blade Beam and Chord Bending at 35-Percent Radius Versus Mast Angle of Attack	IV-48
IV-24	Correlation of Fold Link Load Versus Mast Angle of Attack	IV-49
IV-25	Correlation of Wing Beam Bending at 27 Percent Span	IV-50
IV-26	Steady Spindle Torque Versus Mast Angle of Attack at Different Fold Angles	IV-51
IV-27	Time Histories of Stop Fold Sequence from Run 18 (Wing Alpha, 6 Degrees; Full-Scale Speed, 175 Knots)	IV-52
IV-28	Conversion Link Steady and Oscillatory Loads at 60-Degree Conversion Angle	IV-53
IV-29	Measured Blade Beam Oscillatory Moments at 35-Percent Radius	IV-54
V-1	Model Installed in LTV Wind Tunnel	V-32
V-2	Three View of General Aerodynamic Force Model	V-33
V-3	Complete Aircraft, Flaps Up, Blades Closed, Model Clean	V-34

ILLUSTRATIONS - Continued

<u>Figure</u>		<u>Page</u>
V-4	Complete Aircraft, Flaps Up, Blades Closed, Model Clean	V-35
V-5	Complete Aircraft, Flaps Up, Blades Closed, Model Clean	V-36
V-6	Complete Aircraft, Flaps Up, Blades Closed, Model Clean	V-37
V-7	Complete Aircraft, Flaps Up, Blades Closed, Model Clean	V-38
V-8	Complete Aircraft, Flaps Up, Blades Closed, Model Clean	V-39
V-9	Complete Aircraft, Flaps Up, Blades Closed, Vortex Generators On	V-40
V-10	Complete Aircraft, Flaps Up, Blades Closed, Vortex Generators On	V-41
V-11	Complete Aircraft, Flaps Up, Blades Closed, Vortex Generators On	V-42
V-12	Complete Aircraft, Flaps Up, Blades Closed, Vortex Generators On	V-43
V-13	Complete Aircraft, Flaps Down, Blades Closed, Model Clean	V-44
V-14	Complete Aircraft Flaps Down, Blades Closed, Model Clean	V-45
V-15	Complete Aircraft, Flaps Down, Blades Closed, Model Clean	V-46
V-16	Complete Aircraft, Flaps Down, Blades Closed, Model Clean	V-47
V-17	Effect of Wingtip Pods On Longitudinal Characteristics for the Complete Aircraft, Air Force Pod No. 1	V-48
V-18	Effect of Wingtip Pods on Longitudinal Characteristics for the Complete Aircraft Less Engine Nacelles, Air Force Pod No. 1	V-49
V-19	Effect of Wingtip Pods on Longitudinal Characteristics for the Complete Aircraft Less Empennage, Air Force Pod No. 1	V-50

ILLUSTRATIONS - Continued

<u>Figure</u>		<u>Page</u>
V-20	Effect of Wingtip Pods on Longitudinal Characteristics of the Fuselage and Wing, Air Force Pod No. 1	V-51
V-21	Effect of Air Force Pod No. 2 on Longitudinal Characteristics	V-52
V-22	Summary of Wingtip Pod Effects on Longitudinal Characteristics, Air Force Pod No. 1	V-53
V-23	Summary of the Effects of Other Wingtip-Pod Configurations on Longitudinal Characteristics	V-54
V-24	Effect of Folded Blades on Lift	V-55
V-25	Effect of Folded Blades on Drag	V-56
V-26	Effect of Folded Blades on Pitching Moment	V-57
V-27	Effect of Folded Blades on Rolling Moment	V-58
V-28	Effect of Folded Blades on Yawing Moment	V-59
V-29	Effect of Folded Blades on Side Force	V-60
V-30	Effect of Engine Nacelles on Longitudinal Characteristics for the Complete Aircraft	V-61
V-31	Effect of Engine Nacelles on Longitudinal Characteristics for the Complete Aircraft Less Wingtip Pods	V-62
V-32	Effect of Engine Nacelles on Longitudinal Characteristics for the Complete Aircraft Less Empennage	V-63
V-33	Effect of Engine Nacelles on Longitudinal Characteristics of the Fuselage and Wing	V-64
V-34	Summary of Engine-Nacelle Effects on Longitudinal Characteristics	V-65
V-35	Longitudinal Characteristics with Horizontal Tail Removed from Complete Aircraft	V-66
V-36	Longitudinal Characteristics with Horizontal Tail Removed from Complete Aircraft Less Engine Nacelles	V-67
V-37	Longitudinal Characteristics with Horizontal Tail Removed from Fuselage and Wing	V-68
V-38	Summary of Horizontal Tail Contributions to Longitudinal Characteristics	V-69

ILLUSTRATIONS - Continued

<u>Figure</u>		<u>Page</u>
V-39	Horizontal Stabilizer Contributions to Pitch Static Stability	V-70
V-40	Downwash on the Horizontal Stabilizer	V-71
V-41	Basic Airframe Effects, Model Clean	V-72
V-42	Basic Airframe Effects	V-73
V-43	Effect of Vortex Generators on Wing Contributions to $C_{l\beta}$	V-74
V-44	Effect of Blade Pods on Aircraft Dihedral Stability	V-75
V-45	Aircraft Dihedral Stability, Vortex Generators On	V-76
V-46	Aircraft Dihedral Stability, Vortex Generators On	V-77
V-47	Blade Opening Effects, Air Force Pod No. 1, Flaps Down, Vortex Generators On.	V-78
V-48	Blade Opening Effects, Air Force Pod No. 1, Flaps Down, Vortex Generators On	V-79
V-49	Blade Opening Effects, Air Force Pod No. 1, Flaps Down, Vortex Generators On	V-80
V-50	Blade Opening Effects, Air Force Pod No. 1, Flaps Down, Vortex Generators On	V-81
V-51	Blade Opening Effects, Air Force Pod No. 1, Flaps Down, Vortex Generators On	V-82
V-52	Blade Opening Effects, Air Force Pod No. 1, Flaps Down, Vortex Generators On	V-83
V-53	Aileron Effectiveness, Flaps and Ailerons Up	V-84
V-54	Aileron Effectiveness, Flaps and Ailerons Down	V-85
V-55	Effect of Opening Blades 15 Degrees on Aileron Effectiveness, Flaps and Ailerons Up	V-86
V-56	Effect of Opening Blades 15 Degrees on Aileron Effectiveness, Flaps and Ailerons Down	V-87
V-57	Effect of Roughness on Aileron Effectiveness	V-88

ILLUSTRATIONS - Concluded

<u>Figure</u>		<u>Page</u>
V-58	Effect of Wingtip Pod and Blade Configuration on Aileron Effectiveness with Blades Folded, Flaps Up	V-89
V-59	Effect of Wingtip Pod and Blade Configuration on Aileron Effectiveness with Blades Folded, Flaps Down	V-90
V-60	Effect of Wingtip Pod and Blade Configuration on Aileron Effectiveness with Blades Open 15 Degrees, Flaps Down	V-91
V-61	Elevator Effectiveness, Flaps and Ailerons Up	V-92
V-62	Elevator Effectiveness, Flaps and Ailerons Down	V-93
V-63	Rudder Effectiveness, Angle of Attack Equal Zero Degrees	V-94
V-64	Rudder Effectiveness, Angle of Attack Equal 11 Degrees	V-95
V-65	Rolling Effectiveness of Rudder, Angle of Attack Equal Zero Degrees	V-96
V-66	Rolling Effectiveness of Rudder, Angle of Attack Equal 11 Degrees	V-97
VI-1	C100 Model During Functional Check Runs	VI-14

LIST OF SYMBOLS

a_t	three-dimensional lift curve slope of stabilizer
A_t	stabilizer area
A_w	wing area
AL	left flaperon, subscript indicates deflection where trailing edge down is positive
AR	right flaperon, subscript indicates deflection where trailing edge down is positive
b	wing span
B	fuselage
BL	blades and grips
\bar{c}	wing chord
C	wing chord
C_D	drag coefficient
CF	conversion actuator
C_l	rolling moment coefficient
$C_{l\beta}$	derivative of rolling moment coefficient with respect to sideslip angle
C_L	lift coefficient
$C_{L_{MAX}}$	maximum lift coefficient
$C_{L\alpha}$	slope of the lift curve
$C_{L\delta}$	derivative of lift coefficient with respect to flap deflection angle
C_m	pitching moment coefficient
C_M	pitching moment coefficient
$(C_M)_{STAB}$	contribution of stabilizer to pitching moment
$C_{M\alpha}$	derivative of pitching moment coefficient with respect to angle of attack

LIST OF SYMBOLS - Continued

C_n	yawing moment coefficient
$C_{n\beta}$	derivative of yawing moment coefficient with respect to sideslip angle
C_{RM}	rolling moment coefficient
C_{RMB}	rolling moment coefficient, body axis
$(C_{RM})_\psi$	derivative of rolling moment coefficient with respect to yaw angle
C_T	rotor thrust coefficient
C_Y	side force coefficient
C_{YB}	side force coefficient, body axis
C_{YM}	yawing moment coefficient
C_{YMB}	yawing moment coefficient, body axis
$(C_{YM})_\psi$	derivative of yawing moment coefficient with respect to yaw angle
E	elevator, subscript indicates elevator angle where trailing edge down is positive
f	blade faired to pod; also, equivalent flat plate drag area
F	flaps, subscript indicates flap deflection where trailing edge down is positive
g	acceleration due to gravity
GO	blade grips on
H/D	height to diameter ratio
i_m	mast angle of incidence relative to aircraft longitudinal axis (the complement of the conversion angle from the helicopter attitude)
l_t	stabilizer moment arm
MRP	military rated power
N	jet engine nacelle

LIST OF SYMBOLS - Continued

N_1	flow through, jet engine nacelle
N_2	jet engine nacelle, plugged and faired
N_3	same as N_1 but three inches outboard
N_4	same as N_1 but four inches below that of N_1
OGE	out of ground effect
P^1	Bell tilt-propotor pod, subscript indicates angle relative to perpendicular to fuselage waterline
P^2	Air Force Pod No. 1, subscript indicates angle relative to perpendicular to fuselage waterline
P^3	Bell tilt-propotor pod with folded blades, subscript indicates angle relative to perpendicular to fuselage waterline
P^4	Air Force Pod No. 2, subscript indicates angle relative to perpendicular to fuselage waterline
(PT) ₄₅	Forty-five degree antidiheral pod tip plate
q	test section dynamic pressure corrected for blockage and compressibility
R	rotor radius; also rudder, subscript is rudder angle which is positive for positive side force
S	wing area; also horizontal stabilizer, subscript indicates stabilizer angle where trailing edge down is positive
SLS	sea level standard day
Δt	time interval for stopping or starting the rotor
T	thrust
T'	model test medium temperature ratio
(TS) ₁	boundary layer transition strip on wing
(TS) ₂	boundary layer transition strip on wing and fuselage

LIST OF SYMBOLS - Continued

V	velocity; also vertical stabilizer
$(VG)_1$	partial span vortex generators
$(VG)_2$	full span vortex generators
V_H	maximum level flight speed of aircraft
V_L	limit flight speed of aircraft
W	wing
α	angle of attack
α_m	mast angle of attack
α_w	wing angle of attack
β	sideslip angle, positive for nose left, equal to - ; also blade fold angle, subscript indicates degrees open from folded position
γ	blade fold angle
Γ	wing dihedral angle
δ	flap deflection
δ_3	\tan^{-1} (nose-down change in blade pitch angle as blade flaps up)
ϵ	downwash angle on stabilizer
η	dynamic pressure efficiency at stabilizer
e	air density
σ	rotor blade area divided by rotor disc area
σ'	atmospheric density ratio
ψ	angle of yaw
Ω	rotor rotational speed
Ω_σ	rotor rotational speed at the beginning of the rotor spin-down transition
Ω_F	rotor rotational speed at the end of the rotor spin-up transition

I. SUMMARY

This report summarizes the design studies and presents the results of wind-tunnel test investigations of the folding-prop rotor aircraft concept accomplished under Phase I and II of Contract F33615-69-C-1578 for the USAF Flight Dynamics Laboratory.

The design studies defined the D270A and D270B folding-prop rotor aircraft for USAF rescue and transport missions. Both are VTOL aircraft which can lift off vertically at altitudes over 7000 feet at 95°F and which have speed ranges extending to over 400 knots. Gross weights are in the 66,000-pound category and disc loadings are about 16 pounds per square foot. Risk areas of the concept were found to be in the areas of mechanisms, aerodynamics, stability and control, and dynamics. The D270 designs satisfied the requirements of the missions specified and are possible VTOL design solutions for a high-speed, high-hover-time mission.

Wind-tunnel test investigations of selected risk areas were accomplished during Phase II. Two models were tested. Dynamic investigations were conducted of a one-fifth-scale semispan powered aeroelastic model representing a 25-foot-diameter folding prop rotor. Dynamic data and wind-tunnel balance data were obtained and were scaled to equivalent full-scale values. The dynamic data included time histories of control settings, flapping, and blade and wing loads during the stop/fold process. In addition, data were obtained which included rotor torque, control settings, flapping, and wing loads at two pylon angles with the rotor powered. Investigations of model dynamic stability in the prop rotor mode showed no prop rotor/pylon instability in the conversion speed range tested. With rotor stopped, no flutter was experienced at any fold angle up to 292 knots (1.46 V_H for the stop/fold mode). Rotor stop-start rates were investigated over the range from 1.95 to 4.34 seconds which encompassed the range of optimum rates based on oscillatory and transient loads. The angle of attack envelope for the stop-start process was investigated at a typical speed of 175 knots and was found to extend to approximately 6 degrees wing angle of attack based on blade loads. Blade, wing, and control loads were investigated for several fold angles, including fully folded and fully opened, up to a wing angle of attack of 11 degrees at 175 knots, and 3 degrees at 292 knots. Time histories of continuous stop/fold/unfold/start sequences were obtained for speeds up to 175 knots with a wing angle of attack of 6 degrees. By the conclusion of the test, powered prop rotor data at several torque levels were obtained for the pylon angles representing prop rotor flight and 30 degrees above that angle. Data were correlated with theoretical predictions and compared with full-scale powered tilt-rotor data in the tilt range.

Aerodynamic investigations of cruise-mode drag and stability characteristics of the wingtip folded blade configuration were conducted with a one-fifth-scale model of the Bell Model 306 modified to a folding-prop rotor configuration. For the configuration tested, drag of the folded blades in cruise was found to be the smaller part of the wingtip-pod and folded-blade contribution to total aircraft drag. The larger part is due to the basic transmission and pylon mechanism cowlings generic to the configuration. The blades tend to decrease pitch and yaw stability and increase effective dihedral. These effects were offset in part by contributions of the jet engine nacelles, which

were underslung beneath the wing and which may not be typically generic. Aerodynamic model development testing is desirable for specific folding-proprotor configurations.

A third model was designed, fabricated, and delivered to the Air Force for testing in the NASA-Langley V/STOL wind tunnel. This is a one-tenth-size full-span powered aerodynamic model of the D270A. The purpose of tests with this model is to investigate stability and control and aerodynamic characteristics on the conversion or pylon-tilt range from hover through low- and high-speed helicopter, conversion, and proprotor modes. Test results will give characteristics typical of the larger proprotor aircraft with disc loadings in the 16-pounds-per-square-foot range.

Bell Helicopter Company presents two recommendations to the government which are based on the Phase II results in the light of related small-scale and full-scale proprotor and folding proprotor investigations. These are:

- For the folding proprotor, update component designs of the mechanisms related to proprotor folding to provide an improved basis for assessment of the concept.
- For the tilt rotor, proceed into flight investigations with a 25-foot-diameter proprotor research/technology demonstrator aircraft to validate design criteria and analytical methods which have been thoroughly verified by small-scale model investigations and full-scale component evaluations.

II. INTRODUCTION

A solid background of design, analysis, and wind-tunnel and flight testing has shown that the tilt-rotor configuration is a promising low-disc-loading V/STOL concept for at least doubling the operational speeds of modern helicopters. Efficient hover and helicopter-like low-speed control capability can be provided over greater mission stage lengths and with quicker response times than are possible to obtain with helicopters.

Extensive testing of the XV-3 tilt-rotor aircraft in 1959 demonstrated that flight could be maintained in the hover mode, in the cruise mode, or in any intermediate configuration. The XV-3 test program also identified problem areas associated with proprotor/pylon dynamic stability and low damping of the short-period flight modes. These were subsequently investigated and solutions were reported during the Army Composite Aircraft Program in 1967. Advanced proprotor versions of the Composite Aircraft were shown to have speed potential up to 500 knots by employing advanced airfoils, structural techniques, and mechanical devices to extend performance and aeroelastic stability at the high speeds. However, the additional devices and design requirements for tilt-proprotor operation at high subsonic speeds incur additional weight and complexity. Another approach for increasing the speed capability of the tilt rotor is to employ the folding-proprotor concept. In the high-speed mode, convertible fan/shaft engines provide the propulsive thrust allowing the rotor blades to be stopped and folded after they have been tilted from the helicopter to the proprotor mode. This approach greatly reduces the problems of designing the proprotor to avoid aeroelastic instability at high subsonic speeds, but the stopping and folding of the proprotor impose other design requirements. The question which arises is: does the addition of variable thrust fans to the basic shaft engine and the provision of in-flight blade folding represent less weight than the provision of additional proprotor strength, transmission torque capability, increased tail size, and additional wing stiffness for satisfactory proprotor characteristics in the high subsonic speed range? For a comparison of the folding proprotor and advanced proprotor (or any other V/STOL) approaches for high subsonic speed flight, an investigation of folding-proprotor technology was in order. Such an investigation is the subject of this report. In the following paragraphs, additional detail is provided on the description of the folding proprotor concept, prior and related work, and purposes of the investigations described herein.

A. THE FOLDING-PROPROTOR CONCEPT

The folding-proprotor aircraft concept is an extension of the low-disc-loading, tilt-proprotor VTOL aircraft to a fan-propelled stoppable-rotor configuration suitable for high-speed mission requirements.

The concept is illustrated in its various flight modes in Figure II-1. Takeoff is with proprotor masts vertical, followed by acceleration into forward flight in the helicopter mode. Conversion from helicopter to proprotor mode is identical to that of the tilt proprotor, and is initiated in level flight, while climbing, or during descent by tilting the rotors forward where they produce thrust as conventional propellers. The transition from proprotor to high speed cruise mode is then accomplished by

transferring propulsive thrust from proprotors to fans, then by feathering, stopping, and folding the proprotors.

Steps in the transition process, from tilt-proprotor mode to high-speed cruise mode, as shown in Figure II-2, are initiated by commanding increases in fan mass flow and thus engine propulsive thrust from the compound engines until proprotors are windmilling. The command varies pitch of the fan rotors or stator blades. Concurrently, proprotor blade pitch is being reduced automatically toward the windmilling state by the proprotor rpm governor, which is sensing power turbine speed reductions resulting from increased fan power demands. When the proprotors reach windmilling state, rotors are decoupled from the drive train. Flapping is locked, blades feathered to stop the rotors, masts locked at the azimuth position for folding, blade pitch reset, and blades are folded aft along the wingtip nacelles and locked in place. The steps are stoppable and reversible at any point and are commanded by forward or reverse actuation of a sequence control switch on the cyclic stick. When the blades are folded, rotor drag is reduced, and the aircraft can accelerate to its cruise speed. Since stopping and folding the proprotors removes the speed constraints associated with the tilt-proprotor configuration, the maximum speed capability is then established only by the installed thrust of the powerplants.

The rotors which are folded during cruise, can have blade planform, airfoil sections, and twist which are optimized for hover. The high cruise speed capability of the folding-proprotor VTOL concept increases productivity for logistics support missions, decreases vulnerability during air-assault and aircrew-rescue missions when penetrating a nonpermissive environment, and offers fast response for all missions--frequently the difference between success or failure of a military operation.

There are other operational characteristics which make the folding-proprotor configuration suited for military applications. Among these are:

- The folded proprotors minimize the aircraft radar signature during cruise, and they make air-to-air refueling less hazardous. Both of these considerations are important for missions including aircrew rescue.
- The proprotors, their drive system, and related controls are not turning during the majority of the flight time; i.e., during cruise. This extends their time between overhaul in terms of total aircraft flight hours and reduces maintenance and spares support requirements.
- While redundant design of critical systems makes a failure which would prevent reconversion to vertical flight configuration unlikely, a run-on landing at a conventional airfield can be made with blades folded in cruise configuration without danger of aircraft damage.
- For VTOL aircraft intended for Navy and Marine applications, blade folding is required to achieve maximum shipboard compatibility. In fact, all transport-size helicopters operated from ships already incorporate automatic blade folding. The folding provisions, therefore, do not constitute an additional handicap for VTOL aircraft intended for shipboard operation.

- The low-disc loading of the folding-proprotor VTOL enables it to lift large payloads for short-range external cargo missions normally associated with a flying crane. This versatility of the folding-proprotor configuration in effectively meeting widely differing mission requirements, constitutes one of its principal advantages when compared to other VTOL types. It is this mission versatility that could open new and as yet unrealized applications for the aircraft.

B. PRIOR AND RELATED WORK

1. Basic Tilt Rotor

The wind-tunnel and flight investigations of the XV-3 (Reference 1) demonstrated the feasibility of the tilt-rotor concept. Sustained flight in helicopter, conversion (pylon tilt), and airplane (proprotor) modes was demonstrated. Power-off reconversions from airplane to helicopter mode followed by autorotative landings were conducted. Due to the large aspect ratio effect of the side-by-side rotors, power requirements at low speed, 50 to 60 knots, were considerably reduced from that required to hover which allowed short takeoff and landing (STOL) operations to be demonstrated at overload gross weights. The primary problem areas defined by the XV-3 were: proprotor pylon stability, low damping for the short period modes, and excessive rotor flapping in maneuvers. Secondary problem areas included "lateral darting" tendencies when hovering in ground effect, high pilot workload due to complicated controls, and an underpower situation due to the use of a piston powerplant as described in Reference 1. Following the XV-3 tests, investigations continued and during the Army Composite Program (Reference 2) solutions were employed which were designed to improve the tilt-rotor concept as defined by the XV-3.

The approach on the Composite Aircraft Design was to use two 38.5-foot-diameter, three-bladed, stiff-inplane gimbal-mounted rotor systems with flapping restraint springs and negative delta three control linkage. The rotor was mounted on a "focused mast" pylon assembly which was rigidly attached to a wing of high torsional stiffness. This combination provided a rotor system which was inherently free from ground and air resonance, provided a proprotor/pylon (whirl flutter) stability boundary well in excess of 1.44 times the maximum aircraft speed of 356 knots, minimized the sensitivity of the rotor to flapping during gusts and maneuvers, and provided ample longitudinal control power of the rotor system in the hover mode. In addition, to reduce pilot workload and optimize handling qualities relative to the XV-3, a stability and control augmentation system (SCAS), simplified controls and turbine power were included in the design. The results of that work are described in References 3 through 6. Reference 6 also presents the approach for realizing 400-plus knot speeds with advanced proprotor approaches.

After the conclusion of the Army Composite Program, work was continued on a smaller, 25-foot-diameter tilt-rotor research aircraft design defined as the Model 300 aircraft and reported under NASA Contract NAS2-5386, Reference 7. Since the speed capability of the smaller craft was slightly less (300 knots) than that of the composite aircraft, the design approach was similar, except

that the focused mast concept was eliminated for simplicity without loss of ample margin for proprotor aeroelastic stability. The proprotor dynamic design criteria were verified in two full-scale wind-tunnel tests of the 25-foot proprotor. The first test with the unpowered rotor mounted on simulated wing assemblies of full- and quarter-stiffness wing assemblies proved the design aeroelastically to maximum tunnel speed which represented scale speeds up to 400 knots. The second test with power, showed propulsive efficiencies and static hover capability in excess of predicted values. The results of both tests are provided in References 8 and 9. These tests and related small-scale tests have shown the tilt proprotor dynamic design criteria to be well in hand for application to full-scale aircraft flight programs. In the areas of performance and stability and control, information concerning net effects of overall performance and stability and control derivatives have been obtained. (See for example, Reference 10.) More remains to be done however, on identifying the contributions of isolated components (tail, wing, flaps, etc.) to overall vehicle performance and stability and control characteristics so that designs may be optimized for specific missions.

2. Folding Proprotor

In 1965, in a series of reports for the Army leading to the Composite Aircraft Program, growth potential of the tilt-rotor aircraft was identified and included the "folded-blade proprotor" concept. Following a series of events, the Air Force expressed, late in 1967, interest in this concept for rescue, recovery, and transport missions. In 1968, Bell conducted, under its IR&D program, design studies and model tests of this concept and results were published in References 11 and 12. Based on the background of tilt-proprotor work described above and on the exploratory model tests and analyses conducted under the independent studies, principal effects of adding folding capability to the proprotor in the areas of performance, stability and control, and dynamics were identified in 1968 and are summarized below:

- | | |
|------------------------------|---|
| <u>Performance</u> | <ul style="list-style-type: none"> - Windmilling drag of the proprotors prior to folding are well within the low-speed thrust capability of fans installed for 400-knot cruise speeds. - Cruise drag of folded blades and the wingtip pods represent about 15 percent of total aircraft drag based on tests at low Reynolds and Mach numbers. |
| <u>Stability and Control</u> | <ul style="list-style-type: none"> - As the proprotors are stopped, aircraft neutral point shifts forward and total lift curve slope increases and provides the criteria for sizing the horizontal tail. - During rotor stopping and starting, the longitudinal forces generated at the rotor, due to exchanges between aircraft and rotor kinetic energy, produces aircraft pitching moment variations (as well as longitudinal accelerations) which must be considered in the aircraft design. - Aerodynamic interference of the rotor blades on the wing at blade passage frequency at low rotor rpm could affect aircraft short-period as well as wing structural modes. |

Dynamics

- The flapping freedom of the gimbaled rotor must be locked out at low rotor speed to avoid a flapping instability.
- Wing vibration is excited at low rotor rpm due to wing/rotor aerodynamic interference and could be alleviated by traversing these frequencies quickly. (A trade-off between rotor longitudinal forces on the aircraft and excitation of structural modes results when selecting rotor stop/start rates.)
- Wing divergence speed boundaries with the rotor stopped but not folded are well in excess of the stop/fold speed range when wing stiffness requirements are met for proprotor operation.
- Flutter stability boundaries of the exposed portions of the folded blades are raised into the transonic speed range and beyond.
- Proprotor blade static strength designed for 50-foot-per-second gusts at proprotor cruise speeds is sufficient for gusts up to 66 feet per second with the rotor stopped but not folded at typical stop/start flight speeds.
- One-per-rev blade loads while maneuvering during the stop/start process with flapping locked out and with blade structural configuration representative of proprotor-only operation would result in low-cycle fatigue damage and tend to reduce blade life.

It was found that improved analytical techniques were required in assessing system stability and component loads at very low and zero rotor rpm. There followed a series of contracted efforts sponsored by the Air Force and NASA to further investigate folding proprotor technology. These included analytical studies for predicting stability derivatives at low and zero rpm (Reference 13), prediction of dynamic stability, loads and vibration during the stop/fold process including the effects of wing/rotor aerodynamic interference (Reference 14), and the prediction of wing/rotor aerodynamic interference on aircraft stability in the airplane mode (Reference 15). A program for the wind-tunnel test of a full-scale 25-foot-diameter folding proprotor (the Model 627 rotor) on a simulated wing with full-scale stiffness was completed under Contract NAS2-5461. Design studies of the application of this rotor to a research aircraft (D272) are presented in Reference 16 and final results of that program including wind-tunnel tests of the Model 627 rotor are presented in Reference 17.

Concurrently with the above folding proprotor technology programs the effort described in this report was initiated under Air Force Contract F33615-69-C-1578 for Design Studies and Model Tests of the folding proprotor configuration.

C. PURPOSE OF DESIGN STUDIES AND MODEL TESTS

The contract under which the work reported herein was accomplished was initiated in April 1969 and included both design studies of full-scale aircraft suitable for

Air Force missions (Phase I) and wind-tunnel testing (Phase II). The purpose of the contracted effort including Phase I and II was generation of basic design data for folding-proprotor aircraft to aid in providing a technical base from which the concept can be assessed against competing V/STOL aircraft. Objectives were identification and exploration of potential problem areas and establishment of reliable design criteria through design studies and wind-tunnel testing.

1. Phase I Design Studies

Phase I was completed in October 1969 and consisted of preliminary design studies for aircraft optimized for five specific missions coordinated with the Air Force. A point design was selected from among these for further refinement. Mission tradeoffs were made and sufficient detail design of critical components was performed to identify its technical risk areas. It was recommended that Phase II model work be conducted to investigate risk areas and that a large-scale model be tested to investigate problems such as wear and conversion design requirements.

Results of the study are reported in Reference 18 and a synopsis is included in Section III of this report.

2. Phase II Model Tests

Following completion of Phase I, Phase II model test activities were initiated with guidance from FDL. The Phase II general objectives consisted of wind-tunnel tests of aerodynamically scaled models to validate analytical methods of deriving stability and control derivatives and aerodynamic characteristics, and testing of dynamically scaled models to aid development of reliable prediction techniques and establishment of valid design criteria.

The model program which evolved included tests of two models and fabrication of a third. The first model tested was a one-fifth-scale general aerodynamic force model of the Bell Model 300 tilt-proprotor aircraft modified to a folding proprotor configuration. Tests were with blades folded edgewise alongside the wingtip nacelles, and test results give generic characteristics of this folding-proprotor configuration in the cruise mode, specifically the effects of the folded blades on configuration characteristics. Objectives included determination of component drag, incremental drag due to folded blades, and stability derivatives with the blades in partial and completely folded positions.

The second model was a one-fifth scale semispan powered aeroelastic model of the same aircraft, but modified to have remote-controlled hub lock, blade feathering, mast lock, and blade folding. Tests included dynamic stability, stopping, starting, folding, and continuous sequences. Purpose of tests with this model was the investigation and verification of the planned tilt/stop/fold control procedures and their effect on rotor flapping, pylon accelerations, and rotor and wing component loads. Testing was initiated under proprotor wind-milling conditions and for the stop-fold flight regime including time history records of control settings, flapping, and blade and wing loads during the stop/fold process. Objectives included tests in the transition flight regime at incremental mast tilt angles and with rotor power.

Both models were fabricated by Bell Helicopter Company under IR&D, and the contract supported wind-tunnel time cost, data reduction, and analysis.

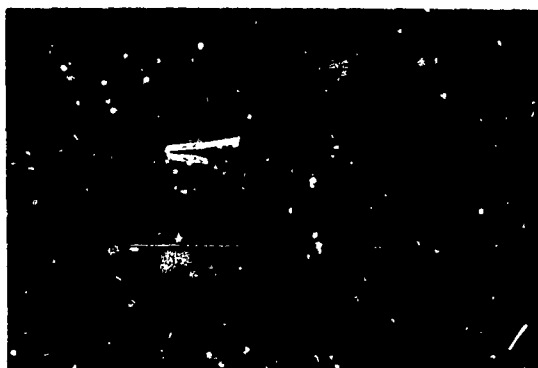
Most emphasis in Phase II was placed on need for stability and control, and aerodynamic testing in the conversion or pylon-tilt range. To satisfy this, a one-tenth-scale full-span powered aeroelastic force model of the Phase I point design, D270A, was designed, fabricated, and checked out. Tests of this model were planned for the NASA-Langley V/STOL Wind Tunnel.



Helicopter Flight



Forward Tilt Conversion



Proprotor Flight



Fan Propulsion
Rotors Stopped and Folding



High-Speed Cruise Mode
Rotors Folded



Cruise Configuration

Figure II-1. Folding Proprotor Conversion

III. DESIGN STUDY SUMMARY

The Phase I Design Studies developed five point designs and were conducted on the basis of folding-proprotor aircraft optimized for several specific Air Force missions. One point design aircraft was selected from among these, for further refinement, and mission tradeoffs. Preliminary design of critical components was performed to identify the technical risk areas associated with the aircraft in question, and a test program was then recommended to investigate each of these risk areas.

The following sections contain a synopsis of the work accomplished during Phase I. For detail information on each area, reference is made to the Phase I Interim Report, "Design Studies of Folding Proprotor VTOL Aircraft," Reference 18.

A. OBJECTIVES

Objectives were to perform parametric and preliminary design studies relating to specific mission performance, identify and analyze potential technical problem areas, and develop data for scaling of a full-scale design down to properly sized model hardware. The tasks performed in Phase I were:

- Establish the impact of mission requirements on folding-proprotor aircraft by optimizing a point design for each of five sets of mission requirements.
- Recommend an aircraft mission and design for future refinement.
- Refine the design of the recommended aircraft.
- Determine the aircraft sensitivity to important design parameter changes.
- Identify technical risk areas.
- Recommend subsequent tests and prepare detailed test plans to investigate the risk areas.

B. APPROACH

Early in the study, key considerations and initial assumptions required to initiate the study effort were identified. These included assumptions relating to rotor and wing aerodynamics, aircraft parameters, and structural requirements. Items such as propulsion system type and its impact on the system's cost and schedule, operational characteristics such as noise and downwash, reliability and battle damage characteristics, and program costs were considered. Where possible, the effects of these items and their interactions were determined. In cases where the effects could not be quantified, assumptions were made for the subsequent efforts.

Where the quantitative approach was used, in determining characteristics of a point design, the optimization and selection of the aircraft parameters were based on considerations of L/D, hover performance, structural weight, and engine specific fuel consumption characteristics. A description of the typical methodology used is presented in Reference 19. For each analysis, the selected parameters generally provided the minimum design gross weight for the mission being considered. The design processes begins with the definition of a mission profile and identification of applicable technology. The missions used for the Phase I study included rescue, recovery, and combinations of these transport profiles. The missions are summarized in the separately bound Appendix A, classified confidential, of Reference 18. The applicable technology is based on prior Bell Helicopter studies (Reference 11) which indicated that the approximate weight growth factor (design gross weight divided by mission invariant weight) associated with the primary mission (and based on existing engines) would be approximately 10.0. This placed the gross weight in the 60,000 to 70,000 pound range for the folding proprotor configuration.

C. POINT DESIGN SUMMARY

A point design was generated for each of five missions. The specific designation for each is as follows:

- Point Design I (Rescue)
- Point Design II (Recovery)
- Point Design III (Rescue and Recovery)
- Point Design IV (Transport)
- Point Design V (Rescue, Recovery and Transport)

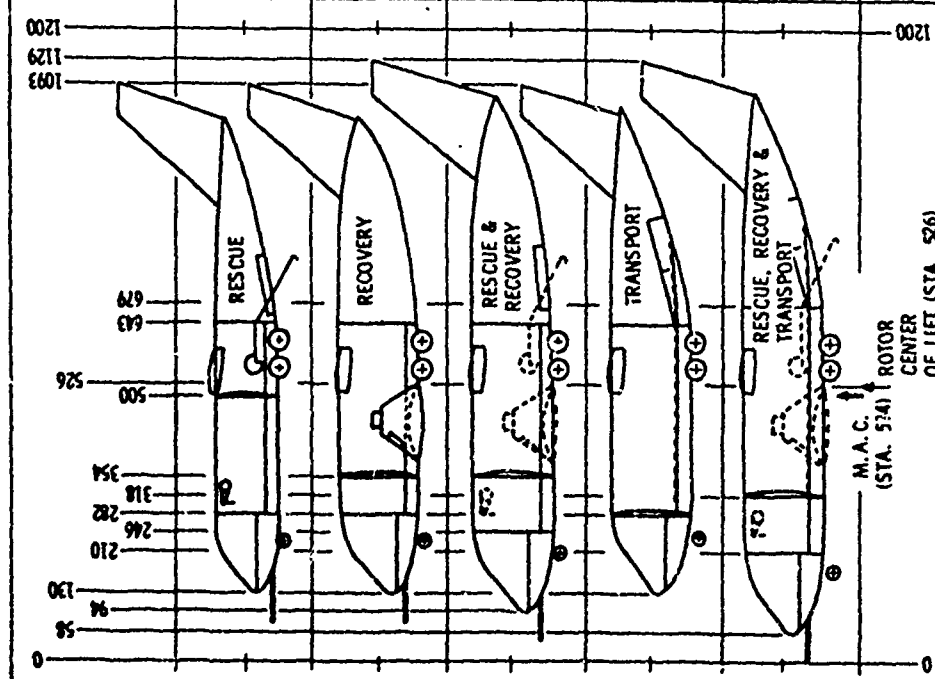
A summary of each is shown in Table III-I.

The most demanding mission requirement was found to be that of the rescue mission. When Point Designs III and V were analyzed for that mission, the fuselage drag resulting from the larger multipurpose fuselage increased mission fuel requirements beyond capacity of the basic design. However, the takeoff weight remained within alternate gross weight capability. Thus, Point Designs I, II, and IV achieved their missions; whereas, Point Designs III and V required an overload takeoff for the rescue mission.

Point Designs I, II, and IV were found to have many features in common. The rotor, propulsion and wing systems are identical. Thus if Point Design I were developed, it was reasoned that Point Designs II and IV could be achieved by the development of a multipurpose fuselage. Layout drawings of the Point Designs are presented in Reference 18.

TABLE III-I. POINT DESIGN SUMMARY

POINT-DESIGN SUMMARY										
POINT DESIGN	ROTOR DIAM. (ft)	ENGINE RATING MIL. SLS (shp)	WEIGHTS			W/HP @ DGW (lb/shp)	L _b		(+5%) SFC	
			DESIGN GROSS (lbs)	MISSION TAKE-OFF (lbs)	OPERATING (lbs)		CRUISE @ DGW	DASH @ DGW	HOVER	CRUISE DASH
I	50	4420	66,000	66,569	46,430	5.70	10.30@ 400 Kn 30,000'	7.13@ 350 Kn 3000'	.525	.635 .694
II	50	4420	66,000	65,967	45,467	5.70	9.24@ 400 Kn 30,000'	N.R.	.525	.637 N.R.
III	53	4420	71,000	77,464	51,579	5.81	9.37@ 400 Kn 30,000'	6.14	.525	.654 .665
IV	50	4420 ²	66,000	66,095	45,730	5.70	10.1@ 400 Kn 30,000'	6.09	.525	.637 .674
V	62.4	4850	84,000	86,225	58,213	6.22	10.37@ 400 Kn 30,000'	6.84	.525	.550 .670
NOTES: 1. Convertible Fan/Shaft Version of LTC4V-1 2. Growth Version of (1.)										



D. RECOMMENDED DESIGN REFINEMENT

It was recommended during the Phase I mid-term briefing of the contract that the aircraft described as Point Design I be the prime development goal and used as the basis for the future program effort. The corresponding lift system was based on a 50-foot-diameter rotor.

The Lycoming LTC4V-1 engines and the 50-foot rotors had sufficient capability for Point Designs II and IV. By providing ample fuselage/blade clearance for the 10-foot-diameter fuselage of Point Design I, it was planned that it would be possible to accommodate a larger 13-foot-diameter fuselage to achieve the requirements of Point Designs II and IV. Thus, the primary dynamic systems would have multimission capability.

Subsequent guidance from the Air Force included the following items:

- Concentrate on technology for one wing rotor system with alternate fuselages.
- Use Point Design I to establish basic vehicle and component size.
- Use Point Design IV performance requirements to establish alternate cargo fuselage for the aircraft sized by Point Design I.

E. REFINED DESIGNS

The D270A is the designation given to the refined design for the rescue mission. It is based on Point Design I, but involved differences due to both design requirements and the approach used. The main differences are:

- Two twin-engine nacelles were changed to four individual engine nacelles resulting in reduced structure and drive system weight and improved survivability and maintenance qualities.
- Empennage size was reduced by designing to minimum requirements per MIL-F-8785 and MIL-F-8785A, and considering stability and control augmentation system operation necessary in the transition mode for optimum handling.
- Major rearrangement of the wing rib spacing and fuel system resulted in reduced fuel system weight and increased fuel capacity in the wing. Fuselage fuel tanks are not required for the rescue mission, thereby improving survivability characteristics.

- Vertical limit load factor was reduced from 3.0 to 2.5 g's.
- Landing gear capacity was increased to accommodate softer fields.

The designation given to the transport version is the D270B. Layout drawings for the aircraft and selected components are presented in Reference 18.

1. D270A

The D270A is illustrated in Figure III-1 and has a design gross weight of 66,000 pounds. In the helicopter mode, hover capability extends to over 7000 feet on a 95°F day and in the airplane mode, the speed range extends to over 450 knots. Four Lycoming LTC4V-1 convertible fan/shaft engines give multiengine reliability in both the rotary wing and fixed wing mode. A shaft version of this engine has completed initial testing.

Its fifty-foot diameter rotors have a design disc loading of 16.8 psf which is optimum (from productivity considerations) for the rescue mission. Design wing loading is 85 psf which is near optimum for the cruise conditions of 400 knots and 30,000 feet.

The primary dynamic system, consisting of rotors, wing and engine, is designed to be suitable for fuselages up to 13-foot diameter. Since the primary mission for the D270A is a rescue mission, a 10-foot-diameter fuselage has been selected, primarily to minimize drag.

The following table shows primary structural design conditions for the D270A lift-propulsion system which are the same for the D270B.

TABLE III-II. PROPROTOR DESIGN CONDITIONS, D270(A & B)

Gross weight	lb	66000
Load factor	g	+2.5 -0.5
Limit torque	ft-lb	230578
Maximum continuous torque	ft-lb	139744
Helicopter rpm		314
Proprotor rpm		191
Limit rpm		345
Maximum velocities		
Helicopter	kt	150
Proprotor level flight (V_H)	kt	250
Proprotor dive (V_L)	kt	288

During the component design study activity of Phase I, criteria such as those shown and assumptions were required as to details of the mechanism design associated with stop/fold process. Details of component load distributions, duty cycles per mission, and wear characteristics which could influence lost motion, stiffness linearity and damping were lacking and showed the need for large scale as well as small scale component tests.

2. D270B

The D270B is designed as a transport aircraft and is illustrated in Figure III-2. Rotor, propulsion, and wing systems are identical to the D270A. The main difference is the fuselage which is increased to a 13-foot external diameter. The landing gear has also been changed to maximize internal volume for cargo. The D270B is based on a modification of Point Design IV described previously.

3. Dimensions and Parameters

Major dimensions and parameters for the D270A and D270B are presented in Table III-III.

TABLE III-III. CHARACTERISTICS DATA SUMMARY

Item	Units	Data	
		D270A	D270B
<u>Airframe</u>			
Length	ft	81.25	81.25
Overall height	ft	30.66	32.33
Maximum fuselage diameter	ft	10.00	13.00
Wing span	ft	64.25	64.25
Wing area	ft ²	706	706
Wing aspect ratio	--	5.85	5.85
Design wing loading	lb/ft ²	85.0	85.0
Vertical tail area	ft ²	205	205
Horizontal tail area	ft ²	250	250
<u>Proprotor</u>			
Diameter	ft	50	50
Number of blades	-	3	3
Design disc loading	lb/ft ²	16.8	16.8
Design C_T/σ	-	0.10	0.10
Tip speed (100% rpm)	ft/sec	822	822
<u>Engine</u>			
Number of engines	-	4	4
Military rating			
Horsepower (SLS)	shp	4420	4420
Thrust (30000 ft, Mach 0.7)	lb	1840	1840

4. Weight and Performance

Group weight empty summaries are shown in Table III-IV. Gross weight summaries for the D270A in the rescue and ferry missions, and the D270B in the 5-ton VTOL, 8.5-ton STOL, and ferry missions, are shown in Table III-V.

Weights were obtained through refinement of the point design weights by:

- Detailed estimation of systems and structural components whenever drawings, stress analyses, component sizing, and other necessary data were available
- Comparison with similar systems with allowances for differences in size, complexity, and design requirements
- Use of statistical equations which had been verified in previous use

Performance characteristics of the D270A and D270B are summarized in Table III-VI and meet or exceed the requirements established for their respective missions. It should be noted that this was based on assuming a technology level representative of conventional structural concepts.

The analysis of the sensitivity of design gross weight as a function of variations in mission parameters and aircraft design parameters was conducted and is reported in Reference 18. In addition, the impact on design gross weight of using advanced structural concepts and composite materials for selected aircraft components for the rescue mission was also assessed and reported in Reference 18. The potential savings were shown to be applicable to reductions in aircraft gross weight or to increased redundancy or survivability characteristics in an aircraft of a given gross weight.

TABLE III-IV. WEIGHT EMPTY SUMMARY

Item	D270A Wt (lb)	D270B Wt (lb)
Rotor Group	7521	7521
Blade Assembly	4004	4004
Hub Assembly	2917	2917
Blade Folding	600	600
Wing Group	5137	5137
Tail Group	1338	1338
Horizontal Tail	790	790
Vertical Tail	548	548
Body Group	4994	7204
Fuselage Basic Structure	2174	2686
Fuselage Secondary Structure	2820	3823
Cargo Handling System	-	695

TABLE III-IV. Continued

Lighting Gear	2631	2764
Main	2011	2122
Nose	620	642
Flight Controls Group	2112	2112
Cockpit Controls	53	53
Automatic Stabilization	30	30
System Controls		
Rotor, Nonrotating	848	848
Rotor, Rotating	883	883
Fixed Wing	268	268
Conversion	15	15
Blade Folding	15	15
Engine Section	1065	1065
Engine Mount	162	162
Firewall	59	59
Cowl	844	844
Propulsion Group	11312	10694
Engine Installation	4100	4100
Conversion System	620	620
Air Induction System	230	230
Exhaust System	35	35
Lubricating System	108	108
Fuel System	1520	1055
In-Flight Refueling System	153	-
Engine Controls	146	146
Starting System	156	156
Drive System		
Gear Boxes	3183	3183
Transmission Drive	477	477
Rotor Drive	584	584
Auxiliary Powerplant Group	182	182
Instrument Group	400	400
Hydraulic and Pneumatic Group	292	292
Electrical Group	775	775
Electronics Group	1500	950
Armament Group	2000	50

TABLE III-IV. Concluded

Furnishings and Equipment Group	752	1580
Accommodations for Personnel	335	335
Miscellaneous Equipment and Furnishings	296	-
Miscellaneous Equipment Without Furnishings	-	296
Furnishings	-	828
Emergency Equipment	121	121
Air-conditioning and Deicing	519	727
Auxiliary Gear Group	40	40
Soundproofing and Insulation	400	750
Rescue Hoists and Equipment	100	-
Manufacturing Variation (1 percent)	435	436
Weight Empty	43505	44017

5. Stability and Control

Analysis and design of the D270 were conducted to determine if the aircraft would be stable and have sufficient controllability in all modes of operation. These modes are:

- Helicopter
- Conversion (tilting rotors)
- Proprotor (rotors turning)
- Transition (stopping and folding rotors)
- Fixed wing (rotors folded)

Constraints placed on the design are a common control system for all modes of operation, a compatible cg range for all modes, and safe flight with the Stability and Control Augmentation System (SCAS) inoperative.

The control system is designed so that rotation of the aircraft about a particular control axis is produced by the same pilot control motions for all modes of operation. In the helicopter mode, fore and aft movement of the cyclic stick produces pitch control by elevator movement or by longitudinal cyclic pitch change in both rotors. Lateral movement of the cyclic stick produces roll control by aileron movement or by differential collective pitch between the rotors. Pedal displacements produce yaw control by rudder movement or by differential longitudinal cyclic pitch between the rotors. During

TABLE III-V. WEIGHT SUMMARY

	D270A Mission Weight		D270B Mission Weight		
	Rescue	Ferry	5-Ton	8.5 Ton	Ferry
Crew	1200	1200	720	720	720
Cargo	-	-	10687	17000	-
Fuel	20271	20271	10055	11000	13000
Unusable	304	304	201	201	201
Auxiliary	-	4079	-	-	15250
Engine Oil	120	120	120	120	120
Drive System Oil	200	200	200	200	200
Rescue Equipment	400	-	-	-	-
Auxiliary Fuel Tank Kit	-	385	-	-	1173
Useful Load	22495	26559	21983	29241	30664
Weight Empty	43505	43505	44017	44017	44017
Gross Weight	66000	70064	66000	73258	74681

TABLE III-VI. PERFORMANCE SUMMARY

Item	D270A	D270B
Design Gross Weight	66000 lb	66000 lb
Hover Ceilings at Design Gross Weight		
Standard Day, Out of Ground Effect	13900 ft	13900 ft
Standard Day, In Ground Effect	14800 ft	14800 ft
95°F Day, Out of Ground Effect	7950 ft	7950 ft
95°F Day, In Ground Effect	8900 ft	8900 ft
Rate of Climb, Design Gross Weight, Sea Level Standard Day		
Helicopter Mode	4150 ft/min at 70 kt	4150 ft/min at 70 kt
Proprotor Mode	5050 ft/min at 135 kt	5050 ft/min at 135 kt
Airplane Mode	4200 ft/min at 240 kt	4200 ft/min at 240 kt
Speed at Design Gross Weight		
Helicopter Mode, Maximum	140 kt	135 kt
Proprotor Mode, Maximum	324 kt	310 kt
Airplane Mode, Maximum	452 kt	433 kt
Airplane Mode, Maximum Cruise	415 kt/30000 ft	400 kt/20000 ft
Airplane Mode, Best Range	340 kt/30000 ft	340 kt/30000 ft
Alternate Gross Weight	82500 lb	82500 lb
Maximum Gross Weight (VTOL, In Ground Effect, Sea Level Standard Day)	93500 lb	93500 lb
Ferry Range (30 Minute Reserve)	2600 nm	2600 nm

conversion from helicopter to airplane mode, the proprotor controls are phased out as a function of pylon angle. In helicopter mode the collective pitch lever controls the pitch on both rotors. After conversion from helicopter to fixed-wing mode, the collective pitch is operated by the rpm governor.

Sizing of each of the control surfaces involved determination of conditions at which maximum performance of the control would be required. This procedure includes examination of the requirements imposed by appropriate military specifications. The following flight conditions were examined for purposes of sizing the empennage.

- Transition - 150 knots, sea level, rotors open and stopped (minimum static margin)
- Dash - 350 knots, 3000 feet altitude, rotors folded (maximum short-period frequency)
- Cruise - 400 knots, 30,000-feet altitude, rotors folded (high-altitude stability)

Stability and control analyses for the D270 were based on analytical techniques including the Bell Helicopter Company Computer Program C-81. Estimations of derivatives in the airplane mode were based on standard methods (Munk, Perkins and Hage, Seckel, DATCOM, etc.) and results from wind-tunnel tests and flight investigations. Further details and references are presented in Reference 18.

The results of the analysis produced the following criteria on which the sizing of control surfaces for the D270 was based.

- Stabilizer size adequate to produce minimum short-period frequency specified in MIL-F-008785A(USAF) (critical flight condition - transition)
- Vertical fin sized to provide a Dutch roll damping ratio of 0.08 (MIL-F-008785A(USAF)) (critical flight condition - transition)
- Elevator size - trim at $C_L = 1.8$ in ground effect (landing with folded rotors)
- Rudder size - trim with asymmetric jet thrust at minimum operating speed (130 knots)
- Flaperon size - level three-roll performance (MIL-F-008785A) at minimum operating speed (roll 30 degrees after 3.6 seconds)
- Hub restraint - desired control response and center of gravity travel in hover (MIL-H-8501A)

Since the conclusion of the Phase I activity, analytical methods associated with the folding proprotor transition from proprotor to high-speed mode were developed under separate Air Force contracts and are reported in References 13 and 15. Further experimental data were required, however, to confirm the

design criteria and approaches for all modes of flight of the folding prop-rotor aircraft (both low-speed and high-speed modes). Important areas in which additional data are required include the flight regime between hover and transition to the high-speed mode (folded blades). Helicopter and conversion mode flight, where rotor downwash affects the contribution of the tail and wing surfaces to aircraft forces and moments, represents an area where additional data are required to optimize the aircraft design for specific mission requirements.

6. Dynamics

A preliminary dynamic analysis of the D270A design was made to determine if basic dynamic and aeroelastic requirements are met. Emphasis was placed on verifying that the estimated structural stiffness and mass parameters are reasonable from a dynamics standpoint to guide the Phase II model program.

The preliminary analysis during Phase I was confined to: (1) determination of proprotor and airframe natural frequencies, (2) estimating critical dynamic loadings, and (3) investigating the aeroelastic stability characteristics. Conservative methods were employed and the results should be viewed in that light. These preliminary results indicated that only minor modifications to the estimated stiffness properties for the proprotor and wing were necessary before proceeding with model development. A more comprehensive dynamic analysis of the D270A was made under "Vibration in V/STOL Aircraft," AFFDL Contract F33615-69-C-1339. Results were reported to the Air Force in Reference 14. The analysis was of sufficient scope to indicate changes required of the parameters to achieve improved dynamic characteristics. The discussion below includes the salient results of the Phase I study and those of Reference 14.

a. Proprotor and Airframe Natural Frequencies

(1) Proprotor

The D270A proprotor natural frequencies were calculated for a range of rotor rpm representing helicopter and airplane modes (tip speeds from 822 to 700 feet per second). The frequencies of the significant natural modes are predicted to be adequately separated from excitation frequencies. The frequency location of the major blade modes of the D270A proprotor is as follows: the first inplane mode varies from 1.8 to 1.38 per rev in helicopter mode (134 rpm) and from 1.5 to 1.85 per rev in airplane mode (225 rpm). The second beam mode is above 4.0 per rev in both helicopter and airplane mode. Thus, these two modes are well located. Close proximity to 4-per-rev resonance is indicated for the second cyclic mode at high pitch in airplane mode (225 rpm) and 6-per-rev resonance for the third collective mode at high collective pitch. However, low airload excitation at these resonances is anticipated. Should the resonances be a problem, tuning weights can be used to raise or lower the frequency as required.

When gimbal freedom is locked out, the second cyclic mode is in resonance with 2 per rev at tip speeds above 750 feet per second. Consequently, when flapping is locked out, the proprotor may have to be restricted to 250 rpm maximum. The collective modes are not affected by locking out flapping.

The frequency of the blade first torsional mode was not calculated, but is estimated to be located at 4.5 per rev. This mode is rigid body blade pitching based on the control system flexibility. The second torsional frequency which involved blade torsional deflection is much higher in semirigid rotor types due to the inherent torsional stiffness of the blades.

(2, Airframe

The basic requirement for placement of wing-pylon-fuselage natural frequencies is the avoidance of resonance with the propotor excitation frequencies. In the case of the D270, these are 1, 3, and 6 per rev. Both helicopter and propotor cruise rpm ranges must be considered. Because of the large rpm range and the variation in natural frequencies as the pylons are converted, it is usually not possible to avoid all resonances. As a rule, resonance with symmetric free-flight modes having antinodes near the hub must be avoided. Transient resonance with antisymmetric modes and with symmetric modes having nodes near the hub is acceptable.

Potential resonance conditions were indicated:

- The proximity to 1 per rev of the first symmetric chord and the first asymmetric torsion modes and resonance during partial conversion of the first asymmetric chord mode, indicate that rpm may have to be scheduled during conversion to avoid prolonged operation at resonance. However, this may not be serious since recent full-scale tests indicate operation in and near 1-per-rev resonance is possible with propotors.
- The wing second beam and torsion modes are indicated to be in 3-per-rev resonance. These modes have nodal points near the hub, thus they are weakly excited by the propotors. These modes can probably be moved out of resonance by spanwise relocation of the engines.

b. Dynamic Loads

(1) Propotor

The design blade loads for the D270A were scaled from loads obtained in tilt-propotor design studies. These past studies have shown that for tilt-propotors two flight conditions impose the design loads. For oscillatory loads, the maximum level flight airspeed in helicopter mode is the most severe. These must be below the endurance limit to achieve a reasonable fatigue life for the propotor. Design limit loads are generally established by a vertical gust encounter in airplane mode. Additional analyses of propotor loads during the stop/fold process were analyzed during the work reported in Reference 14 and are summarized herein. During rotor stopping or starting at 175 knots, the limit vertical gust velocity capability of the propotor was predicted at 80 feet per second or better. The critical component was the blade fold hinge lug and the critical condition was between zero and 20 percent rotor rpm. (Preliminary calculations during Phase I based on cruder methods predicted approximately 45 feet per second capability.) During folding at 175 knots gust capability was predicted to exceed 80 feet per second. Therefore vertical gust requirements during the stop/fold process are satisfied. A small increase in fold hinge strength would result in meeting the required 50-foot-per-second gust at 230 knots. The limit maneuver load factor capability of the folding

proprotor during stop/fold at 175 knots was predicted to be approximately 1.5g and the critical component was the fold lug. When the strength of the fold hinge lug increases to that of the blade and hub, a more acceptable maneuver limit results (to approximately 2.5g).

(2) Airframe

For the airframe, a jump takeoff imposes the most severe loading on the wing. Landing loads have been investigated in earlier studies, but the rotor lift at the wingtips prevents this condition from imposing high loads. Taxi loads have not yet been thoroughly investigated. However, the excellent hover capability of the D270A eliminates the requirement for high-speed taxi over rough terrain which makes this a secondary loading consideration. The gust and maneuver capability of the D270 wing structure was analyzed during the work reported in Reference 14 for the stop/fold process at 175 knots. Gust capability exceeds 80 feet per second. In maneuvers, the wing root becomes critical during blade folding, but maneuver capability exceeds 4g. Dynamic and transient loads experienced by the airframe were analyzed for the rotor starting and stopping process. An additional factor considered was the longitudinal acceleration caused by the transient thrust generated by blade feathering. This in combination with the vibratory response characteristics suggests that a feathering time of three to five seconds is desirable for the D270. It was planned that these effects be investigated during aeroelastic model tests in Phase II.

c. Aeroleastic Stability Characteristics

(1) Proprotor

The calculated proprotor-pylon stability for the D270A is based on several modifications to the D270A design as presented in Reference 18. The pitch-flap coupling was reduced from δ_3 equal -30 to δ_3 equal -25 degrees. The wing torsional stiffness was increased in the wingtip region to achieve 125 percent of the first estimate wingtip torsional spring rate, and the wing chordwise stiffness has been decreased by 30 percent. These changes are required to achieve good dynamic characteristics and are achievable in the D270A design. In the propeller cruise mode rpm range, proprotor/pylon instability can occur in the symmetric wing chord mode. As the blades are feathered, the mode of instability changes to that of the wing beam. For rpm below 60-70 rpm, when the blade flapping restraint has been increased to prevent excessive flapping, instability can occur in a blade flapping mode. The boundary at very low rpm is felt to be conservatively estimated since a small amount of damping (1-2 percent) has a strong stabilizing influence. An elastomeric flapping restraint is employed on the D270A so there will be considerable mechanical damping of blade flapping at low rpm. The stability boundaries as calculated during the work reported in Reference 14 have a minimum of 380 knots at maximum rpm during proprotor mode operation, and increases to higher flight speeds as rpm is reduced during the rotor stopping process. Therefore, the stability margin requirements of 1.15 V_L (331 knots for the D270) as specified in Military Specification MIL-A-8870(ASG) are met by the D270.

Blade motion stability for the D270A proprotor is assured by the selection of rotor parameters that provide stable characteristics. The first inplane frequency is above operating speed which eliminates mechanical instability (ground resonance). The blade is mass balanced such that pitch-flap flutter or weaving will not occur. The blade effective center of gravity is at 24-percent chord with the effective aerodynamic center in hover being at 26.1 percent. The 3-1/2 degrees of pitch axis precone and a stiff control system prevent pitch-lag instability. Positive pitch-flap coupling of 0.466 (δ_3 equal -25 degrees) prevents flap-lag instability.

(2) Airframe

Wing divergence with the blades feathered but prior to folding, the critical condition, was checked to ensure the wing has adequate torsional stiffness to resist the rotor pitching moments. The divergence speed was shown in Reference 14, to be 530 knots equivalent airspeed. The wing forward sweep of 6 degrees was included in the calculation and the wing airload assumed to act at the wingtip. The relatively low divergence airspeed suggested that aileron reversal might be a problem. The reversal speed was estimated using the wingtip torsional spring rate rather than the 0.7 span value used for conventional aircraft. This gave a reversal speed of 320 knots for the blades-unfolded case. This low reversal speed emphasizes the requirement for including aeroelastic effects in stability and control analysis of the feather/fold sequence.

Flutter characteristics in high-speed flight with the blades folded were investigated. The effective mass balancing of the pylon prevents coupling of the fundamental wing beam and torsion modes. The flutter boundary during the blade fold process reaches a minimum speed of approximately 830 knots when the blades are folded 50 degrees. This level is based on analyses reported in Reference 14, and is well removed from required limits. The flutter boundary indicated is a weak, wing-chord-mode flutter. It results from coupling between the blade beamwise bending and the second wing chord mode. The second chord mode contains a large amount of nacelle yawing coupling the mode with blade beam bending at large fold angles. It should be noted that only a small amount of damping is indicated to be required to stabilize this flutter. The blade over mass balancing required for helicopter mode effectively prevents isolated blade flutter during folding.

F. DESIGN STUDY CONCLUSIONS

The D270A and B represent initial designs of folding proprotor aircraft which satisfied the rescue and transport mission requirements defined for the design study. As such, the design criteria used during their formulation put into perspective areas for investigation required during the Phase II and related efforts.

Risk assessments during Phase I in the areas of aerodynamics, stability and control, and dynamics were the bases of model programs initiated in Phase II. In addition, risk areas defined during component design study of folding mechanisms showed the need for large-scale folding-proprotor component tests.

Phase II force model and aeroelastic model tests were planned and, concurrently with the Phase II activity described in subsequent sections of this report, large-scale tests of a twenty-five-foot folding propotor were conducted.

CHARACTERISTICS

WEIGHTS
DESIGN GROSS WEIGHT
WEIGHT EMPTY
OIL AND TRAPPED FUEL
CREW
STOL GROSS WEIGHT

66,000 LB
43,305 LB
624 LB
1,200 LB
82,500 LB

POWER PLANT
MANUFACTURER AND MODEL
MILITARY RATED POWER
MILITARY RATED THRUST
TRANSMISSION POWER LIMIT

LYCOMING LTC4V-1 DERIVATIVE
4 X 4420 (SL STD)
4 X 1,854 (100 KTS 30000 FEET)
2 (2 X 3,380)

12,680 HP
7,416 LB
15,920 HP

EMPENNAGE

HORIZONTAL TAIL AREA
ASPECT RATIO
AIRFOIL

BL (0.0)
BL (200.0)
AFT OF HINGE

250
NACA 64-0
NACA 64-01
51.

ELEVATOR AREA TOTAL

VERTICAL TAIL AREA
ASPECT RATIO
AIRFOIL

WL (192.0) ROOT
WL (408.0) TIP
AFT OF HINGE

205
NACA 64-0
NACA 64-01
42

RUDDER AREA

ROTOR

DIAMETER
NUMBER OF BLADES / ROTOR
DISC AREA/ROTOR
BLADE AREA/ROTOR
DISC LOADING
BLADE AIRFOIL

500 FT
3
1,963.5 SQ-FT
2500 SQ-FT
16.8 LB/SQ-FT

DESIGN GROSS WEIGHT
THEORETICAL \dot{M} TO $\frac{1}{2}$
TIP
CONSTANT

64 X 18
64 X 08
47.0 IN
0.1275
25.0 DEGREES
740-822 FT/SEC
698-780 FT/SEC

\dot{C} TO TIP LINEAR
HELICOPTER MODE (283-314 RPM)
CONVERSION MODE (267-298 RPM)

WING

SPAN
AREA
WING LOADING
ASPECT RATIO
MEAN AERODYNAMIC CHORD
AIRFOIL

DESIGN GROSS WEIGHT

64.25 FT
706.0 SQ-FT
93.5 LB/SQ-FT

BL (108.6)
BL (100)
BL (385.5)

5.85
133.4 IN.
64 X 18
64 X 18

FLAP AREA/SIDE
FLAPERON AREA/SIDE

AFT OF HINGE
AFT OF HINGE

34.94 SQ-FT
23.3 SQ-FT

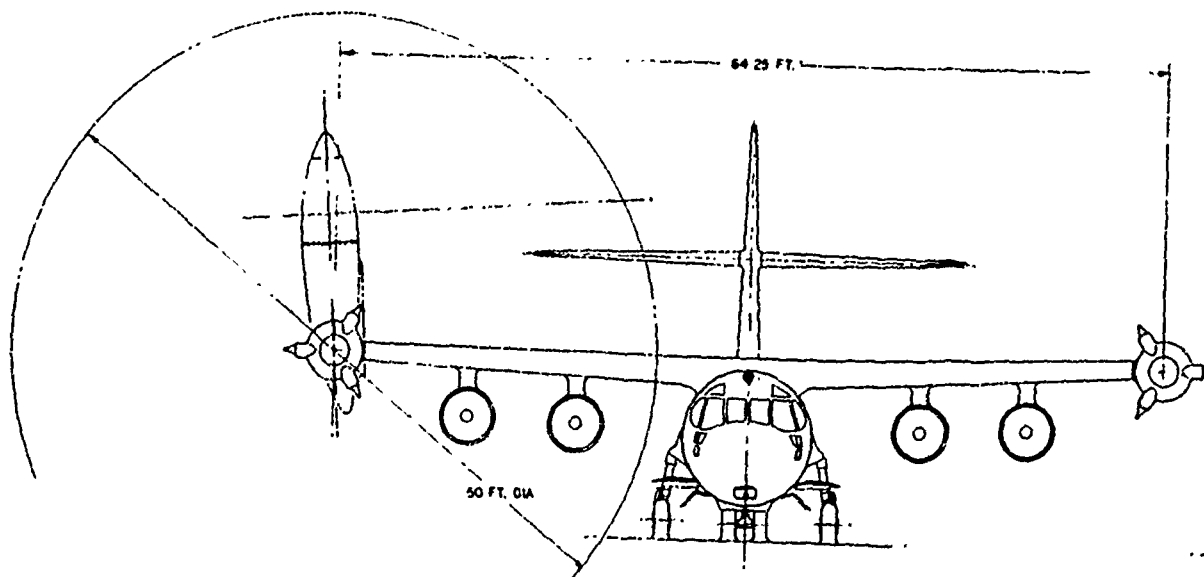


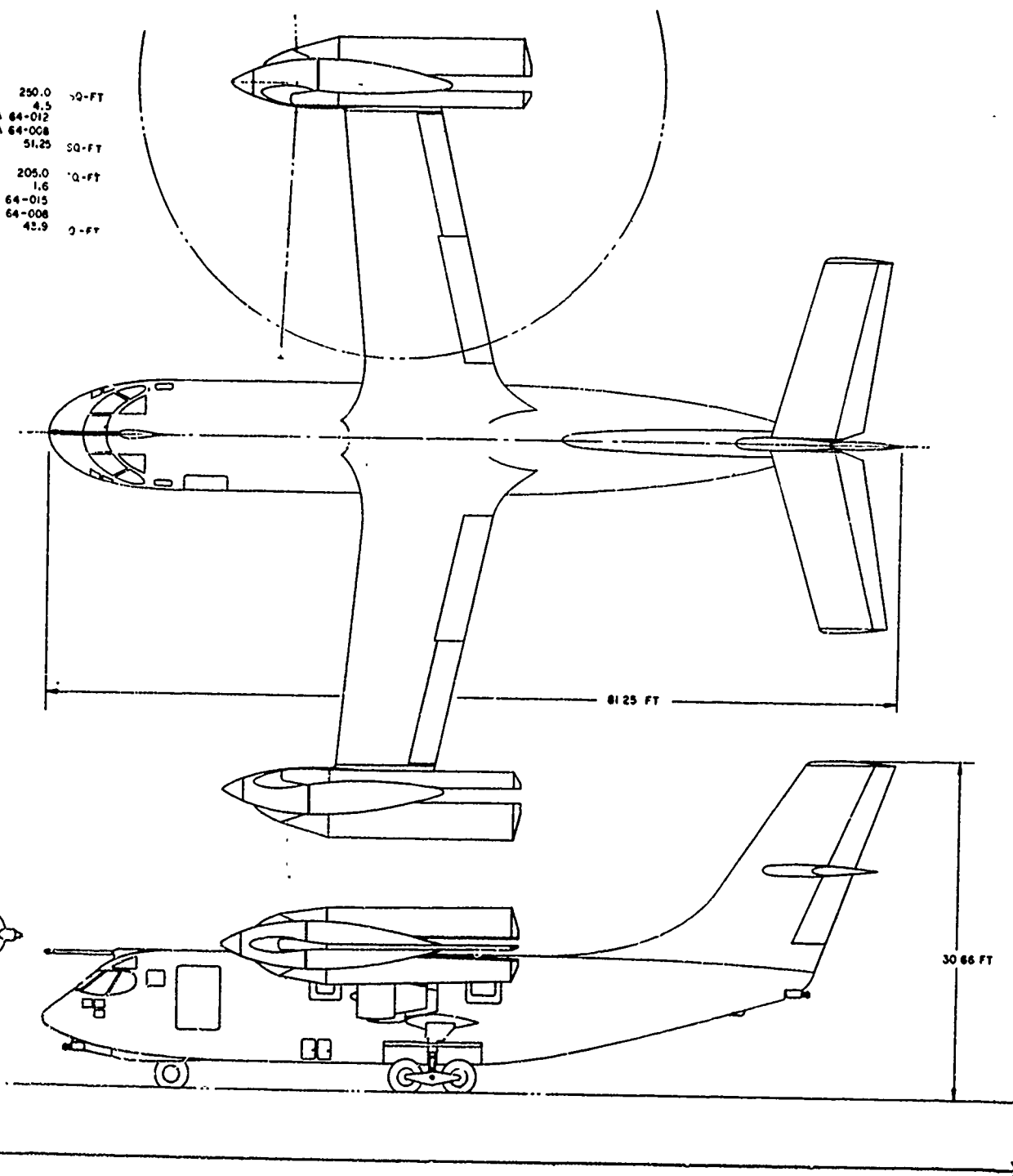
Figure III-1. D270A Thru

III - 18

D270-099-003

A

250.0
4.5
NACA 64-012
NACA 64-008
51.25
SQ-FT
205.0
1.6
NACA 64-015
NACA 64-008
42.9
Q-FT



1. D270A Three View

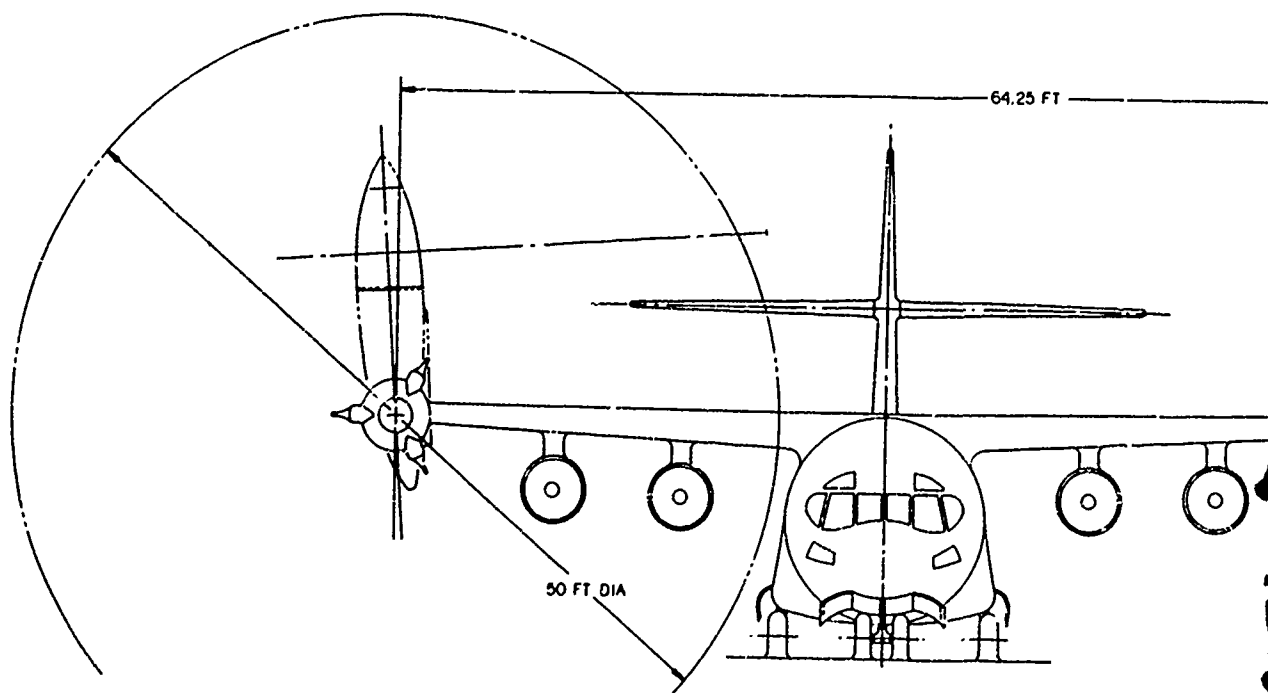
B

III-18 a

C

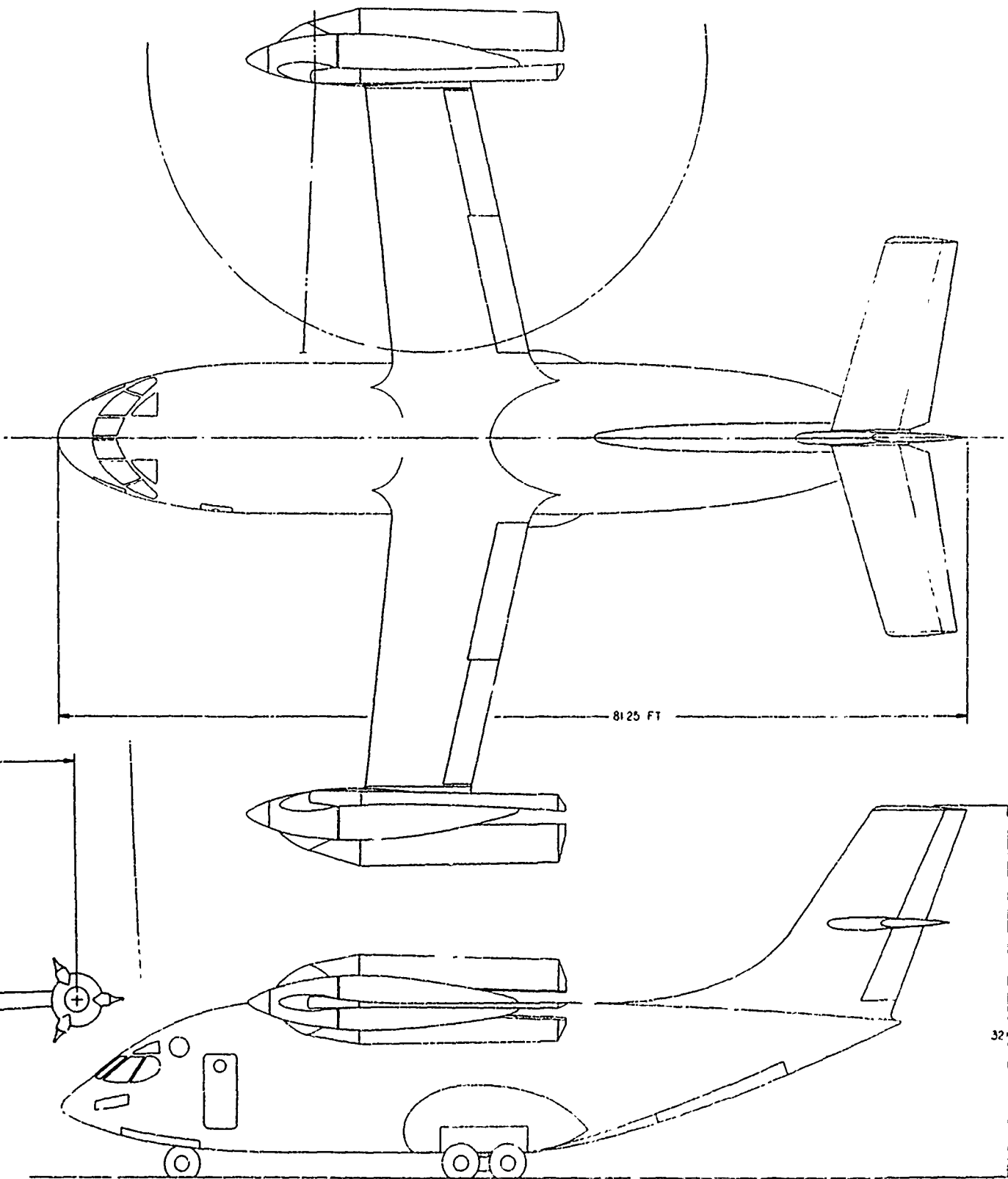
CHARACTERISTICS

WEIGHTS			
DESIGN GROSS WEIGHT	66,000		LB
WEIGHT EMPTY	44,017		LB
OIL AND TRAPPED FUEL	521		LB
CREW	720		LB
STOL GROSS WEIGHT	82,500		LB
POWER PLANT			
MANUFACTURER	LYCOMING LTC 4V-1 DERIVATIVE		
MILITARY RATED POWER	4420 X 4 (SL STD)	17,680	HP
MILITARY RATED THRUST	1854 X 4 (400 KTS 30,000 FEET)	7,416	LB
TRANSMISSION POWER LIVIT	212 X 3,980	15,920	HP
ROTOR			
DIAMETER	500		FT
NUMBER OF BLADES/ROTOR	3		
DISC AREA/ROTOR	1963.5		SQ-FT
BLADE AREA/ROTOR	2500		SQ-FT
DISC LOADING	16.8		LB/SQ-FT
BLADE AIRFOIL	DESIGN GROSS WEIGHT		
	INBOARD END	64 X 18	
	TIP	64 X 08	
BLADE CHORD	CONSTANT	40	IN
SOLIDITY	1 TO TIP LINEAR	0.128	
BLADE TWIST	HELICOPTER MODE (233-314 RPM)	25	DEGREES
TIP SPEED	CONVERSION MODE (267-298 RPM)	740-822	FT/SEC
		698-780	FT/SEC
WING			
SPAN (BETWEEN ROTOR CENTER LINES)	64.25		FT
AREA	706.0		SQ-FT
WING LOADING	93.5		LB/SQ-FT
ASPECT RATIO	5.85		
MEAN AERODYNAMIC CHORD	133.4		IN
AIRFOIL	BL (180.6)	64 X 018	
	BL (C 0)	64 X 015	
FLAP AREA/SIDE	BL (385.5)		
AILERON FLAP/SIDE	AFT OF HINGE	34.94	SQ-FT
	AFT OF HINGE	23.3	SQ-FT
EMPENNAGE			
HORIZONTAL TAIL AREA	2500		SQ-FT
ASPECT RATIO	4.5		
AIRFOIL	NACA 64-012		
	NACA 64-008		
ELEVATOR AREA TOTAL	51.25		SQ-FT
VERTICAL TAIL AREA	205.0		SQ-FT
AIRFOIL	NACA 64-015		
	NACA 64-008		
RUDDER AREA	43.9		SQ-FT
ASPECT RATIO	1.6		



D270-099-002

Figure III-2.



re III-2. D270B Three View

III-19a

B

C

IV. SEMISPAN AEROELASTIC MODEL TEST

In the previous section of this report, the Phase I design study effort was summarized. That effort formed a basis for the model program conducted during the subsequent Phase II effort. The Phase II program involved three different models: a semispan aeroelastic model which is reported in this section, an aerodynamic model of the folding-prop rotor cruise configuration reported in Section V, and a powered force model reported in Section VI.

A. OBJECTIVES

The purpose of the tests of the semispan powered aeroelastic folding prop-rotor model is the investigation and verification of the planned tilt/stop/fold control procedures and their effects on rotor flapping, pylon accelerations, and rotor and wing loads.

The objectives of the test were to:

1. Obtain time history records of control settings, flapping, blade and wing loads during stop/fold process tested under prop rotor windmilling conditions.
2. Obtain wind-tunnel balance forces and moments, drive system torque, control settings, flapping and blade and wing loads in the transition flight regime at incremental mast tilt angles with rotor power.

B. MODEL DESCRIPTION

The model tested, Figure IV-1, was a modification of the semispan portion of Bell's existing scaled aeroelastic model of the Bell Model 300 tilt-rotor aircraft design described in Reference 1. While not an exact scale of the D270 aircraft, several basic design criteria such as the placement of wing and rotor structural natural frequencies in terms of normal rotor rpm are similar and valid test of several dynamic criteria were possible. The model more closely scales the structural parameters of the 25-foot-diameter folding prop-rotor and the D272 folding prop-rotor research aircraft configuration described in Reference 16. Results, however, are applicable to the D270 with appropriate allowances for differences in scale factors. The model was designed to operate in either unpowered or powered modes as required for the test. The unpowered version was designated the C300-A1B, and with the addition of power and cyclic pitch, the C300-A1C. A summary of the scale factors is presented in Table IV-I and primary model dimensional data are presented in Table IV-II. Descriptions of the model components and systems are presented in the following paragraphs.

1. Wing

The wing is composed of a spar which provides the scale bending and torsional stiffness characteristics, and metal covered, nonstructural, segmented fairings which provide the aerodynamic contour. Fuel weight was not simulated during this test.

TABLE IV-I. SUMMARY OF MODEL C300-A1C SCALE FACTORS

Parameters	Scale Factor (Model/Full Scale)
Length	0.2
Density	1.0
Time	0.447
Mass	0.008
Mach Number Ratio	$0.447T^{1/2}$ *
Froude Number Ratio	1.0
Lock Number Ratio	1.0
Reynolds Number Ratio	0.08494
Angular Velocity (rpm)	2.24
Linear Velocity	0.447
Angular Acceleration	5.0
Linear Acceleration	1.0
Force	0
Moment	0.008
Stiffness	0.0016
Stress	0.00032
Power	0.2
Mass Moment of Inertia	0.00358
Linear Spring Rate	0.00032
	0.04
* $T^{1/2}$ = Model temperature/full-scale temperature	

TABLE IV-II. MODEL C300-A1C PRIMARY DIMENSIONAL DATA

Item	Units	Data
Proprotor		
Number of blades per rotor		3
Diameter	in.	60
Blade chord	in.	2.8
Hub spring rate	ft-lb/deg	0.36
Hub precone angle	deg	2.5
Rotor speeds		
100 percent rpm	rpm	1265
81 percent rpm	rpm	1025
Three blades - weight	lb	3.18
Hub (gimbal, yoke, straps) weight	lb	0.5104
Folding gears - weight	lb	0.314
Flapping moment of inertia per blade	slug-in ²	0.416
Pylon		
Conversion axis to rotor	in.	12.7
Shaft axis intersection	in.	11.2
Weight (hub included)	lb	7.62
Mass moment of inertia about center of gravity (hub included)	slug-in ²	0.523
Center of gravity location from conversion axis	in.	5.375
Wing		
Semispan	in.	38.6
Mean aerodynamic chord	in.	12.4
Dihedral	deg	2.1
Flap-chord ratio	-	0.25
Power		
Installed (at 1265 rotor rpm)	hp	3.76
Gear ratio (motor to rotor)	-	17.6:1

The wing is cantilevered at Buttline 5.6 (28 full-scale) and swept forward six and one-half degrees. The basic spar weighs 0.04 pounds per inch and with aerodynamic segments, 0.127 pounds.

An engine weight of 6.2 pounds is simulated and attached on the wing at Buttline 12.4 through the test. Manually adjustable flaps are provided.

Beam and chord linear spring rates determined at the wingtip and torsion spring rate of wing/pylon system about the pylon center of gravity were calibrated and found to be 64.5 pounds per inch, 182 pounds per inch, and 19,800 inch-pounds per radian, respectively. Shake testing of the wing gives natural frequencies at various modes. The results are given in Table IV-III.

2. Pylon

The mass and inertia of the pylon and the interconnect shaft torque characteristics are scaled. The model pylon mass was weighed and the pylon mass moment-of-inertia about its center of gravity was measured. The results are also tabulated in Table IV-III.

3. Proprotors

The construction technique used for the blades is that of duplicating the full-scale cross section and using the appropriate material modulus to obtain the scale stiffness. The blades are scaled in beam, chord, and torsion.

The blades are attached to the hub yoke via fold hinge bearings, pitch change bearings and tension-torsion straps. The hub yoke represents yoke inplane and out-of-plane stiffness properly. The yoke is, in turn, attached on the propotor gimbal which is then mounted on the rotor mast.

The blade pitch-change axis is preconed $2\frac{1}{2}$ degrees. Blade twist and collective pitch are accounted for in the blade natural frequency calculations. Shake testing of the propotor had been conducted prior to the wind-tunnel test. Major propotor blade frequencies are thus obtained and given in Table IV-III.

Remote control of the blade folding mechanism is used. The folding rate is adjustable. Intermediate fold angles are calibrated and marked on a meter.

Fore and aft cyclic to control the blade flapping during powered tests in the pylon-tilt mode is available on the model. Remote control of the propotor collective pitch and of the fore and aft cyclic is provided. Variable collective rate is possible and six collective rates, ranging from $\Delta t = 0.87$ seconds to $\Delta t = 1.94$ seconds model time, were available for changing pitch sixty degrees. Very low collective rates could be achieved by using manual control. Variable (two-step) collective rates were also used during the test to study the variation of the model response during rotor stopping.

Before changing collective pitch to feather the blades, blade flapping freedom was locked out by remote control to eliminate blade rigid-body

TABLE IV-III. MODEL C300-A1C SHAKE TEST RESULTS

Wing/Pylon Frequencies (No Fuel, Engine On)				
Structural Mode	Helicopter Mode		Airplane Mode	
	Rotor On	Rotor Off	Rotor On	Rotor Off
1st Wing Beam	7.5 cps	8.5 cps	7.3 cps	8.77 cps
2nd Wing Beam	27.0	36.3	44.3	50.0
1st Wing Chord	10.6	13.5	12.1	14.2
1st Wing Torsion	28.2	30.7	25.0	31.2
Pylon Yaw	27.0	36.3	47.0	58.8
Node Point from Conversion Axis at Torsion Mode	8.0 in	-	7.5 in	5.375 in
Proprotor Frequencies (Hub-Motion Allowed)				
Mode	Collective Pitch at Blade Tip			
	-5°	+35°	+45°	
1st Collective	20.9 cps	26.4 cps	28.5 cps	
2nd Collective	79.0	70.3	64.5	
1st Cyclic	34.4	22.2	21.8	
2nd Cyclic	42.1	61.0	63.5	

flapping instability. After the feathering procedure is completed, the mast rotation is locked out by remote control prior to folding the blades.

When the proprotor is operated in the airplane mode, the center line of the mast is aligned such that it has three degrees incidence less than that of the wing chordline. The mast (pylon), however, can be converted independently to any conversion angle through a manually adjusted conversion link.

At different conversion angles, the proprotor can be operated either wind-milling or powered by a Task Corporation Model Motor 4074 with an output of 3.76 horsepower at 1265 rotor rpm.

4. Model Instrumentation

The items instrumented, their location on the model, and monitoring or recording method are summarized in Table IV-IV. Motion picture and TV recording was provided.

5. Model Control Panel

Figure IV-2 shows a view of the model control consoles. The left console contains a sequence switch panel for activating various portions of the stop-fold process and meters for monitoring model component loads and rotor rpm variations. The right panel contains a digital rpm readout for setting rpm, two up-down counters for setting collective pitch limits electrically, meters for monitoring model control positions, flapping and fold angles, and rotor torque. Controls are provided for manual adjustment of collective pitch servo position, for trimming cyclic pitch, and for controlling motor power supply frequency. The test was arranged to minimize the number of control and monitoring requirements.

C. CONFIGURATIONS TESTED

The program was planned based on using the 7- by 10-foot test section of Vought Aeronautics Low-Speed Wind Tunnel. A period of ten days of single-shift testing was planned and used. Maximum tunnel speed of 350 feet per second was adequate for tests representing speeds up to $1.15 V_L$ (flutter-free speed requirement) in the stop/fold mode of operation. Wind-tunnel balance data were required. Therefore, the semispan model was mounted with the wing panel vertical directly onto the balance turn table.

The model configuration could be changed between runs with regard to wing flap settings (0, 10, and 30 degrees), and "conversion" angle (pylon tilt angle from the helicopter attitude - 0, 15, 30, 60, and 90 degrees). In addition, remotely controlled geometry variations of the model were possible during a run with regard to collective and cyclic pitch, rotor flapping restraint engagement, mast rotational lock out, and blade folding.

TABLE IV-IV. MODEL C300-A1C INSTRUMENTATION

OSCILLOGRAPH 1		OSCILLOGRAPH 2	
Channel	Parameter	Channel	Parameter
1*	Rotor Torque		
2*	Flapping Amplitude	2*	Wing Beam 27% Span
3*	Cyclic Position	3	Wing Beam 52% Span
4*	Fold Angle	4	Wing Chord 27% Span
5*	Collective Position	5	Wing Chord 52% Span
6*	Blade Beam 35% Radius	6	Wing Torsion 27% Span
		7	Wing Torsion 52% Span
8	Blade Beam 50% Radius		
9	Blade Beam 75% Radius	9	Vertical Forward-Pylon Acceleration
10*	Blade Chord 35% Radius	10	Horizontal Aft-Pylon Acceleration
11	Blade Chord 50% Radius	11	Conversion Axis Vertical Acceleration
12	Blade Chord 75% Radius	12*	Horizontal Forward-Pylon Acceleration
13*	Fold Link Load	13	Axial Pylon Acceleration
14*	Pitch Link Load		
15	Blade Torsion 35%		
16*	Rotor rpm	16*	Rotor rpm
*Also monitored on meters			

The objectives of the test were approached based on dividing the test period into five phases of investigation. These phases and the reasons for them are discussed below.

1. Check Dynamic Stability

Proprotor stability boundaries at typical rotor operating speeds are predicted to be well above speeds where the rotor would be stopped and folded. During the stop/fold process, however, it is necessary to lock out rotor flapping. For the blade stiffness and weight characteristics used with the gimbal-type proprotor, this lockout process causes the inertia of the rotor disc to be effective in lowering the wing natural frequencies and consequently reduces slightly the proprotor stability boundaries. It was necessary to confirm that, after the modification of the aeroelastic model to the folding proprotor configuration, the changes in model weight and stiffness and mass distributions did not lead to unexpected drops in stability boundaries. To check this, the rotor was to be operated first with flapping free then locked out at typical proprotor rpm and excited with wing disturbances to check frequency and damping. This was to be done over the speed range of interest during the test using appropriate flap settings to generate realistic wing-rotor interference flow conditions. At low rotor rpm, rotor flapping would be locked out and proprotor stability boundaries increase rapidly. Another area of interest with regard to dynamic stability characteristics is the blade fold process. Here, the blades act as relatively flexible swept wings added to the wing tip and verification of the dynamic frequency and damping characteristics in response to controlled excitations was desired up to the flutter-free speed requirement of $1.15 V_L$ for the stop/fold mode. These dynamic stability checks were required prior to conducting any other phases of the test to ensure a dynamically stable model for the subsequent investigations.

2. Determine Optimum Stop/Start Rates

Prior model tests as reported in References 12 and 14, indicated that too fast a rate of starting or stopping the rotor will cause excessive rotor-induced axial loads on the wing structure and on the aircraft as a whole while too slow a rate will allow wing beam, chord, and torsional modes to be excited by wing/rotor aerodynamic excitation when the blade passage frequency coincides with the natural frequencies of the structural modes. To verify theoretical predictions of these effects as a function of feathering rates, the capability was required to allow the collective pitch rate to be varied. It was required that the collective pitch settings at a given wind speed be manually set to give the desired high rpm and low (or zero) rpm. These positions were to be "remembered" by the electrical control system and while depressing a switch, the collective pitch would change at the preset rate to the preset position. Desired times for stopping or starting the rotor between zero and 1250 rpm were from 0.9 to 2 seconds in model scale. (This corresponds to 2 to 4.5 seconds full-scale between 0 and 458 rpm for a 25-foot-diameter rotor.) This range was predicted to represent an optimum for the full-scale 25-foot rotor from a loads standpoint. Typical full-scale flight speed for stop-starts is 150 to 175 knots. Tunnel-balance data were of no interest for these "transient" investigations.

3. Define Stop/Start Envelope

Prior work, Reference 14, had shown that blade one-per-rev loads with flapping locked out could exceed the values for infinite blade life at rotor angle-of-attack values representative of maneuver conditions. In addition, there were indications that during the rotor starting or stopping process, a few cycles of blade transient loads might be generated which exceeded the steady-state oscillatory loads for the same angle-of-attack condition. It was required that data be obtained for the scaled rotor which showed, for the condition of flapping locked out, what the angle-of-attack envelope was in terms of scaled infinite-life loads at a typical stop/fold flight speed. For comparison, blade loads with flapping unlocked were also required. Under this condition, the blade loads would be reduced, but steady-state flapping would no longer be zero. Therefore, steady-state flapping with the rotor free was also required over the same angle-of-attack range. These tests were expected to represent the most severe condition for the entire stop/fold process. Wind-tunnel balance data acquisition was planned for this phase of the investigation.

4. Investigate Folding Sequence

With the rotor stopped, and at various fold angles between fully opened and fully folded, the variation of blade and wing loads at various speeds and angles of attack was required for correlation with theory. Other component loads of interest were the equivalent control loads about the pitch change spindle axis and loads on the scaled fold link. While the oscillatory loads were not expected to be critical, static loads would be important for large-scale component detail design and overall loads on the wing would be useful for assessing static trim moment variations during folding. Balance data acquisition was planned as a basis for comparison with wing strain data. Once the "folding" portion of the stop-fold operation was investigated, it was planned to execute a continuous sequence from proprotor operation through the stop/fold/unfold/start process back to proprotor operation. The purpose was to verify the control procedures used for manually commanding the required steps in the overall sequence. (In the aircraft application, this process must be semi-automatic, that is, allowed to continue automatically as long as the pilot continues to command the conversion process by pushing a beep-switch.) The tests which were planned for the 25-foot folding proprotor were similar to that of the model in that each step was to be individually controlled; therefore, procedures during a continuous sequence required verification. Balance data were not planned for the continuous sequences.

5. Investigate Pylon Tilt Mode Dynamics

The variation of rotor and wing loads, flapping, control settings, rotor torque and wind-tunnel balance data at incremental pylon tilt angles was required. These data would be used for comparisons with theoretical predictions and with full-scale data obtained during powered tests of the 25-foot-proprotor as reported in Reference 8. The speed range of interest was to be typical of the pylon tilt range. This phase of the investigation was planned last since it required the activation of additional elements of model complexity, namely, shaft power and rotor cyclic pitch.

D. TEST RESULTS AND ANALYSIS

The test (LSWT Test No. 367) was conducted for the five phases planned after initial rotor track, balance and system functional checks were completed. Data were obtained on oscillograph and the wind-tunnel balance as indicated for each run in the test run schedule presented in Table IV-V. For this test a run generally involved a wind-on period rather than a single parameter sweep. The runs in which various portions of the investigation may be found are as follows:

Track, Balance, and System Functional Check	-	Runs 1 through 6
Dynamic Stability Checks	-	Runs 7, 8, 34
Optimum Stop/Start Rates	-	Runs 7, 8, 27
Stop/Start Envelopes	-	Runs 9, 10, 11, 19, 20, 21, 23, 26
Folding Sequence		
- Folding Only	-	Runs 12, 13, 14, 22, 24, 25, 34
- Continuous Stop-Fold-Unfold-Start	-	Runs 15, 16, 17, 18, 31, 32, 33
Powered/Tilt Mode Dynamics	-	Runs 28, 29, 30, 35, 36, 37, 38, 39

1. Dynamic Test Data

Dynamic data from the test includes dynamic stability characteristics in the conversion airspeed range, dynamic response during proprotor stopping and starting, as a function of feathering rate and angle of attack, and wing and proprotor loads during blade folding. Data on blade loads in the powered pylon-tilt range were also obtained. All model dynamic data were scaled up to full-scale values based on factors in Table IV-I. The computer programs developed under the AFFDL "Vibration in V/STOL Aircraft" program (Contract F33615-69-C-1339), and reported in Reference 14, were used to predict the model dynamic stability, response, and load characteristics for comparison with the test data.

ACTUAL QUN SCHEDULE - FOLDING PROPELLEDE SEMISPAN AIRBALLISTIC POWERED MODEL - 17N 20K 967 (150)

[illegible]

TABLE IV-V. Continued

Run No.	Run No.	FLAP Angle	Roll Angle	Pitch Angle	Yaw Speed	Roll Rate	Pitch Rate	Yaw Rate	Roll Acc	Pitch Acc	Yaw Acc	SEQUENCE COMMANDS												RELATIVE TIME	FILM	COMMENTS	TIME
												1	2	3	4	5	6	7	8	9	10	11	12				
0	10	10	90	30	192	MANUAL	1025	0	0	0	0	+	+	+	+	+	+	+	+	+	+	+	+			DRIVING SYSTEM CHECK - WAS STARTED WITH PLACES	4/6/71 8:00
						MANUAL	1025	0	0	0	0	+	+	+	+	+	+	+	+	+	+	+	+			OPTIONAL OPTICAL CHECK BY RING AT EQUIPMENT TO ITS PARTIAL TABLE	
						MANUAL	1025	0	0	0	0	+	+	+	+	+	+	+	+	+	+	+	+			DRIVING SYSTEM CHECK - WAS STARTED WITH PLACES	
						MANUAL	1025	0	0	0	0	+	+	+	+	+	+	+	+	+	+	+	+			ALPHA SHIP - BARRAGE REPTURE (UNLOCKED) (FLAPPING UNLOCKED)	4/6/71 4:05
						MANUAL	1025	0	0	0	0	+	+	+	+	+	+	+	+	+	+	+	+			ALPHA SHIP - BARRAGE REPTURE (UNLOCKED) (FLAPPING UNLOCKED)	4/6/71 10:25
						MANUAL	1025	0	0	0	0	+	+	+	+	+	+	+	+	+	+	+	+			ALPHA SHIP - BARRAGE REPTURE (UNLOCKED) (FLAPPING UNLOCKED)	4/6/71 11:25
						MANUAL	1025	0	0	0	0	+	+	+	+	+	+	+	+	+	+	+	+			ALPHA SHIP - BARRAGE REPTURE (UNLOCKED) (FLAPPING UNLOCKED)	4/6/71 11:25
10	10	10	90	30	192	MANUAL	1025	0	0	0	0	+	+	+	+	+	+	+	+	+	+	+	+			ALPHA SHIP - BARRAGE REPTURE (UNLOCKED) (FLAPPING UNLOCKED)	4/6/71 11:25
11	10	10	90	30	192	MANUAL	1025	0	0	0	0	+	+	+	+	+	+	+	+	+	+	+	+			ALPHA SHIP - BARRAGE REPTURE (UNLOCKED) (FLAPPING UNLOCKED)	4/6/71 11:25
12	10	10	90	30	192	MANUAL	1025	0	0	0	0	+	+	+	+	+	+	+	+	+	+	+	+			ALPHA SHIP - BARRAGE REPTURE (UNLOCKED) (FLAPPING UNLOCKED)	4/6/71 11:25


JW PAGE 5 OF 14

70 PAGE 6 OF 14

Reproduced from
best available copy.

TABLE IV-V. Continued

[illegible][illegible]

 PAGE 9 OF 14

[illegible][illegible]

TABLE IV-V. Continued

[illegible][illegible]

TABLE IV-V. Concluded

[illegible][illegible]

a. Dynamic Stability

Dynamic stability was investigated for two areas of FPR operation. They were (1) proprotor operation after transition and before feathering and stopping the rotor, and (2) operation with the rotors stopped and feathered and the blades folded at various angles from full open to trailed aft along the wing tip pylons.

Proprotor dynamic stability characteristics were determined only in the range of airspeed corresponding to that for the feather-fold sequence. The principal measurements of interest were wing frequencies and damping for comparison with predicted values and verification that the model would be free of proprotor instabilities before initiating stop-start tests. No attempt was made to determine the high speed stability boundaries since this has been extensively explored in previous investigations. With the rotors stopped and folded at various angles, dynamic stability measurements were made at speeds up to $1.46 V_H$ for the conversion mode.

For reference, Figure IV-3 shows the predicted proprotor dynamic stability boundaries with flapping free and flapping locked. With flapping free, and for rotor speeds between 250 and 600 rpm, the wing beam mode is the mode of instability encountered at the stability boundary which is well beyond the speed for blade folding. Below 240 rpm, a low frequency flapping instability is coupled wing chord bending-wing beam bending, at the wing chord natural frequency. The neutral stability airspeed is above 500 knots for rotor speeds below 350 rpm; again, a margin well in excess of that required for conversion to the stop/fold configuration.

Figures IV-4 through IV-7 compare the measured frequency and damping of the wing beam and wing chord modes with the predicted frequency and damping with flapping free and flapping locked. Although the test data are limited, it is in agreement with the predicted frequency and damping.

For the second area of operation investigated, frequency and damping were measured versus velocity and with the blades folded to various angles. Figure IV-8 shows the measured frequency and damping variation with velocity at a 60-degree fold angle. The frequency trends do not show significant variation with airspeed. The peak of the wing beam damping occurs at an airspeed of approximately 260 knots.

The measured frequency and damping variation with fold angle at 175, 225, and 291 knots are shown in Figures IV-9, IV-10, and IV-11, respectively. The correlation with regard to fold angle at 175 and 225 knots, shown in Figures IV-9 and IV-10, indicates a good trend for the analysis.

b. Determination of Optimum Stop/Start Rate

For the optimum stop/start rate tests, the basic configuration of the model was unpowered, and the rotor was set at propeller tilt angle. Rotor flapping degree-of-freedom was locked out, and cyclic pitch input was zero. The influence of blade feathering rate was evaluated by testing six collective

rates, ranging from that for a $\Delta t = 0.87$ seconds to $\Delta t = 1.92$ seconds model time. These are elapsed times for moving collective pitch through a range which would bring rotor rpm from full rpm to near zero or vice versa. Corresponding full-scale times are $\Delta t = 1.95$ to $\Delta t = 4.34$ seconds respectively.

The vibration levels at the pylon conversion axis were recorded continuously during stopping and starting. Wing chord accelerations were measured by the axial accelerometer, and wing beam and torsional accelerations, by the conversion axis vertical accelerometer (Table IV-IV). For each vibration of interest (i.e., wing beam, wing chord, and wing torsion), the time history records of the particular accelerometer were searched to find the time at which the frequency of the accelerometer output equaled the natural frequency of the mode of vibration. At that time, the amplitude of the vibration was read and is plotted as a function of $1/\Delta t$ (full-scale) in Figures IV-12 and IV-13. The levels shown are not necessarily the maximum that occurred during stopping and starting, but this is probably due to the effects associated with a rate of change of frequency. The steady-state pylon vibrations (i.e., at a feathering rate = 0) were reduced from data taken during run 9, during which rotor rpm was set at each wing natural frequency.

Wing chordwise moments were also recorded, and the reduced data are shown in Figures IV-14 and IV-15. These include both (1) oscillatory loads at the times for load frequencies equal to natural frequencies and (2) the peak transient loads during the stopping or starting cycle.

Correlations between theory and measured response at wing beam, chord, and torsional natural frequencies at different feather/unfeather rates are shown in Figures IV-12 and IV-13, and correlations between theory and measured wing chord bending response during stopping are shown in Figure IV-14. In general, the correlation is fairly good.

From those data, a predicted optimum feathering rate was selected. This was for minimum wing chordwise oscillatory moments and minimum pylon axial vibration at wing beam natural frequency. The corresponding times to stop/start the rotor are 1.1 seconds for the model and 2.46 seconds for the full-scale D272 aircraft.

Sensitivity of the wing/pylon dynamic response to mast angle-of-attack was evaluated at the optimum feathering rate (Figure IV-16). Both theory and measured data show that the pylon vibration at wing chord frequency does not vary with mast angle of attack. Slight variation is seen at wing beam frequency. Significant effect of mast angle of attack on pylon vibration at wing torsional natural frequency is evident. This suggests that, operationally, the feather/stop sequence should be made with a mast angle of attack near zero degrees, or that investigations should be conducted to increase the angle-of-attack range.

The optimum stop/start rate and the effect of mast angle of attack on wing/pylon vibration was determined for linear stop/start rates. Studies of two-step collective rates on the model response during rotor stopping were made. The time to feather with the two step rates was the same as that with the one step rate. Results are shown in Figure IV-17. From this test, a linear feathering rate gives a slightly lower model response.

c. Definition of Stop/Start Envelope

The basic configuration of the model for the conversion envelope tests was the same as the one used to determine the optimum stop/start rate.

The impact of the stop/start rate on blade oscillatory loads was first studied. Figure IV-18 shows the effect of feathering/unfeathering on blade beam oscillatory moments. Figure IV-19 shows the effect on blade chord oscillatory moments. Although the loads are high (probably due to an angle of attack of the model), these figures demonstrate that blade oscillatory loads do not vary with the collective rates, and that less oscillatory loads are observed during starting than stopping.

Figure IV-20 shows blade beam oscillatory loads in the conversion range. For reference, the calculated infinite-life stress limit of the blades is $\pm 20,000$ in-lb, full scale. Good correlation of blade loads is shown.

The influence of mast angle-of-attack on transient blade beam bending is also shown in Figure IV-21. As demonstrated by Figure IV-18, higher blade loads are observed during the stopping than starting.

d. Folding Sequence Investigation

For the folding sequence investigation, the model was unpowered with the rotor mast initially set at propeller tilt angle relative to the free stream velocity in the tunnel. Proprotor gimbal degree-of-freedom was locked out. The mast was locked to prevent the rotor from rotating and cyclic pitch was set at zero. Blade fold angle was remotely controlled.

(1) Blade and Fold-Link Loads During Folding

The steady blade beam and chord moments during folding were recorded during the test. Figure IV-22 shows the steady blade beam loads versus fold angles; Figure IV-23 shows the loads versus mast angle of attack. The correlation of the blade beam bending is excellent as seen in both figures.

The measured steady chord bending moments are not shown because they are believed to be in error. At 90 degrees fold angle, the calculated chord loads should be primarily due to gravitational force, but the measured data showed much higher values--on the order of 10 times the calculated values. The errors in the measurement of steady blade chord loads may be due to temperature zero shifts of the output signal from the strain gages used on a fiberglass blade. As a check on the assumption that the measured blade chord loads were in error, the calculated steady blade chord bending moment just out-board of the blade fold hinge was used to calculate the fold link loads and the results are then compared with measured data in Figure IV-24. The measured loads are less than those calculated in this manner, thus tending to indicate that the calculated blade chord loads shown in Figures IV-22 and IV-23 are more nearly correct than the measured loads.

(2) Wing Beam Steady Bending During Folding

Wing steady bending moments versus mast angle of attack at 0-, 15-, 30-, 60-, 75-, and 90-degrees blade fold angle were measured. Figure IV-25 shows the data at 0- and 90-degrees fold angle. Those loads measured at other fold angles fall in between and follow the trends shown in Reference 14. Correlation for the wing beam steady moment at these two extreme fold angles is shown in Figure IV-25, and the calculated data are in good agreement with the measured data.

(3) Steady Spindle Torque During Folding

The measured spindle torque is shown in Figure IV-26, which demonstrates how the spindle torque varies with angle of attack and fold angle at 175 knots simulated airspeed. A peak at a fold angle of about 15 degrees is evident.

Only positive angle-of-attack data are shown in Figure IV-26. The reason is that the test model was set up such that the pitch link was against the pitch horn stops when the mast was at a negative angle of attack. This resulted in a transmittal of pitch link forces to the mast, thus by-passing the pitch links and resulting in zero reading in steady pitch link loads.

Steady spindle torque at 30-degree blade fold angle is calculated and shown in Figure IV-26 for comparison.

(4) Continuous Stop/Fold Sequences

Continuous stop/fold/unfold/start sequences were made at two angles-of-attack at a 175 knot full scale speed, continuously from powered proprotor flight, through the stop/fold process, and return to powered proprotor operation at 90 percent torque. The operation was accomplished as quickly as the model operator could determine that a step was completed and operate a switch to command the subsequent step. Movies and continuous oscillograph records are available of the process. Data are compatible with quasistatic data described above. Oscillograph records of a continuous stop/fold sequence taken during Run 18 (6 degrees wing angle of attack at 175 knots full-scale speed) are shown in Figure IV-27.

e. Pylon-Tilt Mode Dynamics

For the pylon-tilt mode dynamics investigation, the model was powered and provided with cyclic control.

(1) Pylon Link Loads at 60-Degree Conversion Angle

The model was tested at a 60-degree conversion angle (rotor 30 degrees from propeller mode) at 106 ft/sec tunnel speed (140 knots full scale) and 1265 model rpm (565 rpm full scale). Figure IV-28 shows the conversion link loads for different percentages of power (100 percent corresponding to 187 lb-in torque model scale). For the same model configuration, steady conversion link loads were recorded at 121 ft/sec tunnel speed (160 kt full scale) while the rotor was windmilling.

(2) Blade Beam Oscillatory Loads at 60-Degree Conversion Angle

The variation of blade beam oscillatory loads versus power is seen in Figure IV-29. Measured and predicted results from Model 300 tilt proprotor tests at NASA-Ames, November 1970, are included in Figure IV-29 for comparison.

2. Wind-Tunnel Balance Test Data

Tabulated data acquired on the Vought Aeronautics tunnel balance through Run 39 are presented in the test document prepared by the wind-tunnel staff, Reference 20. In addition reduced data plots are presented in terms of full scale lift, drag, and pitching moment divided by dynamic pressure for Runs 5, 7 through 14, and 20 through 25.

3. Model Incident

a. Related Runs Prior to Incident

During the fifth phase of the investigation, powered/pylon tilt-mode dynamics, the model was severely damaged after entering a rotor overspeed condition. Data had been obtained during earlier runs at a conversion angle of 90 degrees (airplane attitude) at a full-scale wind speed of 175 knots for various prop-rotor thrusting conditions representing torque levels, in terms of percent design value of 0, 30, 60, 90, and windmilling (drive system tare torque). Data were also obtained at a conversion angle of 60 degrees at 80 knots (full-scale), and 140 knots in increments of torque up to 100 percent. At the 160-knot condition, the zero torque data had been recorded and adjustments were being made in collective pitch to reach the next torque level when the incident took place.

b. Procedure for the Fifth-Phase Tests

The test procedure called for setting collective pitch to obtain predetermined levels of rotor torque while rpm was maintained by vernier adjustments of motor power supply frequency. Torque was the primary parameter being monitored by direct readout meters to set pitch remotely by a knob-controlled position servo during this phase of the test. Since this parameter was critical, loss of this signal was established before the test as a condition for shutting down the test run.

c. Events Leading to the Incident

As collective pitch was being changed to reach the next torque level, no response in meter indication was noted, the meter indicating a constant level at around 50-percent torque. Collective was manipulated over a small range in an unsuccessful attempt to generate a response in indicated torque level. The drive motor temperature monitor then indicated an over temperature condition and drive power was immediately turned off allowing the drive motor to coast. The rotor then speeded up to approximately a 25-percent overspeed condition indicating the motors had been applying a braking rather than a driving torque. The collective pitch was then commanded, in approximately

0.8 seconds, to a pitch for still higher rpm and the model was severely damaged at approximately 240 percent of maximum nominal operating speed. During the post-test inspection, no malfunction of the servo control system or rotor mechanical components was detected which could have caused the overspeed.

d. Reflection

Ordinarily in any powered rotor wind-tunnel or whirl testing, the collective pitch is operated by slow acting control actuators commanded by beep switches. These are more forgiving in that inadvertent control can be detected and corrected before conditions change much. The "hot", high authority, servo system used during this test was necessary for the rotor stop/start tests in automatic mode. The manual adjustment of collective to establish precise rpm limits for the stop/start tests was done in a windmilling condition where motor torque constraints were not present. While operation to and from powered operation was conducted earlier in the test, it depended heavily on the availability of torque and rpm cues. The loss of primary cues for the model operator when using "hot" controls means that integrated backup information must be made available instantaneously. The control of the servo in manual mode proved satisfactory under practiced conditions but contains an element of ambiguity under emergency conditions; a lever may provide a more natural interface with the operator than a control knob.

An alternative to simply continuing the use of slow, beep-type trim controls, where variable geometry or transient conditions are required in a test, could involve providing a model control station with integrated cues in the form of a simulated flight panel containing synthesized rate of climb, normal g, integrated altitude, etc. derived from a model balance. In addition, cockpit-type lever servo controls could be provided with sufficient operator checkout time for operating the system. Such a model-simulator experiment would be appropriate, initially, with a free-to-pitch powered semispan model with controllable horizontal tail for maintaining trim flight as the rotor pylons are tilted between the helicopter and airplane modes. Operator work loads for various control gains, conversion rates, etc., could be assessed in the presence of wing and rotor interactions on the tail as well as acquiring data on performance, stability and control trim conditions, and dynamic loads during continuous conversion in trimmed flight. Where powered rotor tests involve only steady-state data acquisition at discrete operating conditions, however, the simpler beep-type low-speed trim controls provide a lower risk and lower cost solution.

The occurrence of the incident meant that the planned test objectives to obtain data at still higher speeds at the 60-degree conversion angle and for other mast-tilt angles were not achieved; however, the data which were obtained showed good agreement with the powered tilt test results of the contractor's 25-foot proprotor at Ames in November 1970 under similar conditions (Figure IV-29).

E. CONCLUSIONS

Based on the results of this small-scale test, the following conclusions can be drawn relative to full scale characteristics:

Dynamic Stability

- No proprotor instabilities should be experienced in the stop/fold speed range due to adding folding mechanisms to a basic proprotor system. Test data confirmed predicted frequencies and damping.
- No flutter-type instabilities should be encountered at any fold angle up to $1.46 V_H$ for the stop/fold mode (292 knots full scale). Damping of the folded blades and wing assembly reduces as predicted as the blades are folded but does not indicate any tendency to drop below structural damping values in the speed range tested.

Optimum Stop/Start Rates

- The ability to predict the effects of stop/start rates on wing beam and chord loads and vibrations has been demonstrated. Based on these tests and analyses which also consider aircraft longitudinal accelerations, optimum stop/start rates for the full-scale 25-foot-diameter folding proprotor are in the range of 2.5 to 4 seconds.

Stop/Start Envelope

- Rotor blade loads at operating rpm are a minimum when rotor flapping is free and are predicted by theory and remain below the infinite life load levels over a wide range of angle of attack. Flapping amplitudes are acceptable.
- Rotor blade loads at operating rpm as a function of angle-of-attack increase significantly when rotor flapping is restrained by a flapping lock-out mechanism. The loads are predictable. For the full-scale rotor allowables, loads would be expected to exceed the infinite life level at 175 knots when the rotor shaft angle of attack exceeds ± 4 degrees. This represents, however, a usable maneuver range. Means for opening this range by softening the flapping restraint should be explored, however. This condition is a major design consideration for folding-proprotor blade structural design.
- As the rotor stops or starts, a few cycles of transient loads are generated which exceed the loads at rpm with flapping locked out. From a fatigue-life damage standpoint these are of lesser significance than the loads at rpm with flapping locked out.

- When the rotor operates at very low rpm, while indexing to the proper azimuth for engaging the rotational lock, the blades are exposed to the effects of wing/rotor aerodynamic interference. The variation of blade loads with angle of attack is almost identical to the oscillatory load levels experienced when the rotor is at rpm with flapping locked out. However, the load cycles are accumulated at an insignificant rate. These loads are predictable by theory.

Folding Investigation

- Blade, wing and component static loads during folding are predictable and do not appear to be critical at any fold angle.
- Planned control procedures for continuous sequence operation from powered proprotor operation through the entire stop/fold/unfold/start process and return to powered proprotor operation were executed and shown to be feasible. Reliable feedback information concerning the completion of each step is required to make the process semiautomatically controlled by operation of a single beep switch to command sequence progression, regression or stopping at any point. Such a device should be provided in any future component tests to simplify operator workload. Mechanical interlocks to, for example, prevent a rotor-start collective pitch change while the mast lock is engaged must be considered.

Pylon-Tilt Mode Dynamics

- By the conclusion of the test period, the dynamic data that were obtained during the powered tilt mode tests showed excellent agreement not only with theory but with the 25-foot tilt-proprotor tests conducted at NASA-Ames in November 1970 as reported in Reference 8. This indicates that dynamic design criteria can be applied with confidence.



Figure IV-1. Installation of Semispan Aeroelastic Powered Folding Propotor Model (C300-ALC) in the LTV Wind Tunnel, February 1971.

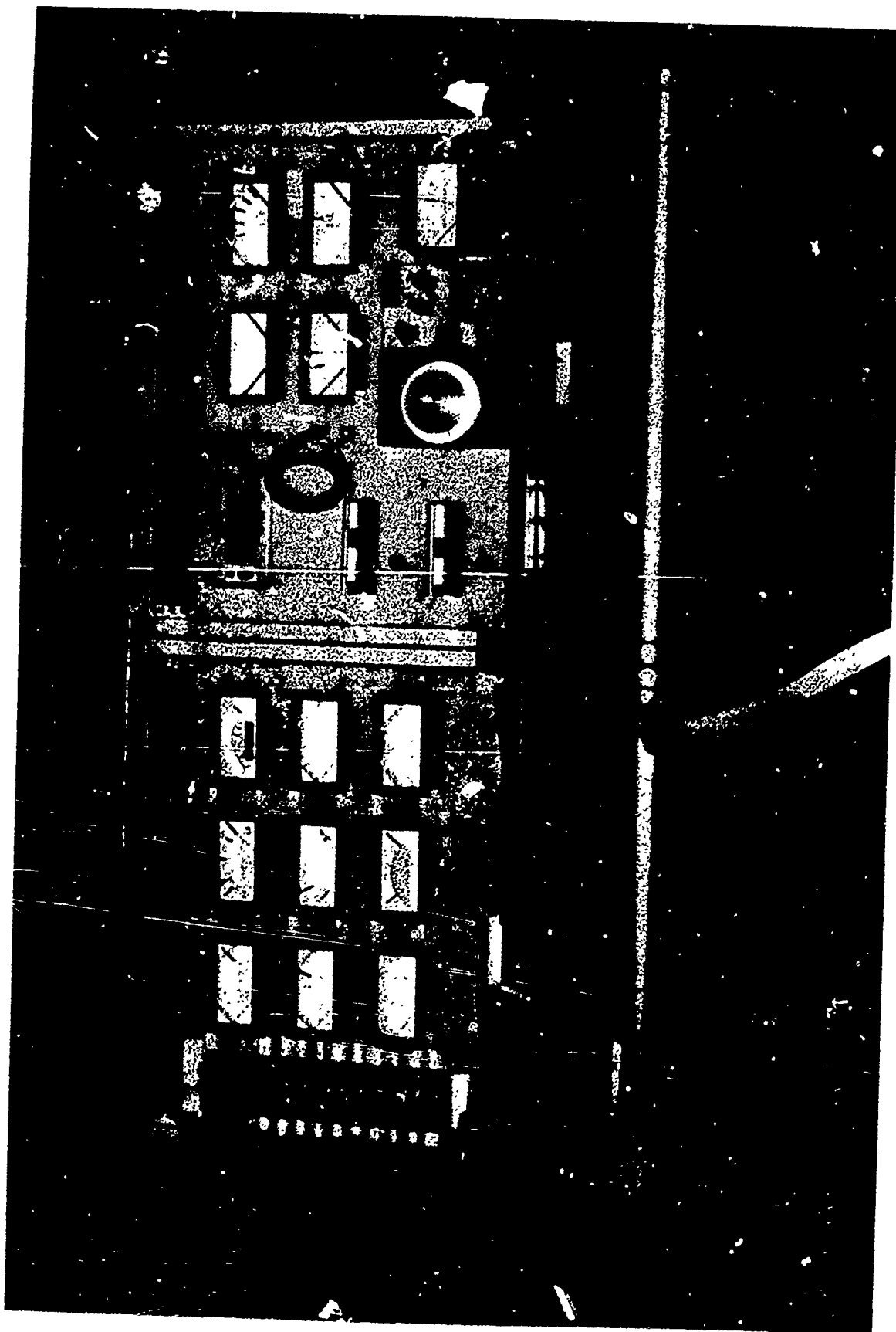


Figure IV-2. Control Console for Semispan Powered Aeroelastic Folding Propotor Model.

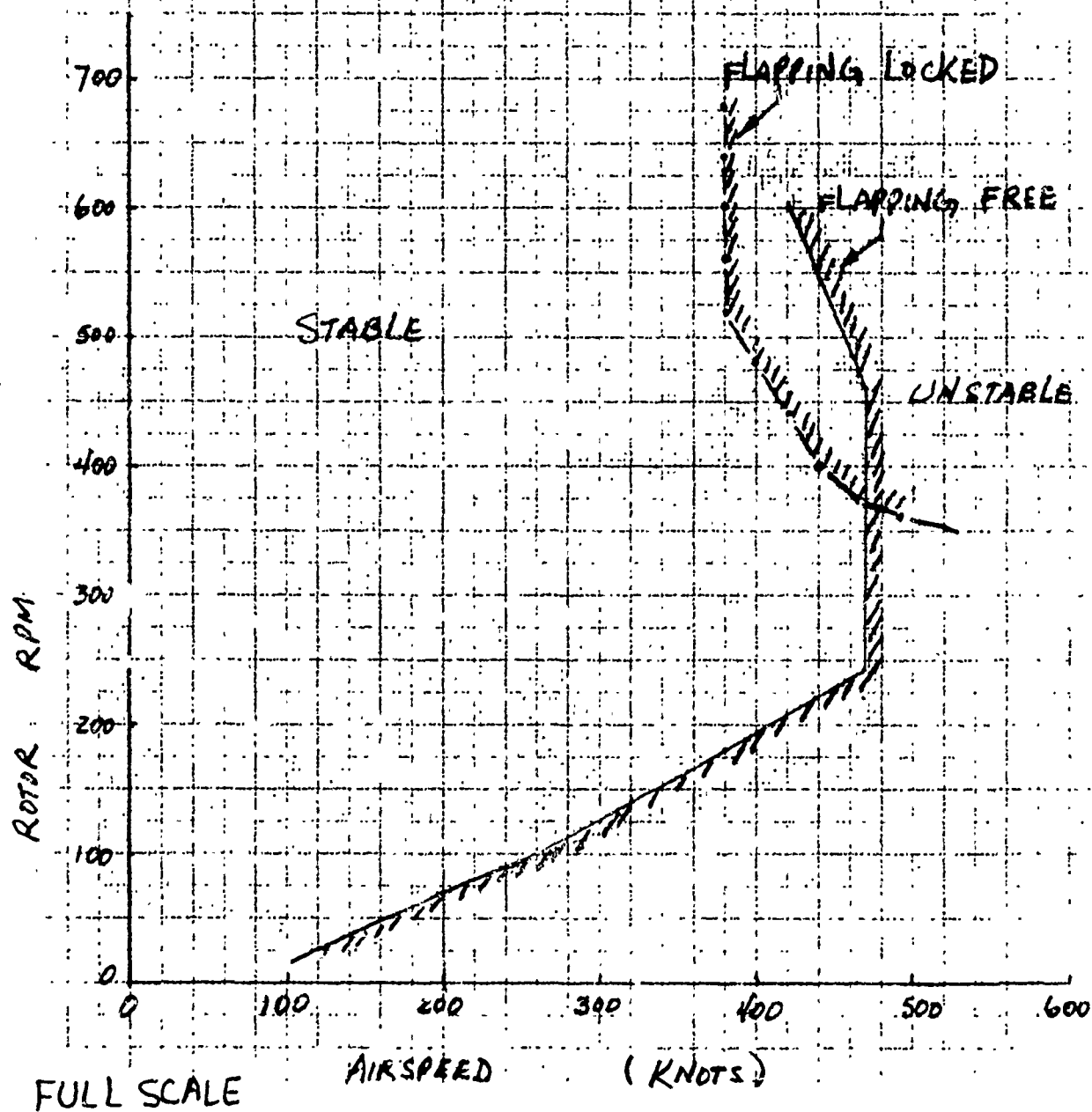


Figure IV-5. Model C300-A1C Predicted Proprotor Stability Boundaries with Flapping Free and Flapping Locked Out.

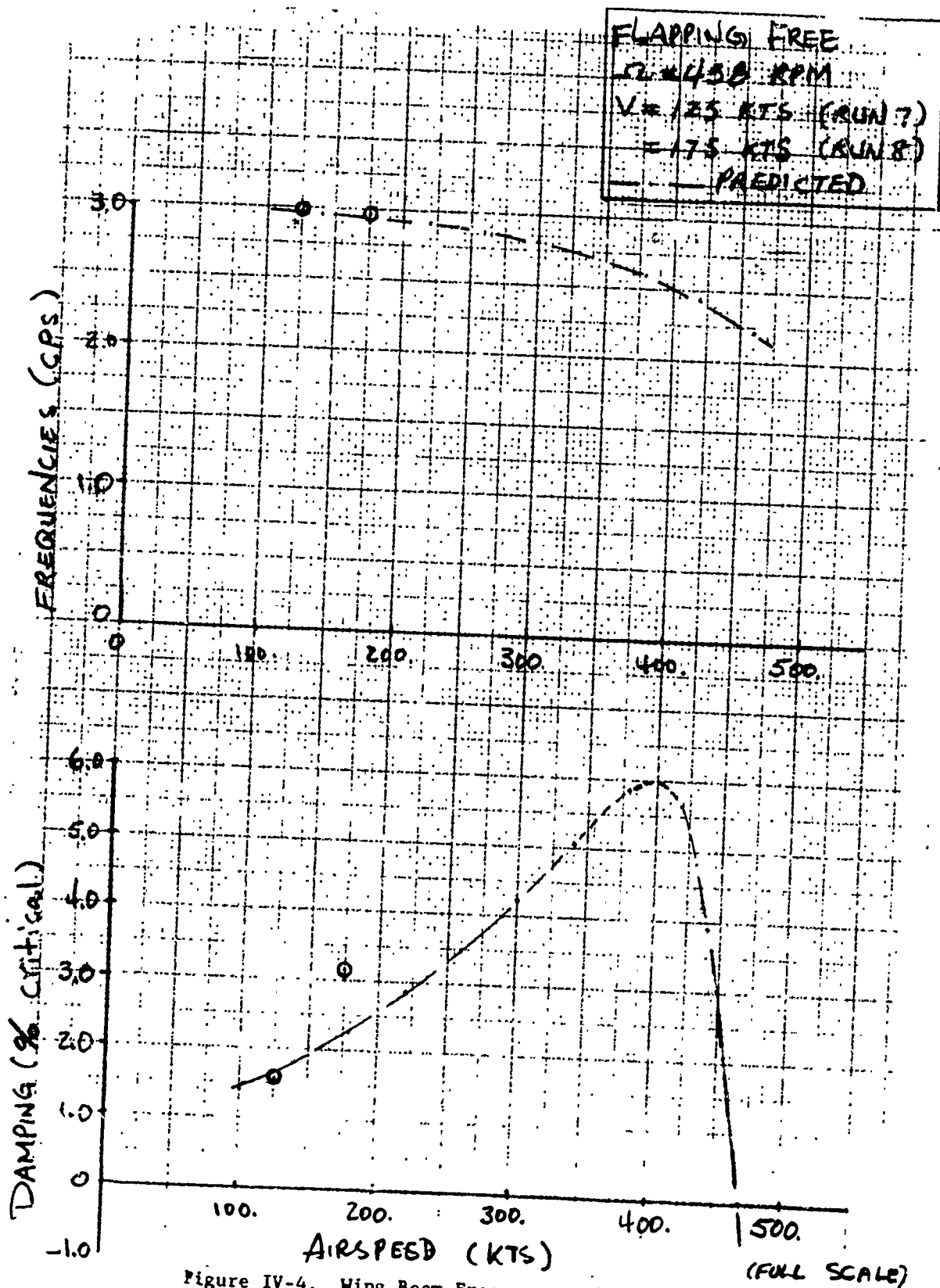


Figure IV-4. Wing Beam Frequency and Damping Versus Airspeed.

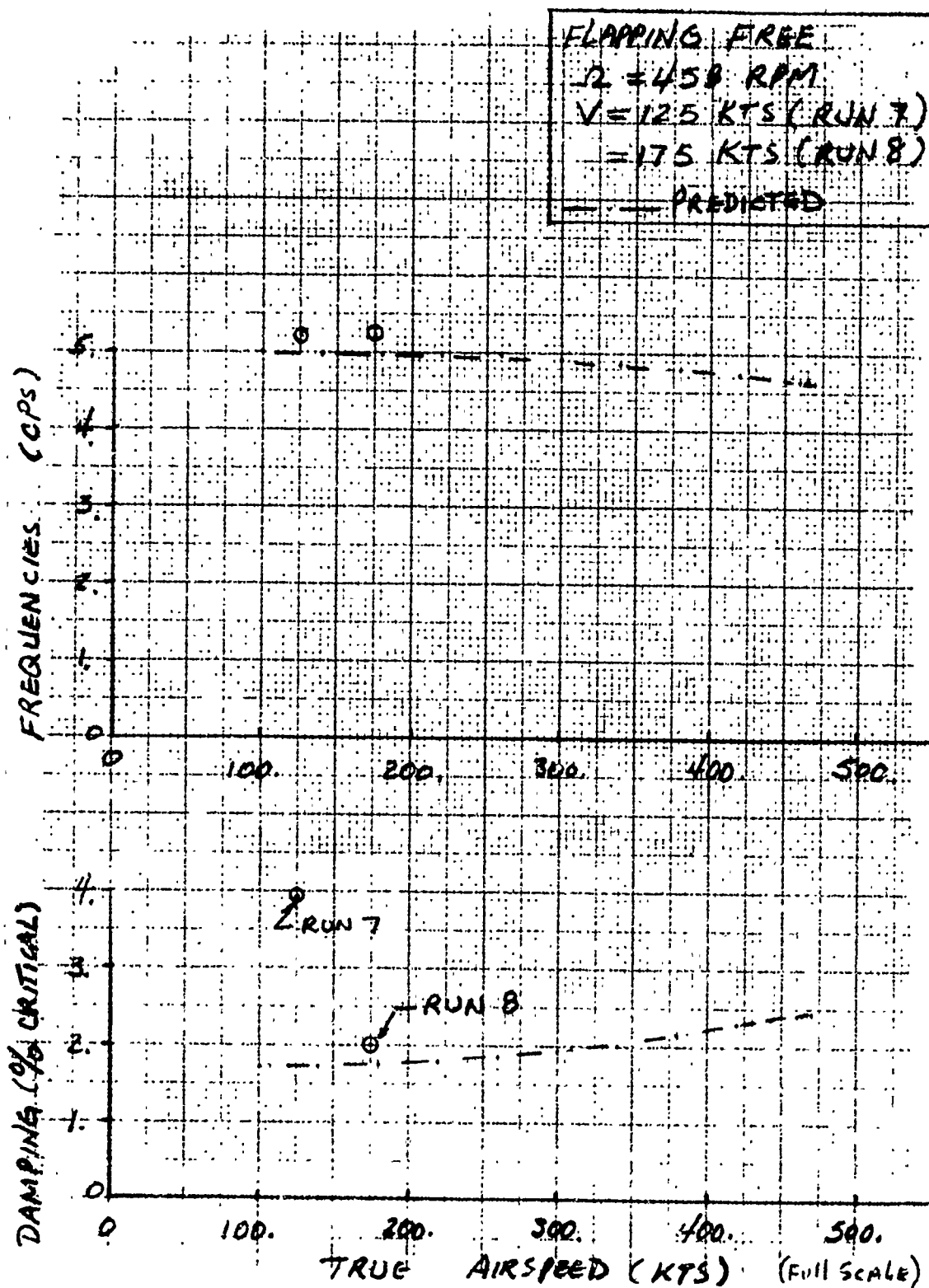


Figure IV-5. Wing Chord Frequency and Damping Versus Airspeed.

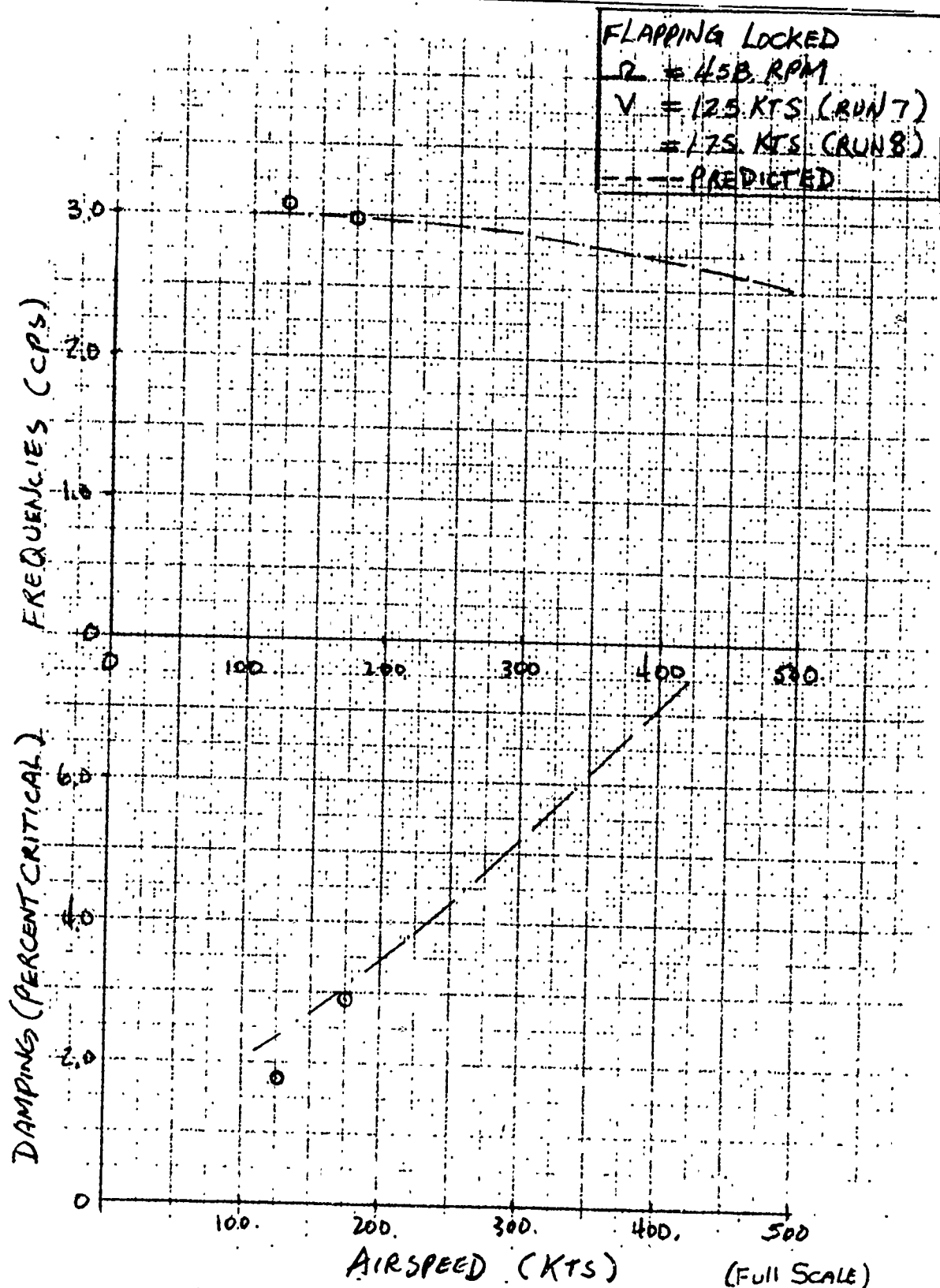


Figure IV-6. Wing Beam Frequency and Damping Versus Airspeed.

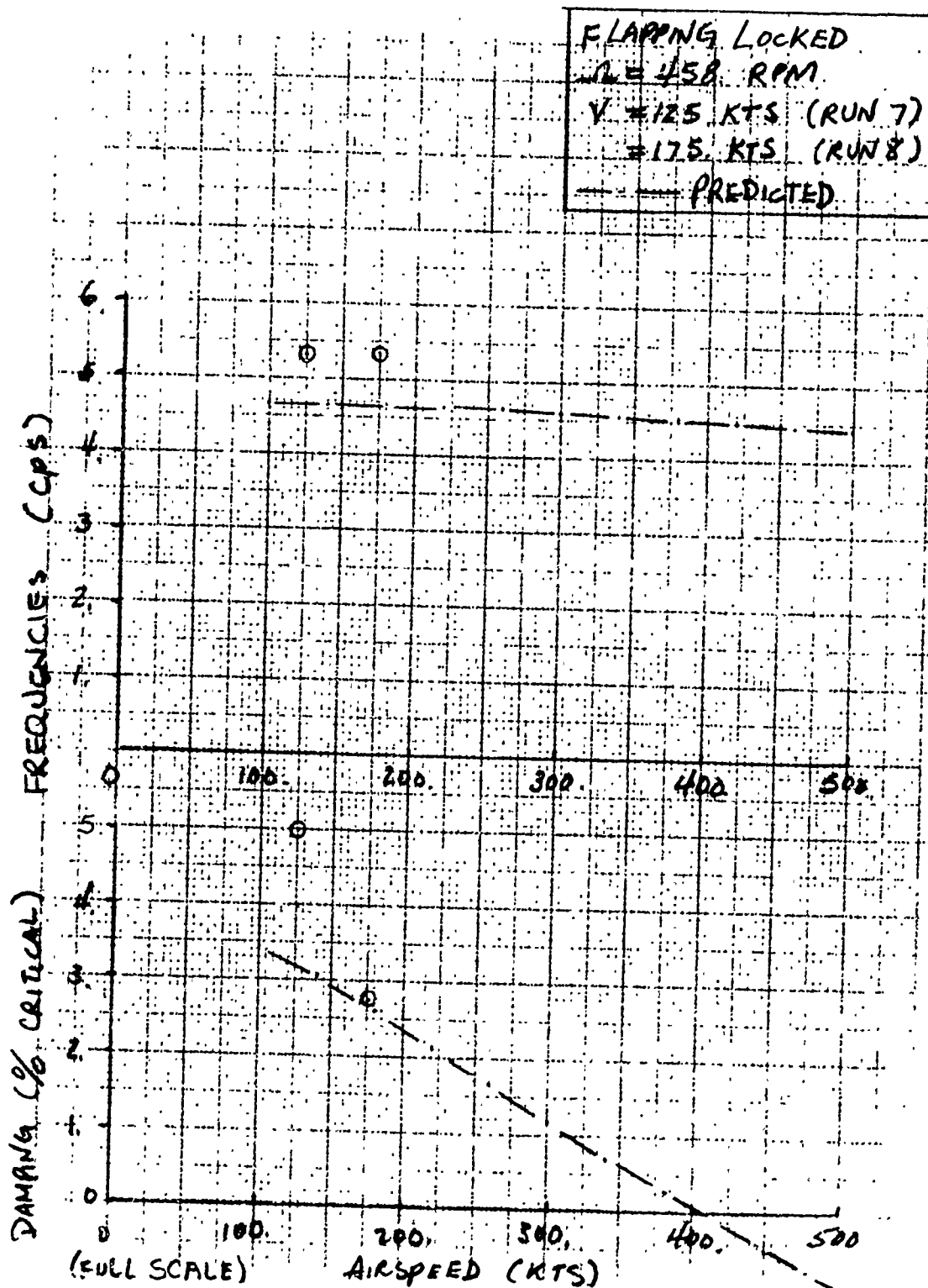


Figure IV-7. Wing Chord Frequencies and Damping Versus Airspeed.

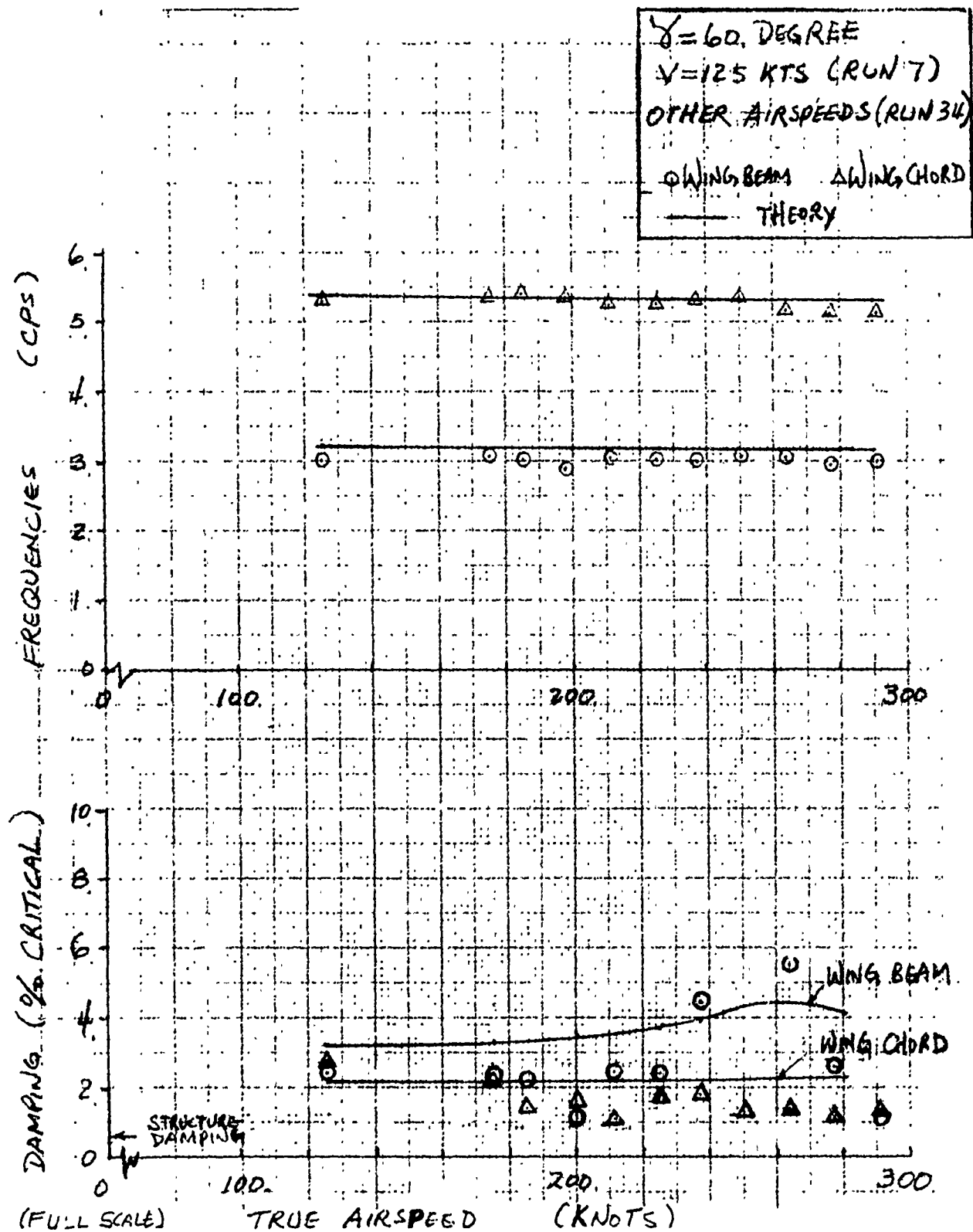


Figure IV-8. Wing Beam and Chord Frequency and Damping at 0-Degree Mast Angle, 60-Degrees Fold.

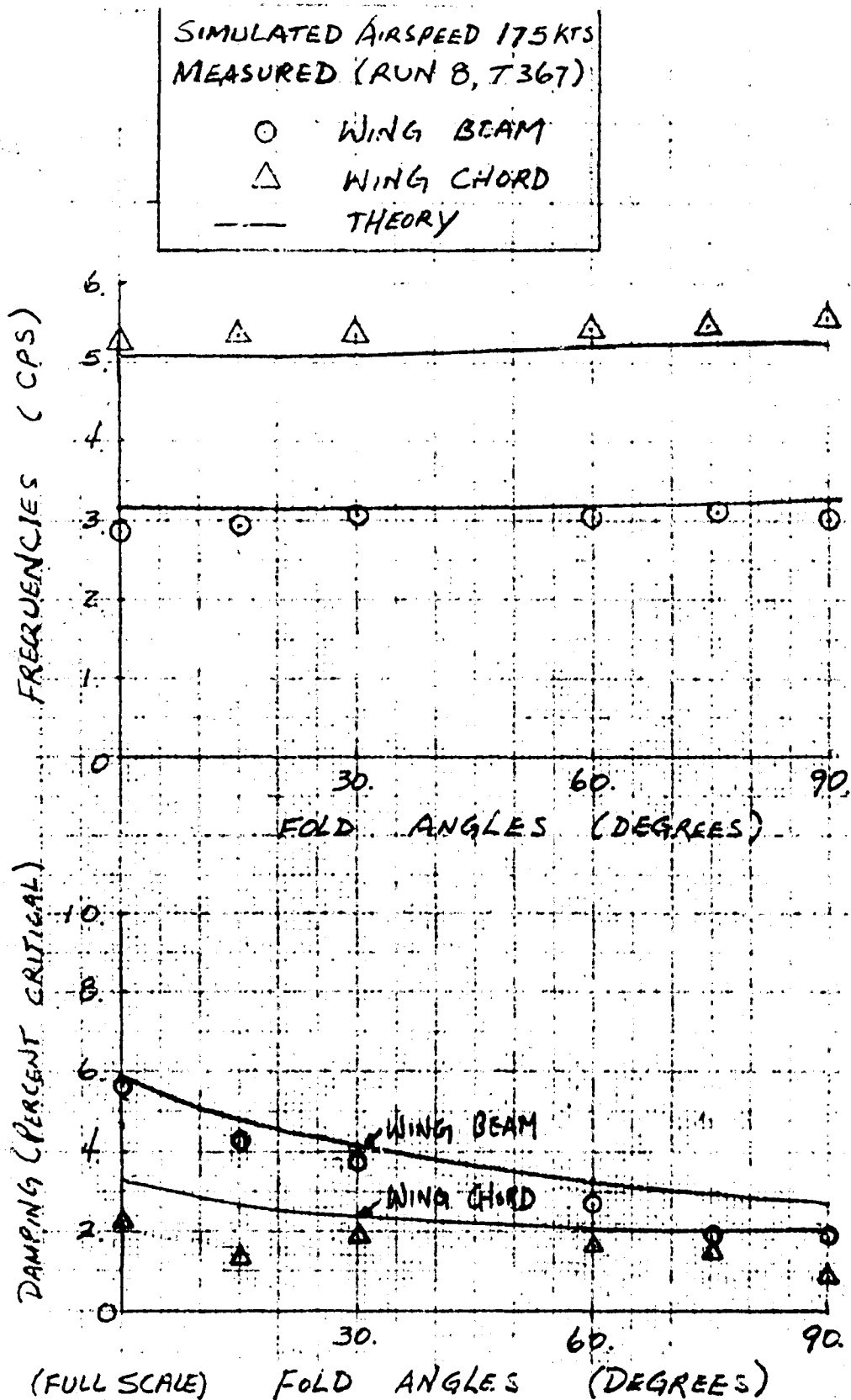


Figure IV-9. Correlation Between Theory and Measured Frequency and Damping Versus Fold Angle.

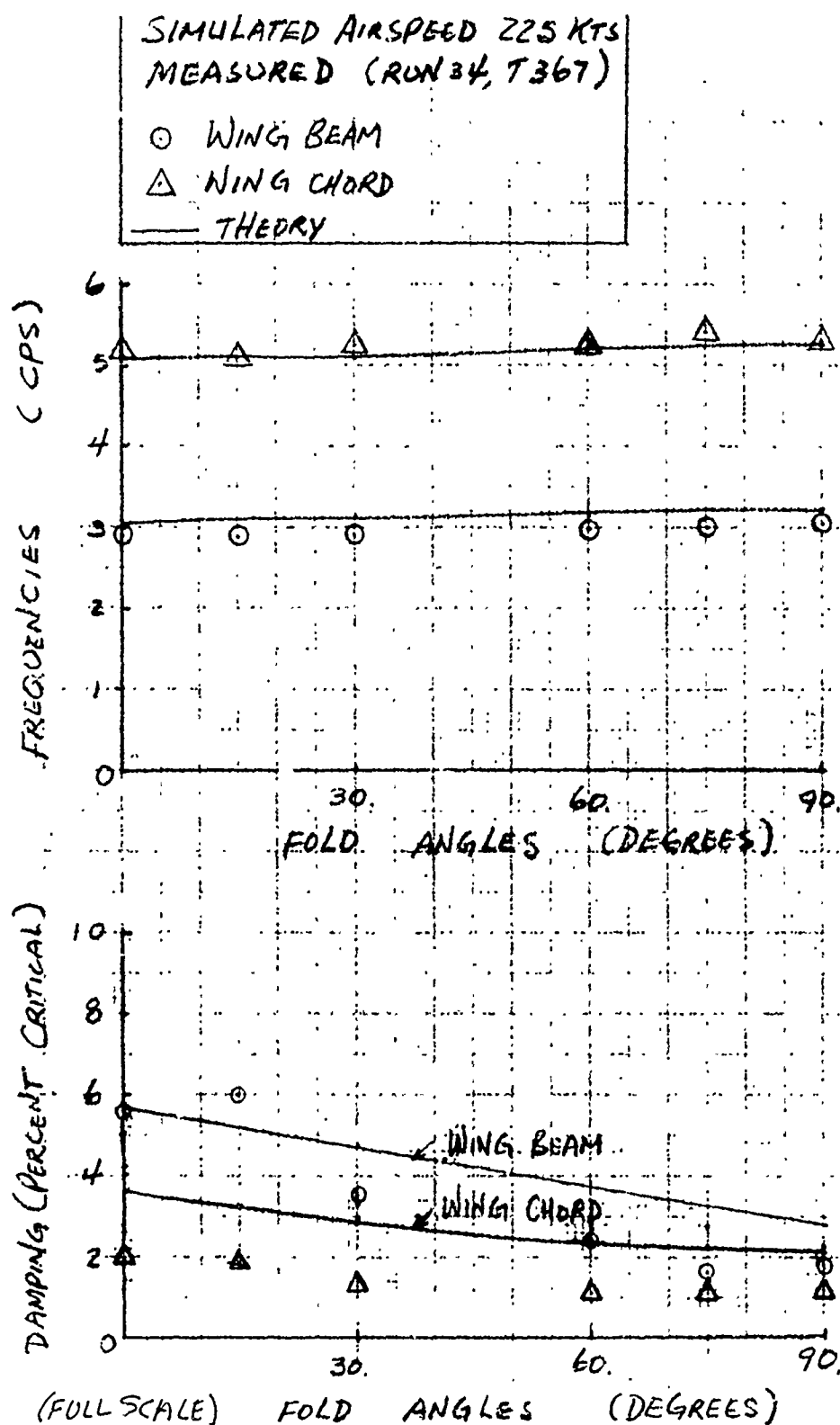


Figure IV-10. Correlation Between Theory and Measured Frequency and Damping Versus Fold Angle.

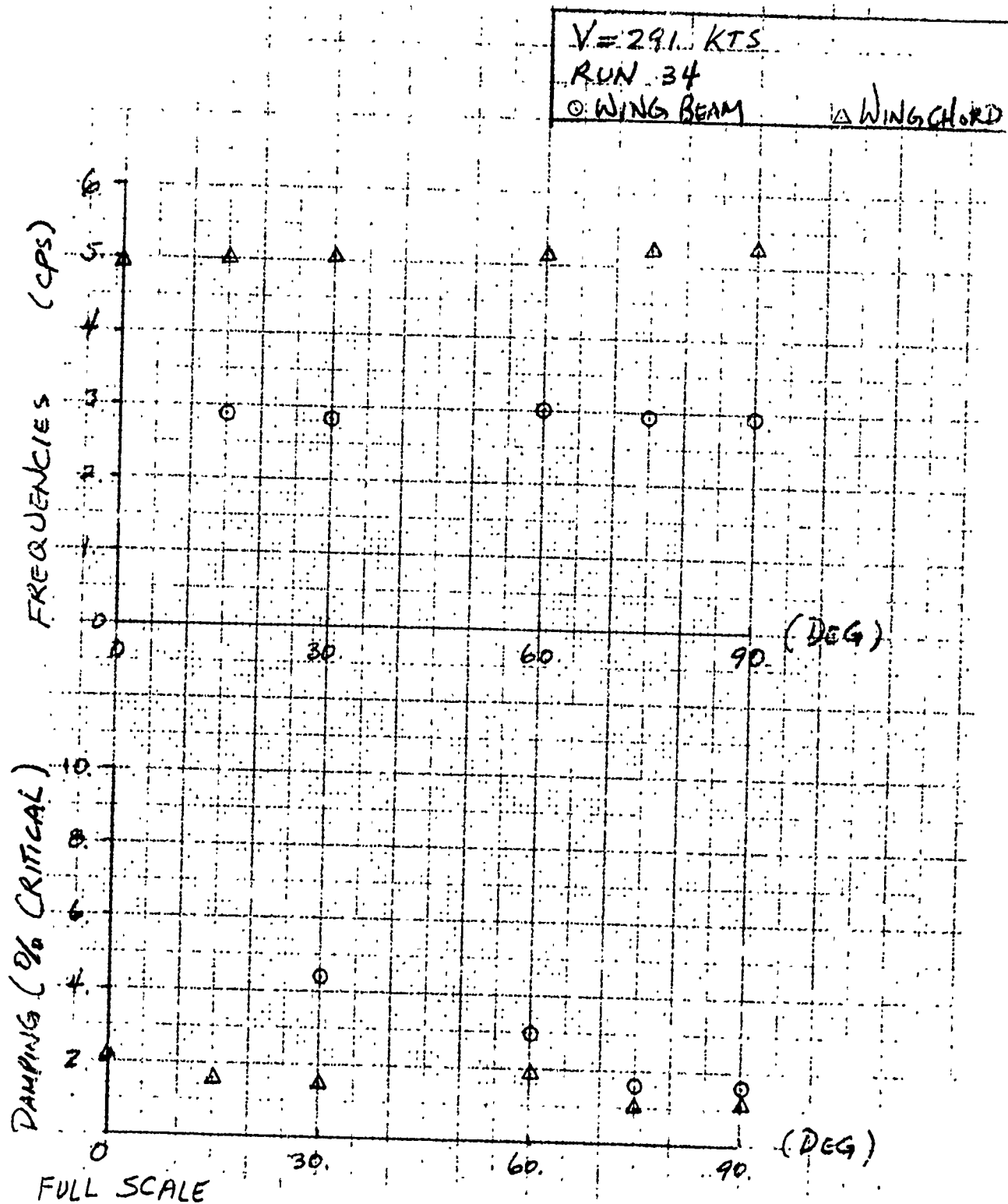


Figure IV-11. Wing Beam and Chord Frequency and Damping at 0-Degree Mast Angle of Attack.

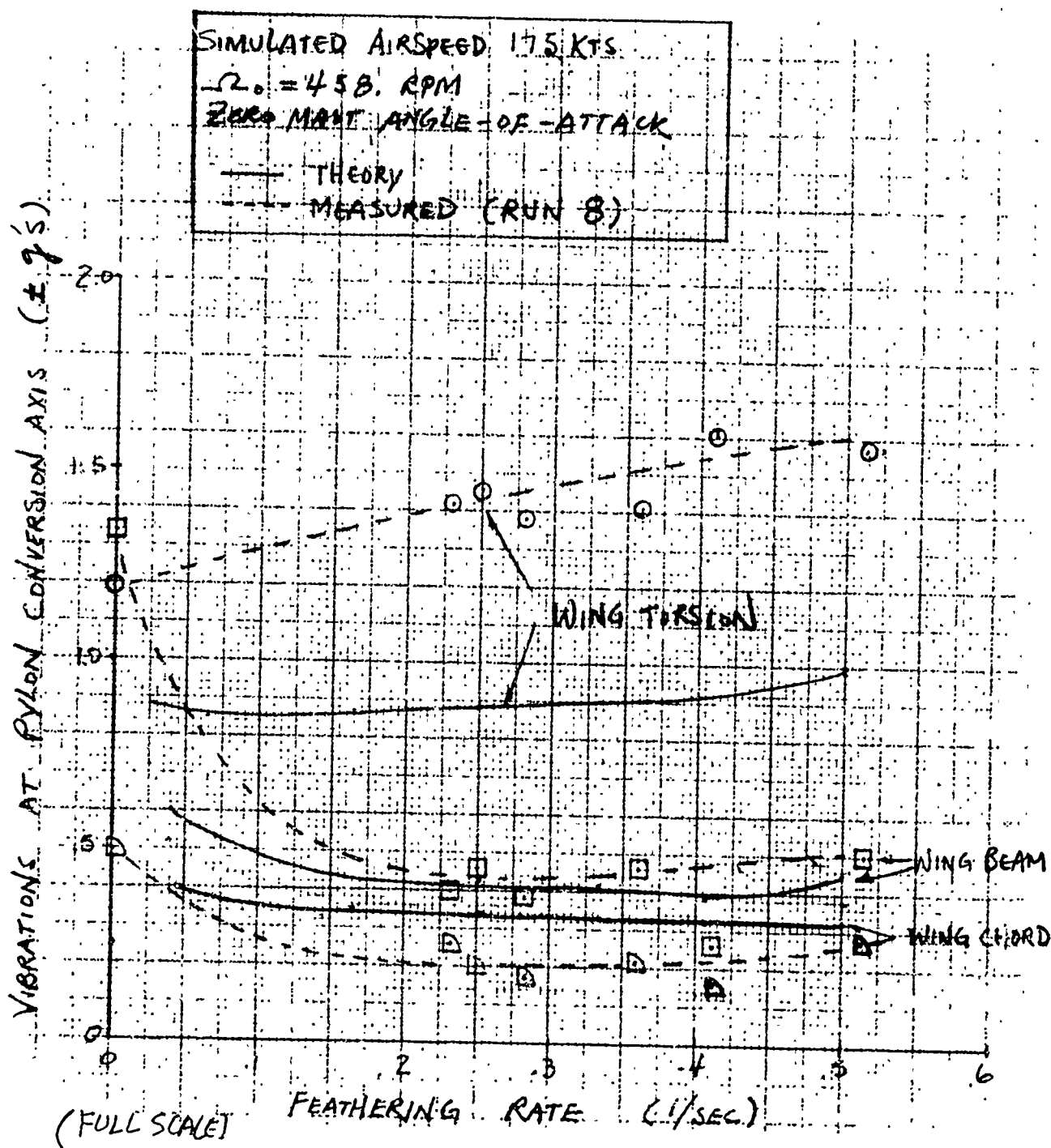


Figure IV-12. Correlation Between Theory and Measured Response at Wing Beam, Chord, and Torsional Natural Frequencies.

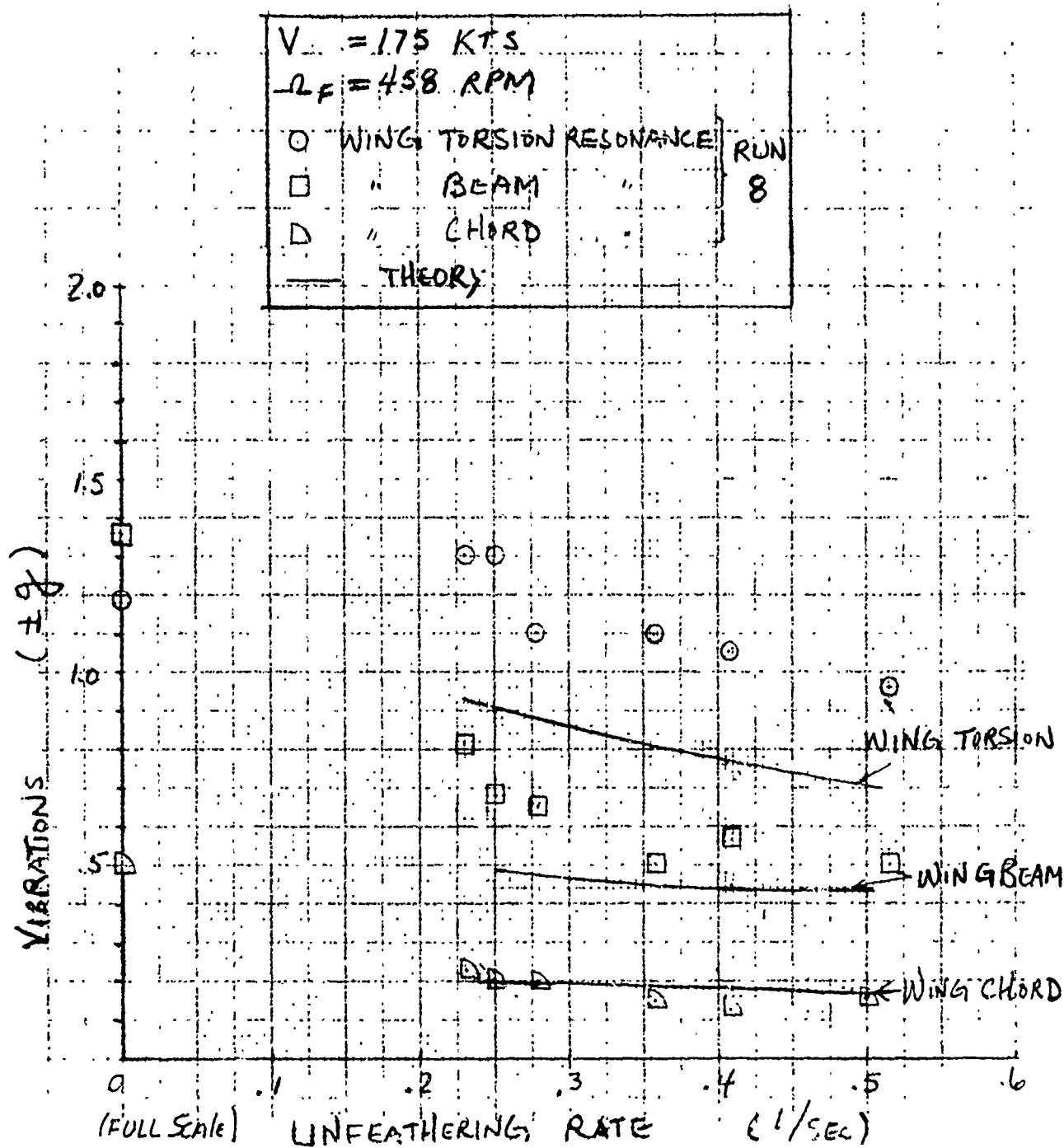


Figure IV-13. Conversion Axis Vibration at 0-Degree Mast Angle of Attack During Starting.

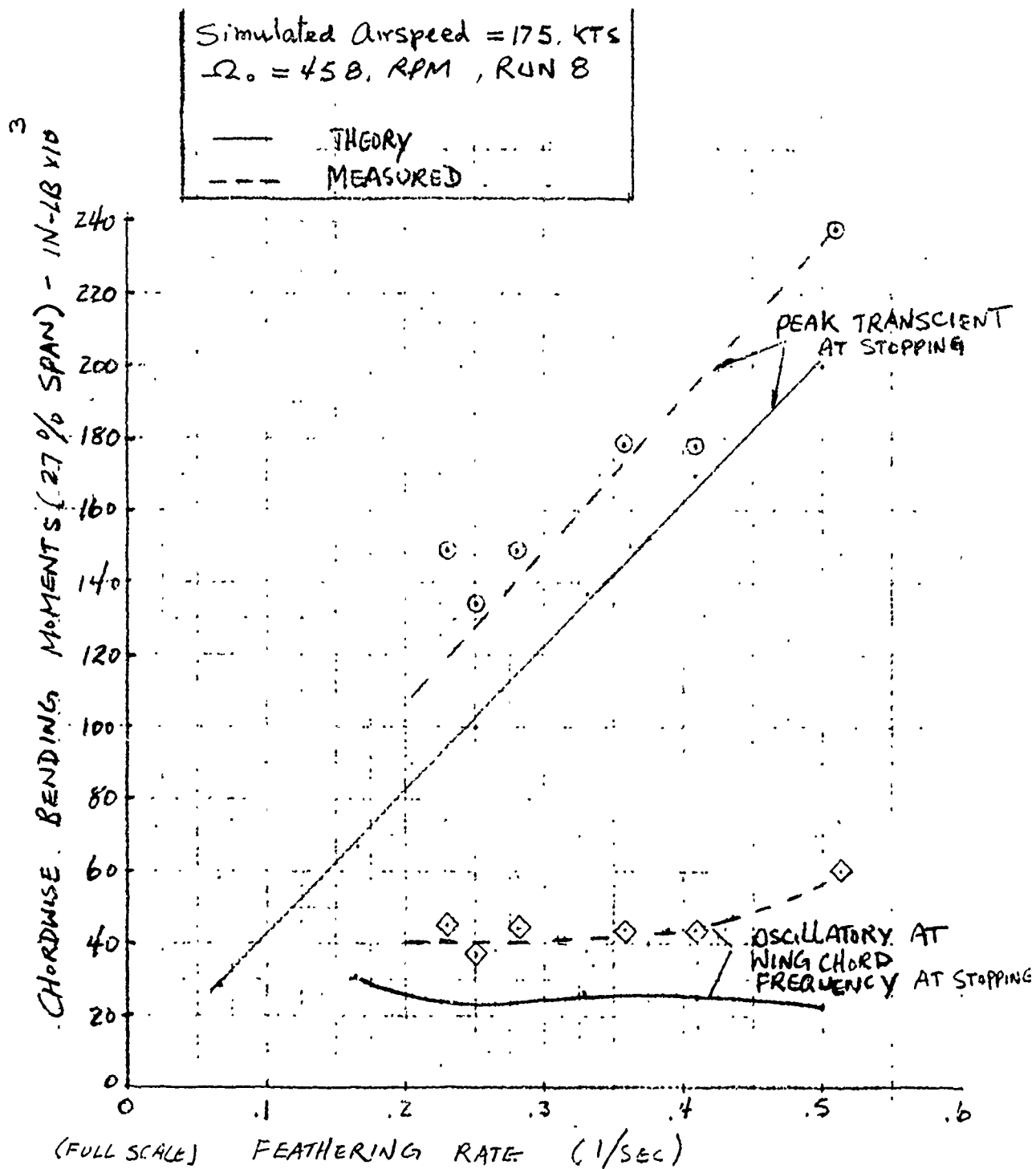


Figure IV-14. Correlation Between Theory and Measured Wing Chord Bending Response During Stopping.

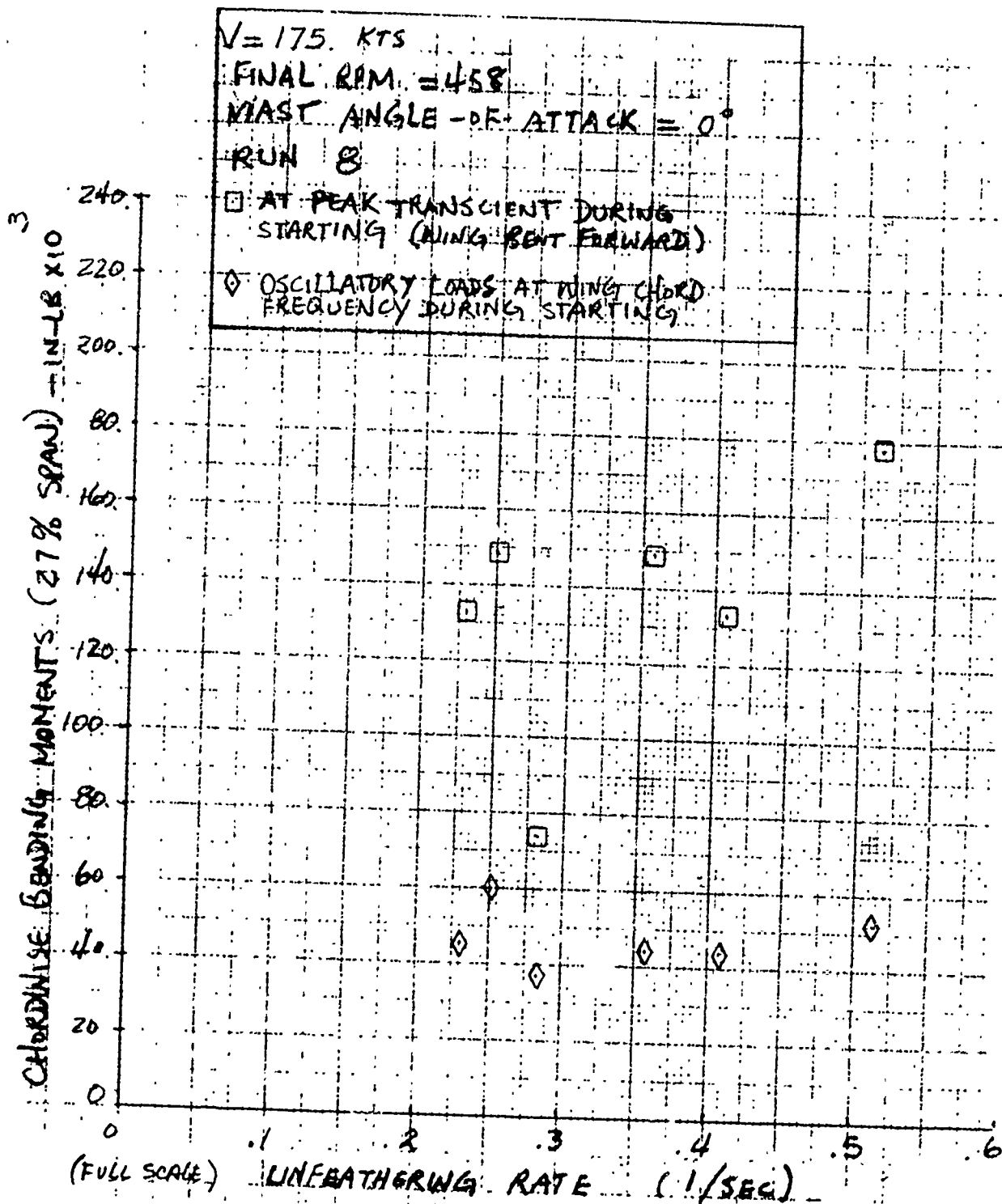


Figure IV-15. Wing Chord Bending Response During Starting.

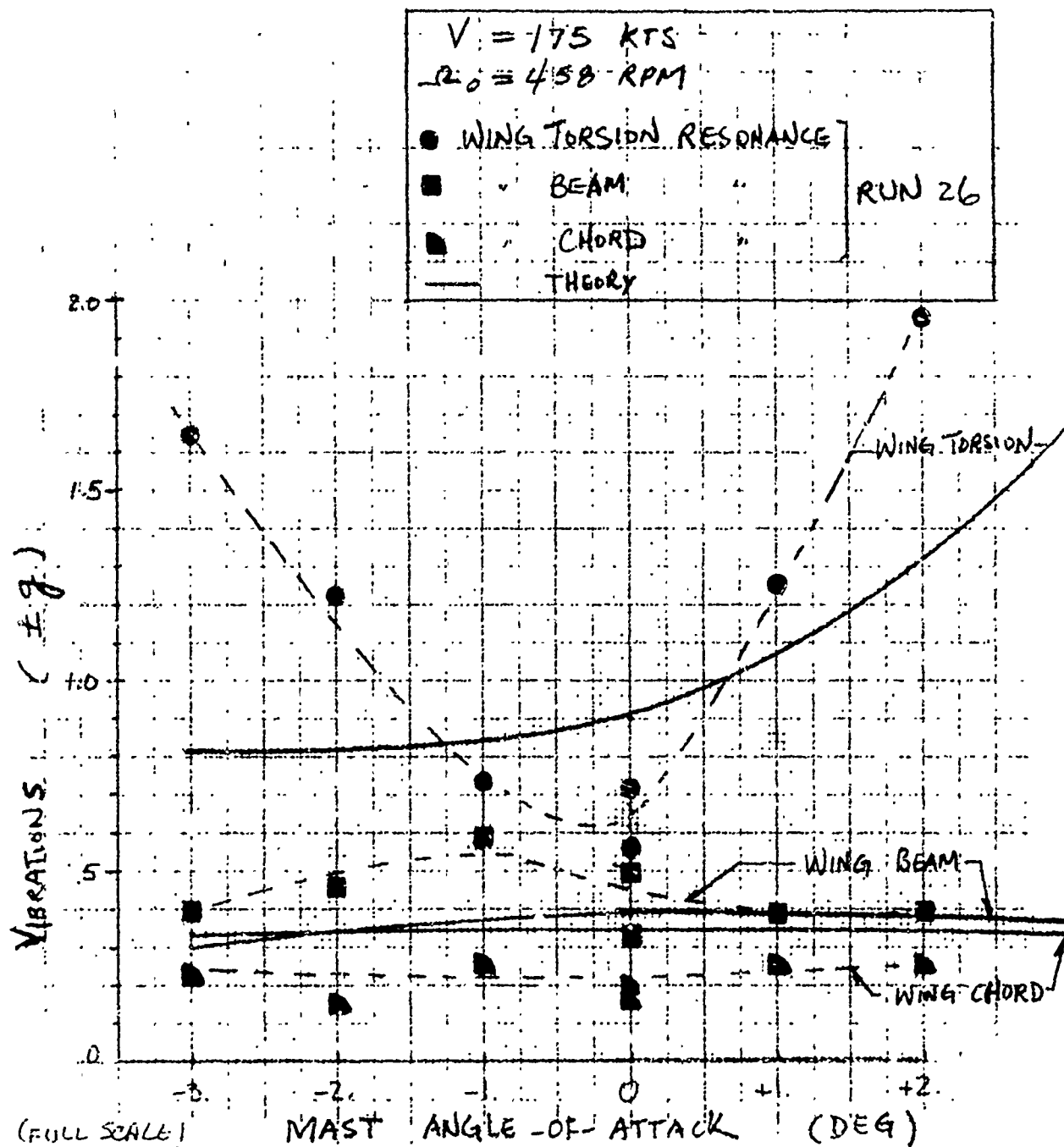


Figure IV-16. Conversion Axis Vibration During Stopping
 at $\Delta t = 2.46$ Seconds.

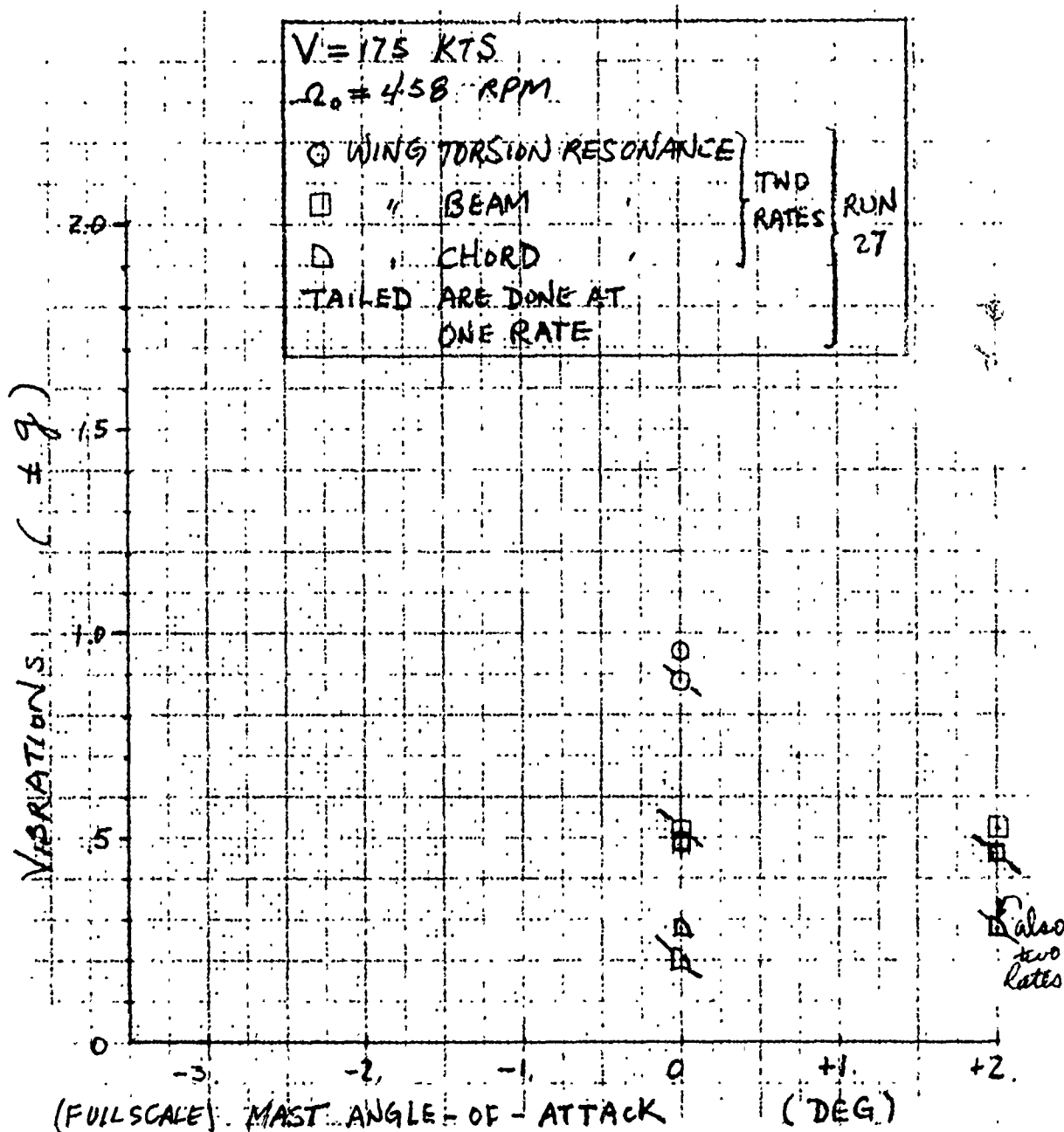


Figure IV-17. Conversion Axis Vibration During Feathering at $\Delta t = 3.56$ Seconds.

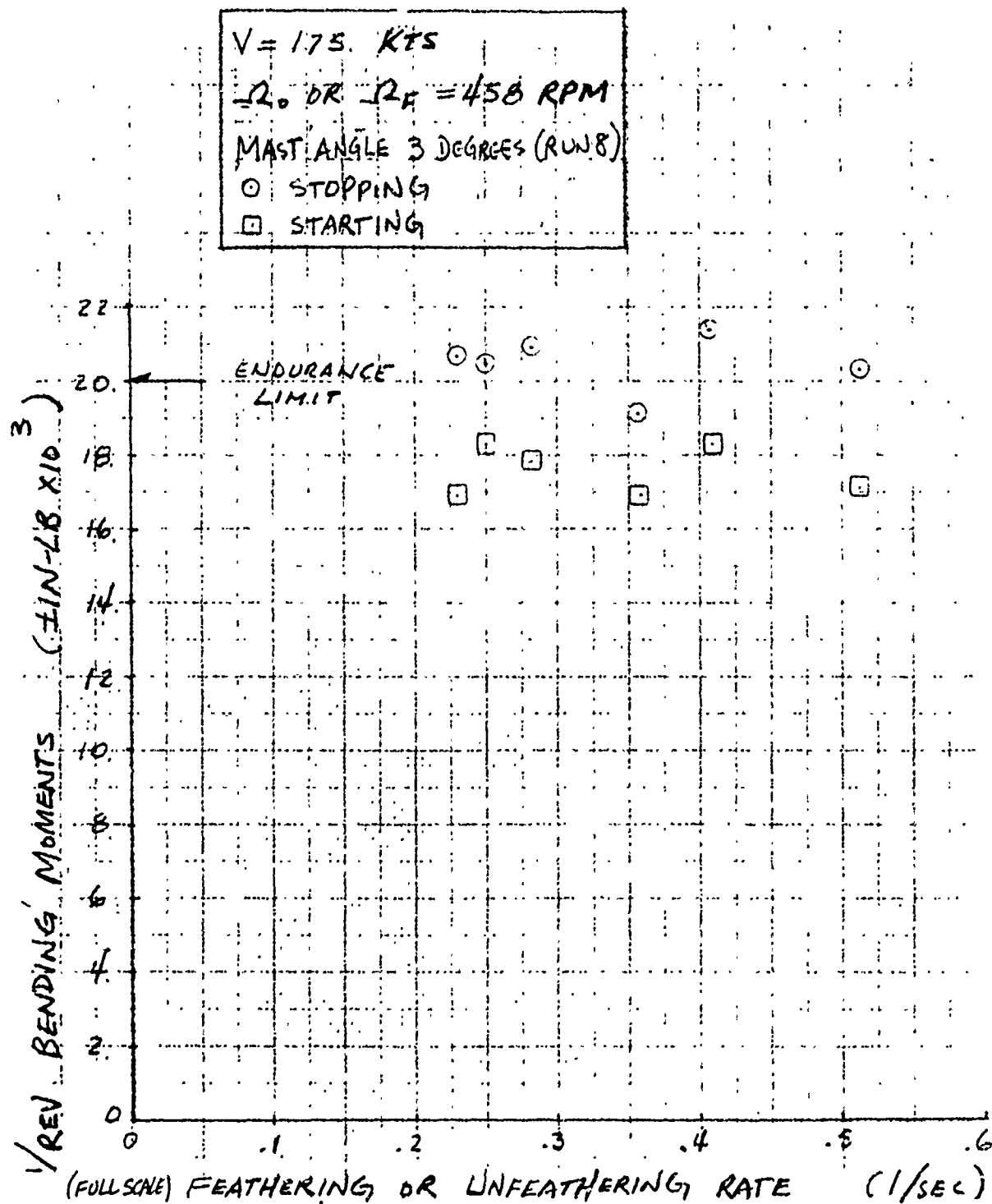


Figure IV-18. Maximum Blade Beam Oscillatory Moments at 35 Percent Radius.

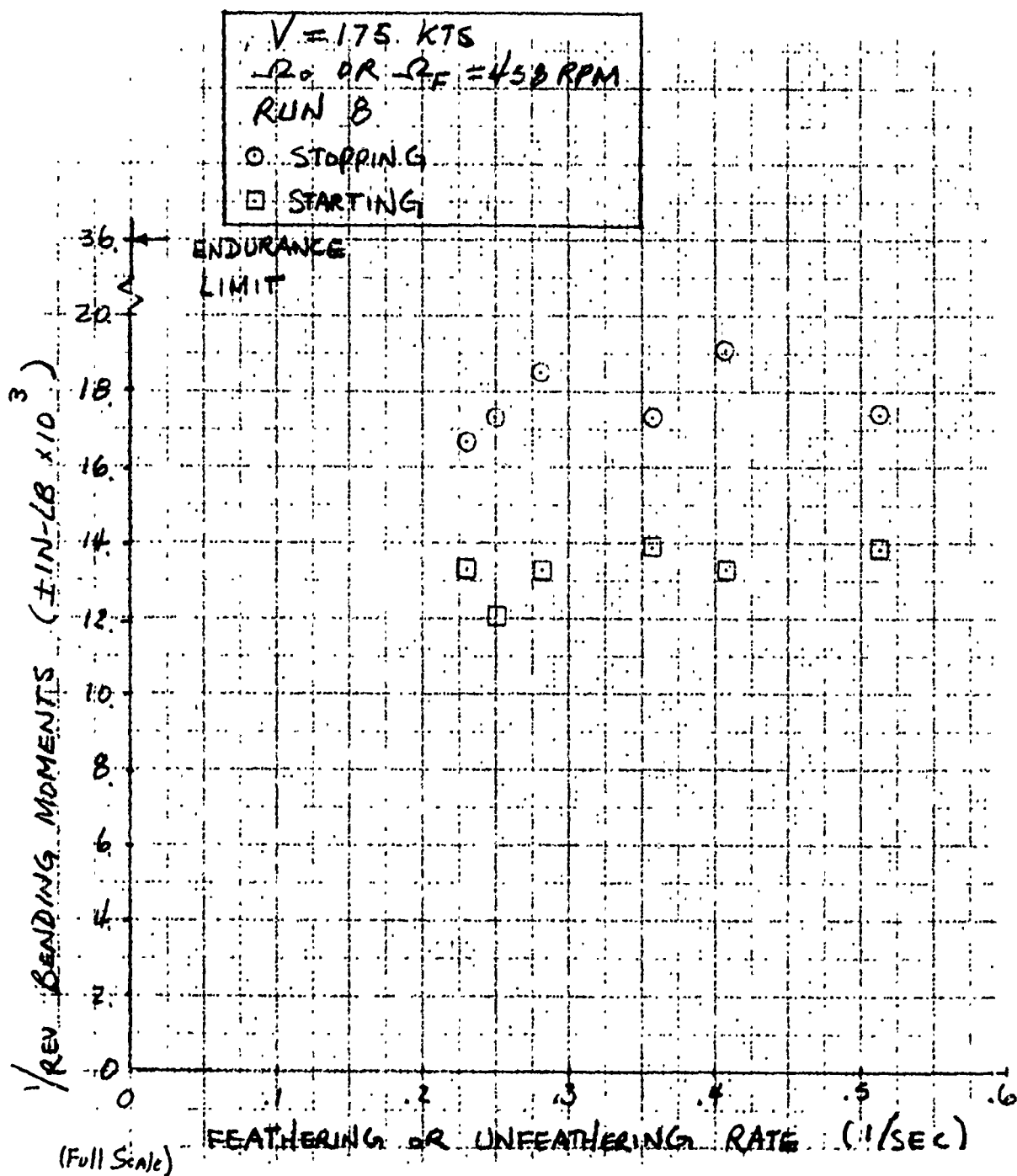


Figure IV-19. Blade Chord Oscillatory Moment at 25 Percent Radius.

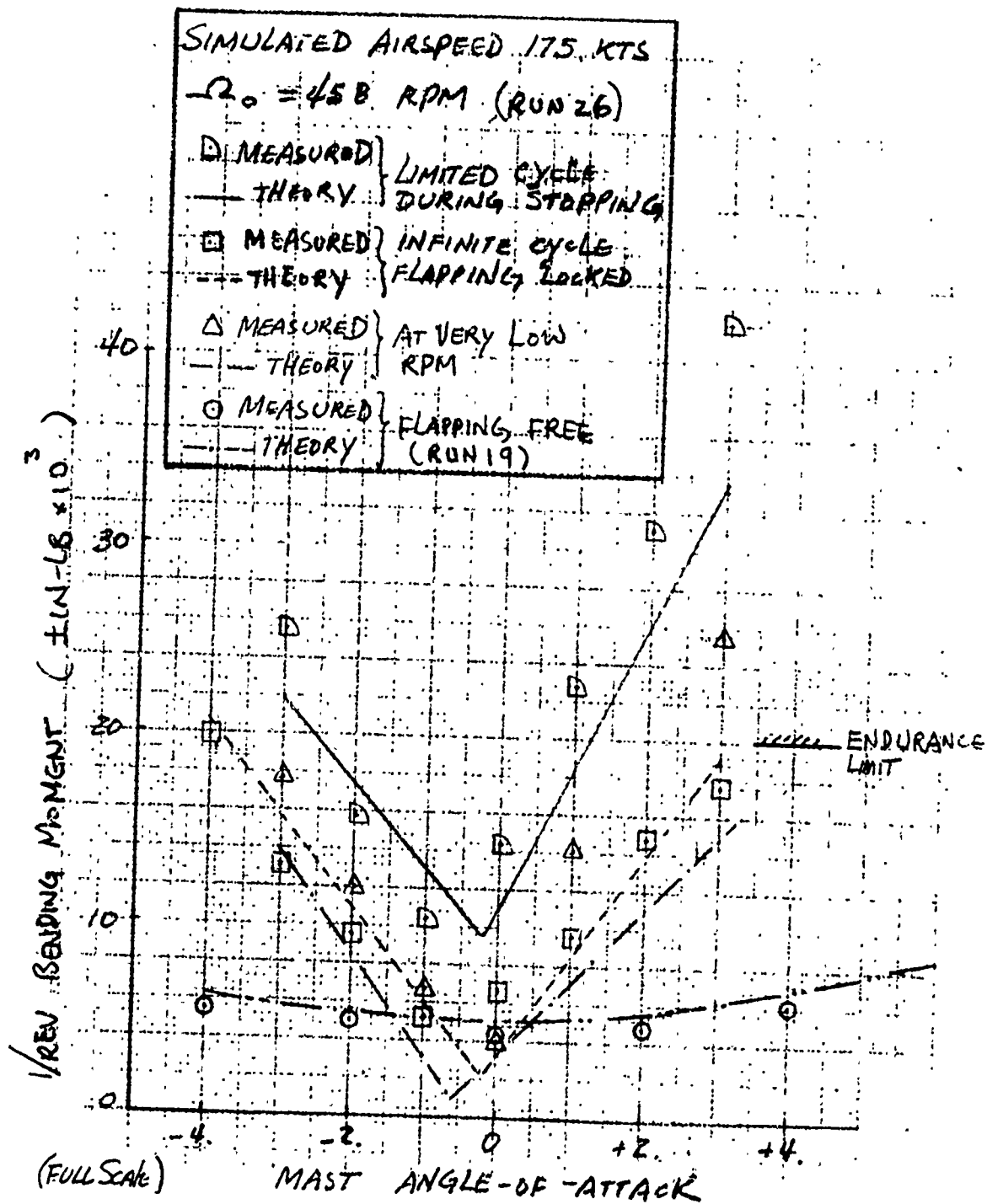


Figure IV-20. Correlation Between Theory and Measured Blade Beam Loads at 35-Percent Radius.

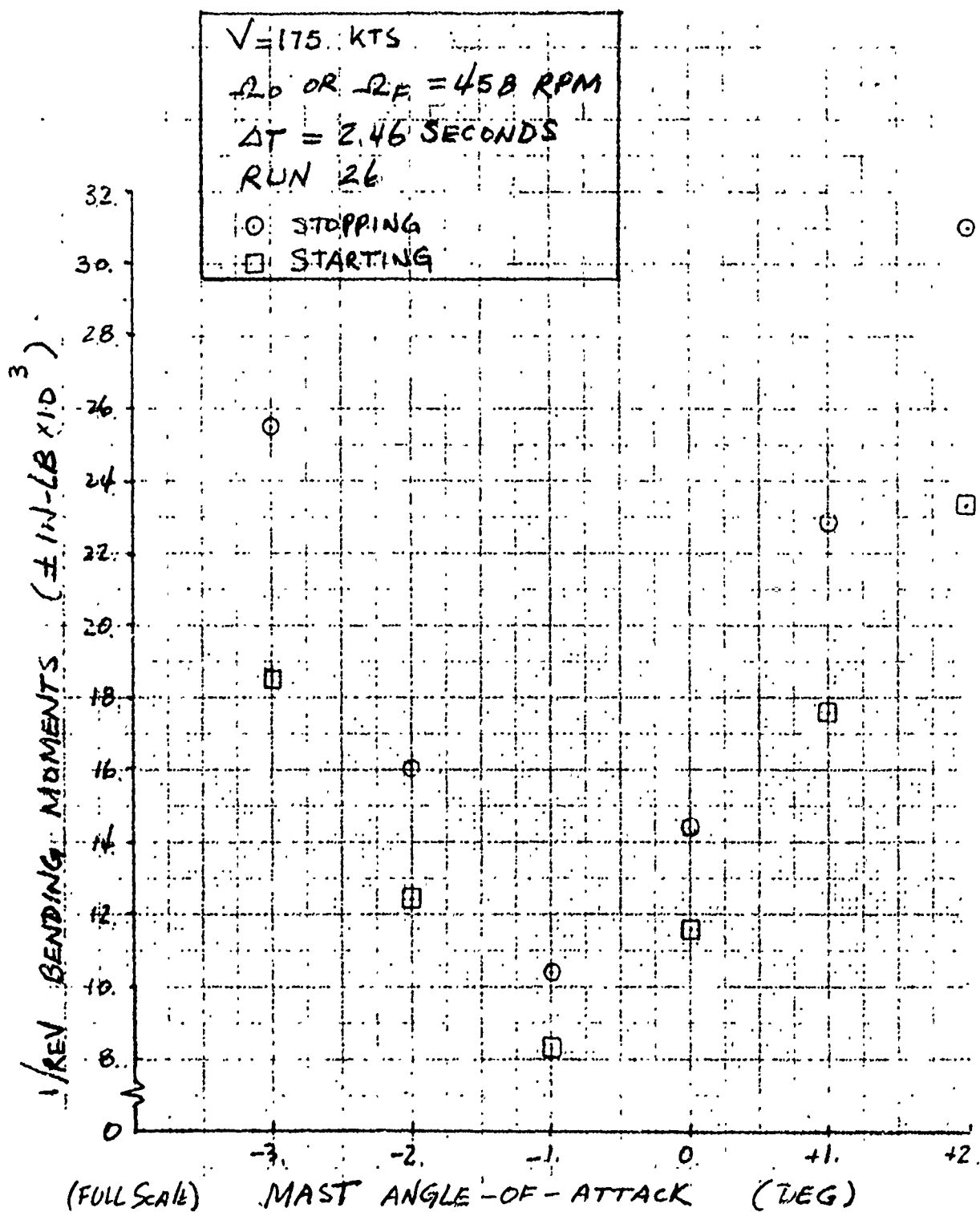


Figure IV-21. Transient Blade Beam Oscillatory Loads at 35-Percent Radius.

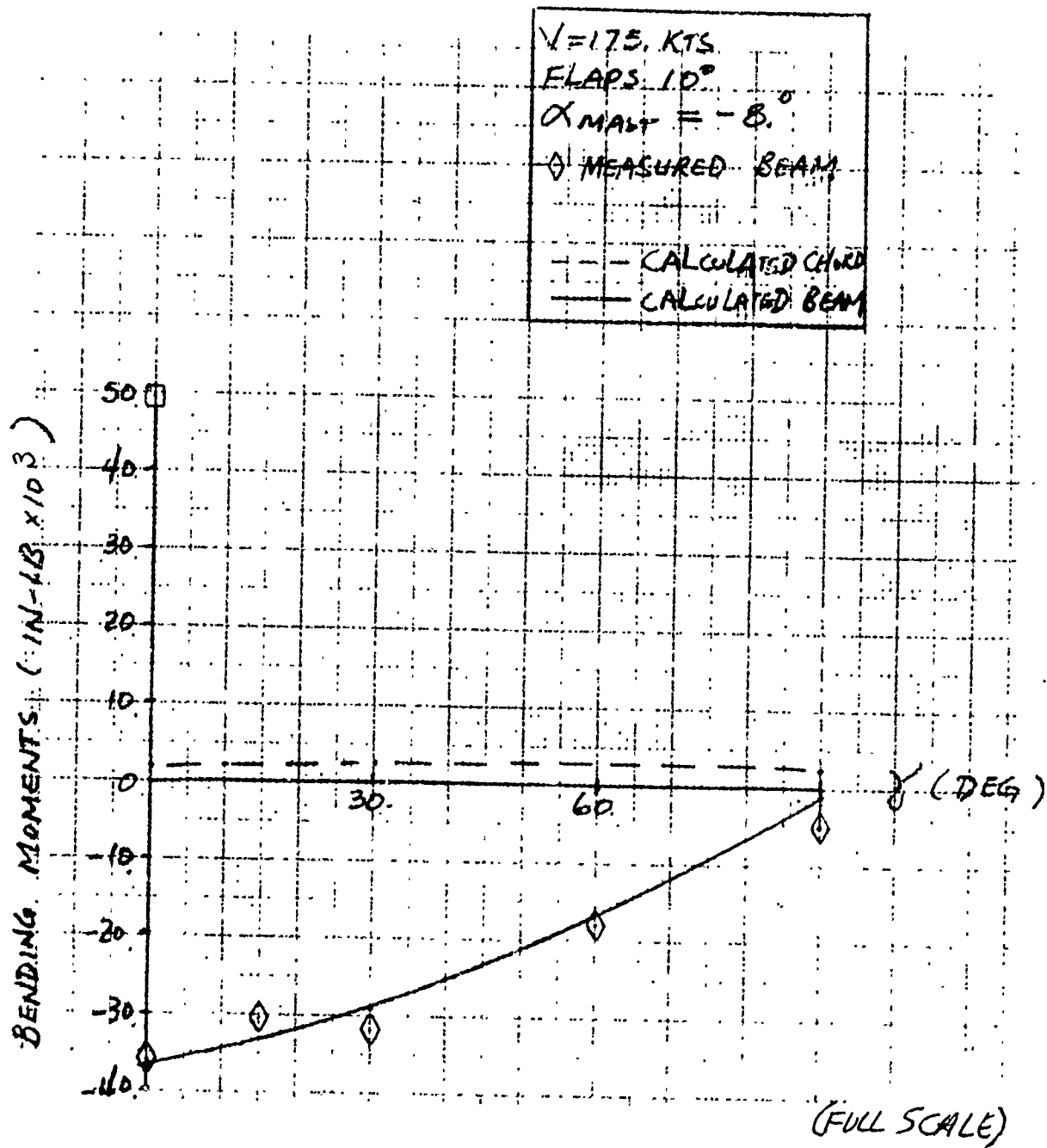


Figure IV-22. Correlation of Blade Beam and Chord Bending at 35-Percent Radius Versus Fold Angle.

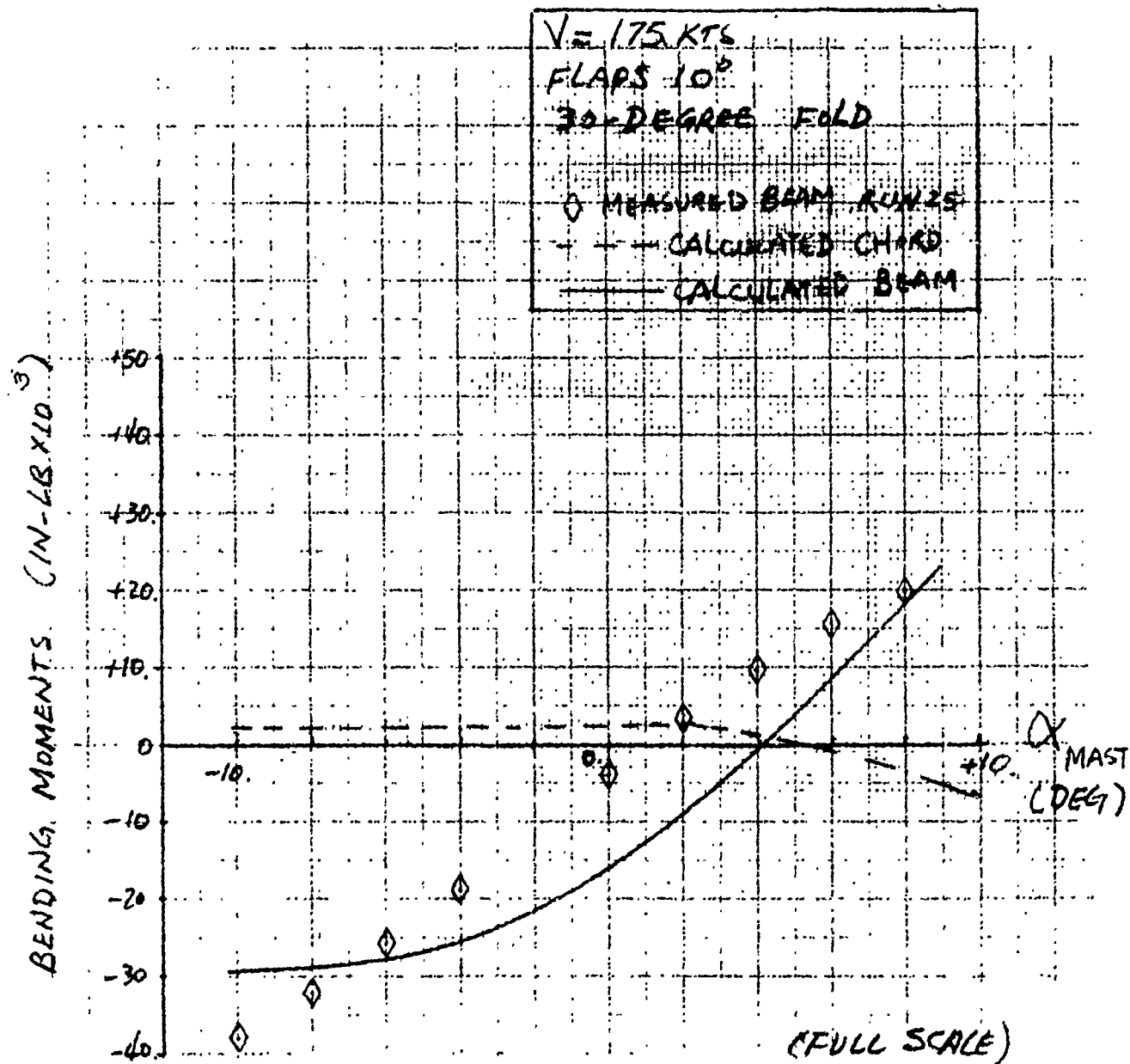


Figure IV-23. Correlation of Blade Beam and Chord Bending at 35-Percent Radius Versus Mast Angle of Attack.

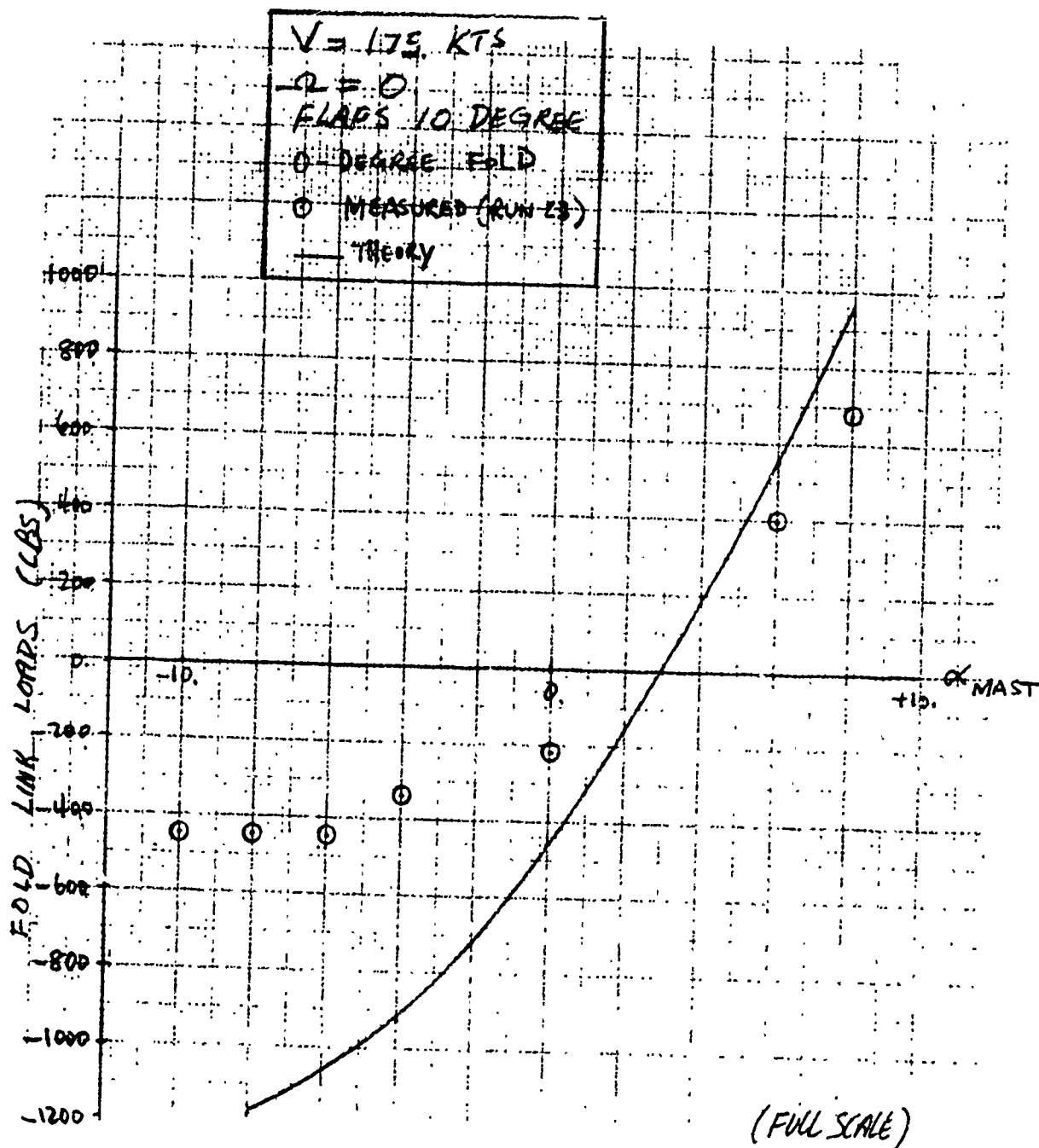


Figure IV-24. Correlation of Fold Link Loads Versus Mast Angle of Attack.

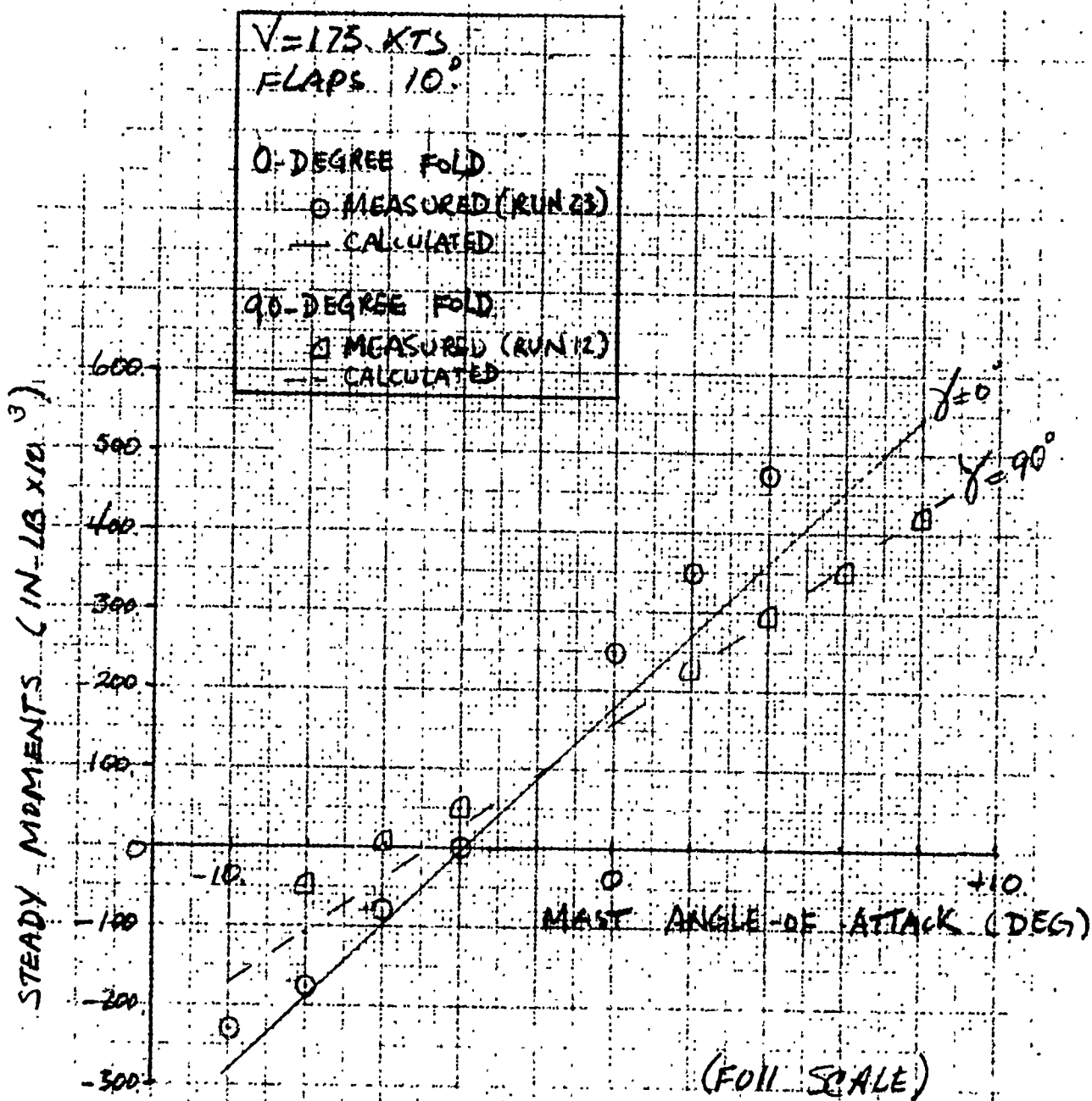


Figure IV-25. Correlation of Wing Beam Bending at 27 Percent Span.

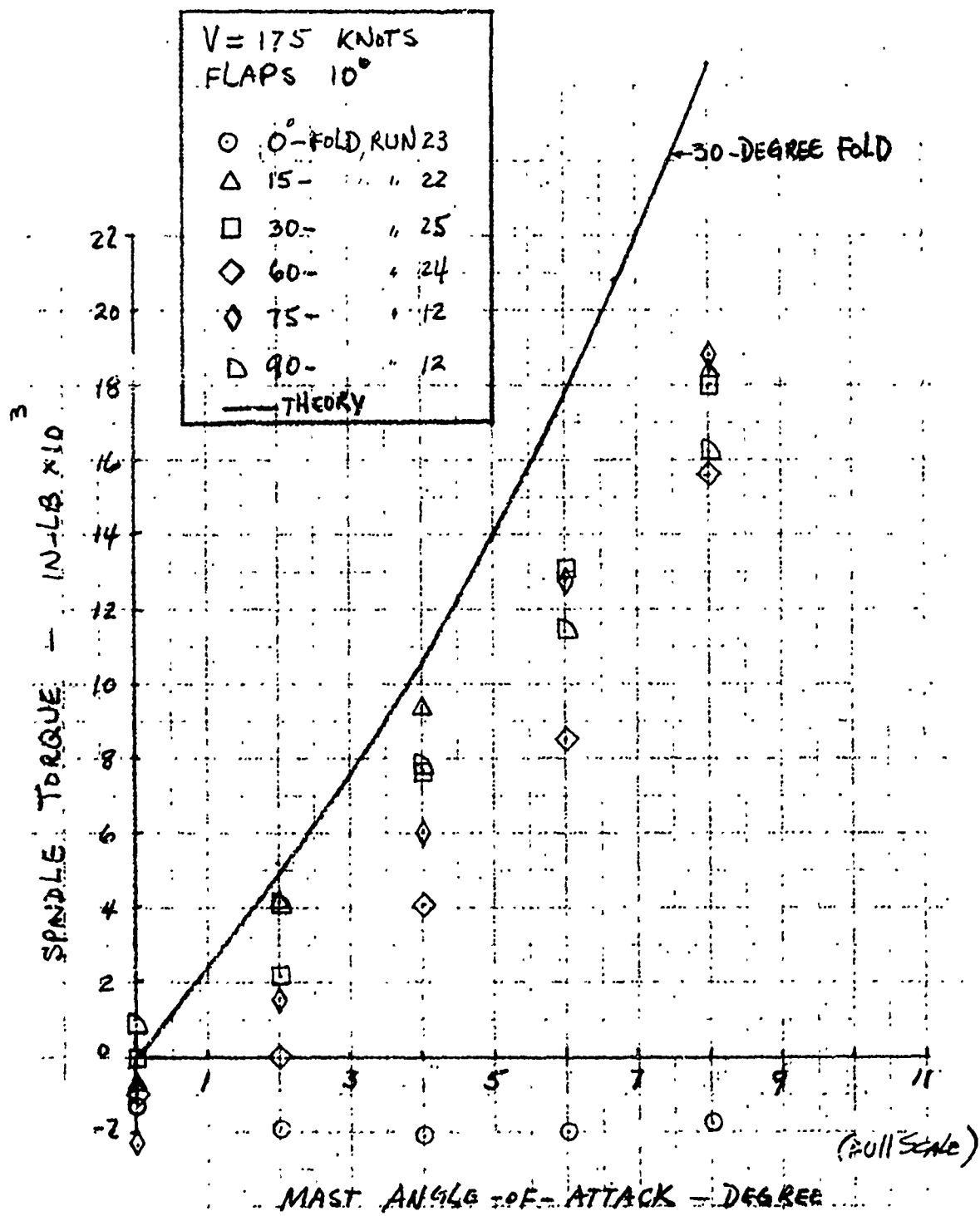


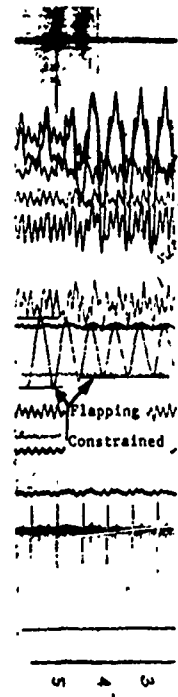
Figure IV-26. Steady Spindle Torque Versus Mast Angle of Attack at Different Fold Angles.

OSCILLOGRAPH 1 - RUN 18			
Channel	Parameter	Oscillograph Trace Scale Factor per Inch	
1	Rotor Torque	125	in-lb
2	Flapping Amplitude	3.8	deg
3	Cyclic Position	5.94	deg
4	Fold Angle	101	deg
5	Collective Position	17.5	deg
6	Blade Beam 35% Radius	37.5	in-lb
8	Blade Beam 50% Radius	29.5	in-lb
9	Blade Beam 75% Radius	13.02	in-lb
10	Blade Chord 35% Radius	92	in-lb
11	Blade Chord 50% Radius	109	in-lb
12	Blade Chord 75% Radius	38.8	in-lb
13	Fold Link Load	479	lb
14	Pitch Link Load	8.57	lb
15	Blade Torsion 35%	40.4	in-lb
16	Rotor rpm	-	

DATA FROM
OSCILLOGRAPH NO. 1 →

SEQUENCE STARTS
WITH ROTOR AT Ω_0 AND →
FLAPPING FREE

FLAPPING RESTRAINT
ENGAGE



CONTIN
ROTOR

OSCILLOGRAPH 2 - RUN 18			
Channel	Parameter	Oscillograph Trace Scale Factor per Inch	
2	Wing Beam 27% Span	697	in-lb
3	Wing Beam 52% Span	656	in-lb
4	Wing Chord 27% Span	2350	in-lb
5	Wing Chord 52% Span	581	in-lb
6	Wing Torsion 27% Span	412	in-lb
7	Wing Torsion 52% Span	924	in-lb
9	Vertical Forward-Pylon Acceleration	2.23	g
10	Horizontal Aft-Pylon Acceleration	1.37	g
11	Conversion Axis Vertical Acceleration	1.63	g
12	Horizontal Forward-Pylon Acceleration	1.97	g
13	Axial Pylon Acceleration	1.25	g
16	Rotor rpm	-	

DATA FROM
OSCILLOGRAPH NO. 2 →

ONE INCH OF
TRACE DEFLECTION

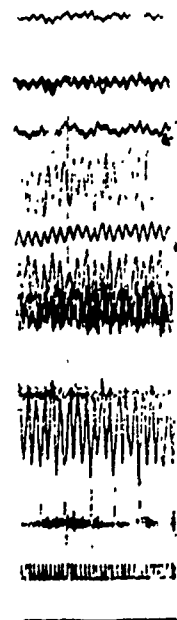
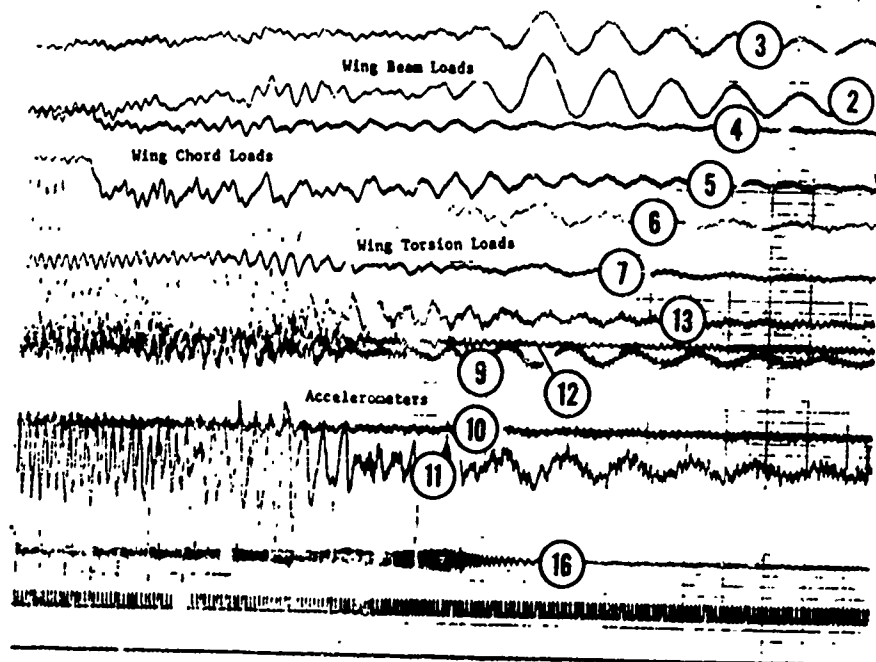
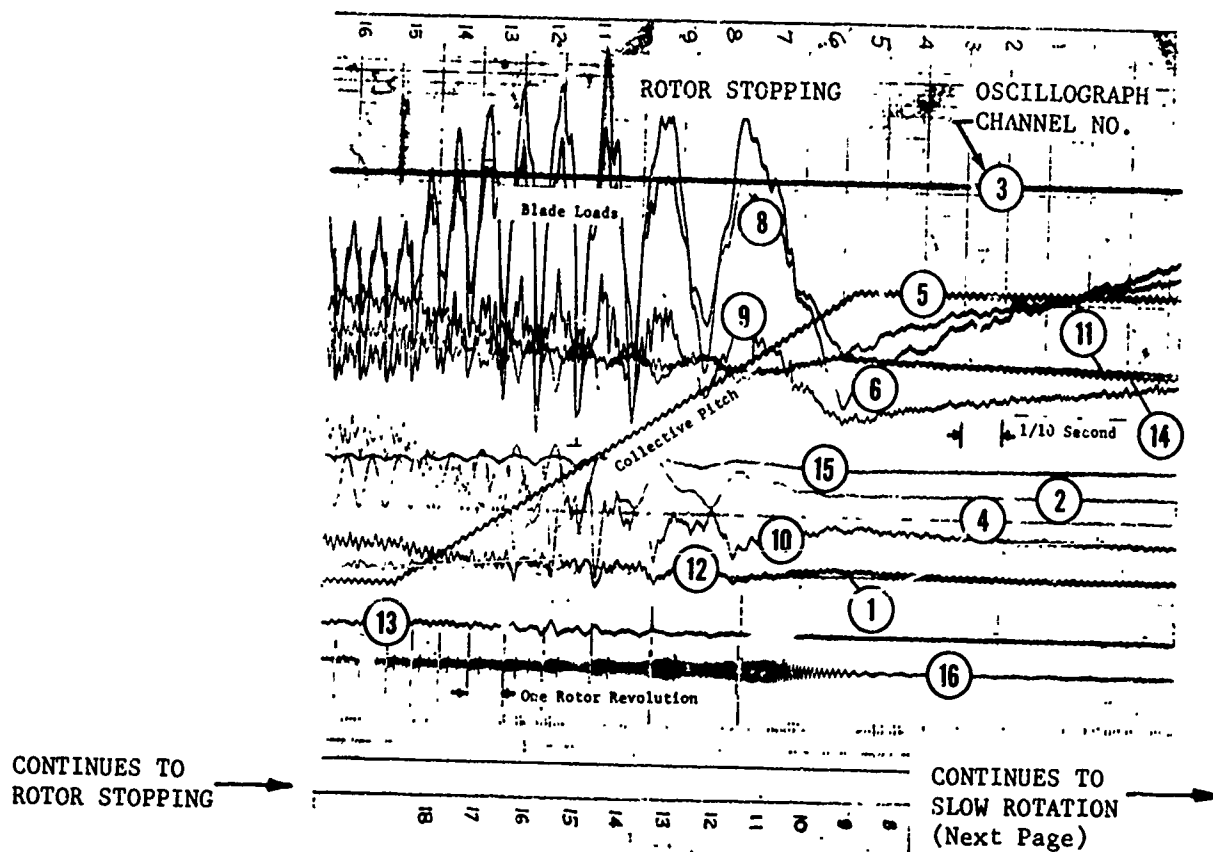


Figure IV-27. Time Histories of Stop-Fold Sequence From Run 18 (

STRAINT



From Run 18 (Wing Alpha, 6 Degrees; Full-Scale Speed, 175 Knots).

IV-52 a

B

C

OSCILLOGRAPH 1 - RUN 15			
Channel	Parameter	Oscillograph Trace Scale Factor per Inch	
1	Rotor Torque	125	in-lb
2	Flapping Amplitude	3.8	deg
3	Cyclic Position	5.94	deg
4	Fold Angle	101	deg
5	Collective Position	17.5	deg
6	Blade Beam 35% Radius	37.5	in-lb
8	Blade Beam 50% Radius	29.5	in-lb
9	Blade Beam 75% Radius	13.02	in-lb
10	Blade Chord 35% Radius	92	in-lb
11	Blade Chord 50% Radius	109	in-lb
12	Blade Chord 75% Radius	38.8	in-lb
13	Fold Link Load	479	lb
14	Pitch Link Load		lb
15	Blade Torsion 35%	40.4	in-lb
16	Rotor rpm		

OSCILLOGRAPH 2 - RUN 18			
Channel	Parameter	Oscillograph Trace Scale Factor per Inch	
2	Wing Beam 27% Span	697	in-lb
3	Wing Beam 52% Span	656	in-lb
4	Wing Chord 27% Span	2350	in-lb
5	Wing Chord 52% Span	581	in-lb
6	Wing Torsion 27% Span	412	in-lb
7	Wing Torsion 52% Span	924	in-lb
9	Vertical Forward-Pylon Acceleration	2.23	g
10	Horizontal Aft-Pylon Acceleration	1.37	g
11	Conversion Axis Vertical Acceleration	1.63	g
12	Horizontal Forward-Pylon Acceleration	1.99	g
13	Axial Pylon Acceleration	1.25	g
14	Rotor rpm		

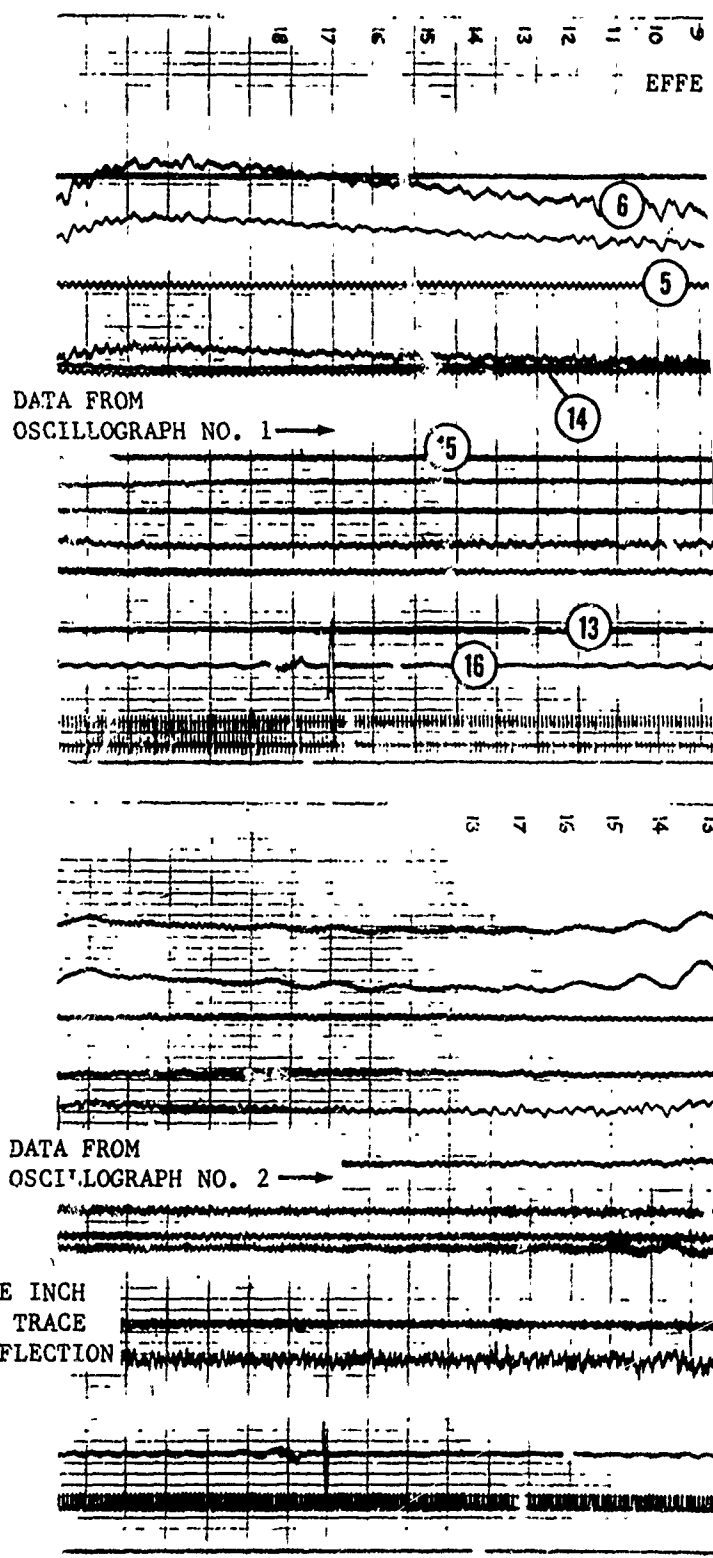
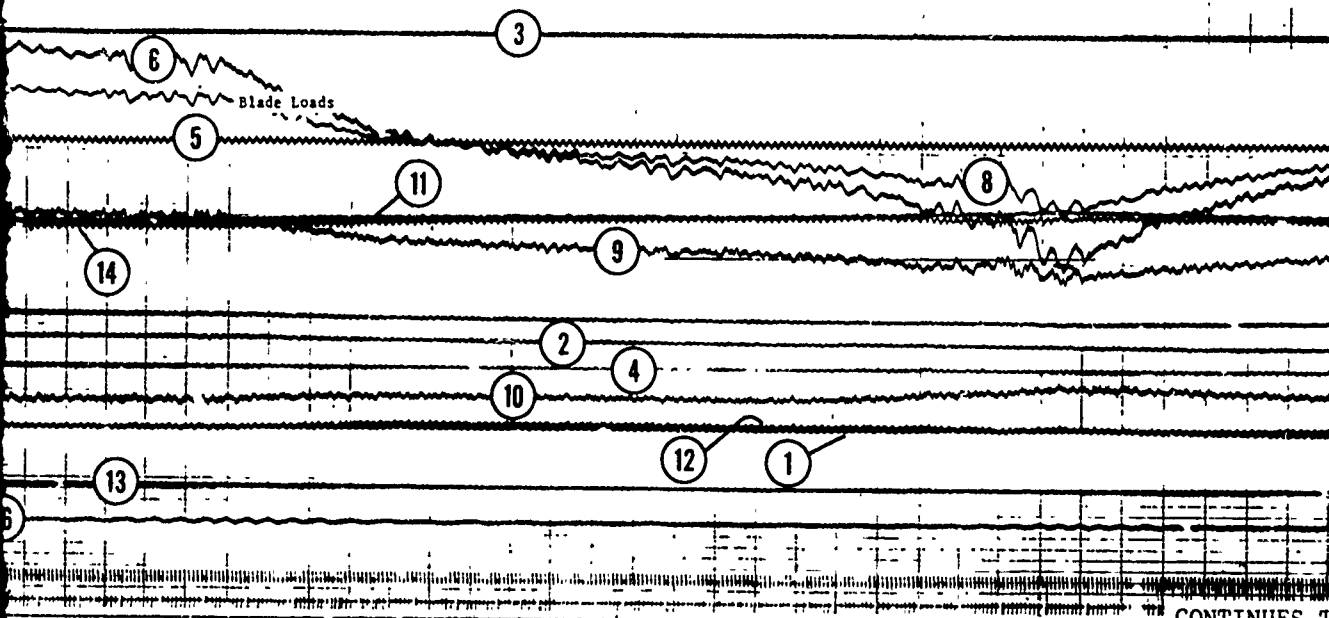


Figure IV-27. Time Histories of Stop-Fold Sequence from Run 18 (W

EFFECT OF WING ROTOR INTERFERENCE
(VERY SLOW ROTATION)



CONTINUES TO ROTATION
LOCK ENGAGED
(Next Page)

ce from Run 18 (Wing Alpha, 6 Degrees; Full-Scale Speed, 175 Knots). Continued

B

IV-53 a

OSCILLOGRAPH 1 - RUN 18			
Channel	Parameter	Oscillograph Trace Scale Factor per Inch	
1	Rotor Torque	125	in-lb
2	Flapping Amplitude	3.8	deg
3	Cyclic Position	5.94	deg
4	Fold Angle	101	deg
5	Collective Position	17.5	deg
6	Blade Beam 35% Radius	37.5	in-lb
8	Blade Beam 50% Radius	29.5	in-lb
9	Blade Beam 75% Radius	13.02	in-lb
10	Blade Chord 35% Radius	92	in-lb
11	Blade Chord 50% Radius	109	in-lb
12	Blade Chord 75% Radius	38.8	in-lb
13	Fold Link Load	479	lb
14	Pitch Link Load	8.57	lb
15	Blade Torsion 35%	40.4	in-lb
16	Rotor rpm	-	

OSCILLOGRAPH 2 - RUN 18			
Channel	Parameter	Oscillograph Trace Scale Factor pe. Inch	
2	Wing Beam 27% Span	697	in-lb
3	Wing Beam 52% Span	656	in-lb
4	Wing Chord 27% Span	2350	in-lb
5	Wing Chord 52% Span	581	in-lb
6	Wing Torsion 27% Span	412	in-lb
7	Wing Torsion 52% Span	924	in-lb
9	Vertical Forward-Pylon Acceleration	2.23	g
10	Horizontal Aft-Pylon Acceleration	1.37	g
11	Conversion Axis Vertical Acceleration	1.63	g
12	Horizontal Forward-Pylon Acceleration	1.99	g
13	Axial Pylon Acceleration	1.25	g
16	Rotor rpm	-	

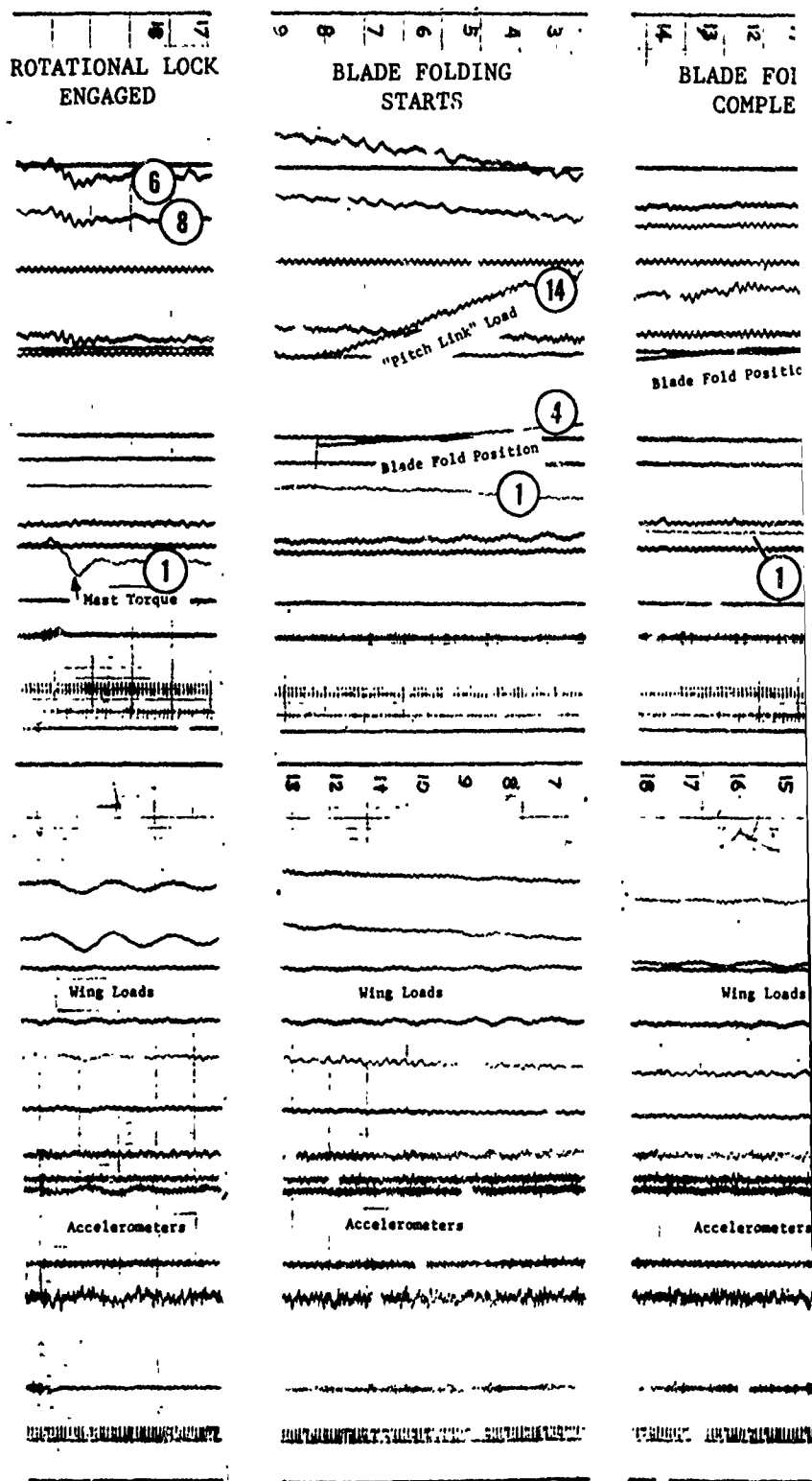


Figure IV-27. Time Histories of Stop-Fold Sequence From Run 18 (Wing Alpha)

D270-099-003

IV-54

BLADE FOLDING
COMPLETE

Blade Fold Position

DATA FROM
OSCILLOGRAPH
NO. 1

BLADES UNFOLD,
ROTATIONAL LOCK
DISENGAGED, AND
CONTINUES TO ROTOR
STARTING

Wing Loads

DATA FROM
OSCILLOGRAPH
NO. 2

Accelerometers

ONE INCH OF
TRACE DEFLECTION

ROTOR STARTING

Blade Loads

Collective Pitch

Rotor Azimuth slips

CONTINUES TO
FLAPPING RESTRAINT
DISENGAGED AND
SEQUENCE CONCLUDED.

Wing Beam Loads

Wing Torsion Loads

Accelerometers

8 (Wing Alpha, 6 Degrees; Full-Scale Speed, 175 Knots). Concluded

IV-54 a

c

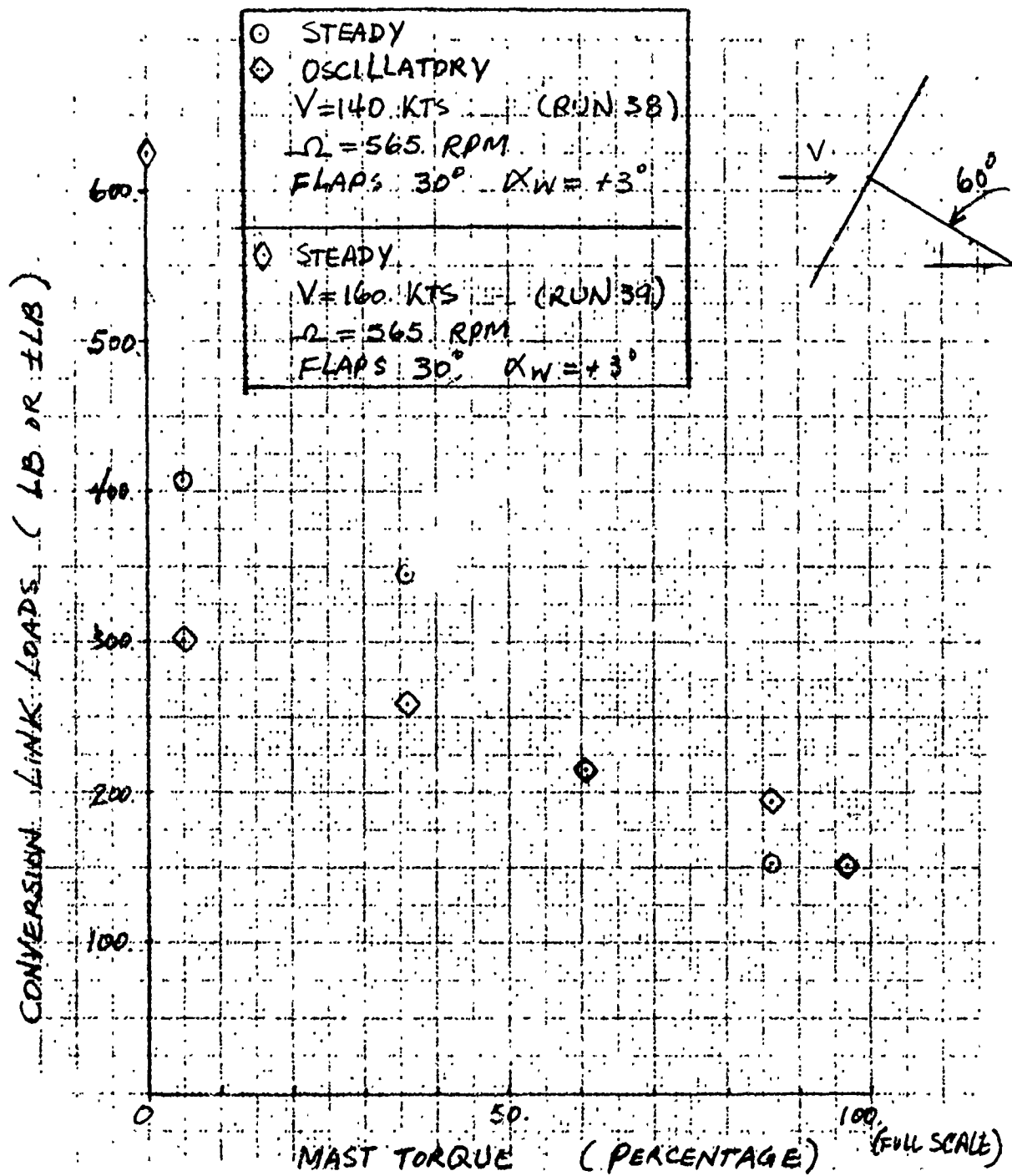


Figure IV-28. Conversion Link Steady and Oscillatory Loads at 60-Degree Conversion Angle.

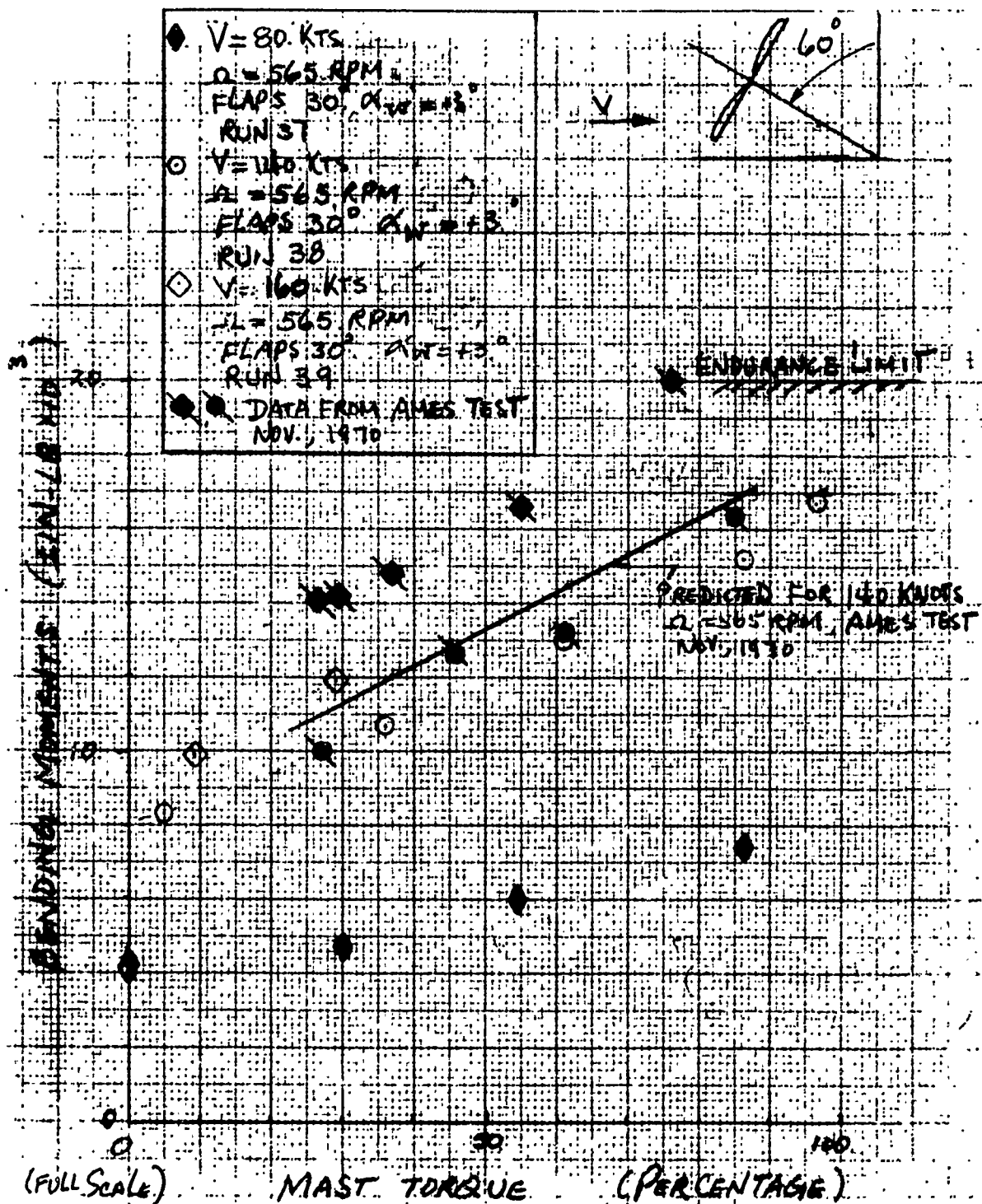


Figure IV-29. Measured Blade Beam Oscillatory Moments at 35-Percent Radius.

V. GENERAL AERODYNAMIC FORCE MODEL TEST

The aerodynamic model tested as part of the Phase II effort is reported in this section. The model was a force and moment airframe model with no rotor rotation involved but with propotor blades folded aft along wing tip nacelles in the high speed cruise mode configuration of the folding propotor aircraft. The purpose of the test was investigation of the aerodynamic characteristics of the wingtip folded blade configuration in cruise mode flight. This section gives a description of the model, run schedule, significant test results including related data plots with corrections included for tares, interference, alignment and wall effects, and conclusions.

A. OBJECTIVES

Objectives of the test were determination of component drag, incremental drag due to folded blades, and stability derivatives with blades in partial and completely folded positions.

B. MODEL DESCRIPTION

1. General

The model tested was a modification of a one-fifth-scale airframe model of the Bell Model 300 tilt-propotor aircraft. Modifications to the tilt-propotor model included changes to the wingtip nacelles, addition of folded blades, and addition of compound jet-engine nacelles mounted beneath the wing panels at an inboard wing station. A photograph of the model installed in the wind tunnel is shown in Figure V-1 and a three view drawing is shown in Figure V-2.

The wingtip nacelles were designed to enclose the transmissions, pylons, and wingtip mechanisms of the aircraft but not to include the gas-turbine engines which in the tilt-propotor configuration are integral with the wingtip propulsion system. There were three blades at each nacelle, and each had scale twist, thickness, airfoil contours. Blade roots were modified for folding in the chord direction. Two configurations of blade fold-hinge radius and trail angle were tested. One had a fold-hinge radius at 15.6 percent radius and blades trailed straight aft from the hinge, parallel to the fuselage waterline. The second configuration had the hinge radius moved toward the pod centerline and the blades folded an additional four degrees. These configurations are identified as AF Pod No. 1 and AF Pod No. 2, respectively. Fairings were constructed between the blade trailing edges and nacelles and to enclose the propotor hub blade-fold mechanism. These were based on a scale kinematic working model of the configuration. During the test, blades could be opened 30 degrees from the folded position.

Flaps, ailerons, horizontal stabilizer, elevator, and rudder were adjustable to fixed incidences. The empennage had a single vertical stabilizer with the horizontal stabilizer mounted above the root. With the wingtip nacelles and blades removed, the model was fitted with a set of wingtip extensions.

The model had smooth wing and fuselage surfaces. For tests with roughness added, boundary layer transition strips consisting of No. 60 grit wire were placed on the wing at the 5-percent chord and on the fuselage for some tests. Vortex generators, when used, were placed on the upper surface of the wing at the 20-percent chord. These had the following dimensions:

Vortex generators - height/wing chord	0.02
Vortex generators - length/height	4.0
Vortex generators - spacing/height	6.0

Recessed adapters in the fuselage accepted bayonets for both normal and inverted two-support-system wind-tunnel mounting and for dummy struts when used for interference and alignment runs. No internal model balances were involved.

For data runs, the model was mounted upright in the wind tunnel test section. A forward support strut positioned the model near the center of the section and was shielded from the wind by a fairing aligned with the airstream. A knurled rear strut was used for the aft support, which was actuated to vary the model angle of attack. Support-strut interference runs were made in the conventional manner with the model inverted and with/without the presence of dummy struts. Alignment data runs were made with the model upright but with the dummy struts installed.

The Vought Aeronautics Division low speed wind tunnel was used for this test. It is a closed single-return facility having tandem test sections of 15 x 20 feet and 7 x 10 feet. The model was mounted in the 7 x 10 foot test section, which operates at atmospheric pressure at speeds up to 240 miles per hour. Test section dynamic pressure was maintained at 50 pounds per square foot during these test runs. The two support struts of the model mounting system extend through the tunnel floor and attach to the wind tunnel facility's six-component force and moment external balance to measure forces and moments. All six components of data were monitored on a visual display and recorded on an IBM typewriter and card punch machine for subsequent data reduction.

2. Dimensions

Table V-1 gives principal dimensions and areas of the model and those used in data coefficients.

The moment resolving center for data reduction, plots, and analysis was model Fuselage Station 58.6 and Waterline 16.3. This point is 0.21-inches aft and 3.26-inches below the one-quarter chord of the model wing MAC and represents an aft center of gravity.

TABLE V-I. MODEL DIMENSIONAL DATA

Overall Model Length	8.38 ft
Overall Model Width with Folded Blades AF Pod No. 1	7.33 ft
Folded-Proprotor and Wingtip Nacelle	
Number of blades per propotor	3
Diameter, if unfolded	5 ft
Fold-hinge radius, AF Pod No. 1 configuration	4.67 in.
Blade chord	2.8 in.
Aerodynamic blade twist from root cutout to tip	27 deg
Direction of rotation if unfolded, inboard tip motion, propotor mode	up
Distance from one-fourth chord of wing MAC to rotor hub	9.46 in.
Hub precone	2.5 deg
Distance from hub to nacelle/spinner leading edge	7.46 in.
Nacelle and spinner length	31.2 in.
Nacelle diameter, maximum	5.43 in.
Wing	
Span with folded blades, AF Pod No. 1	7.33 ft
Span which if multiplied by wing chord will result in wing area used in aerodynamic coefficients	6.874 ft
Span between outermost lines of nacelle spinner	6.85 ft
Span used in yaw and roll moment coefficient, and span between propotor centerlines in airplane mode	6.43 ft
Span of wing with nacelles removed and wingtip extensions installed	6.84 ft
Root chord (BL 5.6)	1.03 ft
Tip chord (BL 41.0)	1.03 ft
Wing area used in aerodynamic coefficients	7.08 sq ft
Mean aerodynamic chord	
Chord (BL 20.55)	1.03 ft
One-fourth chord at fuselage station	58.26
Airfoil section (constant)	NACA 64A223 modified
Aspect ratio	6.63
Forward sweep	6.5 deg
Dihedral	2.167 deg
Incidence	3.0 deg
Twist	0 deg

TABLE V-I. Continued

Aileron

Area per side (aft of hinge line)	0.416 sq ft
Span (along hinge line) (1.608 feet)	19.3 in.
Chord per wing chord	0.25

Flap

Area per side (aft of hinge line)	0.22 sq ft
Span (along hinge line) (0.85 feet)	10.2 in.
Chord per wing chord	0.25

Fuselage

Length (7.62 feet)	91.5 in.
Maximum breadth	13.2 in.
Maximum depth	14.8 in.

Vertical Tail

Span (1.77 feet)	21.2 in.
Total area	2.10 sq ft
Rudder area (aft of hinge)	11.55 sq ft
Rudder chord/total chord	0.25
Aspect ratio	1.49
Sweep of one-fourth chord	42.53 deg
Root chord (WL 15.0)	19.4 in.
Airfoil section	NACA 64A015
Tip chord (WL 36.2)	9.2 in.
Airfoil section	NACA 64A012
Mean aerodynamic chord (WL 24.34)	14.91 in.
Mean aerodynamic chord	
One-quarter chord at fuselage station	105.22
Distance from one-quarter chord of wing mean aerodynamic chord to one-quarter chord of vertical tail mean aerodynamic chord	46.96 in.

Horizontal Tail

Total area	2.0 sq ft
Span (2.87 feet)	34.4 in.
Aspect ratio	4.09
Angle of incidence	0 deg
Elevator area (aft of hinge), total	0.553 sq ft
Elevator chord/total chord	0.30
Root chord (BL 0)	9.80 in.
Airfoil section	NACA 64A015

TABLE V-I. Concluded

Tip chord (BL 17.2)	7.00 in.
Airfoil section	NACA 64A015
Mean aerodynamic chord (BL 8.122) (WL 20.4)	8.48 in.
Mean aerodynamic chord	
One-quarter chord at fuselage station	109.15
Sweep of one-quarter chord line	22.43 deg
Distance from one-quarter chord of wing mean aerodynamic chord to one-quarter chord of horizontal tail mean aerodynamic chord	50.89 in.

C. CONFIGURATIONS TESTED

The test period comprised 80 hours of wind tunnel occupancy time. The sequential run schedule is shown in Table V-II beginning with Run 99 and continuing through Run 331; between these run numbers, those runs with other than Air Force Pods No. 1 and 2 or with no pods, are excepted. The schedule gives a brief description of the purpose of each run, the model configuration, and identifies the run as an angle of attack or yaw sweep. Configuration nomenclature for the test is given in Table V-III. Only data related to Air Force Pods No. 1 and 2 are the subject of the test and subsequent discussion.

A summary tabulation of configurations and variable settings tested is given in Table V-IV arranged according to test purposes. The sequential run schedule orders the test for minimum occupancy time. The summary identifies the data run numbers. It gives the figures (in this Section of the report) on which results are plotted.

Reduced data in the figures of this section and discussed in the following paragraphs include corrections for strut tare and interference, solid and wake blockage, flow alignment, static weight tares and tunnel wall corrections. The tunnel wall corrections due to boundary constraint were derived in accordance with Reference 26 and were applied to angle of attack, drag, and pitching moments. Corrections, additional data plots, and tabulated data in wind, body and stability axes for all data runs are reported in the 1013-page wind tunnel test facility data report, Reference 27. A copy of the report has been forwarded to the Prototype Division of the Air Force Flight Dynamics Laboratory.

TABLE V-II. RUN SCHEDULE

RUN NO	PURPOSE	CONFIGURATION	W	U	REMARKS
1	Tilt Proprotor Exploratory Test	(TS)	0	0	Model tufted, without lower counting plate, q = 75 PSF
2					Model tufted, without lower counting plate, q = 50 PSF
3					Model tufted, begin runs with lower counting plate installed
4					Model tufted
5					
6					
7					
8					
9					
10					
11					
12					
13					
14					
15					
16					
17					
18					
19					
20					
21					
22					
23					
24					
25					
26	Tilt Proprotor Exploratory Test	(TS)	0	0	No data, tuft study only
27					
28					
29					
30					
31					
32					
33					
34					
35					
36					
37					
38					
39					
40					
41					
42					
43					
44					
45					
46					
47					
48					
49					
50					

TABLE V-II. Continued

RUN NO	PURPOSE	CONFIGURATION	RANGE DEG	RANGE DEG	REMARKS
51	Tilt Proprotor Exploratory Test	BWP 30 0 0 V 0 0 F 90 (VO) ₂ (TS) ₁	-9/+21	0	Model tufted
52			0	+2/+12	
53			+6		
54			+12		
55			+18		
56		(AL) ₄₅ (AR) ₁₅	-9/+21	0	
57		(AR) ₁₅			
58					
59					
60		(AL) ₁₅			
61		F ₃₀ (AL) ₃₅ (AR) ₅			
62		F ₃₀ (AL) ₃₅ (AR) ₅			
63		F ₀			
64			0	-2/+12	
65			+6		
66			+12		
67			+18		
68			-9/17	0	q = 100 PSF
69			0	-2/+12	
70			+6		
71			+12		
72			+15		
73		(PT) ₄₅	0	-2/+12	
74			+6		
75			+12		
76	Tilt Proprotor Exploratory Test	BWP 0 0 0 V 0 0 F 90	-9/17	0	q = 100 PSF
77			-9/21	0	
78			0	-2/12	
79			+6		
80			+12		
81			-9/+17	0	q = 100 PSF
82		F ₃₀	-9/+17	0	q = 100 PSF
83			-9/+15		q = 100 PSF
84		(AL) ₄₅ (AR) ₁₅	-9/+21		
85		(AL) ₄₅ (AR) ₁₅ (TS) ₁			
86	Evaluation of Fuselage Fairings	(TS) ₂	-12/+20		
87		F ₀			
88			0	-12/+20	
89			-10		
90			+5		
91			+10		
92			+16		
93	Y & Y's Model Inverted, Image Out		-12/24	0	Begin testing model on two support system
94			0	-12/20	
95			-10		
96			+5		
97			+10		
98			+16		
99		F ₉₀ A ₀	-12/24	0	
100			0	-12/20	

TABLE V-II. Continued

REF NO	PURPOSE	CONFIGURATION				RANGE DEG	RANGE DEG	REMARKS
		M_1	S_1	V_1	P_1			
101	T & I's Model Inverted, Image Out	0	0	0	90	-10	-12/20	T & I
102						5		
103						+10		
104						+16		
105		F_{30}				-12/+24	0	
106						0	-12/+20	
107						-10		
108						+5		
109						+10		
110						+16		
111						-12/+24	0	
112						0	-12/+20	
113						-10		
114						+5		
115						+10		
116						+16		
117		F_0				-12/+24	0	
118						0	-12/+20	
119						-10		
120						+5		
121						+10		
122						+16		
123						-12/+24	0	
124						0	-12/+20	
125						-10		
126	T & I's Model Inverted, Image Out	0	0	0	90	+5	-12/+20	T & I
127						+10		
128						+16		
129	T & I's Model Inverted, Image In					-12/+24	0	
130						0	-12/+20	
131						-10		
132						+5		
133						+10		
134						+16		
135						-12/+24	0	
136						0	-12/+20	
137						-10		
138						+5		
139						+10		
140						+16		
141						-12/+24	0	
142						0	-12/+20	
143						-10		
144						+5		
145						+10		
146						+16		
147						-12/+24	0	
148						0	-12/+20	
149						+10		
150						+5		

TABLE V-II. Continued

ROW NO	PURPOSE	CONFIGURATION	RANGE DEG	RANGE DEG	REMARKS
151	T & I's Model Inverted, Image In	SWP 0 0 0 V 0 0 P 90 0 (TS) ₂	+10	-12/+20	
152			+16		T&I
153			-12/+24	0	
154			0	-12/+20	
155			+5		
156			+10		
157	Ppa Exploratory Tests	P 30 (AL) ₃₅ (AR) ₅	-12/+24	0	
158		P 30 (AL) ₃₅ (AR) ₅	-12/+24	0	
159		P 0	-12/+24	0	Data at 6° -12°, 16°, 20°, & 24° in error
160			0	-12/+20	
161			+5		Void Run
162			+10		
163		(TS) ₂	-12/+20	0	
164			0	-12/+20	
165			+10		
166			0	-12/+20	
167			0	-12/+20	
168	T & I's, Model Inverted, Image Out		-12/+20	0	T&I
169		P 90 0			
170					
171	T & I's, Model Inverted, Image In				
172					
173					
174		P 30 0 0 V 0 0 P 90 0 (TS) ₂	0	-12/+20	
175					
176	T & I's, Model Inverted, Image In	SWP 30 0 0 V 0 0 P 90 0 (TS) ₂	+10	-12/+20	
177			+5		
178			+10		
179			+16		
180			-12/+24	0	
181			0	-12/+20	
182			-10		
183			+5		
184			+10		
185			+16		T&I
186	Evaluation of Flow Through Macelle, Macelle Closed	F 0	-12/24	0	
187			0	-12/20	
188	Alignment Data, Flaps Up		-12/24	0	
189	Alignment Data, Flaps Down 30°	P 30			
190	Component Evaluation, No Macelle	F 0			
191	Component Evaluation, Macelle at Outboard Location				
192	Baseline Data, AF Pod #1, Flaps Up, Without Vortex Gen		0	-12/+20	
193					
194			-10		
195			+5		
196			+10		
197			+16		
198	Component Evaluation, Flaps 50°	P 30	-12/+24	0	
199		P 30	0	-12/+20	
200	Baseline Data, AF Pod #1, Flaps down, Without Vortex Generators	P 30 (AL) ₂₀ (AR) ₂₀	-12/+24	0	

TABLE V-II. Continued

RUN NO	PURPOSE	CONFIGURATION	RANGE DEG	RANGE DEG	REMARKS
201	Baseline Data, A.F. Pod #1, Flaps Down, Without Vortex Generators	BW^2 S_0^2 E_0^2 V_0^2 R_0^2 N_1 (AL) ₂₀ (AR) ₂₀	Q	-12/+20	
202			-10		
203			+5		
204			+10		
205			-16		
206	Component Evaluation, FPR, Effect of Actuator Pairings, A.F. Pod #1, Flaps Down, Vortex Gen Off	(AL) ₂₅ (AR) ₁₅	-13/+24	0	
207		(AL) ₃₅ (AR) ₋₅			Actuator Pairing Off
208		(AL) ₃₅ (AR) ₅			Actuator Pairing Off
209					
210	Component Evaluation, FPR, Effect of Actuator Pairings, A.F. Pod #1, Flaps Up, Vortex Gen Off	F_0	0	12/+20	
211			-12/+24	0	
212		(AL) ₅ (AR) ₋₅			
213		(AL) ₁₅ (AR) ₋₁₅			
214	Baseline Data, FPR, A.F. Pod #1, Flaps Up, Vortex Generator Off				
215	Component Evaluation, FPR, Effect of Macellie, Macellie Off, A.F. Pod #1, Flaps Up, Vortex Gen Off	$S_0 E_0$ $V_0 R_0$ N_1 (TS) ₂	0	-12/+20	
216	Baseline Data, FPR, Effect of Roughness, A.F. Pod #1, Flaps Up, Roughness On		-12/+24	0	
217	Same as 216		0	-12/+20	
218	Baseline Data, FPR, Effect of Roughness, A.F. Pod #1, Flaps Down, Roughness On	F_{50}	-12/+24	0	
219	Same as 218		0	-12/+20	
220	Aileron Control, FPR, A.F. Pod #1, Flaps Down, Roughness On	(AL) ₂₀ (AR) ₂₀	-12/+24	0	
221	Baseline Data, FPR, A.F. Pod #1, Flaps Down, Vortex Generator	(AL) ₃₅ (AR) ₅			
222		(AL) ₂₀ (AR) ₂₀ (VG) ₂	0	-12/20	
223			+5		
224			+10		
225	Aileron Control, FPR, A.F. Pod #1, Flaps Down, Vortex Generator On	(AL) ₂₅ (AR) ₁₅	-12/+24	0	
226	Aileron Control, FPR, A.F. Pod #1, Flaps Down, Vortex Gen On	BW^2 S_0^2 E_0^2 V_0^2 R_0^2 N_1 (AL) ₃₅ (AR) ₅ (VG) ₂	-12/+24	0	
227	Aileron Control, FPR, A.F. Pod #1, Flaps Up Gen On	(AL) ₅ (AR) ₋₅			
228	Same as Run 227	(AL) ₁₅ (AR) ₋₁₅			
229	Elevator Effectiveness, FPR, A.F. Pod #1, Flaps Up, Vortex Gen On	E_{15}			
230		E_5			
231		E_{10}			
232		E_{15}			
233	Rudder Effectiveness, FPR, A.F. Pod #1, Flaps Up Vortex Gen On	E_0 R_5	0	-12/+20	
234		S_5	+10		
235		R_{10}	0		
236		R_{10}	+10		
237	Elevator Effectiveness, FPR, A.F. Pod #1, Flaps Down, Vortex Gen	F_{50} E_5 R_0	-12/+24	0	
238		E_{10}			
239		E_{15}			
240	Aileron Control, A.F. Pod #1, Flaps Down, Vortex Gen On	F_0			
241	Aileron Control, A.F. Pod #1, Flaps Up, Vortex Gen On	(AL) ₃₀ (AR) ₁₀			
242	Baseline Data, FPR, A.F. Pod #1, Flaps Up, Vortex Gen On	(AL) ₁₀ (AR) ₋₁₀			
243			0	-12/+20	
244			+10		
245			+16		
246	Aileron Control, FPR, A.F. Pod #1, Flaps Up Blades Open 150, Vortex Gen On	R_{90}^2 E_{15}	-12/+24	0	
247		(AL) ₅ (AR) ₋₅			
248	Blade Opening Effects, FPR, A.F. Pod #1, Flaps Down, Blades Open 150, Vortex Gen On	(AL) ₁₅ (AR) ₋₁₅			
249		(AL) ₂₀ (AR) ₂₀	-10	-12/20	
250			0		

TABLE V-II. Continued

RUN NO	PURPOSE	CONFIGURATION	RANGE DEG	RANGE DEG	REMARKS
251	Blade Opening Effects, FFR, A.F. Pod #1, Flaps Down, Blades Open 15°, Vortex Gen On	$S_0 F_0$ $V_0 R_0$ $F_{90} R_{15} N_1$ (AL) ₂₀ (AR) ₂₀ (VG) ₂	+5	-12/+20	
252			+10		Void Run
253			+10		Repeat of Run 253
254			+16		Large Hysteresis Effects
255	Aileron Control, FFR, A.F. Pod #1, Flaps Down, Blades Open 15°, Vortex Gen On	(AL) ₂₅ (AR) ₁₅	-12/+24	0	
256	Same as Run 255	(AL) ₃₅ (AR) ₅			
257	Blade Opening Effects, FFR, A.F. Pod #1, Flaps Down, Blades Open 30°, Vortex Gen On	R_{30} (AL) ₂₀ (AR) ₂₀	-10	-12/+20	
258			0		
259			+5		
260			+10		
261			+16		
262					
263	Comparison to Run 221, A.F. Pod #1, Flaps Down, Vortex Gen On, Elevator Inverted	R_0	-12/+24	0	Elevator of Horizontal Stabilizer Invert
264	Elevator Effectiveness, FFR, A.F. Pod #1, Flaps Down, Gen On	E_{-15}			
265	Elevator Effectiveness, FFR, A.F. Pod #1, Flaps Up, Vortex Gen On	E_{-15}			
266	Blade Opening Effects, FFR, A.F. Pod #1, Flaps Down, Blades Open 15°, Vortex Gen Off	F_{30} E_0 R_{15} (AL) ₂₀ (AR) ₂₀	+10	-12/+20	
267			+15	0	
268			+16		
269					
270	Component Evaluation, FFR, Effect of Blades, A.F. Pod #1, Flaps Up, Blades Off, Vortex Gen Off	F_0 (AL) ₀ (AR) ₀	-12/+24		Blade Slots Sealed
271	Component Evaluation, FFR, Effect of Blade & Grips A.F. Pod #1, Flaps Up, Vortex Gen Off		0	-12/+20	
272			-12/+24	0	
273	Component Evaluation, FFR, Effect of A.F. Pod #1, Flaps Up, Vortex Gen Off		0	-12/+20	
274			+10		
275					
276	Component Evaluation, Basic Ship, Effect of Tail Surfaces, Flaps Up, Vortex Gen Off	$S_0 F_0$ $V_0 R_0$ $F_{90} R_{15} N_1$ (AL) ₀ (AR) ₀	-12/+24	0	
277	Component Evaluation, Effect of Engine No. 1, Flaps Up, Tail Surfaces Off, Vortex Gen Off				
278	Baseline Data, Effect of Roughness, Body & Wing Only, Flaps Up, Roughness On				
279	Baseline Data, FFR, Bell Pod #2, Flaps Up, Vortex Gen On	$S_0 F_0$ $V_0 R_0$ $F_{90} R_{15} N_1$ (AL) ₀ (AR) ₀ (TS) ₂	0	-12/+20	
280			+10		
281			+16		
282					
283	Aileron Control, FFR, Bell Pod #2, Flaps Up, Vortex Gen On	(AL) ₂₅ (AR) ₁₅	-12/+24	0	Void
284	Aileron Control, FFR, Bell Pod #2, Flaps Up, Vortex Gen On	(AL) ₃₅ (AR) ₅			Void
285	Aileron Control, FFR, Bell Pod #2, Flaps Down, Vortex Generators On	(AL) ₃₅ (AR) ₅			
286	Same as Run 285	(AL) ₂₅ (AR) ₁₅			
287	Aileron Control, FFR, Bell Pod #2, Flaps Down, Blades Open 15°, Vortex Gen On	R_{15} (AL) ₂₅ (AR) ₁₅			
288	Same as Run 287	(AL) ₃₅ (AR) ₅			
289	Blade Opening Effects, FFR, Bell Pod #2, Flaps Down, Blades Open 15°, Vortex Gen On	(AL) ₂₀ (AR) ₂₀	-10	-12/+20	
290		(AL) ₂₀ (AR) ₂₀			
291			0		
292			+5		
293			+10		
294			+16		
295	Aileron Control, FFR, Bell Pod #2, Flaps Up, Blades Open 15°, Vortex Gen On	F_0 (AL) ₂₅ (AR) ₁₅	-12/+24	0	
296	Baseline Data, Basic Ship, Pods Off, Flaps Up, Vortex Gen Off	(AL) ₀ (AR) ₀		0	
297			0	-12/+20	
298			+15	-12/+12	
299	Aileron Control, FFR, Bell Pod #2, Flaps Up, Blades Open 15°, Vortex Gen On	$F_{90} R_{15} N_1$ (AL) ₁₅ (AR) ₋₁₅ (VG) ₂	-12/+24	0	

Reproduced from
best available copy.

TABLE V-II. Concluded

RUN NO	PURPOSE	CONFIGURATION	BARGE DEG	BARGE DEG	REMARKS
300	Blade Opening Effects, FPR, Bell Pod #2, Flaps Up, Blades Open 15°, Vortex Gen On	$W_0, S_0, E_0, V_0, R_0, F_{90}, A_1, N_1, (AL)_0, (AR)_0, (VQ)_2$	-12/+24	0	
301			-10	-12/+20	
302			0		
303			+5		
304			+10		
305			+16		
306	Blade Opening Effects, FPR, Bell Pod #2, Flaps Up, Blades Open 30°, Vortex Gen On	F_{30}	-12/+24	0	
307			-10	-12/+20	
308			0		
309			+5		
310			+10		
311			+16		
312	Blade Opening Effects, FPR, Bell Pod #2, Flaps Down, Blades Open 30°, Vortex Gen On	$F_{30}, (AL)_{20}, (AR)_{20}$	-12/+20	0	
313			-10	-12/+20	
314			0		
315			+5		
316			+10		
317			+16		
318	Aileron Control, FPR, Bell Pod #2, Flaps Up	$F_0, \beta_0, (AL)_{15}, (AR)_{-15}$	-12/+24	0	
319		$\beta_0, (AL)_5, (AR)_5$			
320	Baseline Data, FPR, A.F. Pod #2, Flaps Up, Blades Folded -4°, Vortex Gen On	F_{90}, β_{-4}			
321			-10	-12/+20	
322			+10		
323			+16		
324	Baseline Data, FPR, A.F. Pod #2, Flaps Up, Blades Folded -4°, Vortex Gen Off	$W_0, S_0, E_0, V_0, R_0, F_{90}, A_1, N_1$	-12/+24	0	
325			0	-12/+20	
326			-10		
327			+5		
328			+10		
329			+16		
330	Component Evaluation, Effect of Macallie Location, FPR, AF Pod #2, Blades Folded, Vortex Gen Off	N_h	-12/+24	0	
331	Same as Run 330	N_h	0	-12/+20	
332	Baseline Data, Tilting Proprotor, Bell Pod #1, Flaps Up, Vortex Gen Off	F_{90}, A_1, N_1	-12/+24	0	
333	Same as Run 332	F_{90}, A_1, N_1	0	-12/+20	
334	Baseline Data, 300 FPR, Bell Pod #2, Flaps Up, Vortex Gen Off	F_{90}, A_1, N_1	-12/+24	0	
335			0	-12/+20	
336			+5		
337			+10		
338	Baseline Data, 300 FPR, Bell Pod #2, Flaps Down, Vortex Gen Off	$F_{30}, (AL)_{20}, (AR)_{20}$	-12/+24	0	
339			0	-12/+20	
340			+5		
341		$W_0, S_0, E_0, V_0, R_0, F_{90}, A_1, N_1, (AL)_{20}, (AR)_{20}$	+10		

TABLE V-III. NOMENCLATURE

Configuration

B	fuselage on
BL	blades and grip on
CF	conversion actuator fairings off
f	blade faired to pod
GO	blade grips on
N ₁	jet engine nacelle, flow through, on
N ₂	jet engine nacelle on but plugged and faired
N ₃	same as N ₁ but three inches outboard
N ₄	same as N ₁ but four inches below that of N ₁
P ₁	Bell tilt propotor pod on
P ₂	Air Force Pod No. 1 on
P ₃	Bell tilt propotor pod with folded blades, on
P ₄	Air Force Pod No. 2 on
(PT) ₄₅	Forty-five degree antidiheral pod trip plate on
S	horizontal stabilizer on
(TS) ₁	boundary layer transition strip on wing
(TS) ₂	boundary layer transition strip on wing and fuselage
V	vertical stabilizer on
(VG) ₁	partial open vortex generators on
(VG) ₂	full open vortex generators on
W	wing on

Variable

AR	left aileron, plus trailing edge down
AL	right aileron, plus trailing edge down
β	blade fold angle, degrees open from folded position
E	elevator, plus trailing edge down
F	flaps, plus trailing edge down
R	rudder, plus for positive side force
S	horizontal stabilizer, plus trailing edge down
V	vertical stabilizer

TABLE V-IV. SUMMARY OF CONFIGURATIONS AND VARIABLE SETTINGS TESTED - FOLDING PROTOTROR CONFIGURATION - AP POD #0, 1 AND 2

Purpose of Test	Configuration	Boundary Layer Condition		Test Run and Figure Number V-													
				α Sweep											φ Sweep		
				Figure No.													
		Model Surface Clean	Roughness Applied	Vortex Generators On	F	AL	AR	β	S	E	V	R	Run No.	C _L , C _D , and C _H Versus α	C _{RM} Versus C _L	Run No.	C _{RM} and C _{TH} Versus φ
Component Characteristics	BW S V	x	x		0	0	0	0	0	0	0	0	277	20,33,37		297	42
	BW S V	x	x										296	18,31,37,41		298	
	BW S V P90 ² BL N ₁	x	x				0					190	18,30,36,41		193	5,27,28,29	
	BW S V P90 ² BL N ₁	x	x									192	3,17,24,25,26,30,35		194	4	
	BW S V P90 ² BL N ₁	x	x												195	6	
	BW S V P90 ² BL N ₁	x	x												196	7	
	BW S V P90 ² BL N ₁	x	x												197	8	
	BW S V P90 ² BL N ₁	x	x												211		
	BW S V P90 ² BL N ₁	x	x												187		
	BW S V P90 ² BL N ₁	x	x														
	BW S V P90 ² BL N ₁	x	x														
	BW S V P90 ² BL N ₁	x	x														
	BW S V P90 ² BL N ₁	x	x														
	BW S V P90 ² BL N ₁	x	x														
	BW S V P90 ² BL N ₁	x	x														
Flap Effects	BW S V P90 ² BL N ₁	x	x														
	BW S V P90 ² BL N ₁	x	x														
	BW S V P90 ² BL N ₁	x	x														
	BW S V P90 ² BL N ₁	x	x														
	BW S V P90 ² BL N ₁	x	x														
	BW S V P90 ² BL N ₁	x	x														
	BW S V P90 ² BL N ₁	x	x														
	BW S V P90 ² BL N ₁	x	x														
	BW S V P90 ² BL N ₁	x	x														
	BW S V P90 ² BL N ₁	x	x														
	BW S V P90 ² BL N ₁	x	x														
	BW S V P90 ² BL N ₁	x	x														
	BW S V P90 ² BL N ₁	x	x														
	BW S V P90 ² BL N ₁	x	x														
	BW S V P90 ² BL N ₁	x	x														

TABLE V-IV. Concluded

Purpose of Test	Configuration	Boundary Layer Condition	Test Run and Figure Number V-									
			α Sweep					ϕ Sweep				
			Variable Setting		Figure No.		Figure No.		Figure No.		Figure No.	
			F	AL	AR	β	S	E	V	R	Run No.	Run No.
Blade Opening Effect	BW S V P902 BL N1	Model Surface Roughness Clean Applied On	50	20	20	15	0	0	0	0	266	267, 268
											269	269
											270	270
											271	271
Aileron Characteristics	BW S V P902 BL N1 CF	Model Surface Roughness Clean Applied On	50	20	20	15	0	0	0	0	212	53
											213	53
											214	53, 55, 58
											215	53, 55, 58
Elevator Characteristics	BW S V P902 BL N1	Model Surface Roughness Clean Applied On	50	20	20	15	0	0	0	0	206	54
											207	54, 7
											208	57
											209	54, 56, 59
Rudder Characteristics	BW S V P902 BL N1	Model Surface Roughness Clean Applied On	50	20	20	15	0	0	0	0	225	54, 56, 57, 59
											226	54
											227	55
											228	55, 60

(1) C_M only (2) C_{RM} only (3) C_{YM} only

D. TEST RESULTS AND ANALYSIS

The test results presented herein are the significant results of the test to the extent that could be determined with the available resources.

1. Aerodynamic Characteristics and Stability Derivatives of Complete Aircraft with Blades Folded

Aerodynamic characteristics and stability derivatives of the complete model in the folding-prop rotor configuration are presented in Tables V-V and V-VI. For these data, flaps are up and blades are folded aft along the wingtip nacelles. Table V-VII presents the characteristics with flaps down 50 degrees and ailerons down 20 degrees. All slopes in the tables are average values taken between ± 2 degrees and are derived from Figures V-3 through V-16, and Figures V-47 through V-51. The data are the basis for subsequent comparisons and analysis of the effects of individual components, the effects of opening the blades, and the full-scale analyses.

2. Component Lift, Drag, and Pitching Moment

a. Wingtip Pods Including Blades

The singular contributions of the wingtip pods including folded blades to lift, drag, and pitching moment of the configuration are shown in Figures V-17 through V-23 and summarized in Table V-VIII.

As expected, the additional area or end plate effect of the pods and blades results in lift and drag increases. As will be found in the next section, part is due to the nacelle (transmission cowling and spinner) and part to the blades. A complete theoretical analysis of the effect on lift has not been completed; however, a comparison of test and predicted values of drag is included in a later section.

The pods cause a pitch trim change, but their contribution to pitch stability varies depending upon the presence of other components. When the stabilizer is off, the pods decrease longitudinal stability. However when the stabilizer is on, they have practically no effect--for an angle of attack range of 0 to 4 degrees. At greater or lesser angles, they are slightly destabilizing. The conclusion is that, while the pods are destabilizing, the interference effects created on the horizontal stabilizer result in almost no change in pitch stability.

b. Blades Only

Table V-IX shows the contribution of the blades. These data are derived from Figures V-24 through V-29.

The increase in drag due to both blades and wingtip nacelles is 18.1 percent at a cruise angle of attack of 0 degrees. From this, one calculates that the blade and nacelle drag represents 15 percent of total aircraft drag in cruise. (At higher lift coefficients, their drag contribution is a much smaller percentage.) Of the total drag increase, that due to just the blades is about 25 percent and the remainder is due to the nacelles.

TABLE V-V. CHARACTERISTICS OF COMPLETE AIRCRAFT, FLAPS UP,
MODEL CLEAN

Aerodynamic Coefficient or Stability Derivative	Air Force Pod No. 1 Value	Air Force Pod No. 2 Value
$C_{L\alpha}$ at $\psi = 0$	0.095/deg	0.088/deg
$C_{L_{MAX}}$ at $\psi = 0$	1.54	1.50
C_D at $\alpha, \psi = 0$	0.047	0.054
f-full-scale	8.26 ft ²	9.50 ft ²
$C_{M\alpha}$ at $\psi = 0$	-1.92/rad	-1.83/rad
$(C_{RM})\psi$ at $\alpha = 0$	0.186/rad	0.135/rad
$(C_{YM})\psi$ at $\alpha = 0$	-0.056/rad	-0.086/rad
$(C_{RM})\psi$ at $\alpha = -11^\circ$	-0.016/rad	0.028/rad
$(C_{YM})\psi$ at $\alpha = -11^\circ$	-0.201/rad	-0.122./rad
$(C_{RM})\psi$ at $\alpha = 5^\circ$	0.227/rad	0.224/rad
$(C_{YM})\psi$ at $\alpha = 5^\circ$	-0.018/rad	-0.036/rad
$(C_{RM})\psi$ at $\alpha = 10^\circ$	0.330/rad	0.344/rad
$(C_{YM})\psi$ at $\alpha = 10^\circ$	-0.066/rad	-0.079/rad
$(C_{RM})\psi$ at $\alpha = 17^\circ$	0.244/rad	0.259/rad
$(C_{YM})\psi$ at $\alpha = 17^\circ$	-0.008/rad	0.037/rad

TABLE V-VI. CHARACTERISTICS OF COMPLETE AIRCRAFT, FLAPS UP, VORTEX GENERATORS ON

Aerodynamic Coefficient or Stability Derivative	Air Force Pod No. 1 Value
$C_{L\alpha}$ at $\psi = 0$	0.098/deg
C_{LMAX} at $\psi = 0$	1.76
C_D at $\alpha, \psi = 0$	0.063
f-full scale*	11.09 ft ²
$C_{M\alpha}$ at $\psi = 0$	-1.50/rad
$(C_{RM})_\psi$ at $\alpha = 0$	0.189/rad
$(C_{YM})_\psi$ at $\alpha = 0$	-0.074/rad
$(C_{RM})_\psi$ at $\alpha = 11^\circ$	0.242/rad
$(C_{YM})_\psi$ at $\alpha = 11^\circ$	-0.034/rad
$(C_{RM})_\psi$ at $\alpha = 17^\circ$	0.121/rad
$(C_{YM})_\psi$ at $\alpha = 17^\circ$	-0.014/rad
*Based on a one-fifth-scale model	

TABLE V-VII. CHARACTERISTICS OF COMPLETE AIRCRAFT,
FLAPS DOWN, AIR FORCE POD NO. 1

Aerodynamic Coefficient or Stability Derivatives	Model Clean Values	Vortex Generators On Values
$C_{L_{\alpha}}$ at $\psi = 0$	0.088/deg	0.094/deg
$C_{L_{MAX}}$ at $\psi = 0$	1.80	2.12
C_D at $\alpha, \psi = 0$	0.132	0.145
f-full scale*	23.21 ft ²	25.49 ft ²
$C_{M_{\alpha}}$ at $\psi = 0$	-1.53/rad	-1.26/rad
$(C_{RM})_{\psi}$ at $\alpha = 1$	0.260/rad	0.298/rad
$(C_{YM})_{\psi}$ at $\alpha = 1$	-0.118/rad	-0.069/rad
$(C_{RM})_{\psi}$ at $\alpha = 6^{\circ}$	0.144/rad	0.189/rad
$(C_{YM})_{\psi}$ at $\alpha = 6^{\circ}$	-0.155/rad	-0.057/rad
$(C_{RM})_{\psi}$ at $\alpha = 11^{\circ}$	0.283/rad	0.201/rad
$(C_{YM})_{\psi}$ at $\alpha = 11^{\circ}$	-0.104/rad	-0.002/rad
*Based on one-fifth-scale model		

TABLE V-VIII. SUMMARY OF WINGTIP POD CONTRIBUTIONS
TO LONGITUDINAL CHARACTERISTICS

Aerodynamic Characteristics	Air Force Pod No. 1	Air Force Pod No. 2
$\Delta C_{L_{\alpha}}$ at $\psi = 0$ per deg	0.027	0.002
$\Delta C_{L_{MAX}}$ at $\psi = 0$	0.23	0.17
ΔC_D at $\psi = 0$	0.007	0.014
ΔC_M at $\psi = 0$ per rad	-0.114	-0.029

TABLE V-IX. CHANGE IN LONGITUDINAL AND LATERAL CHARACTERISTICS
DUE TO FOLDED BLADES

Aerodynamic Coefficient or Stability Derivative (1)	Percent Change in Coefficient			
	Reference Configuration (2)	Add Wingtip Pods but no Blades or Blade Grips	Add Blade Grips Only (3)	Add Blades
$C_{L\alpha}$	0	7.7	10.3	23.1
$C_{L_{MAX}}$	0	7.5	9.0	16.4
C_D at $\alpha = 0$	0	13.1	36.9	18.1
C_D at $\alpha = 6$	0	9.8	25.8	22.7
C_D at $C_L = 0.6$	0	4.9	21.3	5.7
C_M	0	Negligible	Negligible	Negligible
C_Y	0	5.5	-	44.9
$(C_{RM})\psi$	0	13.0	-	41.3
$(C_{YM})\psi$	0	19.5	-	47.2
<p>(1) A positive sign indicates a "more positive" slope. Drag coefficients and stability derivatives are at α and/or $\psi = 0$.</p> <p>(2) Complete aircraft less wingtip pods and blades.</p> <p>(3) Grips had blunt afterbodies.</p>				

c. Jet Engine Nacelles

The general effects produced by the presence of these nacelles are to (1) slightly decrease the lift-curve slope at low to moderate angles of attack, (2) decrease maximum lift coefficient, (3) increase drag in most cases, (4) increase static longitudinal stability at low angles of attack when the empennage is present, and (5) cause no noticeable change in static longitudinal stability at high angles of attack when the empennage is present and at all angles when the empennage is not present. Data are presented in Figures V-30 through V-33.

The summary curve in Figure V-34 shows two unusual effects. They are: (1) a favorable interference between the wing and nacelles as evidenced by a decreasing and low value of drag due to the nacelle at angles of

attack between 0 and 10 degrees, and (2) a favorable but nonlinear interference of the nacelles at low angles of attack so as to increase static longitudinal stability with the empennage on. It appears that the latter may be related to a reduction in downwash at the tail, as indicated by the slight reduction in lift-curve slope over the same angle.

Effects of changing nacelle configuration and location were investigated. Three changes were made. One involved plugging the inlets and outlets and adding forebody and afterbody fairings. This change then made the nacelle equivalent to a streamlined body having a diameter-to-length ratio of 0.4. Other changes involved relocation of the nacelles three inches outboard (at the same distance below the wing), and lowering of the nacelles four inches (at the same wing spanwise station). Results of these tests are that the streamlined nacelles made small changes in comparison to that for the model with flow-through nacelles. Moving the nacelle outboard three inches had no appreciable effect, and lowering the nacelle four inches has no appreciable effect on either longitudinal or lateral characteristics.

d. Empennage

Figures V-35 through V-37 show the contribution of the empennage. There are some differences depending upon the configuration of the model when the tail was removed, and these are summarized in Figure V-38.

A comparison was made of measured and theoretical values of the horizontal stabilizer contribution to static stability. For the fuselage-wing-empennage combination, the measured horizontal stabilizer contribution to $C_{M\alpha}$ is -2.45/radian, determined by taking the slope of the difference between Run 296 (tail on) and Run 277 (tail off). This difference is plotted as a solid line in Figure V-39. The calculated horizontal-stabilizer contribution to pitching moment is shown by the dashed line. The calculation was based on the following:

$$(C_M)_{STAB} = -a_t \frac{A_t l_t}{A_w \bar{c}} (\alpha - \epsilon) \eta_q$$

where

a_t = three-dimensional lift curve slope of stabilizer

A_t = stabilizer area (2.00 ft², model scale)

l_t = stabilizer moment arm (4.29 ft, model scale)

A_w = wing area (7.06 ft², model scale)

\bar{c} = wing chord (1.03 ft, model scale)

α = fuselage angle of attack

ϵ = downwash angle on stabilizer

η_q = dynamic pressure efficiency at stabilizer

A lift curve slope, a_t of 0.061 per degree was used for the stabilizer which has an aspect ratio of 4.1 and a sweep of 25 degrees. The downwash angle, ϵ , was estimated as a function of wing lift by use of charts in Appendix B.6 of Reference 21. Wing lift was derived from the lift of Run 277 corrected to account for fuselage lift. Results of the downwash calculation are shown in Figure V-40. At $\alpha = 0$, the value of $\partial\epsilon/\partial\alpha$ is approximately 0.29.

e. Comparison of Component Drag with Predictions

(1) Wing

Table V-X shows comparisons of wind-tunnel test and predicted values of lift curve slope, and change in lift coefficient with flap deflection for the model wing without wingtip pods and engine nacelles.

The test values indicate that 100-percent carry through is affected by the fuselage.

The effect of roughness on the wing is greater than predicted. With roughness, the measured value of $C_{L\alpha}$ is sensitive to the value used for the two-dimensional slope of the lift curve of the wing airfoil section at the Reynolds number of the model test. On this, very little data are available.

Flap effectiveness varies as a function of angle of attack. (The slope of the lift curve with flaps up is not the same as that with flaps down.) Values of $C_{L\delta}$ shown in the table are averages of two values. For the wing alone, the low value was 0.0157, measured at the angle of attack for zero lift with flaps up, and the high value was 0.0174, measured at a zero angle of attack. For the wing and fuselage, the values were 0.0217 to 0.0230. In either case, measured values of flap effectiveness are greater than predicted.

TABLE V-X. COMPARISON OF MEASURED AND PREDICTED VALUES OF LIFT CURVE SLOPE AND FLAP EFFECTIVENESS FOR THE WING

	Aerodynamic Characteristic			
	$C_{L\alpha}^*$		$C_{L\delta}$	
	Wing Alone /deg	Wing-Fuselage /deg	Wing Alone /deg	Wing-Fuselage /deg
Measured Values				
With leading edge roughness	0.058	0.058	0.0165	0.0223
Clean configuration	-	0.076	-	-
Predicted Values				
Using Reference 21				
Wing transition at 0.05C	0.066	0.066	-	-
With transition at 0.5C	0.071	0.071	-	-
Using Reference 22	-	-	0.0137	0.0202
Using References 21 and 22	-	-	0.0143	0.0202
*at $\alpha = 0$				

(2) Other Components

Comparisons for the other components are given in Table V-XI. Predicted values were derived during or from related work, as indicated by the references shown in the Table.

TABLE V-XI. COMPARISON BETWEEN MEASURED AND PREDICTED
CRUISE DRAG DATA⁽¹⁾

Component	Measured Drag Coefficient ⁽²⁾	Predicted Drag Coefficient	
		Values	Reference
Wing	0.0115	0.0120	23
Fuselage	0.0104	0.0127	23
Air Force Pod No. 1	0.0060	0.0064	18
Air Force Pod No. 2	0.0115	-	
Empennage ⁽³⁾	0.0026	0.0053	23
Engine Nacelles	0.0034	0.0020	24

(1) All data are based on a full-scale wing area of 176 ft². This value includes fuselage carry through and pod carry through out to outer edge of pod spinner.

(2) The measured drag data have been corrected for Reynolds number and trim conditions.

(3) This value listed for Bell Pod No. 1.

3. Component Contributions to Lateral Stability

a. Yaw Stability

(1) Wingtip Pods for Folded Blades

For cruise angles of attack, the basic airframe (fuselage-wing-empennage) has some yaw stability ($C_{Y\beta} = 0.046$ per radian). This is shown in Figure V-42 and Table V-XII.

Addition of Pod No. 1 with blades folded reduces stability and essentially makes the aircraft neutrally stable for small to moderate yaw angles. The change in yaw stability is approximately 18 percent of the tail contribution to $C_{Y\beta}$.

TABLE V-XII. BASELINE DATA, BASIC AIRFRAME

Aerodynamic Coefficient or Stability Derivative	Basic ⁽¹⁾ Airframe value ⁽²⁾	Addition of Blade Pods Alone value ⁽²⁾	Addition of Jet Engine Nacelles Alone value ⁽²⁾	Addition of Blade Pods and Jet Engine Nacelles value ⁽²⁾
$C_{L\alpha}$ at $\psi = 0$	0.082/deg	0.098/deg	0.079/deg	0.095/deg
$C_{L_{MAX}}$ at $\psi = 0$	1.37	1.56	1.33	1.54
C_D at $\alpha, \psi = 0$	0.035	0.045	0.039	0.047
f-full scale ⁽³⁾	6.16 ft ²	7.92 ft ²	6.86 ft ²	8.26 ft ²
$C_{M\alpha}$ at $\psi = 0$	-1.47/rad	-1.56/rad	-1.88/rad	-1.92/rad
$(C_{RM})_\psi$ at $\alpha = 0$ ⁽⁴⁾	0.127/rad	0.184/rad	0.127/rad	0.186/rad
$(C_{YM})_\psi$ at $\alpha = 0$ ⁽⁵⁾	-0.046/rad	0	-0.095/rad	-0.045/rad
<p>(1) Fuselage plus wing plus empennage, model clean</p> <p>(2) Model wing reference areas and lengths are: $S = 7.08 \text{ ft}^2$, $\bar{c} = 1.03 \text{ ft}$, and $b = 6.43 \text{ ft}$</p> <p>(3) Length scale factor of one-fifth</p> <p>(4) Effective wing dihedral angle (degree) $\cong -(C_{RM})_\psi / 0.016$</p> <p>(5) Contribution of vertical stabilizer to $(C_{YM})_\psi \cong -0.25/\text{rad}$</p>				

Cause of the reduction in stability may be an increased sidewash effect on the fin, mostly due to the blades. This is indicated in Figure V-28 which shows that removal of the folded blades alone increases stability from $C_{n\beta} = 0.056$ per radian to 0.080 per radian. Thus, the effects of the blades are destabilizing, and most of the destabilizing contribution of the pod-blade combination seems to be caused by the blades.

A summary of pod effects is included in Table V-XIII, along with a summary of the effects of other components.

(2) Engine Nacelles

One might expect the engine nacelles to produce a decrease in stability in that the side forces on the nacelles might increase the sidewash gradient at the fin. However, the nacelles actually produced a large increase in yaw stability. No data are available to determine how much of the change is due to improvement in the flow conditions at the fin. The increase appears to be present with or without the wing-tip-pods. The addition of the nacelles to the basic airframe results in an increase in $C_{n\beta}$ from 0.046 per radian to 0.095 per radian, which is equivalent to a 20 percent increase in fin effectiveness. On the aircraft with Pod No. 1, the difference between the nacelles-off and nacelles-on static stability is even larger -- a $C_{n\beta}$ of 0.064 or 26 percent of the fin effectiveness. Additional testing would be required to determine to which parameters the change is sensitive.

(3) Vertical Stabilizer

The vertical stabilizer effectiveness and flow conditions were examined in a prior test with the same fuselage, empennage, and wing. Consequently, it was not investigated again during this test. The previous findings are reported in Reference 25.

From the results of the prior tests, the vertical stabilizer configuration used in this test was known to provide low yaw static stability at small sideslip angles, particularly at high angles of attack; however, for generic tests, this was believed to be acceptable for the purpose of examining the effects of other components on lateral characteristics. Consequently, the actual levels of static stability of the model tested should be considered secondary to the changes noted for the different aircraft components. As a means of comparison, however, the fin contribution to yaw stability, which is approximately $C_{n\beta} = +0.25$ per radian at small sideslip angles, is used as a baseline in evaluating the component effects on yaw stability.

(4) Blades Open

Yaw stability seems very little affected by blade fold angles within 30 degrees of the fully-folded position. The variations in yaw stability were within about 5 percent of the vertical tail contribution to $C_{n\beta}$.

TABLE V-XIII. SUMMARY OF COMPONENT EFFECTS ON AIRCRAFT YAW STABILITY ($C_{n\beta}$)*

Change	Basic Aircraft		AF Pod No. 1		AF Pod No. 2	
	$\Delta C_{n\beta}$	Percent of Tail ($C_{n\beta}$)	$\Delta C_{n\beta}$	Percent of Tail ($C_{n\beta}$)	$\Delta C_{n\beta}$	Percent of Tail ($C_{n\beta}$)
Add blades, pods, nacelles to basic aircraft	-	-	0.010	+ 4	0.040	+16
Add blades and pods to basic aircraft	-	-	-0.046	-18	-	-
Remove blades from baseline configuration	-	-	+0.024	+10	-	-
Add jet nacelles	+0.049	+20	+0.064	+26	-	-
Unfold blades by 30 degrees	-	-	+0.002**	+ 1	-	-
Add vortex generators	-	-	+0.018	+ 7	-0.100	- 4
*Tail contribution to $C_{n\beta} = 0.25$ per radian (negative $C_{n\beta}$ values indicate a reduction in stability for the change noted).						
**Flaps down.						

(5) Vortex Generators

The vortex generators do not influence the yaw stability significantly. They appear to increase the stability very slightly for AF Pod No. 1 configurations and reduce it for AF Pod No. 2. The maximum change noted was 7 percent of the fin effectiveness.

b. Dihedral Stability

The aircraft design at the time of the test had a high-wing location positive wing dihedral angle, and single vertical stabilizer, all of which contribute to negative dihedral stability. The wing, in addition, has a relatively thick airfoil section which either by itself or due to wingtip pod or fuselage interference, may be contributing to an increasing dihedral effect with increasing lift coefficient. Tests were conducted to examine the wing contribution alone, and results of adding the folding-proprotor appendages.

In reviewing these data, it may be helpful to note that effective wing dihedral angle in degrees can be approximated by $(\Gamma)_{\text{effective}} = -C_{l\beta}/0.016$, with $C_{l\beta}$ per radian, or that the effective dihedral is approximately equal to -62 times the value of $C_{l\beta}$ shown on the curves.

(1) Wing Alone

The wing alone was tested early in the program and the data, uncorrected for tare and interference are shown in Figure V-43. From this, one concludes that the wing alone without fuselage or protuberances experiences a significantly increasing effective dihedral with angle-of-attack. Vortex generators on the upper surface were found to delay the increase in effective dihedral. Tests were conducted both with and without the vortex generators until more was learned about the phenomenon.

(2) Wingtip Pods

Wingtip pod and blade geometry appear to have a large effect on dihedral stability. On Figure V-44 are shown the variations in $C_{l\beta}$ with C_L for three different pod configurations with flaps up and without vortex generators, and for the basic aircraft without pods. At $C_L = 1.0$, the AF pod configurations have a considerably higher $C_{l\beta}$ than the Bell Pod No. 2 configuration, and the pods off value lies between them. All of the configurations exhibit an increase in $C_{l\beta}$ with C_L .

Some indication of the contribution of the blades only to $C_{l\beta}$ may be obtained from Figure V-27. It shows at an angle of attack of zero that if the blades are removed from the AF Pod No. 1 configuration with vortex generators off, $C_{l\beta}$ decreases from -0.186 per radian to -0.141 per radian. More testing is required to determine how blade-pod geometry, including folded blade positioning can be optimized to reduce dihedral stability.

(3) Engine Nacelles

The effect of engine nacelles varied. When wingtip pods were not present, the engine nacelles had no effect on dihedral (at $\alpha = 0$). This is shown in Figure V-42 and Table XII. When wingtip pods were present, the nacelles reduced $C_{l\beta}$ by approximately 0.10. (The latter configuration had Air Force Pod No. 1, leading edge roughness, and no vortex generators.) This change is equivalent to about -6 degrees of effective wing dihedral angle.

(4) Blades Open

For a configuration having Air Force Pod No. 1, flaps down, and vortex generators on, blade fold angle did not influence dihedral stability significantly. $\Delta C_{l\beta}$ was -0.015 as the blades were unfolded to 30 degrees. With Pod No. 2, flaps up, and vortex generators on, $C_{l\beta}$ decreased from -0.127 to -0.061 as the blades were unfolded to 30 degrees. A somewhat smaller change was indicated for the flaps-down case.

(5) Effect of Vortex Generators

The vortex generator produced large but unpredictable changes in dihedral stability at high lift coefficients above $C_L = 1.0$. With flaps up, values of $C_{l\beta}$ are shown for the several configurations (with vortex generators on) in Figure V-45. Comparisons of $C_{l\beta}$ with those in Figure V-44 indicate that at a C_L between 1.5 and 1.6, the vortex generators reduce $C_{l\beta}$ up to 50 percent. The largest change is for the Bell Pod No. 1 configuration, which does not have folded blades or jet engine nacelles.

Flaps-down data, in Figure V-46 show that at lift coefficients between 1.0 and 1.5, the value of $C_{l\beta}$ is nearly the same with or without vortex generators.

4. Blade Opening Effects

The effects on lift, drag, and moments caused by opening the blades 15 and 30 degrees from the folded position are shown in Figures V-47 through V-52 for the Pod No. 1 configuration with flaps down.

a. Lift

The lift curve slope as well as the zero-lift angle changes slightly as the blades are opened. The variations are fairly uniform. Only small variations in maximum lift occur.

b. Drag

Variation in drag is uniform. Minimum drag is 0.120, 0.126, and 0.129 for 0-, 15-, and 30-degrees blade-open angles.

c. Pitching Moment

There is a significant change in the trim value, but only a slight change in the pitching moment derivative. The trim change occurs during the first 15 degrees of blade opening.

d. Rolling Moment and Yawing Moment

Only small changes are noted in the yawing moment curves. The largest changes seem to occur in rolling moment and its derivative.

5. Aileron Effectiveness

A complete aerodynamic investigation of the folding-propeller configuration should include aileron, elevator, and rudder effectiveness tests for control data. Some tests were accomplished in each area and are reported herein. Most interest was in aileron effectiveness because of their use to help the flaps increase maximum lift during conversion and transition. Also the wing thickness is relatively high and very little data were available.

a. Blades Folded

(1) Flaps Up, Model Clean

These data are shown in Figure V-53. For aileron deflection angles up to ± 10 degrees, they are quite effective at lift coefficients up to about 0.8, and effectiveness is greater than would be predicted for a wing without pods. Test values of $C_{l\delta}$, for example are 0.006 per degree, while the predicted value is 0.00464 per degree. Thus the aileron aspect ratio is effectively increased by the pods.

At lift coefficients above 0.8, aileron effectiveness is reduced until at or slightly below maximum lift, they become ineffective. The causes of this reduction were not well established at the time of the test.

(2) Flaps Down, Model Clean

Data with flaps down 50 degrees are shown in Figure V-54. Ailerons are drooped nominally 20 degrees, and they act as flaperons.

In general, rolling moments are 50 to 75 percent of those with flaps up. They are nearly constant for lift coefficients up to about 1.3, above which they decrease to zero at or slightly below the maximum lift coefficient. At a given lift coefficient, the variation in rolling moment of aileron deflection is nonlinear. In contrast to the more nearly uniform variation with flaps up, it increases for settings up to aileron deflections of ± 15 degrees.

(3) Effects of Vortex Generators

Test results with vortex generators on the wing upper surfaces are also shown in Figures V-53 and V-54.

With flaps up, rolling moments due to a ± 15 -degree aileron deflection are increased somewhat for lift coefficients up to 0.8. The most pronounced effect is an increase in moments at the higher coefficients, and an increase in the percent of maximum lift coefficient at which a given level of aileron control power is maintained.

With flaps down, rolling moments due to aileron deflection are reduced at low to moderate lift coefficients but increased at the highest coefficients. The decrease in rolling moments at low to moderate lift coefficients is believed caused by a nonlinear influence of the generators on aileron effectiveness. Evidently, they improve effectiveness up to some value of deflection, beyond which they have a less effect. With flaps down, the percent of maximum lift coefficient for a given level of aileron control power is increased.

b. Blades Open

For lift coefficients up to 1.4 (flaps up) and 1.7 (flaps down), differences between moments with blades folded and blades open 15 degrees are small (Figures V-55 and V-56).

c. Other Effects

The effect of roughness applied to the wing leading edge is shown in Figure V-57. It appears that the effects are small and insignificant.

Some differences in aileron effectiveness might be expected for different wing-tip-pod and blade configurations because of differing end conditions for the ailerons, or interference with the edgewise-folded blades. When blades are folded for cruise flight no significant differences were found (Figures V-58 and V-59). With blades open 15 degrees, a large difference is shown (Figure V-60). This was unexpected because opening the blades had no significant effect on aileron effectiveness with the Air Force pod configuration. There was no significant difference in effectiveness between the two pod configurations with blades folded. The effect shown is largely the result of an increase in aileron effectiveness for the Bell pod No. 2 configuration when blades are open. One may conclude from this that interference exists with airflow about the ailerons when blades are folded with the Bell pod No. 2 configuration, and that the deeper tilt-propeller-pod, which has engines mounted below the transmission, results in increased aileron effectiveness in comparison to the reduced diameter folding propeller pod.

6. Elevator and Rudder Effectiveness

Pitching moment coefficients as a function of elevator deflections and air-frame angle of attack are presented in Figures V-61 and V-62. Yawing moments due to rudder deflection and yaw angle are given in Figures V-63 and V-64 for angles of attack of 0 and 11 degrees. The related rolling effectiveness of the rudder is given in Figures V-65 and V-66. At the high angle of attack, there is a noticeable increase in static directional stability for rudder deflections of 5 and 10 degrees. Cause of this effect is not established.

7. Conclusions

The folded-blade drag of the folding-propotor configuration tested is the smaller part of the wingtip pod and blade contributions to aircraft drag. The blades were completely exposed and had first-iteration hub and trailing-edge fairings. The greater part of the contribution is due to the basic pylon mechanism, transmission, and spinner cowlings which are basically generic to both the tilt- and folding-propotor configurations. The folding-propotor configuration tested had relatively high-drag jet engine nacelles underslung between the wings and these may not be representative of larger aircraft. But with these nacelles and the folded blades, the equivalent full-scale equivalent flat-plate drag is about one square foot greater than that of the tilt propotor not including blade drag or propulsive efficiency in the latter. The comparison above does not include considerations of fuel flow, fan or propotor efficiencies, altitude, system weights, speeds, or Mach number effects.

The blades when folded for cruise, tend to reduce pitch and yaw stability and to increase effective dihedral. In the case of pitch stability, this is offset by a favorable influence which they have on wing downwash such that horizontal stabilizer effectiveness is increased. This results in a negligible net effect of the folded blades on pitch stability. In the configuration tested, jet engine nacelles are underslung beneath the wing at an inboard station. The arrangement can be expected to vary for different configurations but for the configuration tested, they introduced compensating yaw stability and dihedral effects tending to offset those of the blades.

Opening the blades 30 degrees from the folded position changed longitudinal trim, but did not affect pitch stability. The fold angle was limited by model and wind-tunnel size, but future tests should be conducted with blades fully open, which is critical for empennage sizing. A number of areas discussed in the text, such as Reynolds number effect, directional stability and effective dihedral, and aileron effectiveness, have subsequently been investigated for the tilt-propotor configuration, but these do not appear to be unique to the folded-blade configuration. However, there are sufficient differences in many characteristics to require developmental model testing for specific folding-propotor configurations.

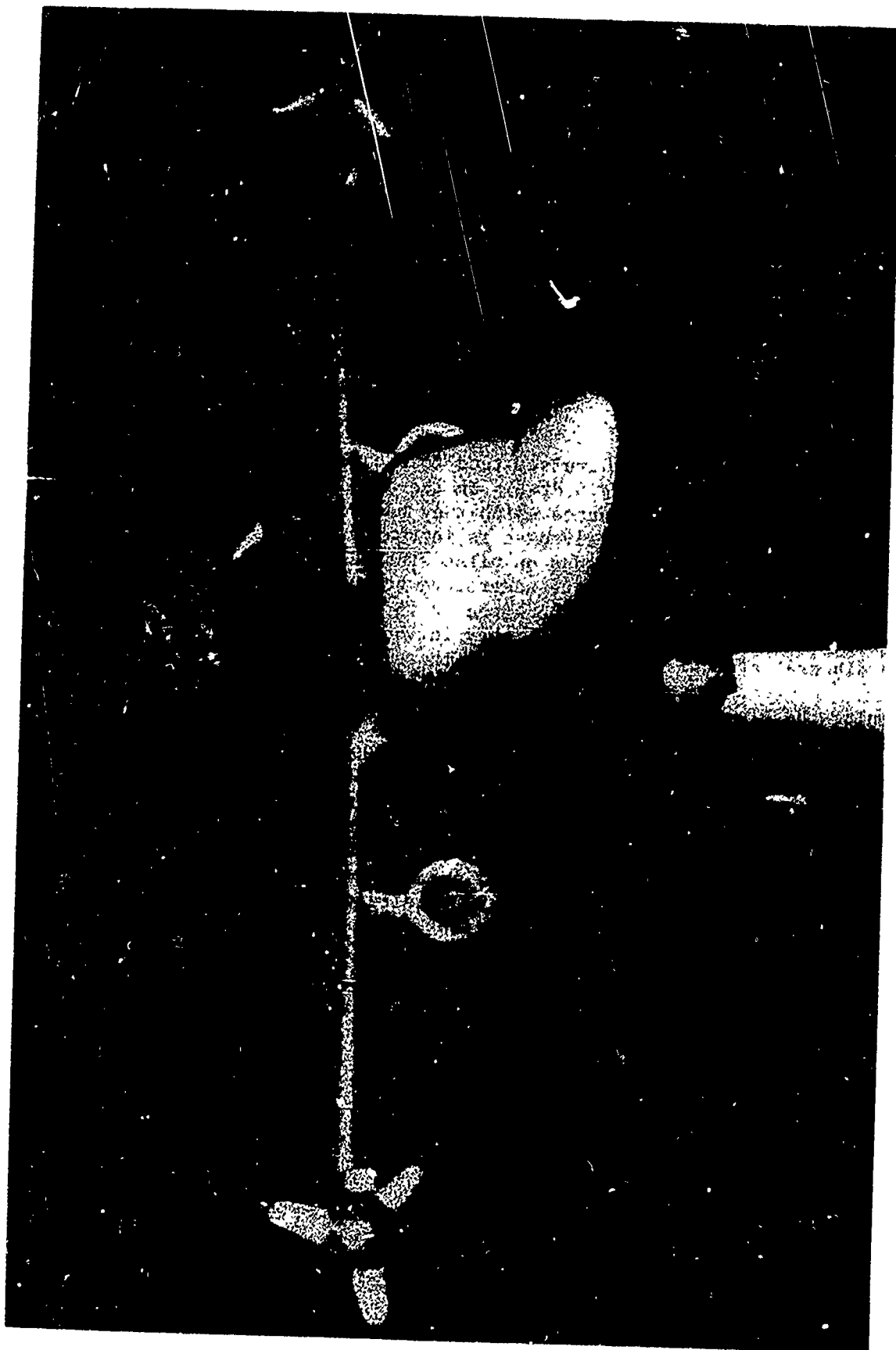


Figure V-1. Model Installed in LTV Wind Tunnel.

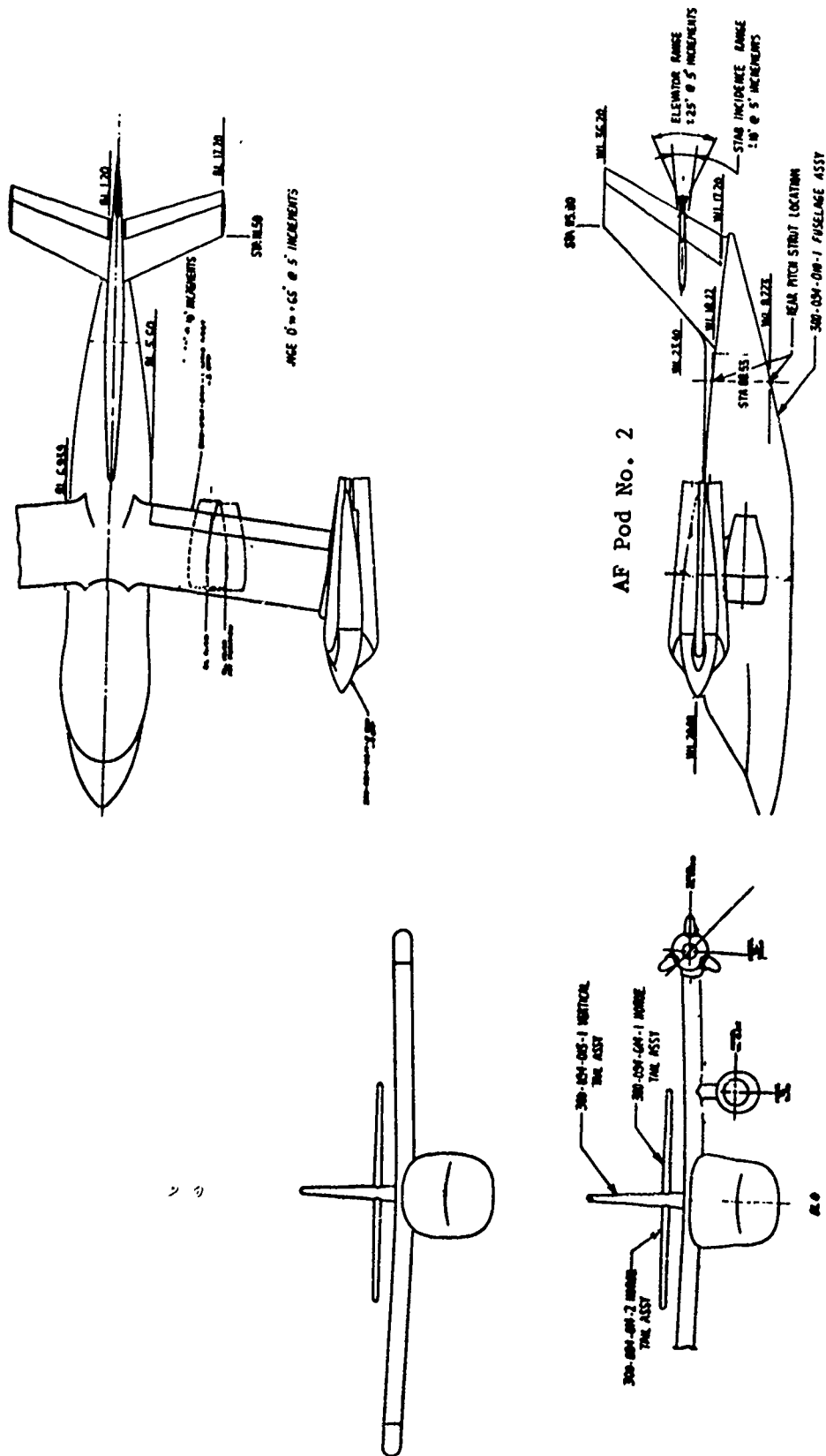


Figure V-2. Three View of General Aerodynamic Force Model.

Figure V-3. Complete Aircraft, Flaps Up, Blades Closed,
Model Clean.

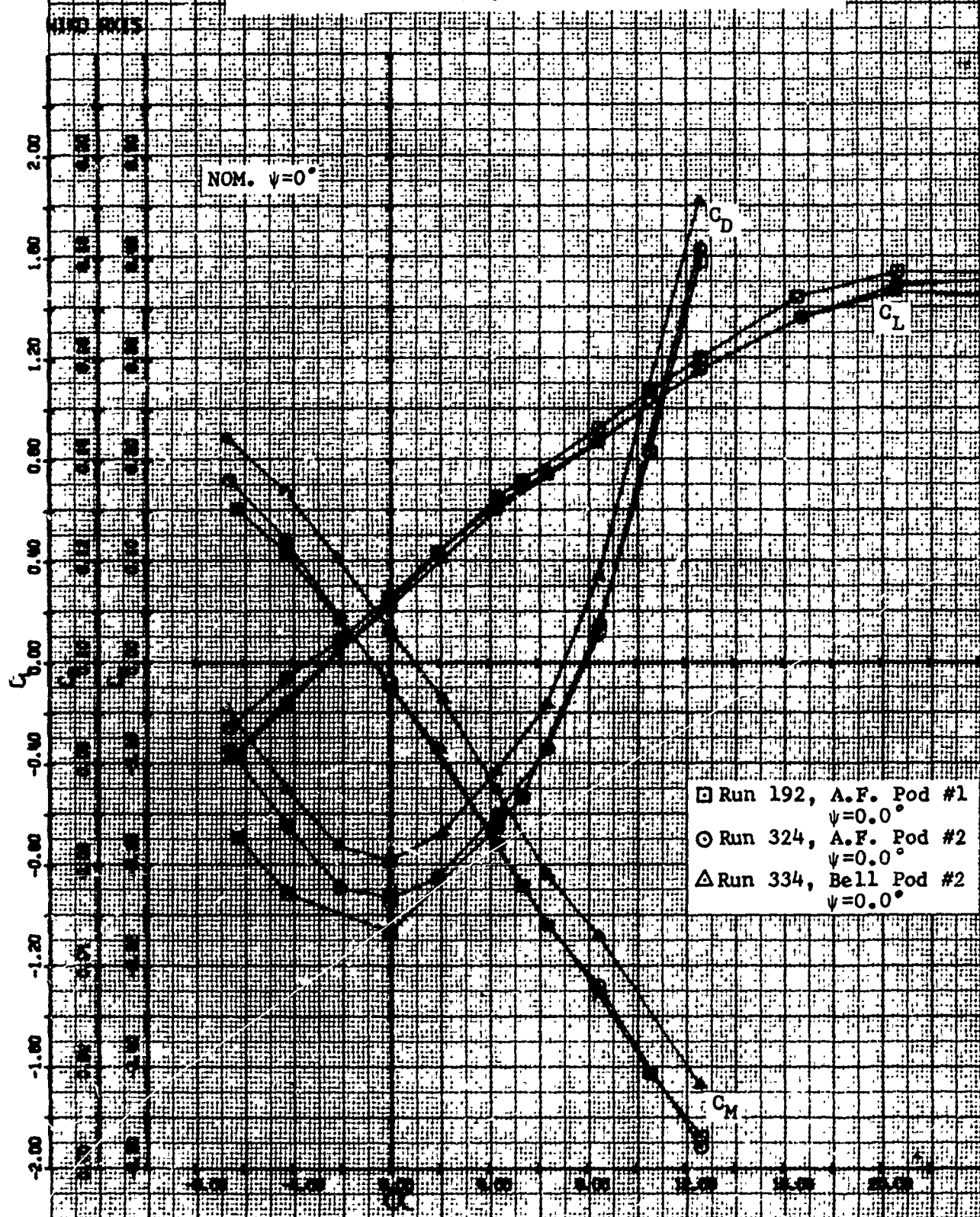


Figure V-4. Complete Aircraft, Flaps Up, Blades Closed,
Model Clean.

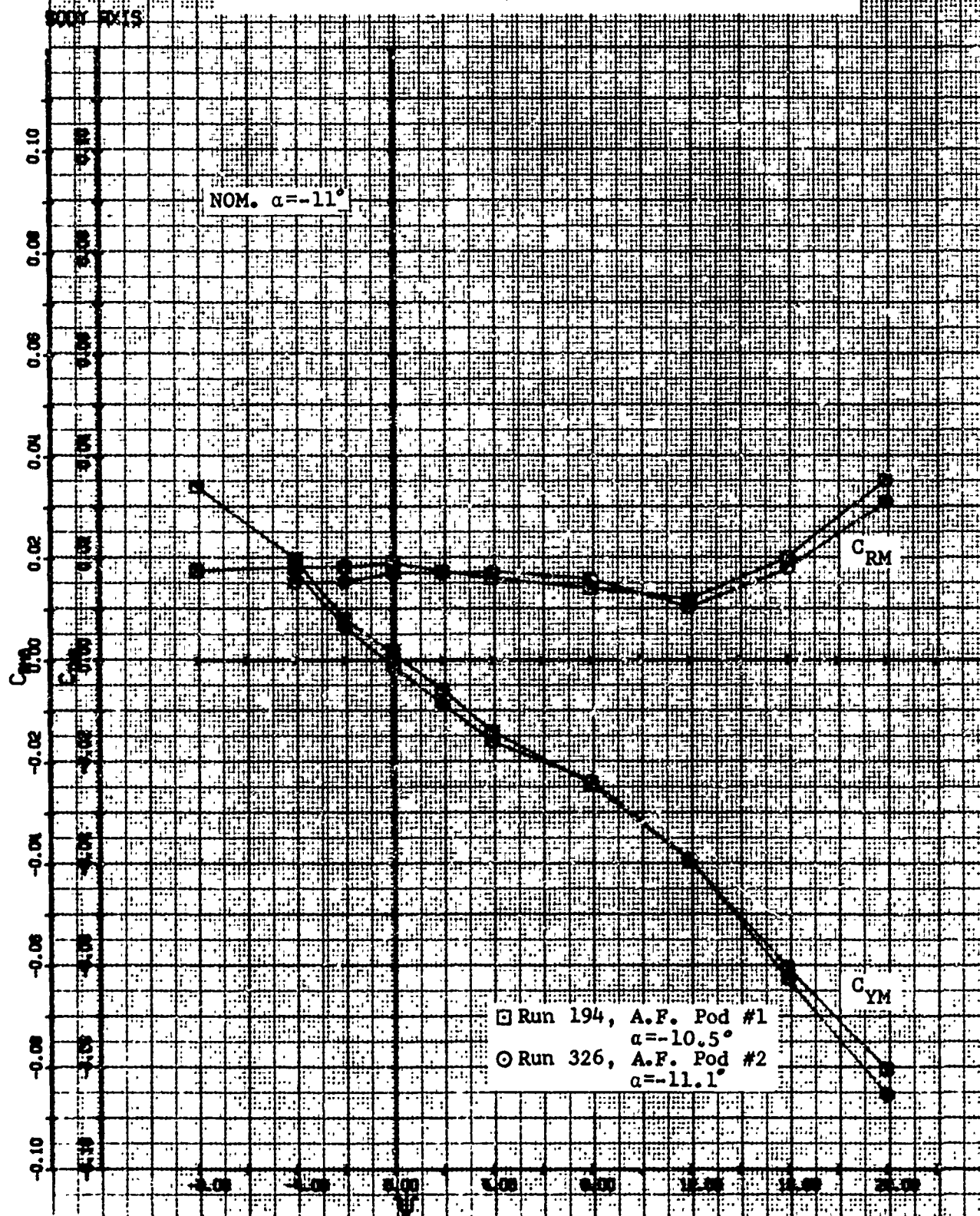


Figure V-5. Complete Aircraft, Flaps Up, Blades Closed,
Model Clean.

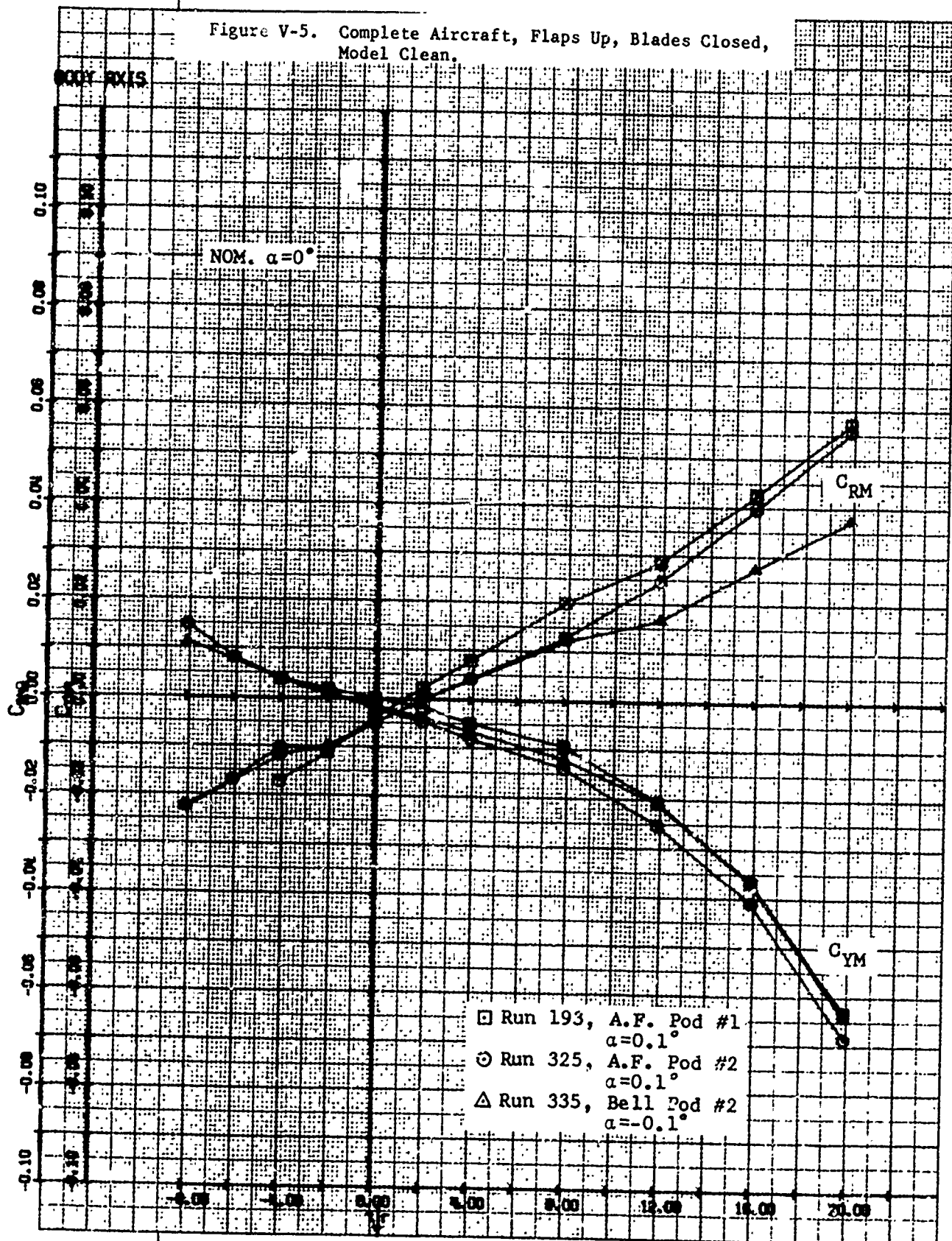


Figure V-6. Complete Aircraft, Flaps Up, Blades Closed,
Model Clean.

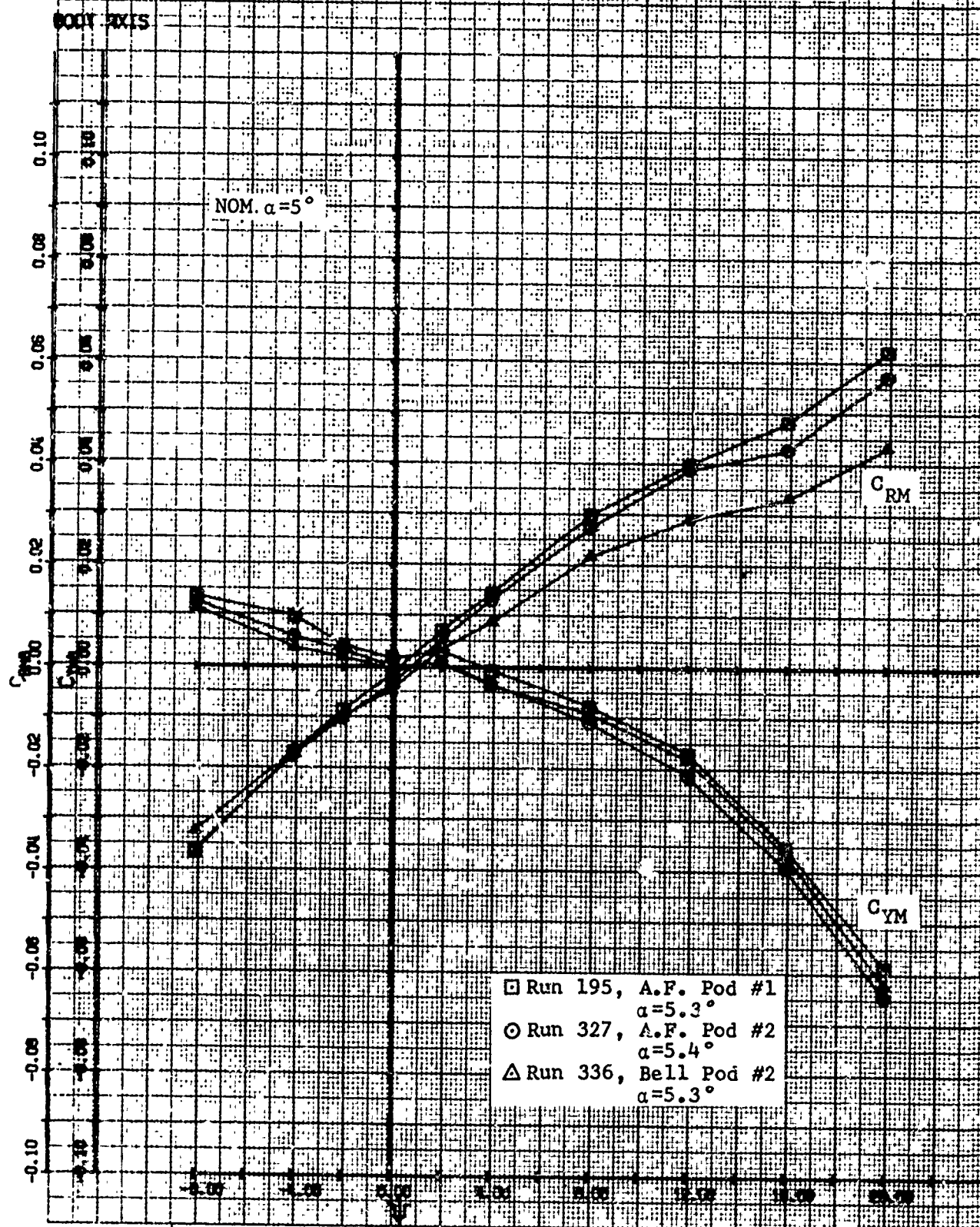
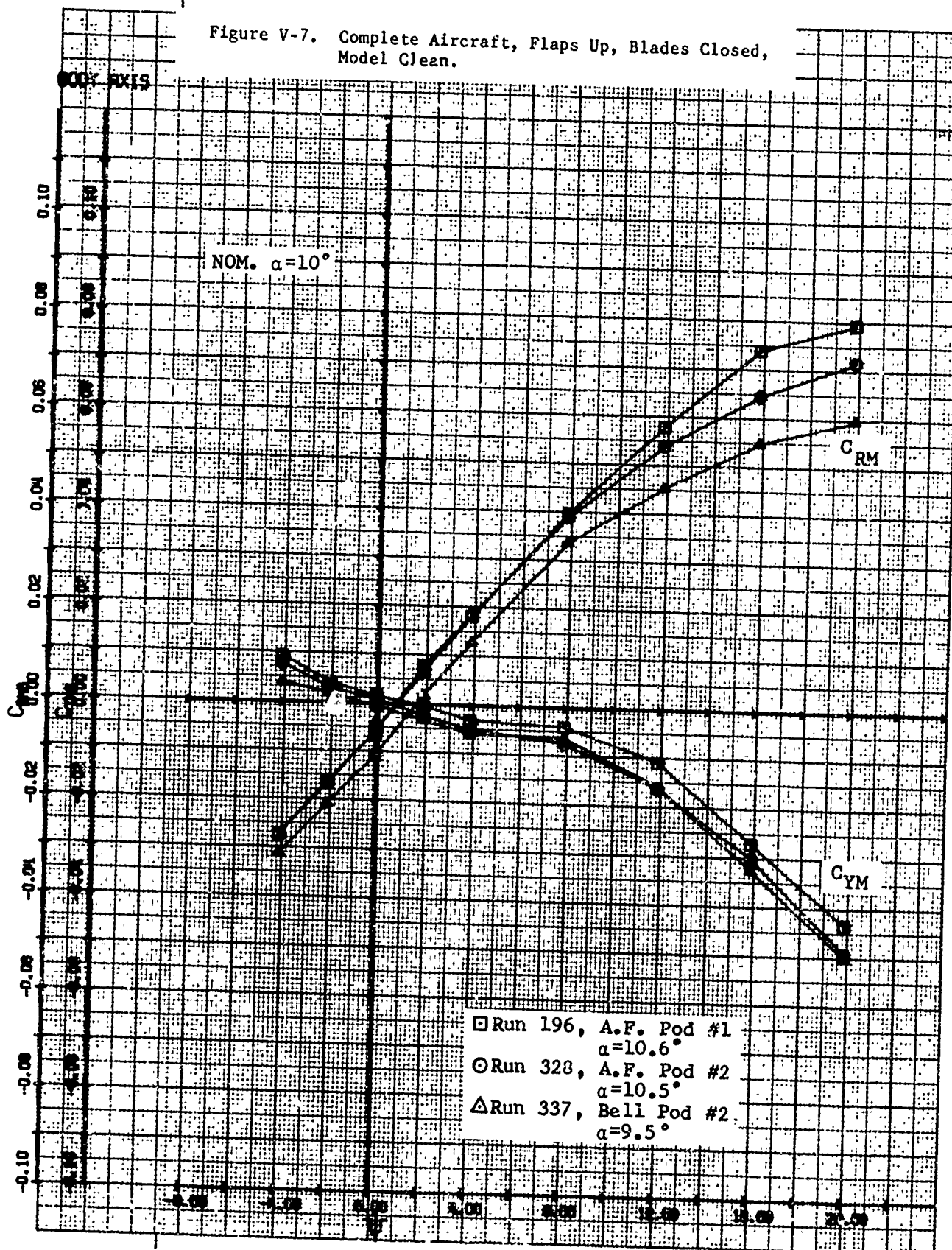


Figure V-7. Complete Aircraft, Flaps Up, Blades Closed,
Model Clean.



1270-099-003

Figure V-8. Complete Aircraft, Flaps Up, Blades Closed,
Model Clean.

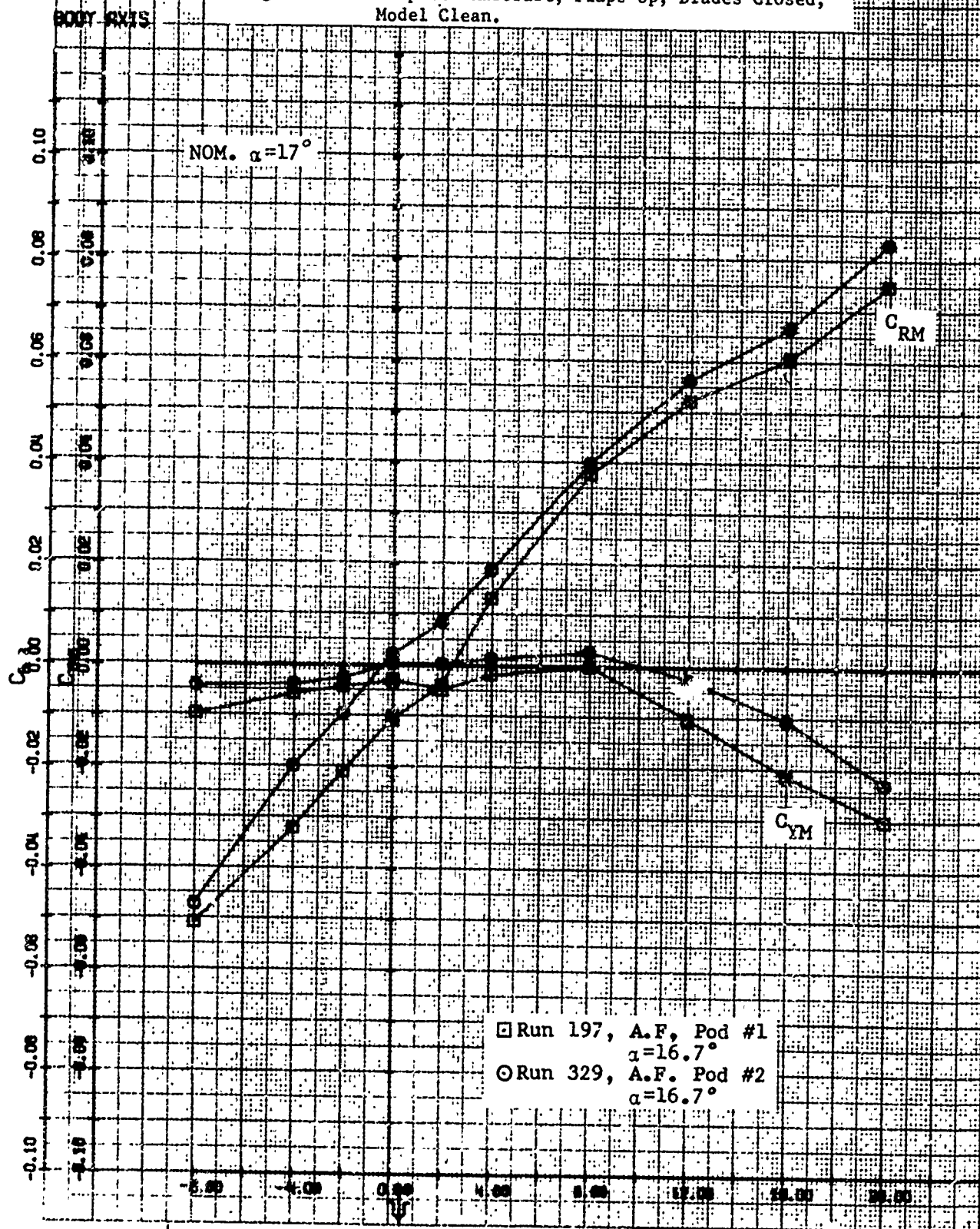
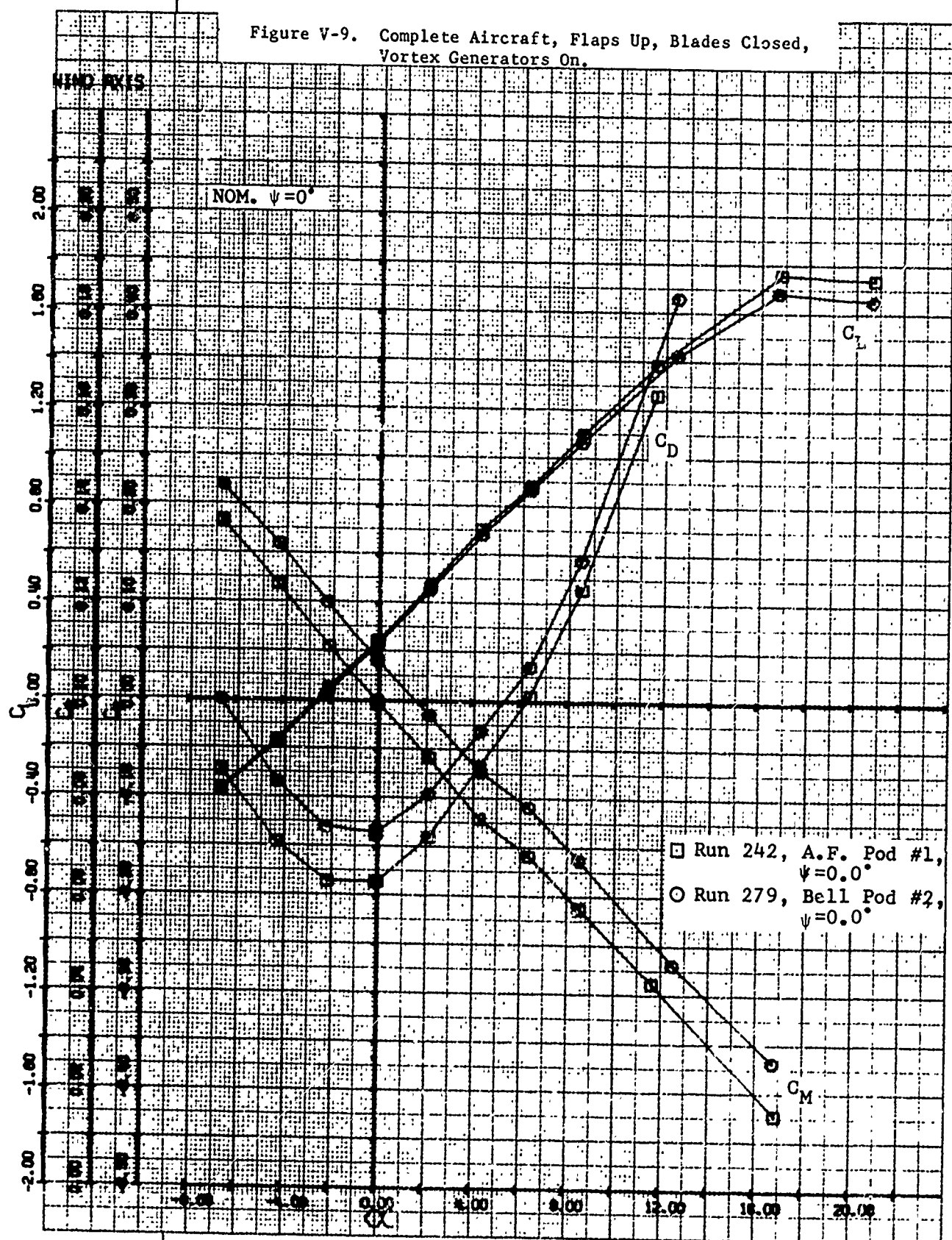


Figure V-9. Complete Aircraft, Flaps Up, Blades Closed,
Vortex Generators On.



D270-099-003

BODY AXIS

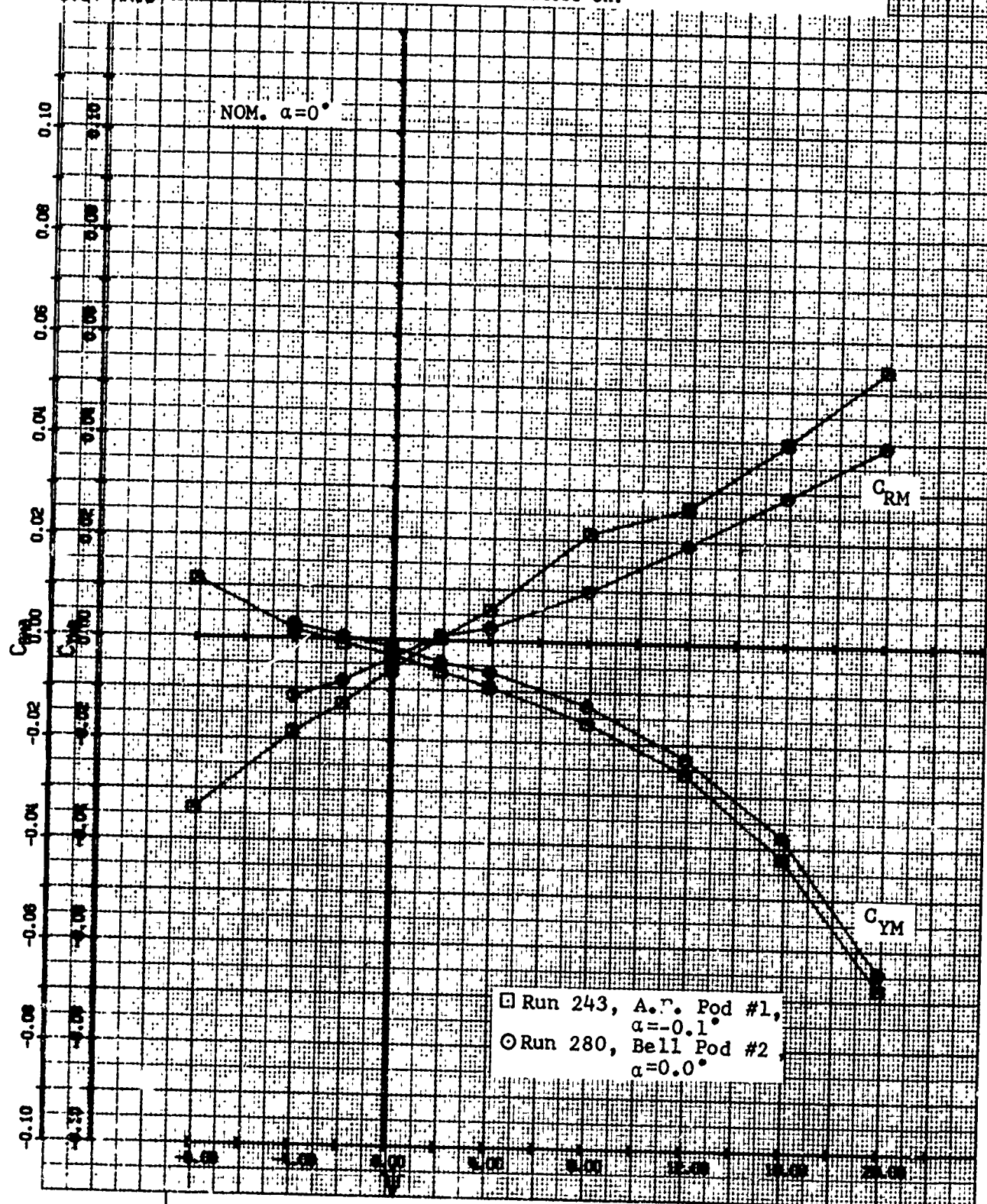
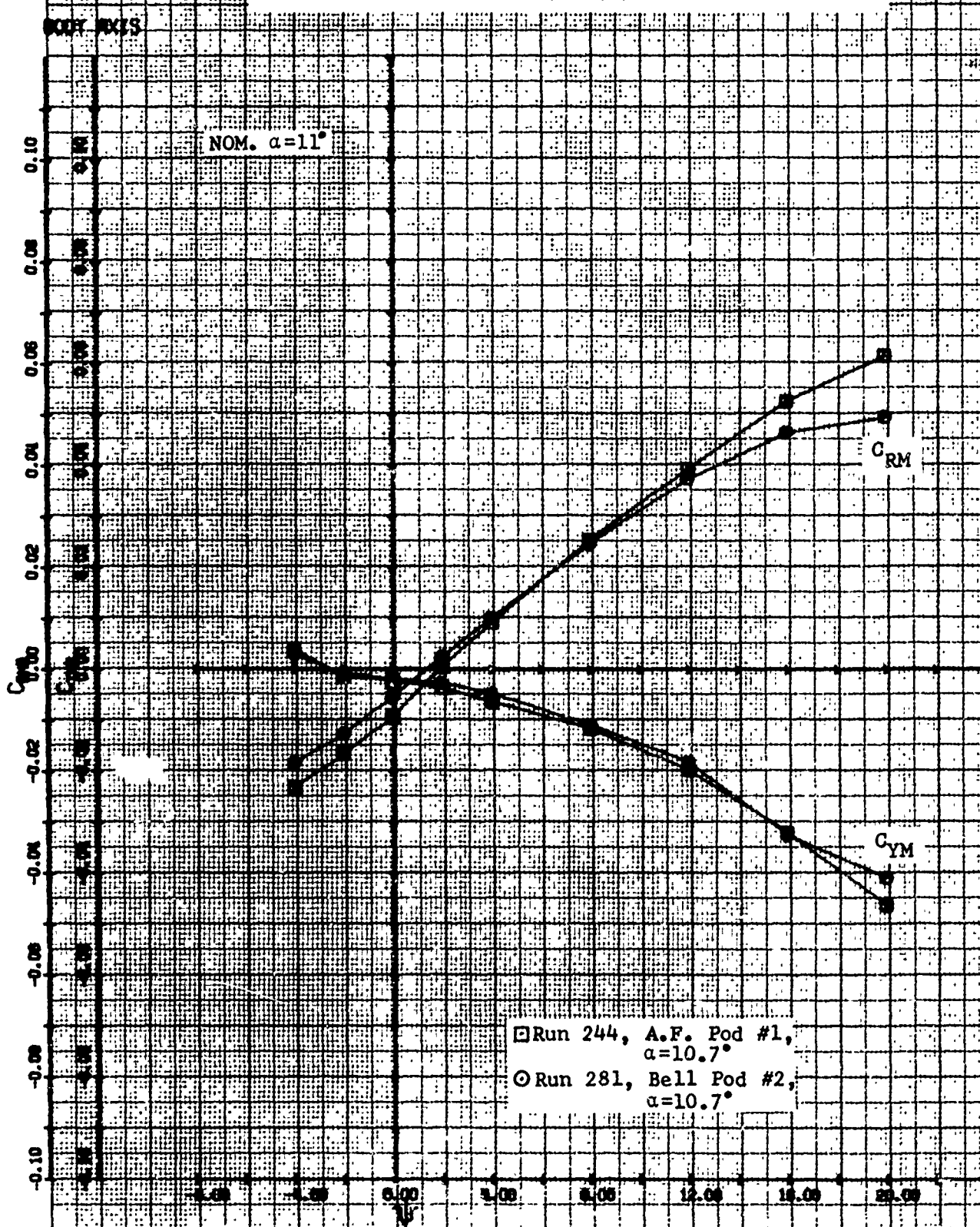


Figure V-11. Complete Aircraft, Flaps Up, Blades Closed,
Vortex Generators On.



D270-099-003

Figure V-12. Complete Aircraft, Flaps Up, Blat's Closed,
Vortex Generators On.

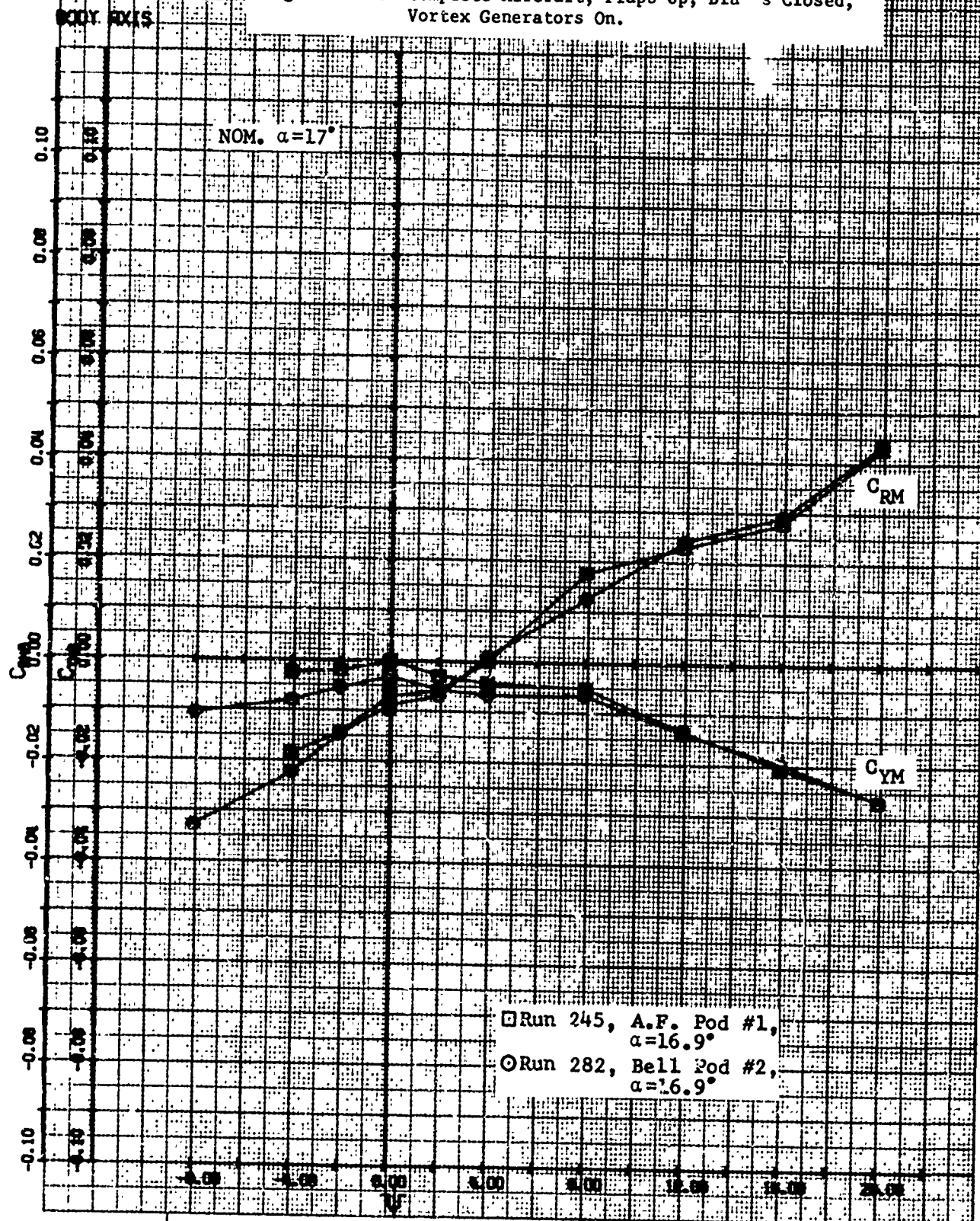


Figure V-13. Complete Aircraft, Flaps Down, Blades Closed, Model Clean.

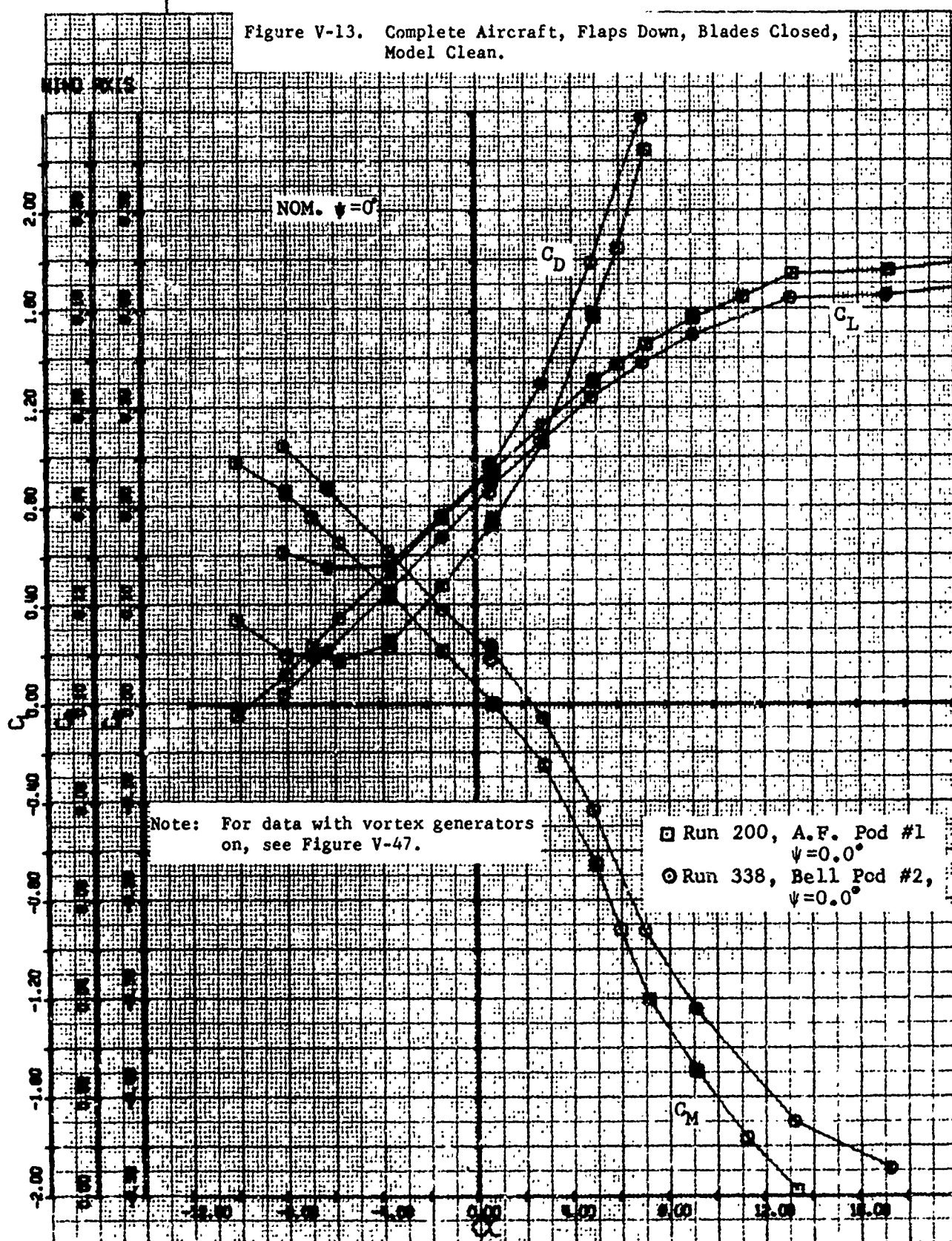


Figure V-14. Complete Aircraft, Flaps Down, Blades Closed, Model Clean.

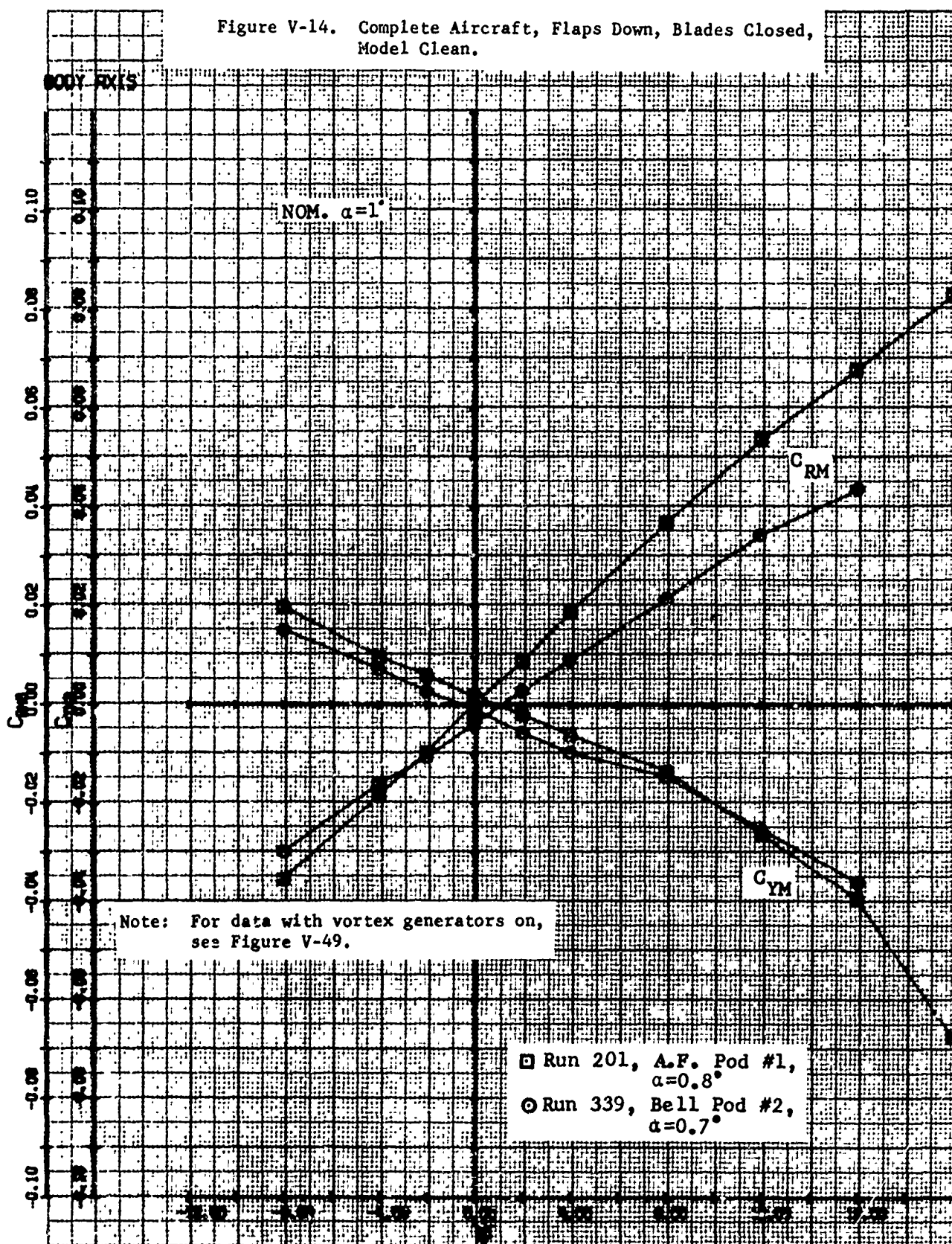


Figure V-15. Complete Aircraft, Flaps Down, Blades Closed,
Model Clean.

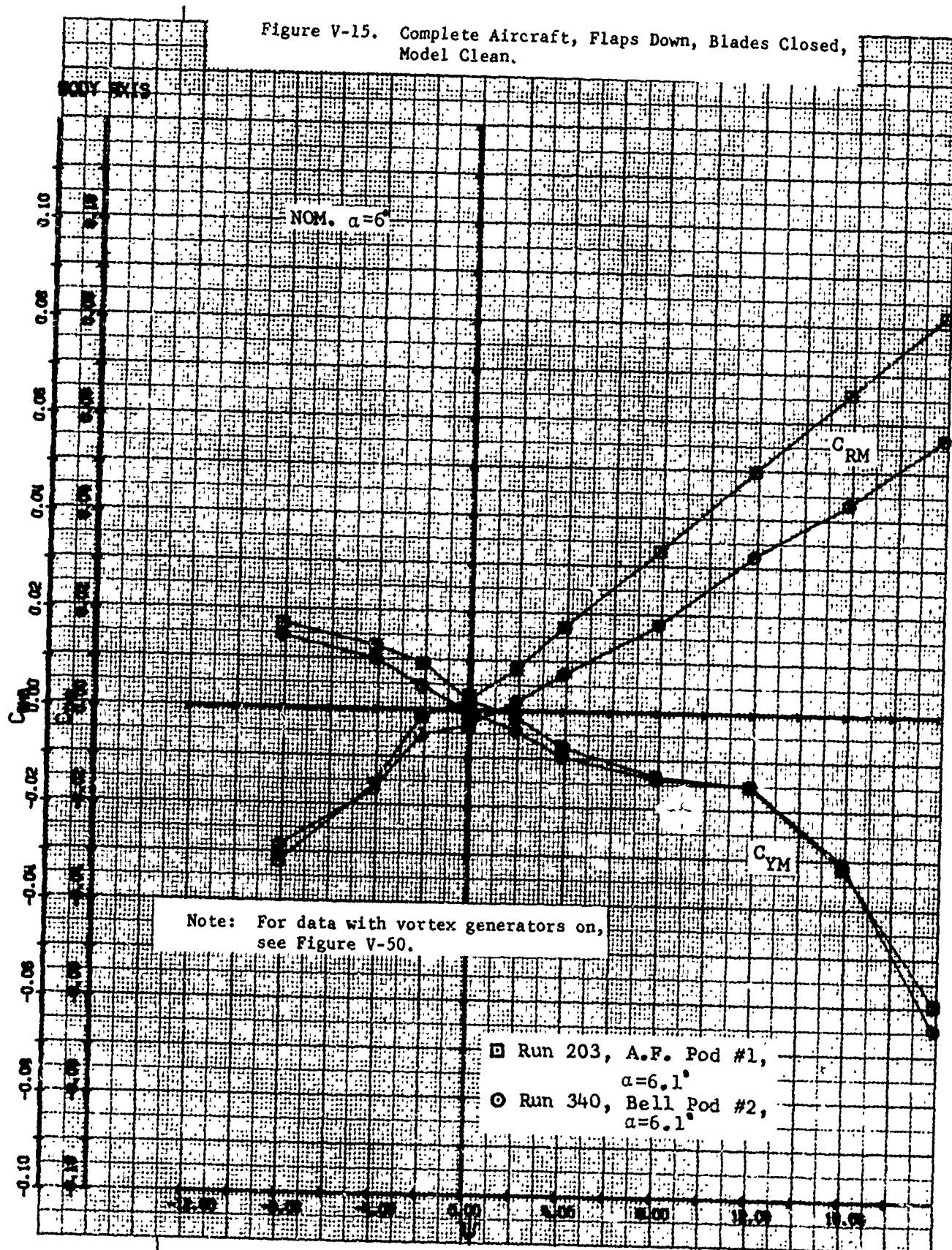


Figure V-16. Complete Aircraft, Flaps Down, Blades Closed, Model Clean.

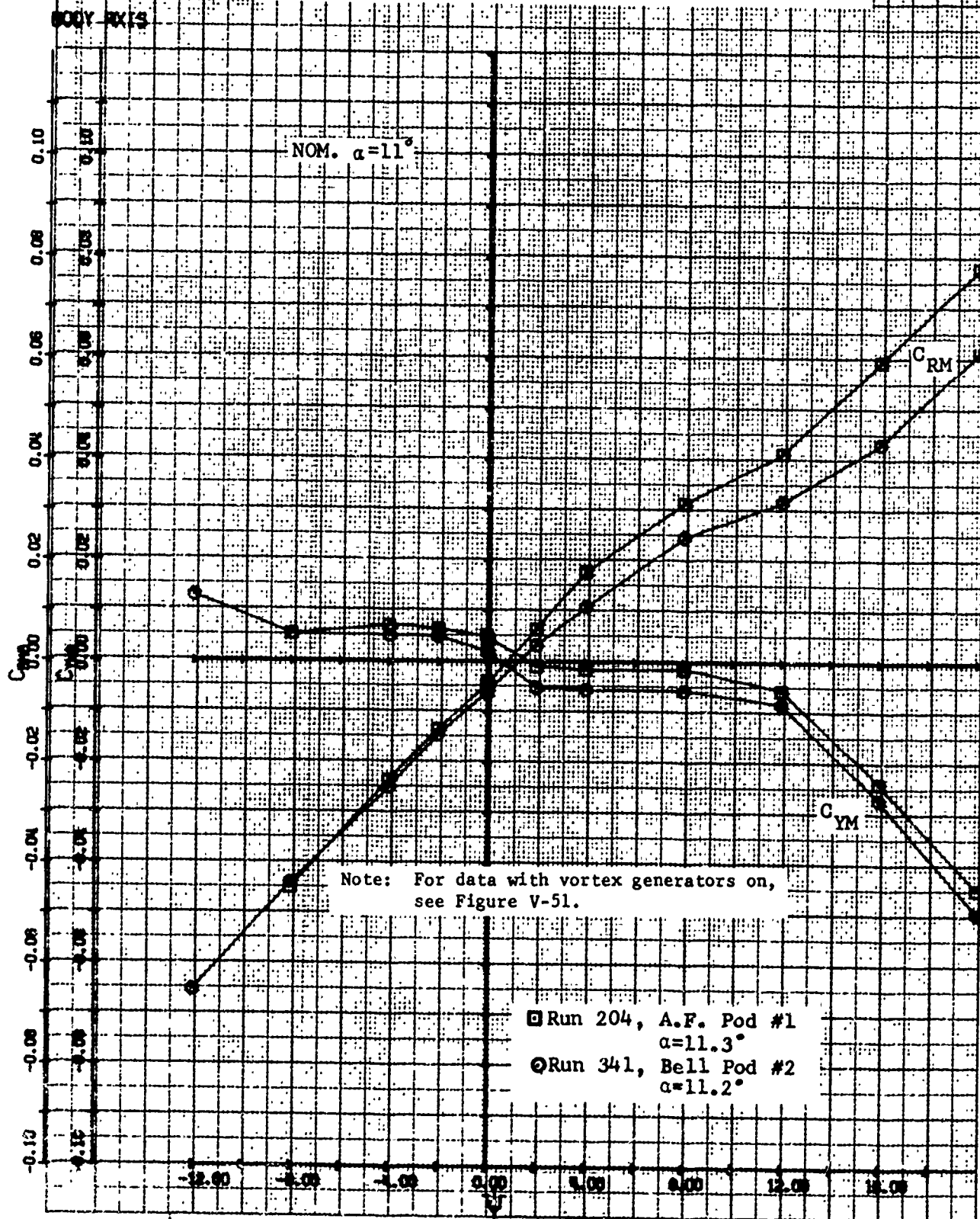


Figure V-17. Effect of Wingtip Pods on Longitudinal Characteristics for the Complete Aircraft, Air Force Pod No. 1.

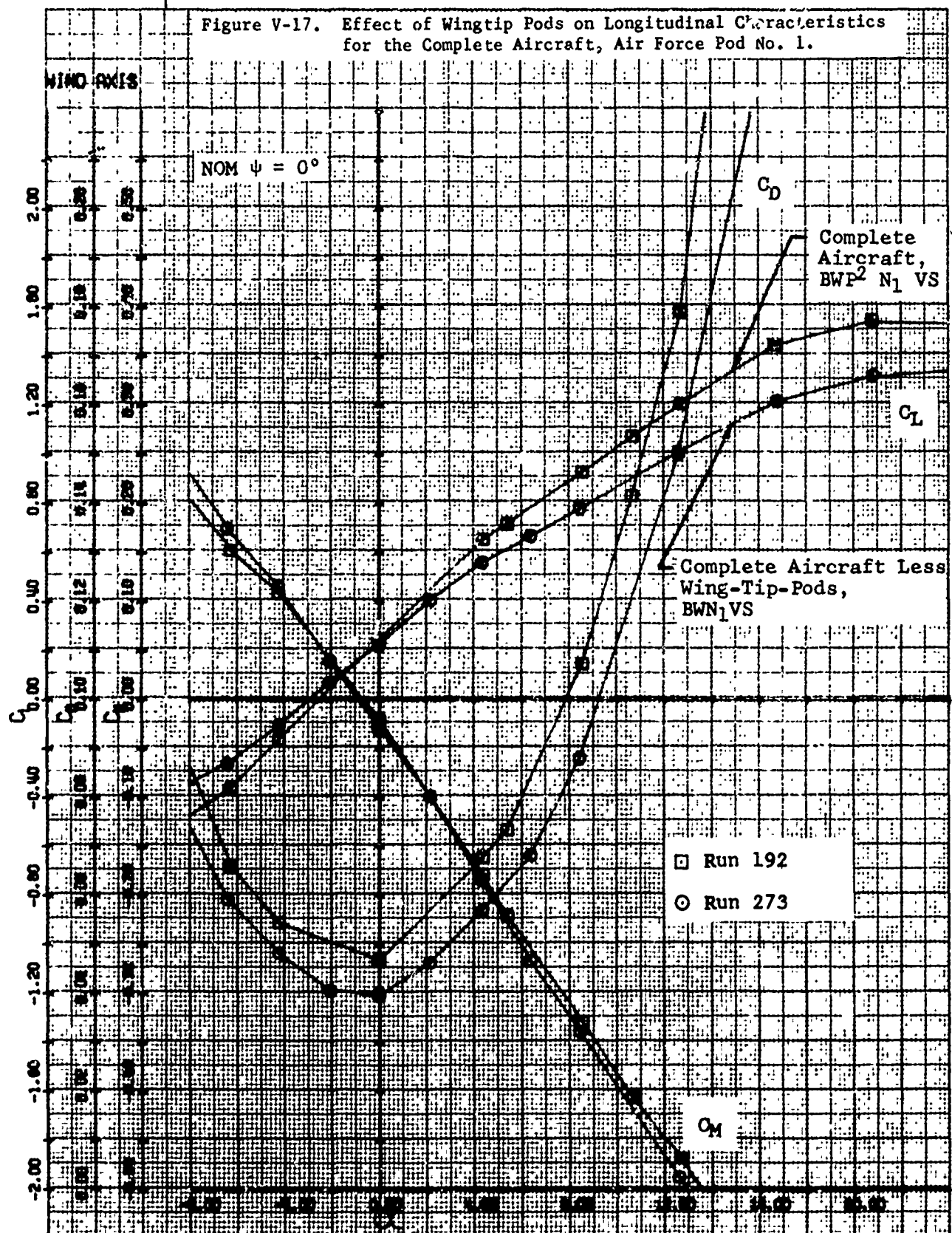


Figure V-18. Effect of Wingtip Pods on Longitudinal Characteristics for the Complete Aircraft Less Engine Nacelles, Air Force Pod No. 1.

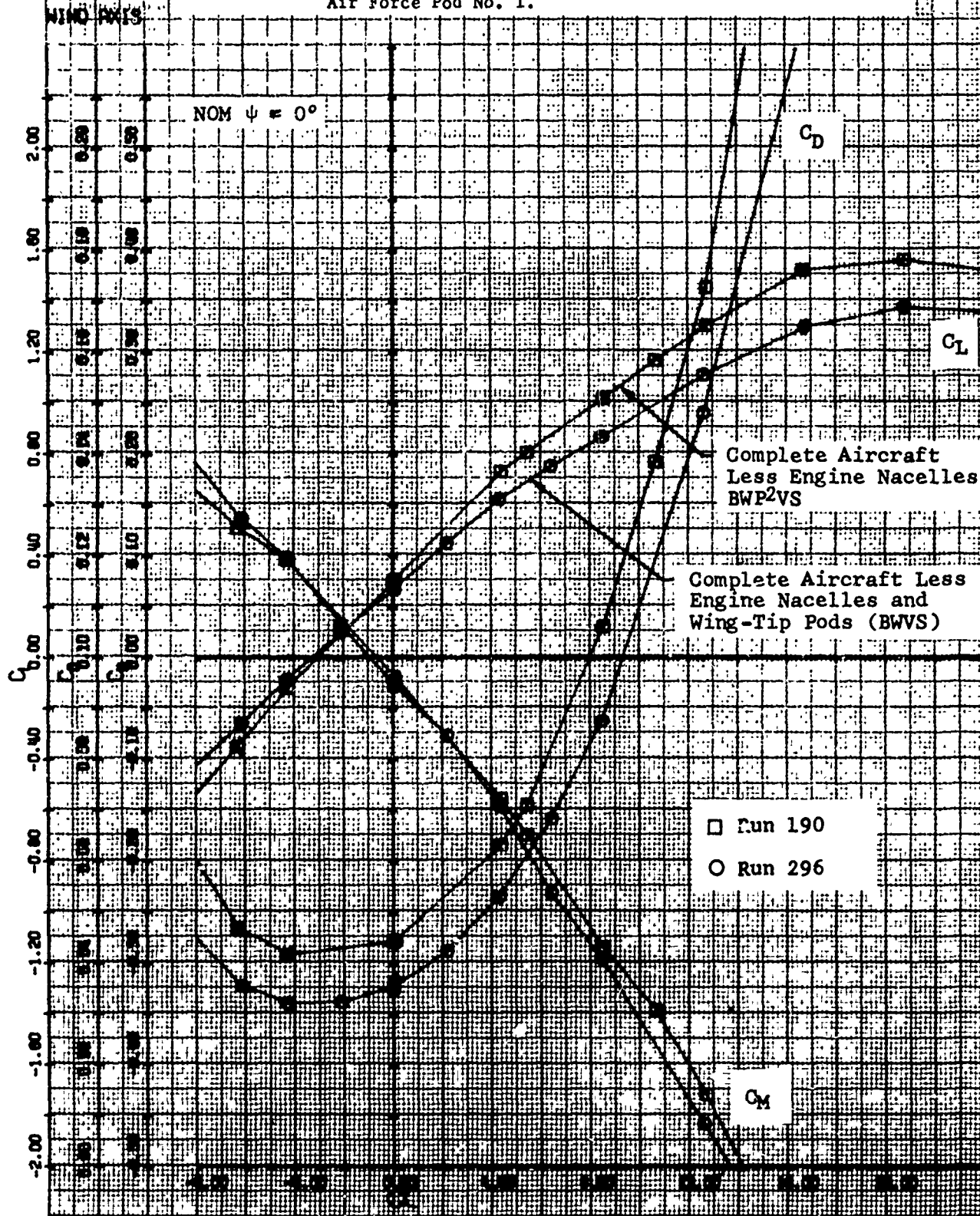
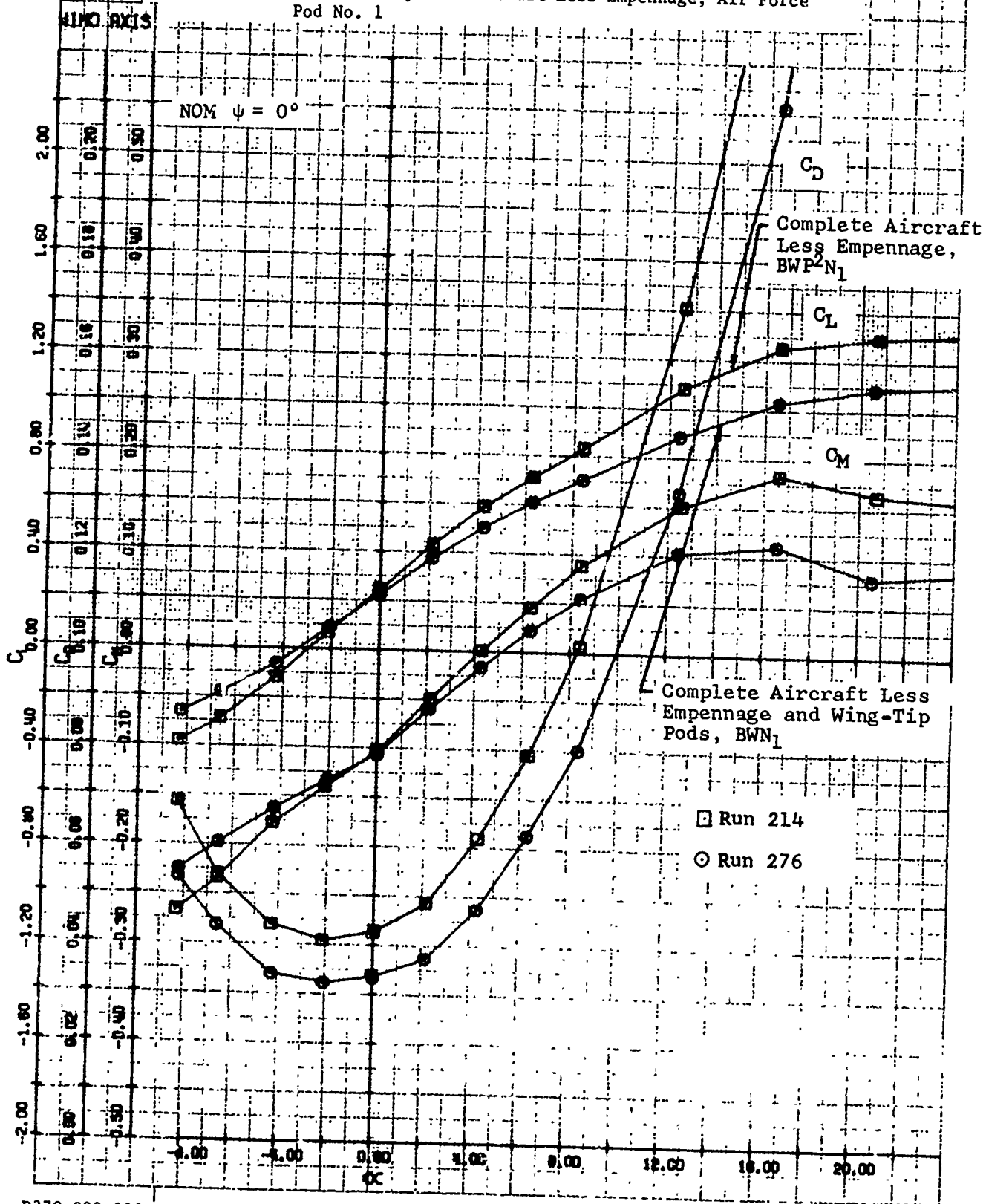


Figure V-11. Effect of Wingtip Pods on Longitudinal Characteristics for the Complete Aircraft Less Empennage, Air Force Pod No. 1



D270-099-003

Figure V-20. Effect of Wingtip Pods on Longitudinal Characteristics of the Fuselage and Wing, Air Force Pod No. 1

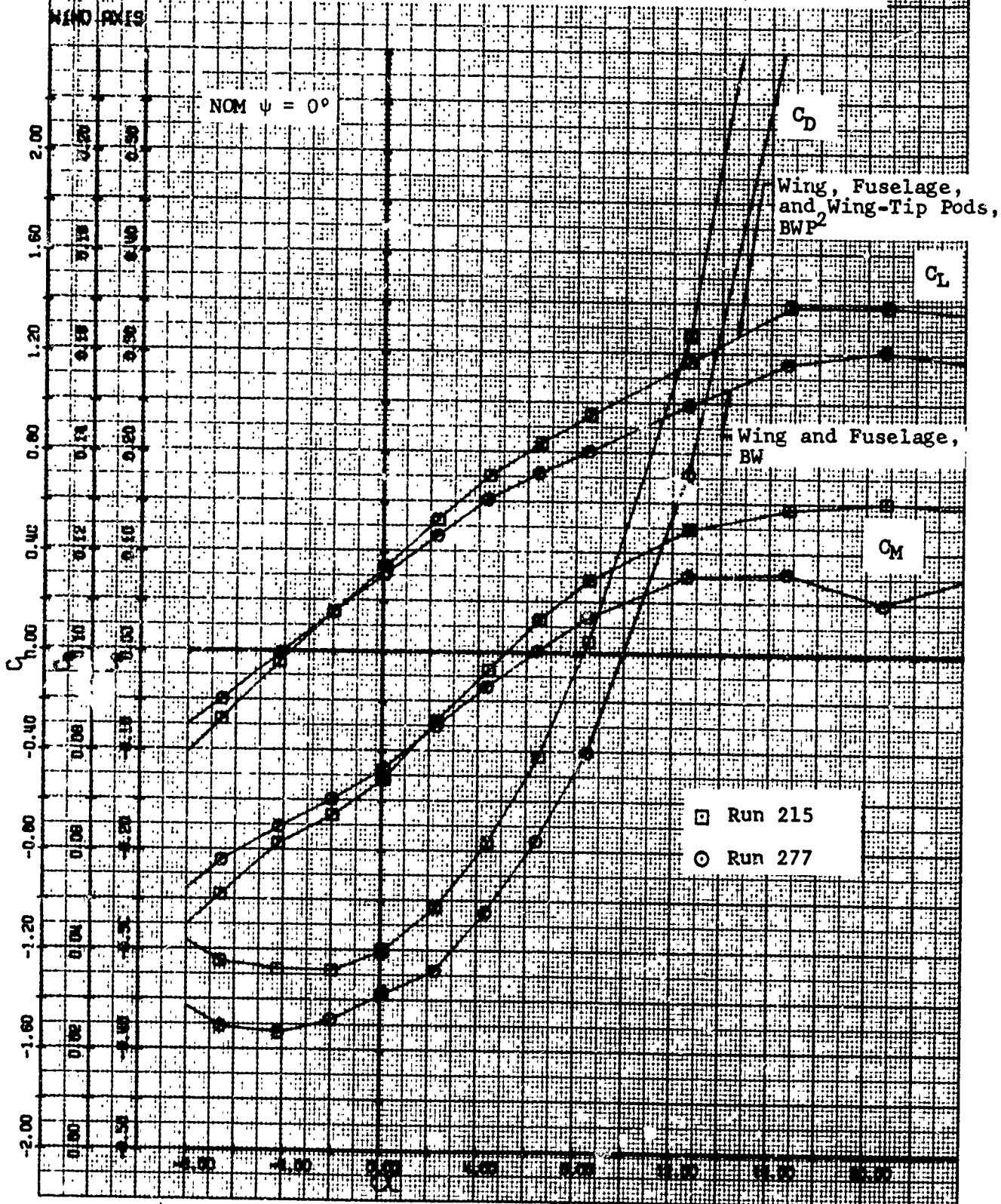
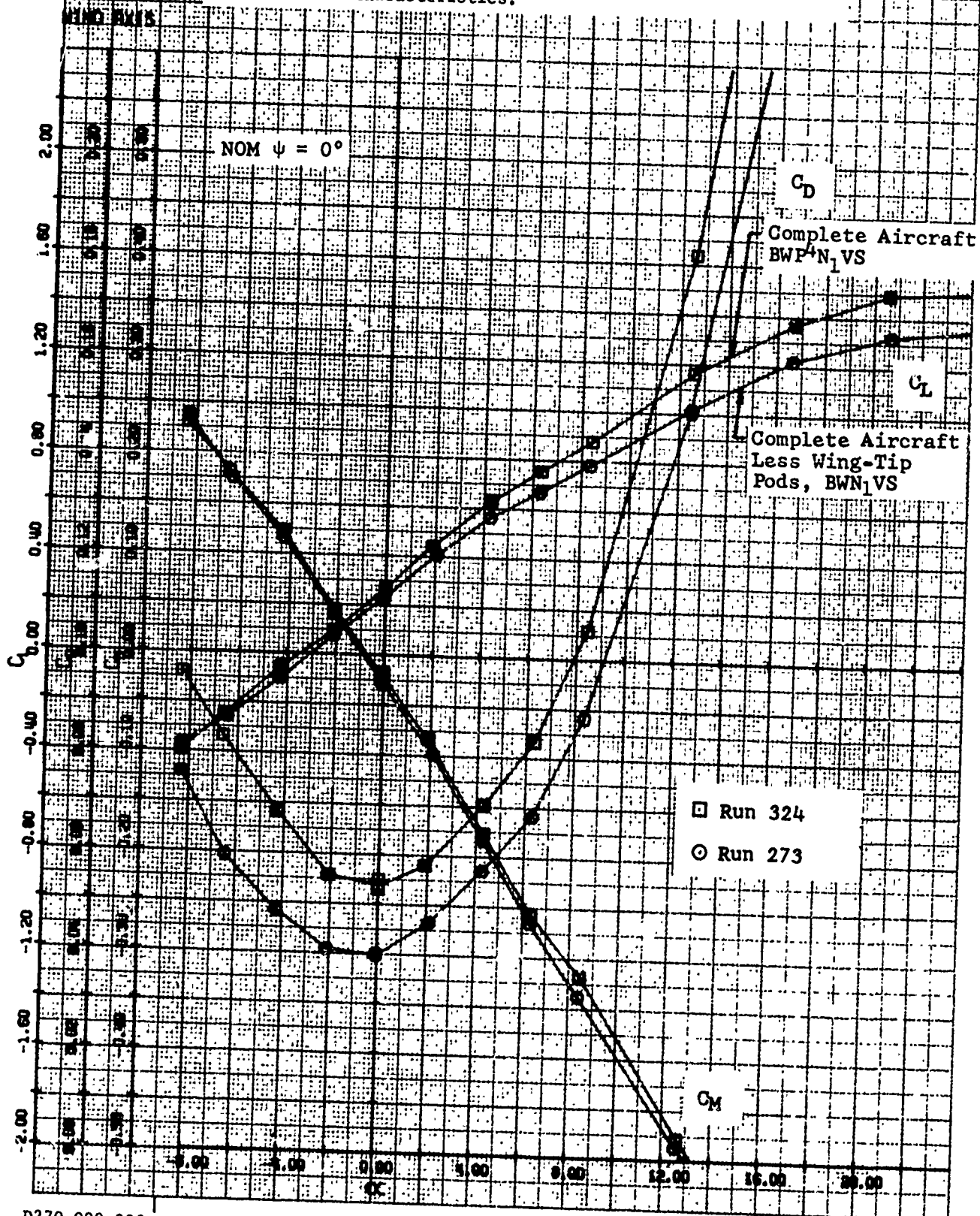


Figure V-21. Effect of Air Force Pod No. 2 on Longitudinal Characteristics.



D270-099-003

Figure V-22. Summary of Wingtip Pod Effects on Longitudinal Characteristics, Air Force Pod No. 1

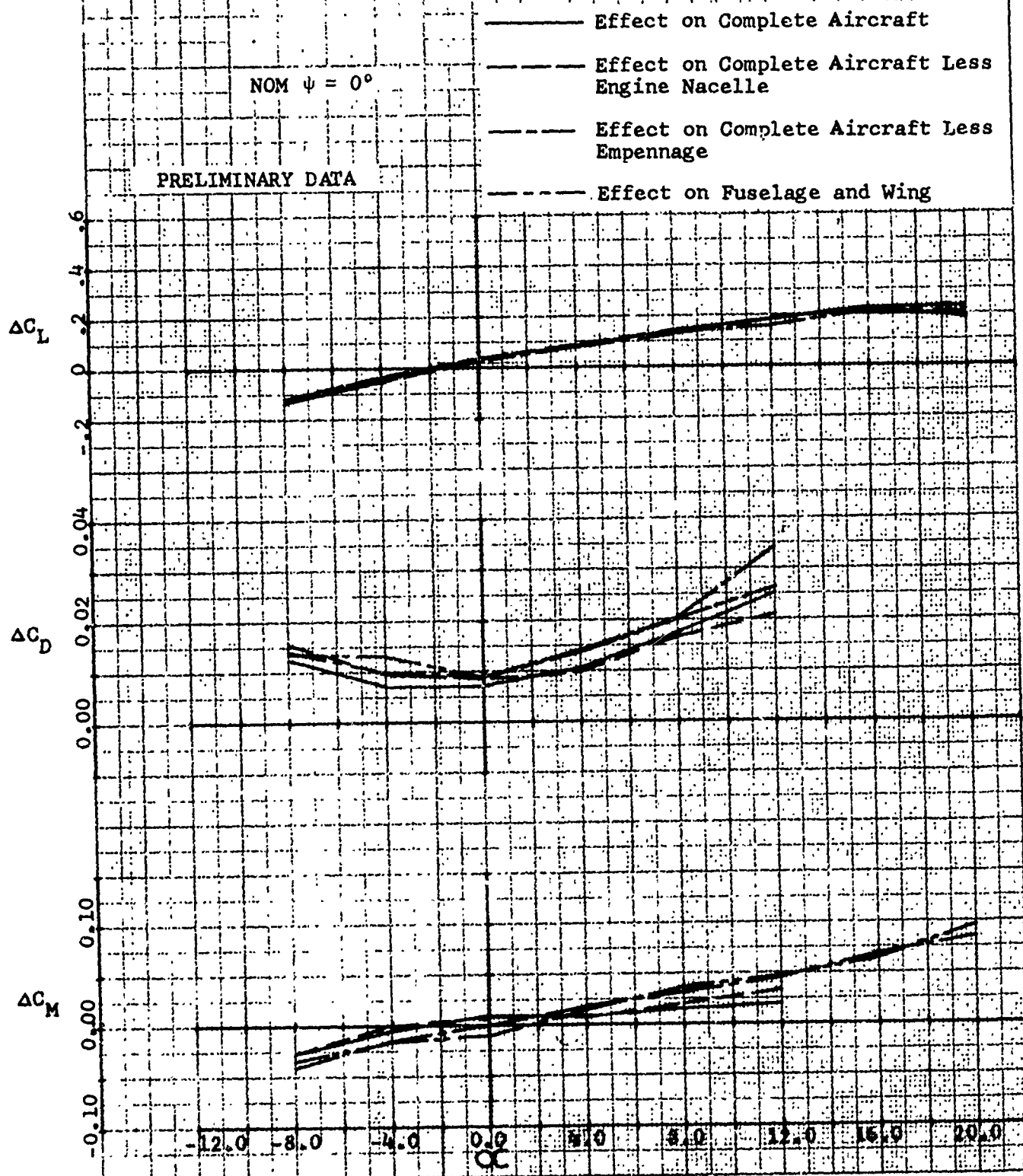


Figure V-23. Summary of the Effects of Other Wingtip-Pod Configurations on Longitudinal Characteristics.

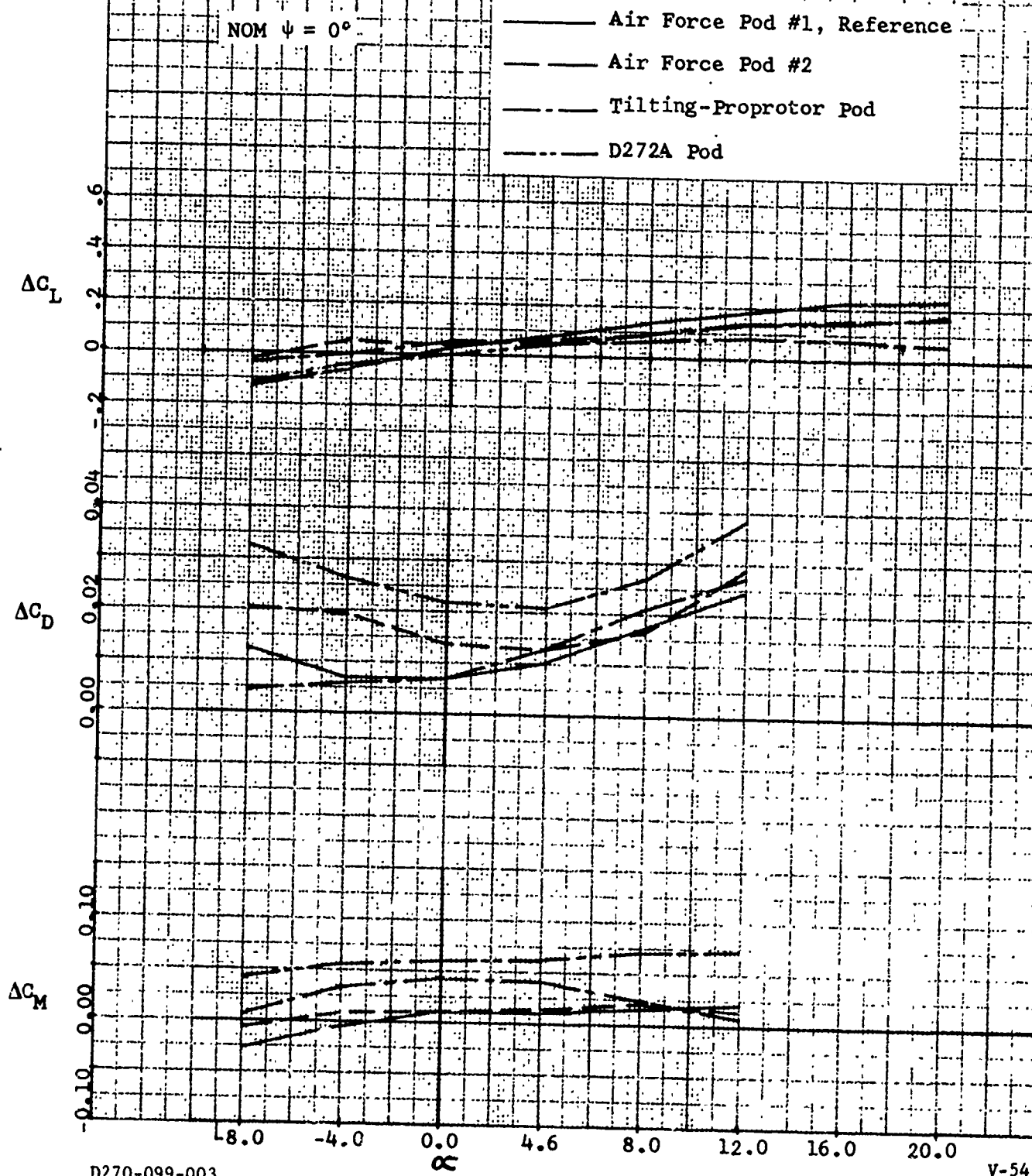


Figure V-24. Effect of Folded Blades on Lift.

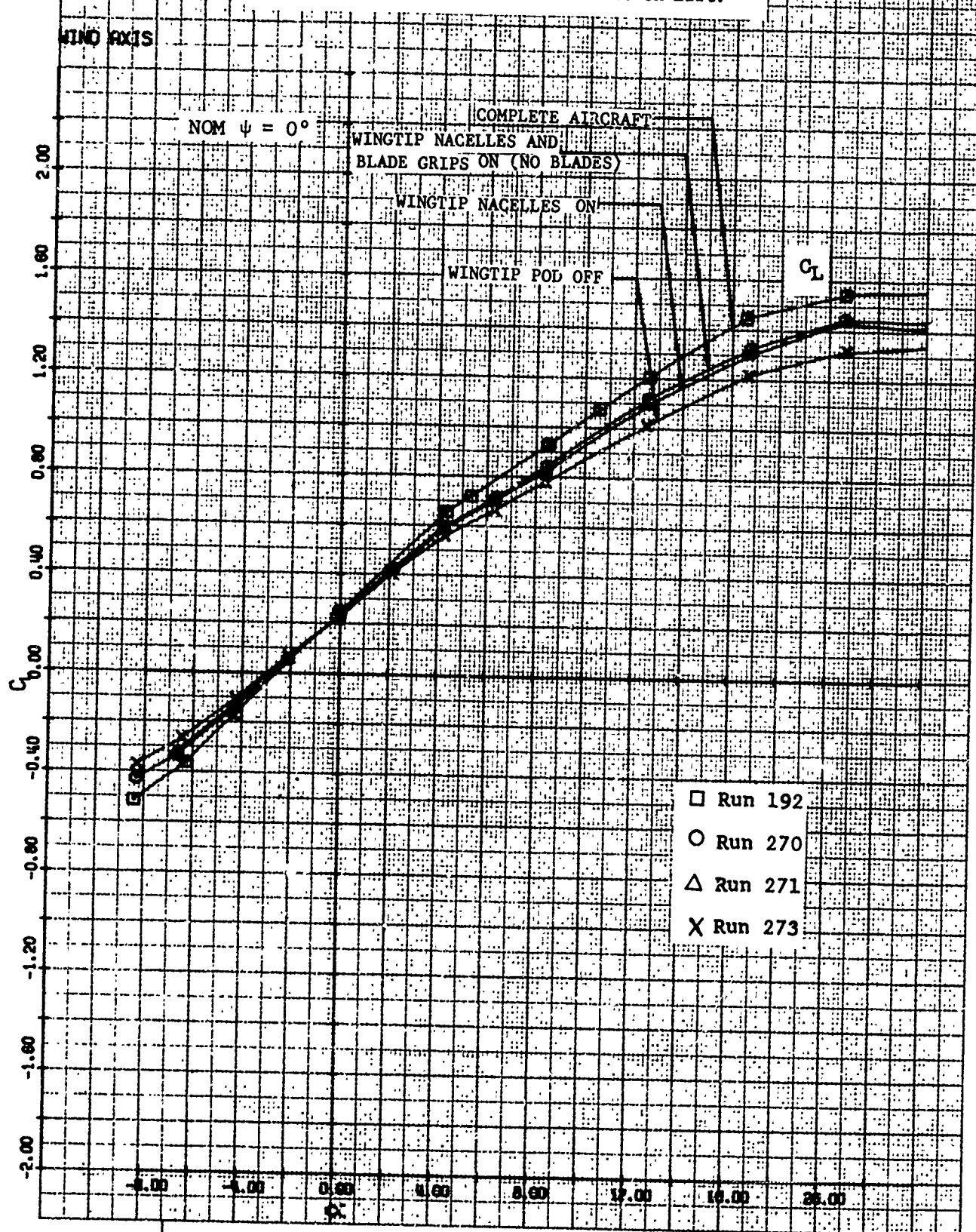


Figure V-25. Effect of Foiled Blades on Drag.

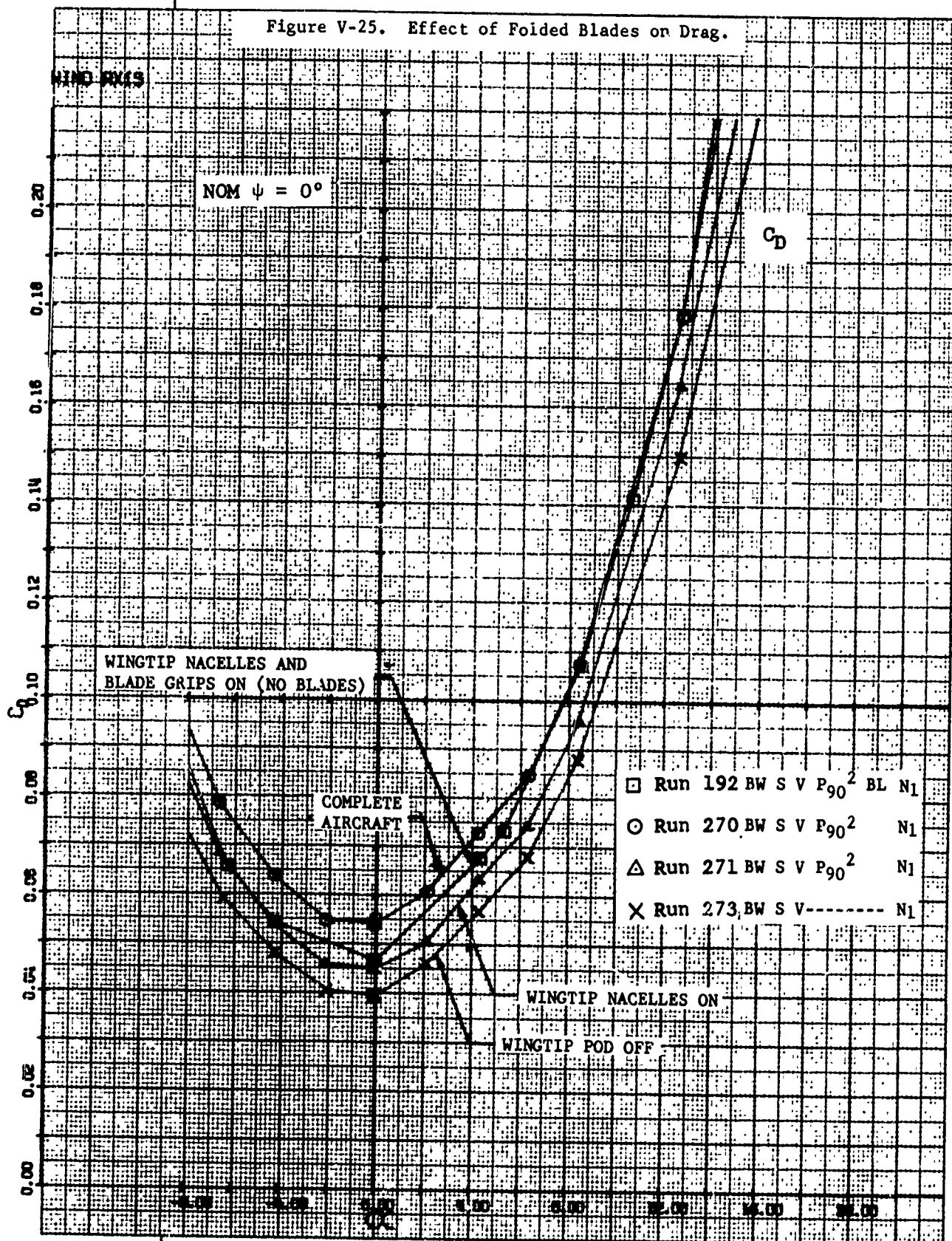


Figure V-26. Effect of Folded Blades on Pitching Moment.

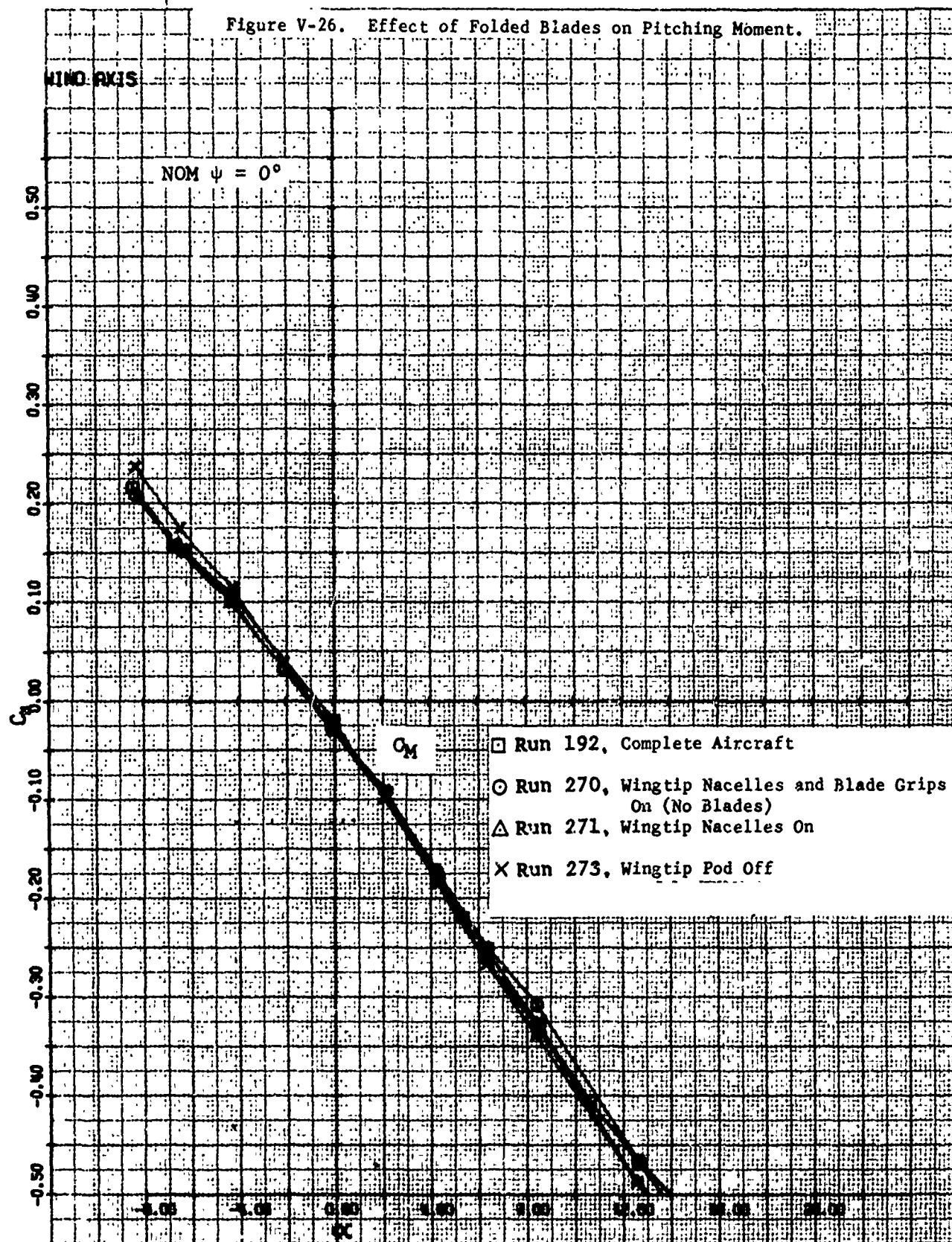


Figure V-27. Effect of Folded Blades on Rolling Moment.

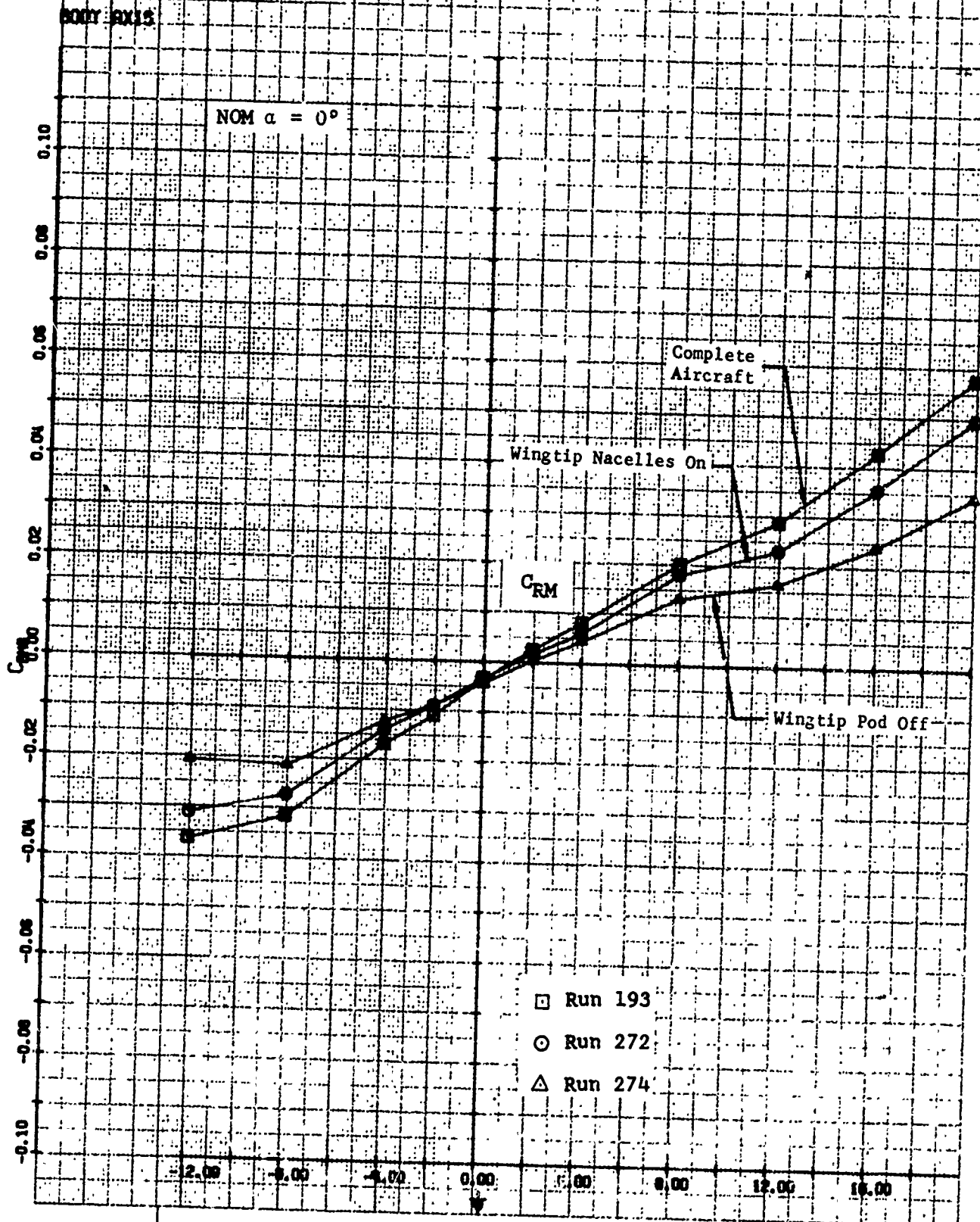


Figure V-28. Effect of Folded Blades on Yawing Moment.

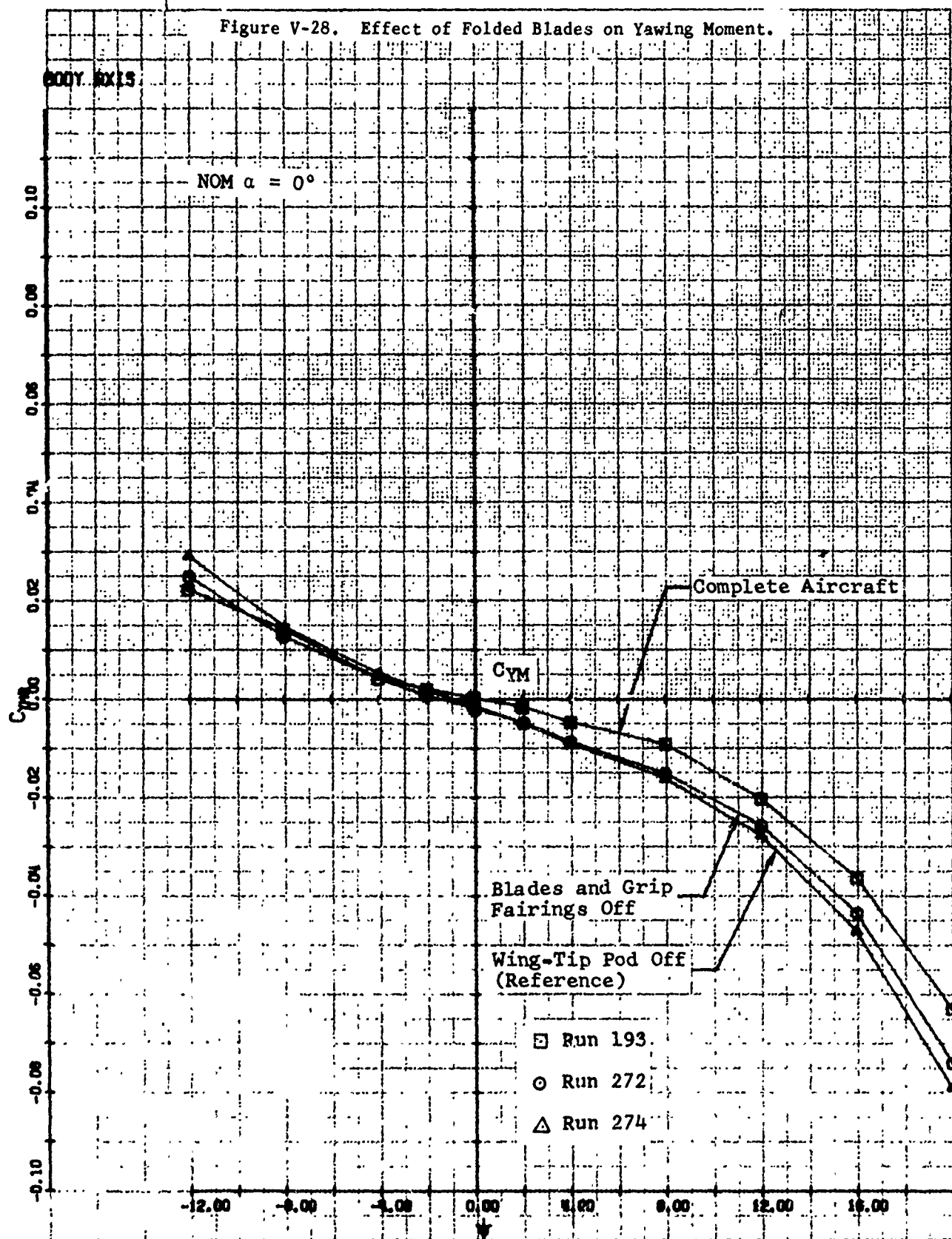
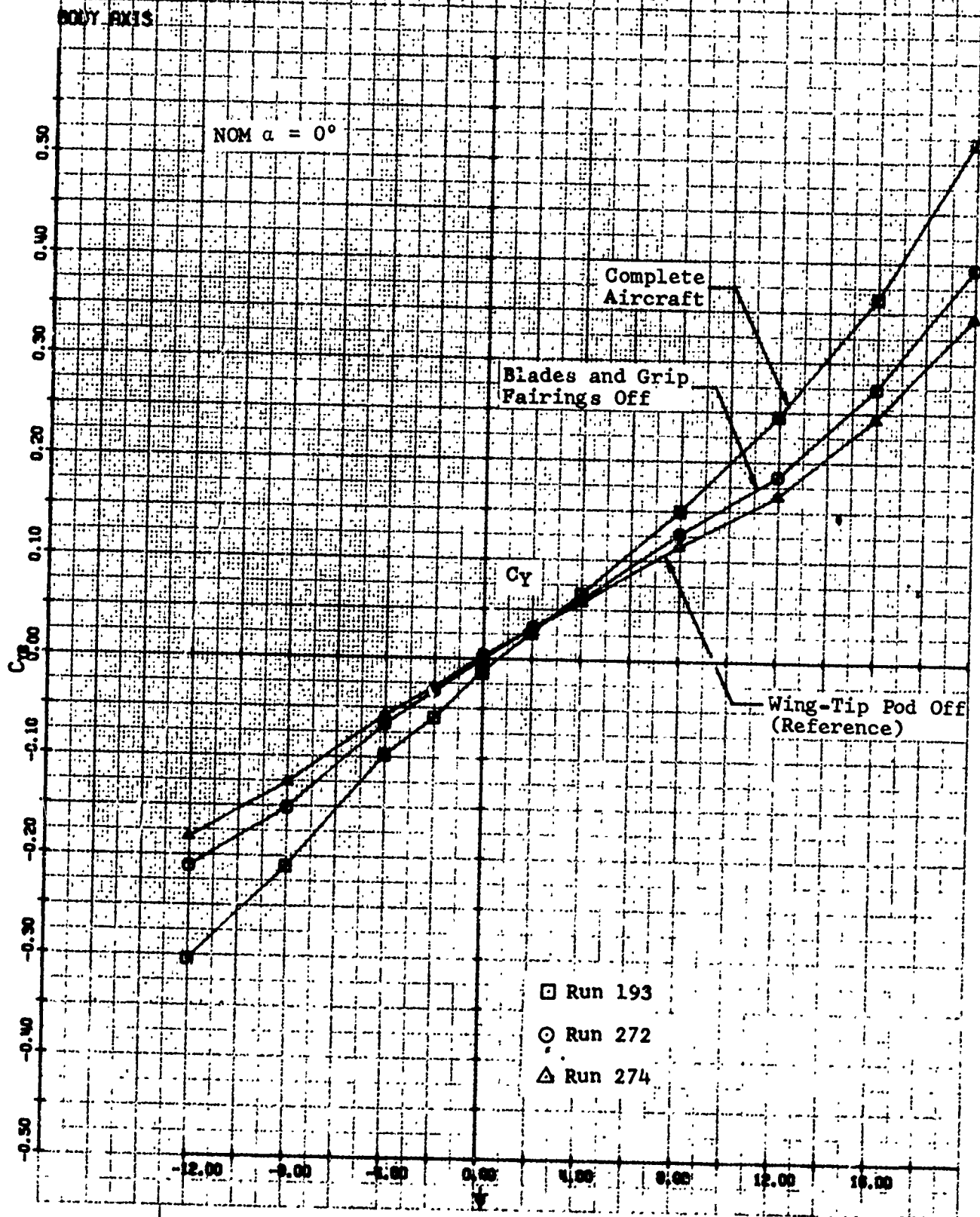


Figure V-29. Effect of Folded Blades on Side Force.



HIND AXIS

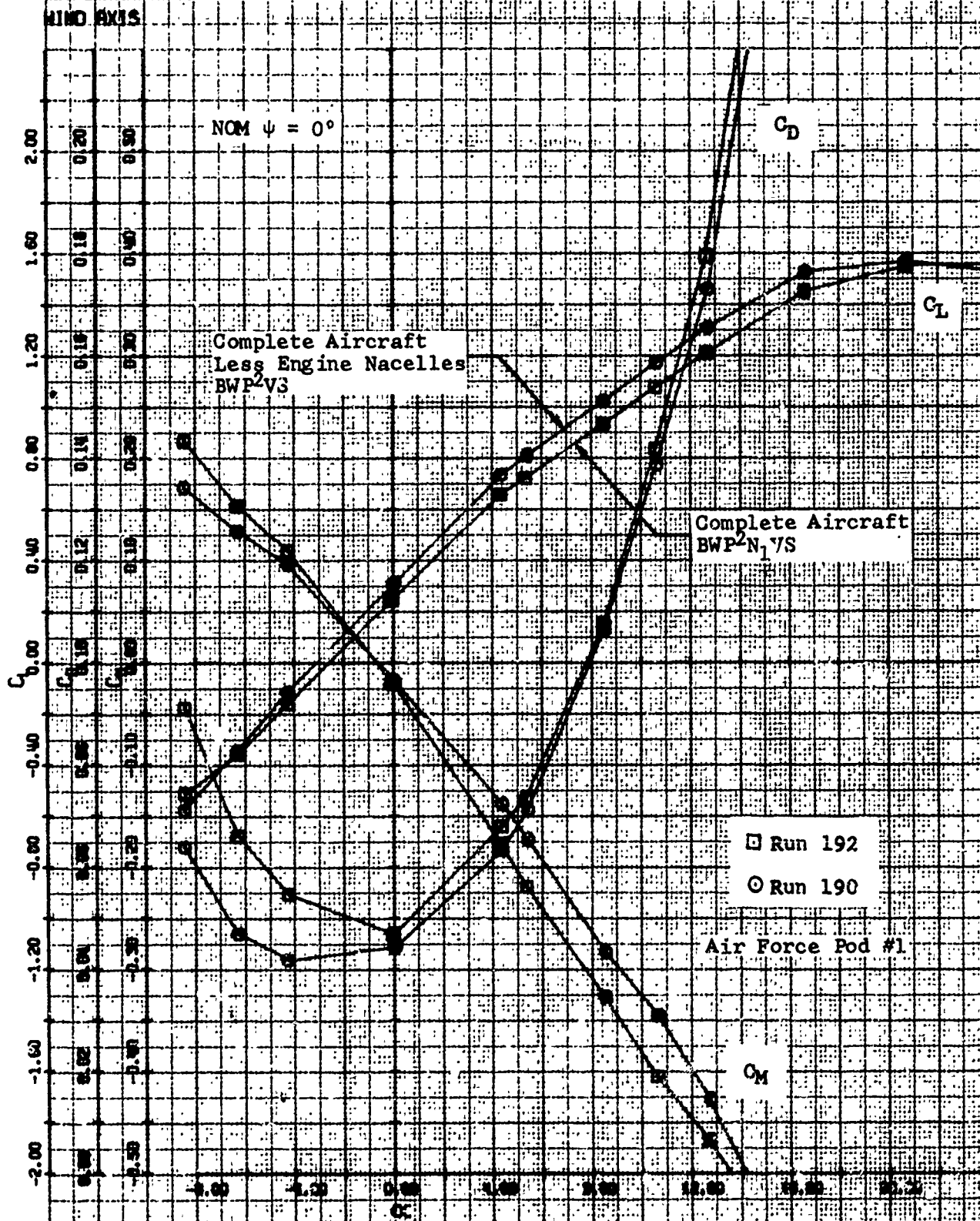


Figure V-31. Effect of Engine Nacelles on Longitudinal Characteristics for the Complete Aircraft Less Wingtip Pods.

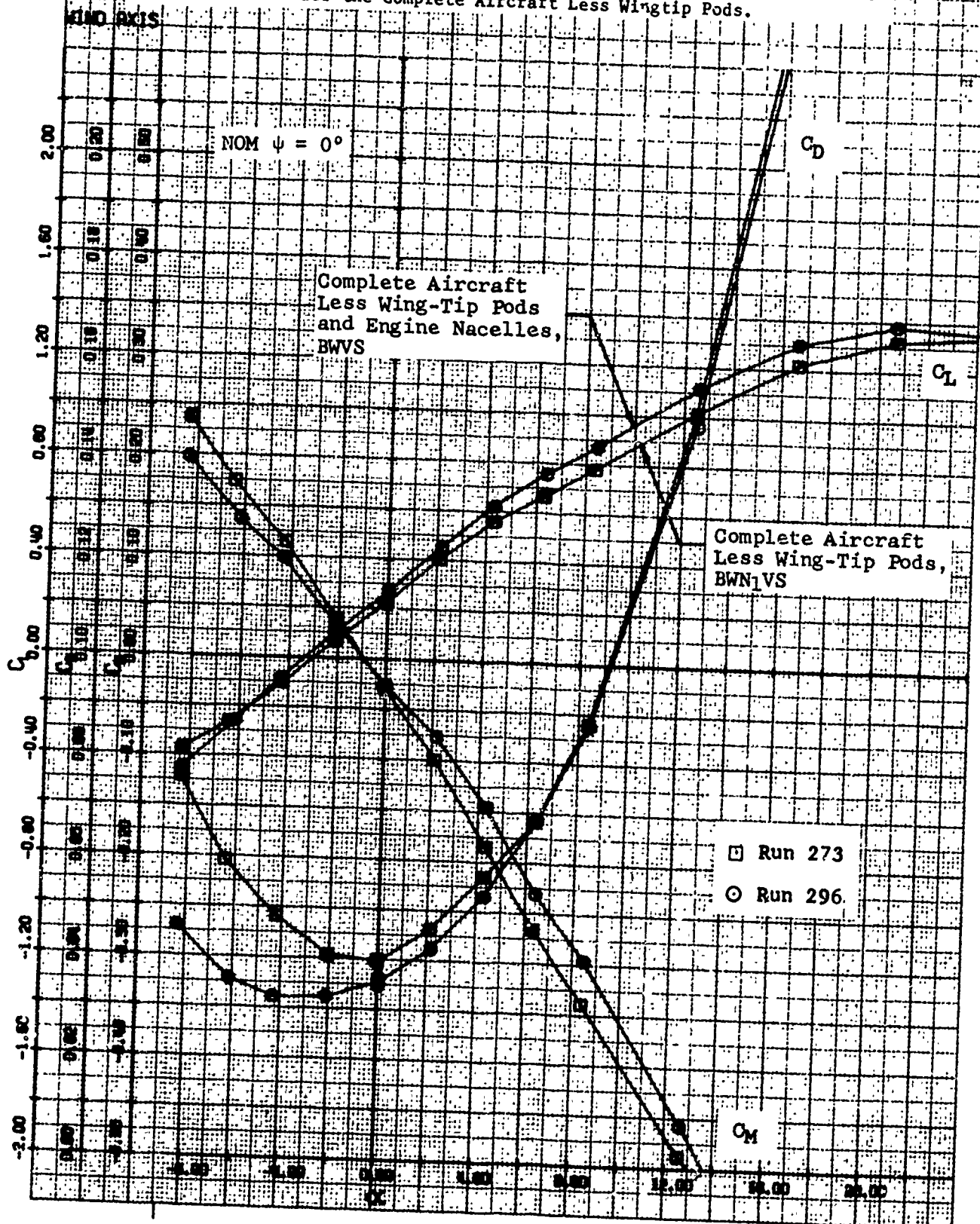


Figure V-32. Effect of Engine Nacelles on Logitudinal Characteristics for the Complete Aircraft Less Empennage.

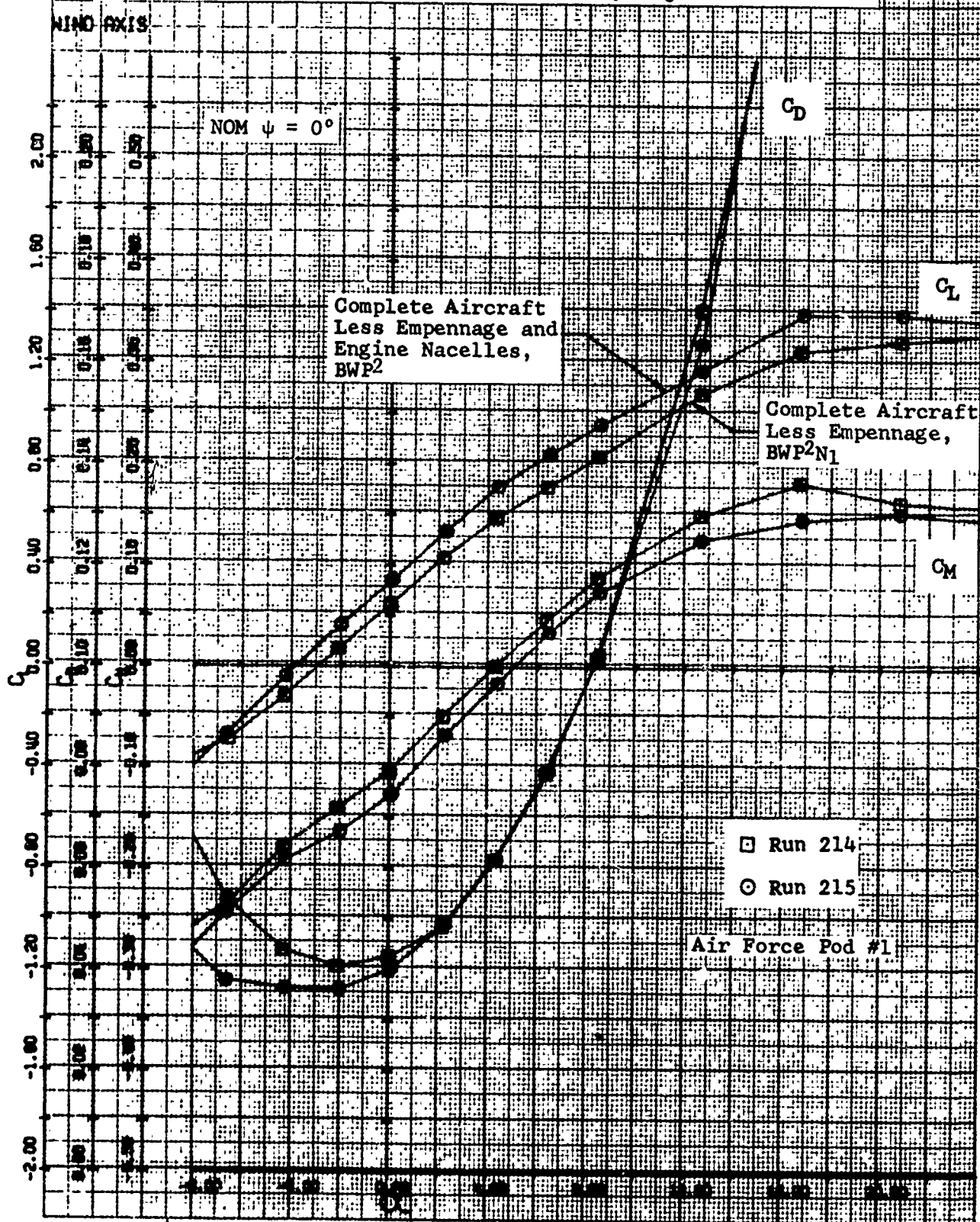


Figure V-33. Effect of Engine Nacelles on Longitudinal Characteristics of the Fuselage and Wing.

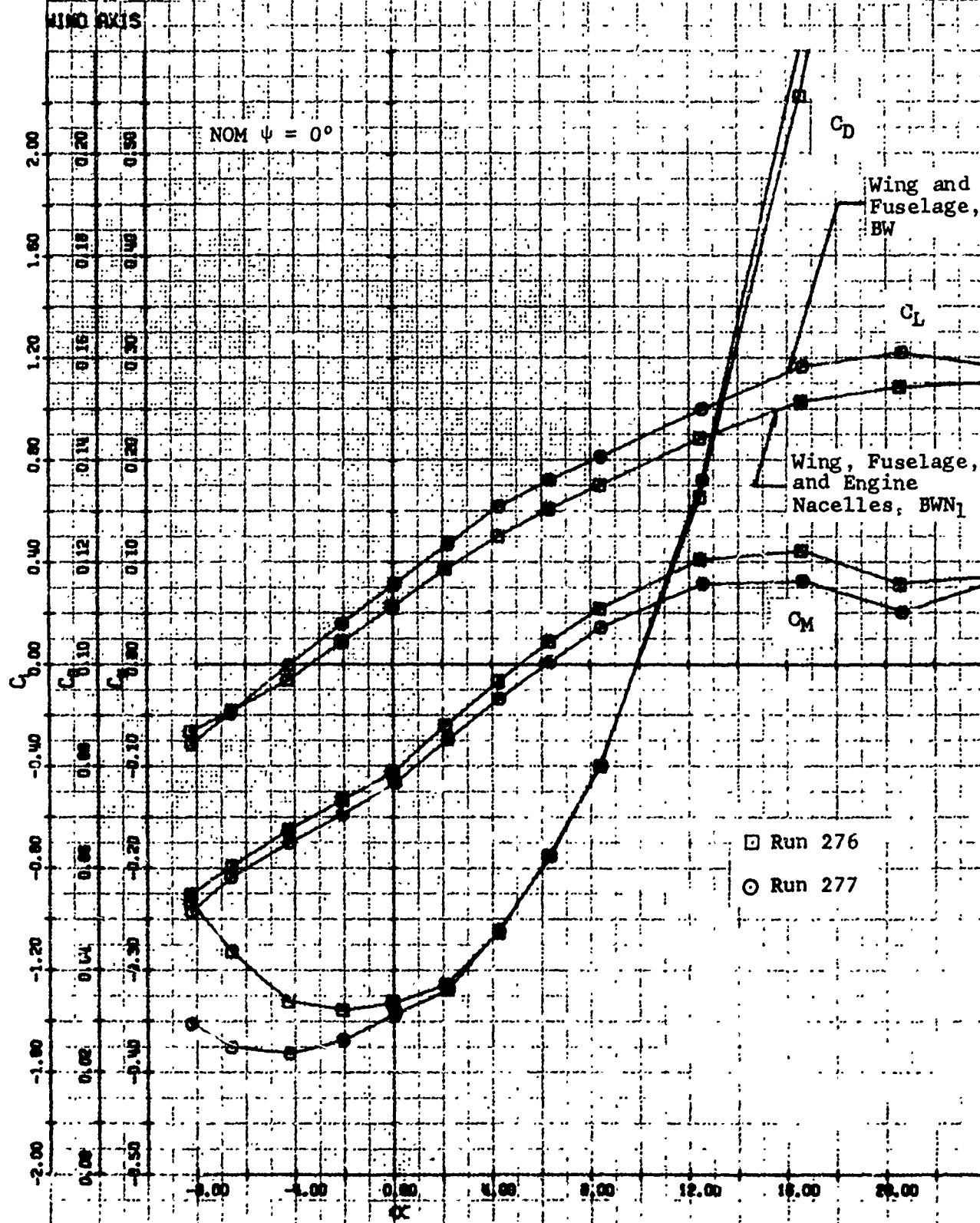


Figure V-34. Summary of Engine-Nacelle Effects on Longitudinal Characteristics.

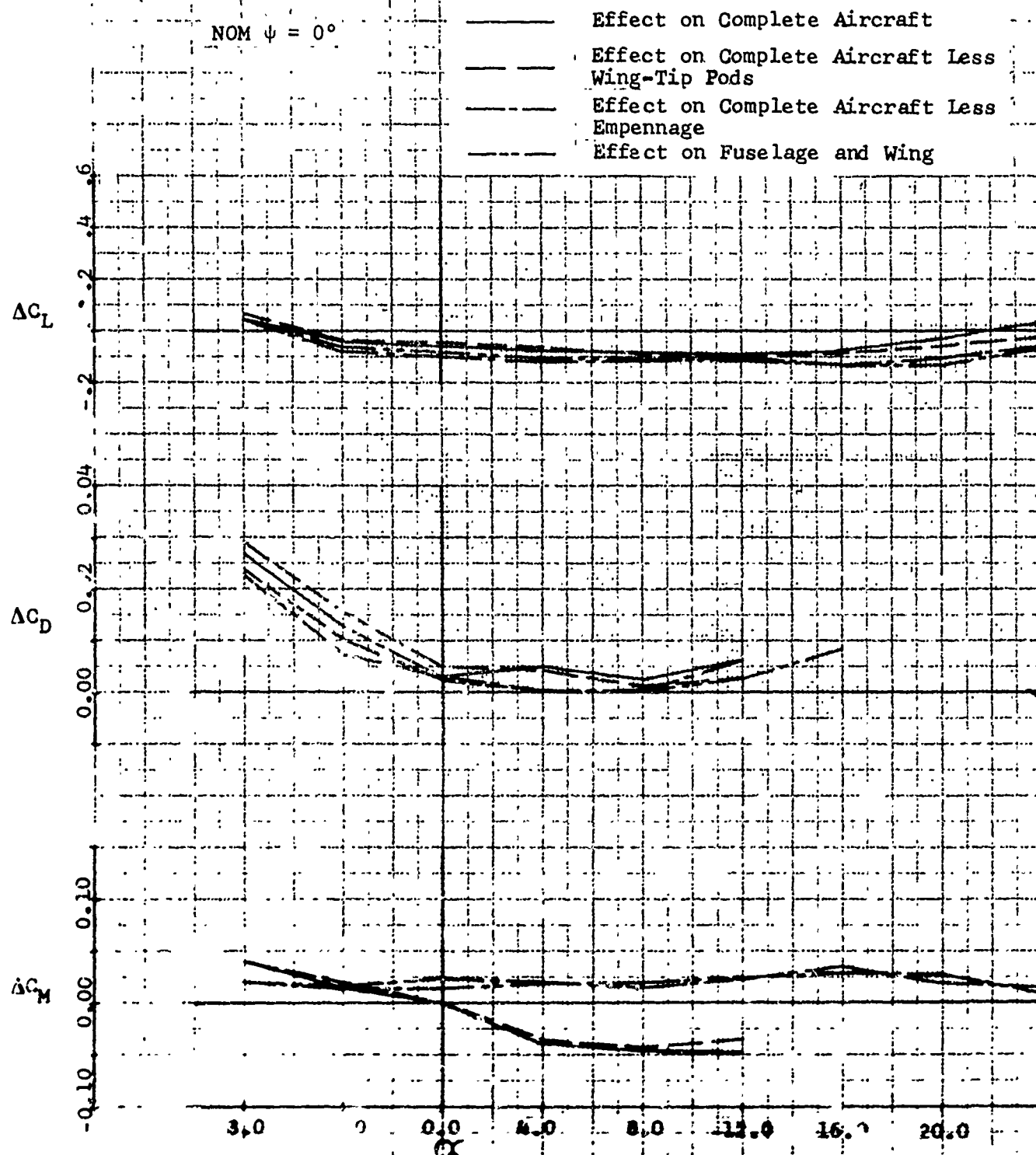
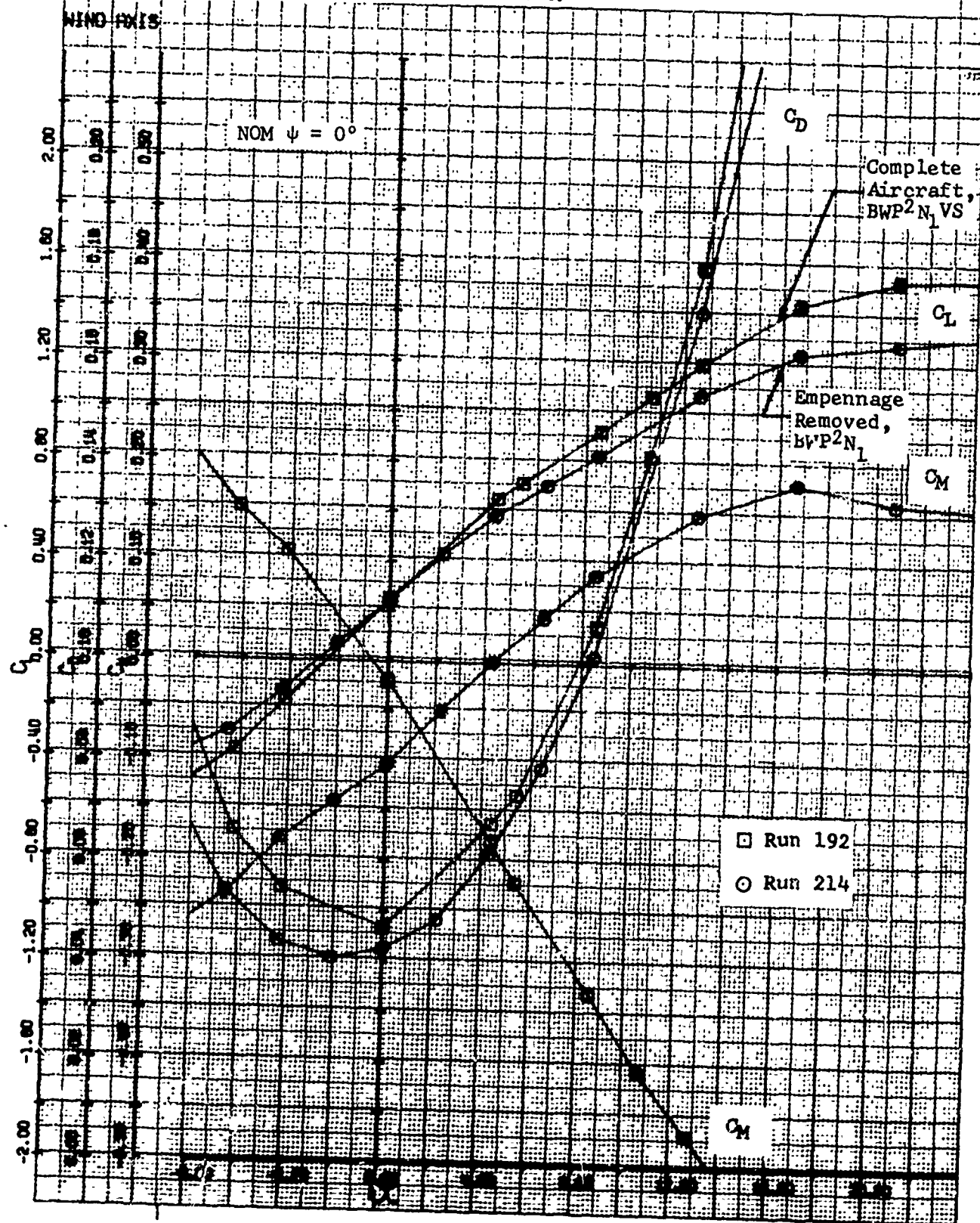


Figure V-35. Longitudinal Characteristics with Horizontal Tail Removed from Complete Aircraft.



5270-099-001

Figure V-36. Longitudinal Characteristics with Horizontal Tail Removed from Complete Aircraft Less Engine Nacelles.

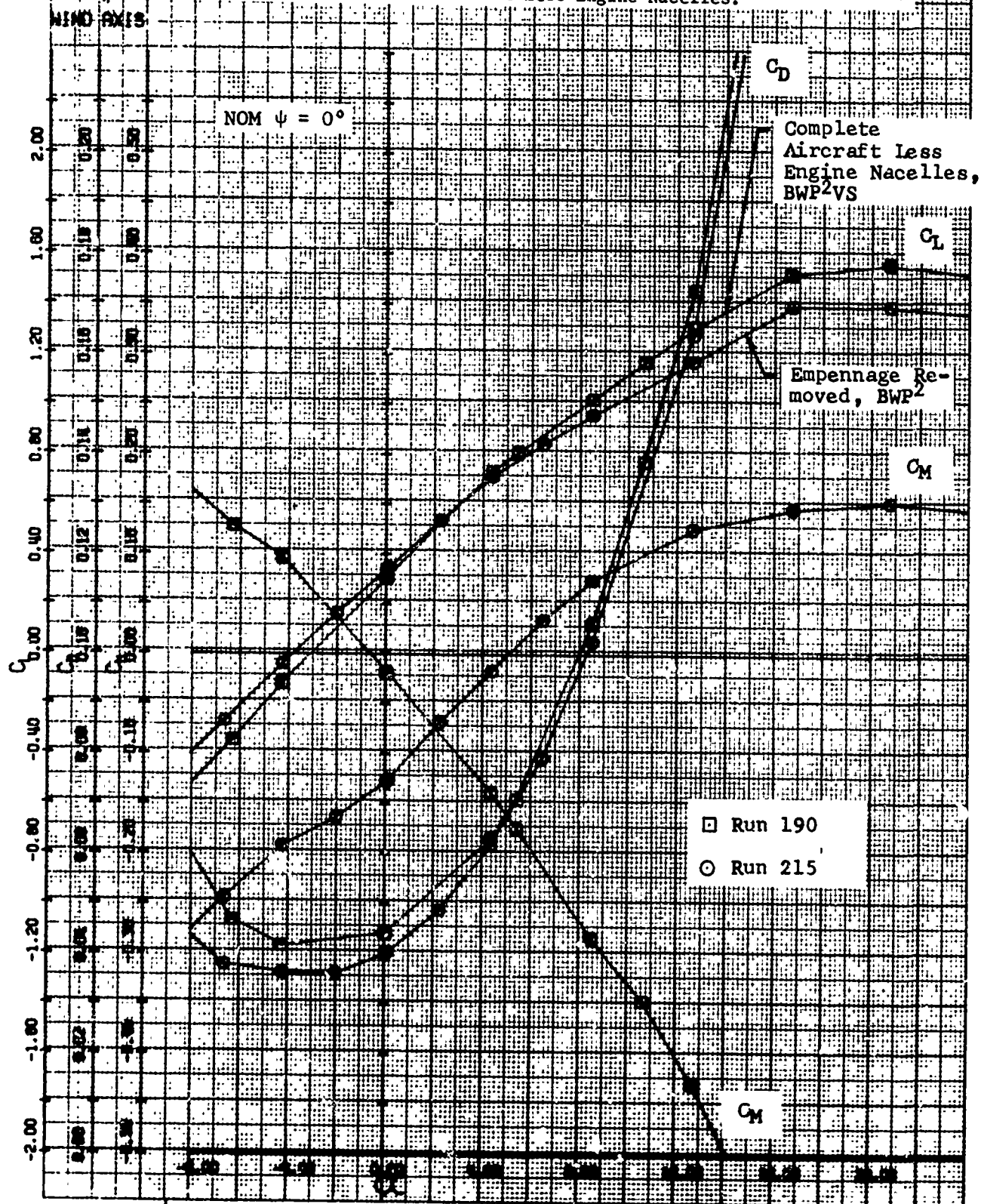


Figure V-37. Longitudinal Characteristics with Horizontal Tail Removed from Fuselage and Wing.

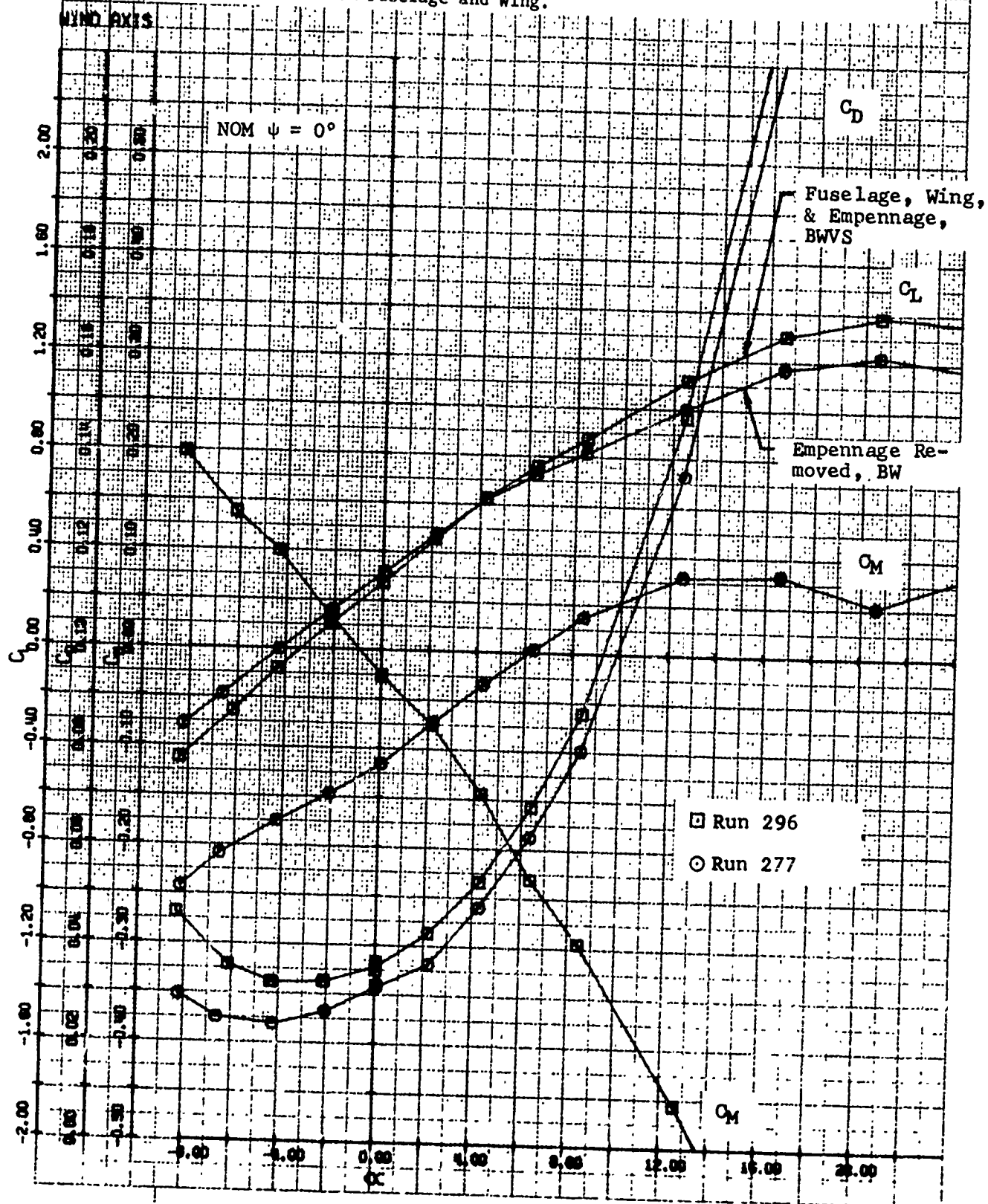


Figure V-38. Summary of Horizontal Tail Contributions to Longitudinal Characteristics.

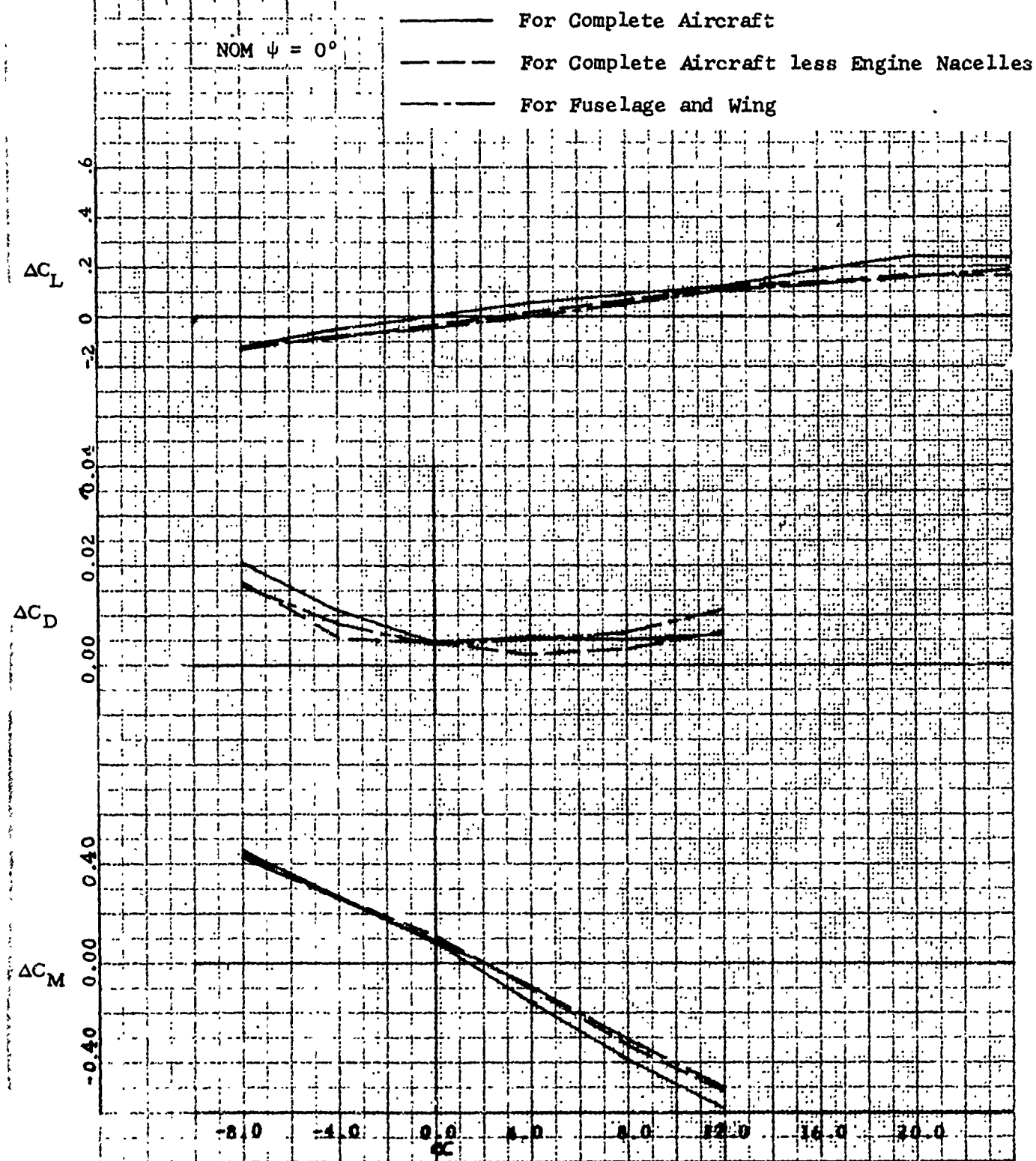


Figure V-39. Horizontal Stabilizer Contributions to Pitch Static Stability.

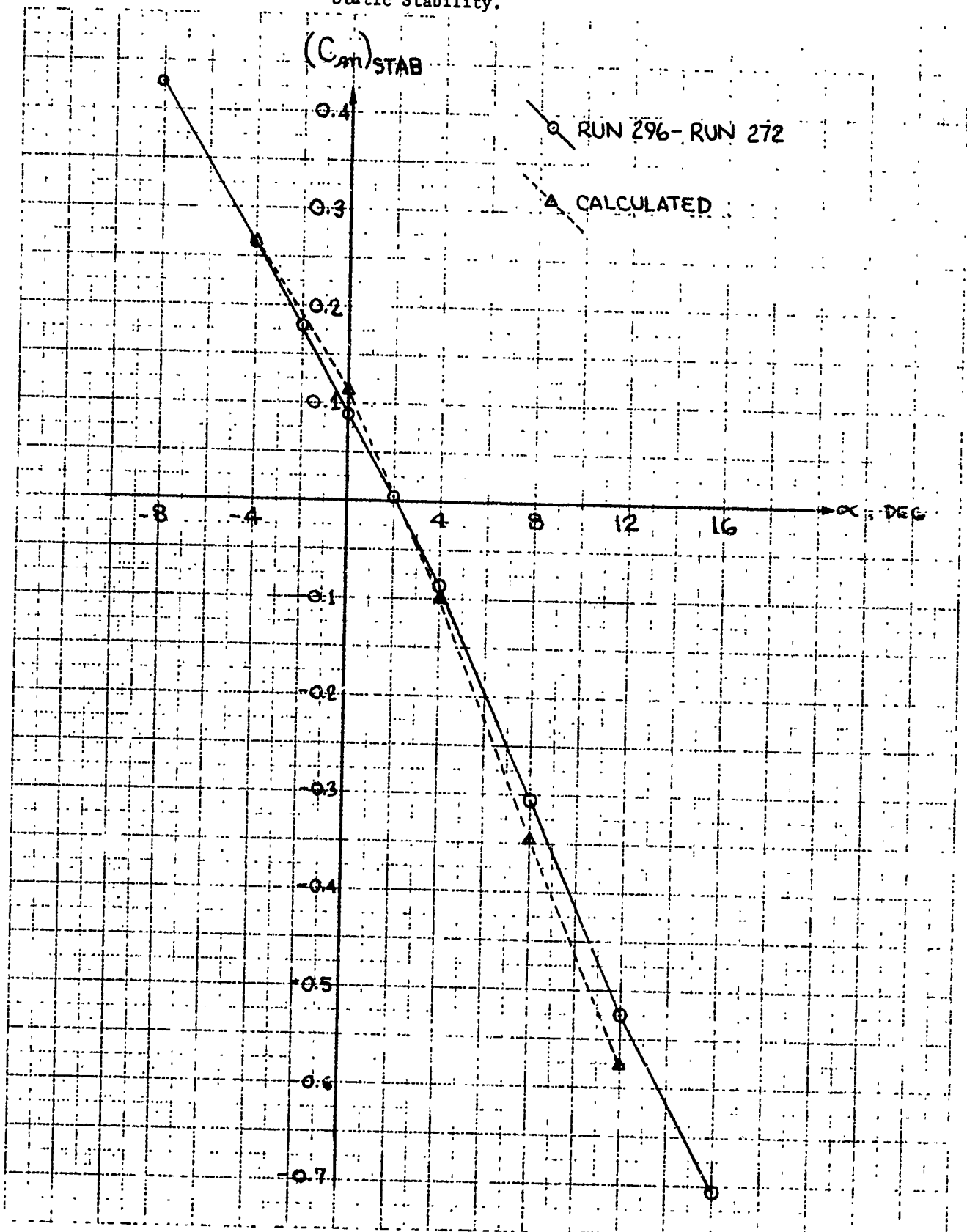


Figure V-40. Downwash on the Horizontal Stabilizer.

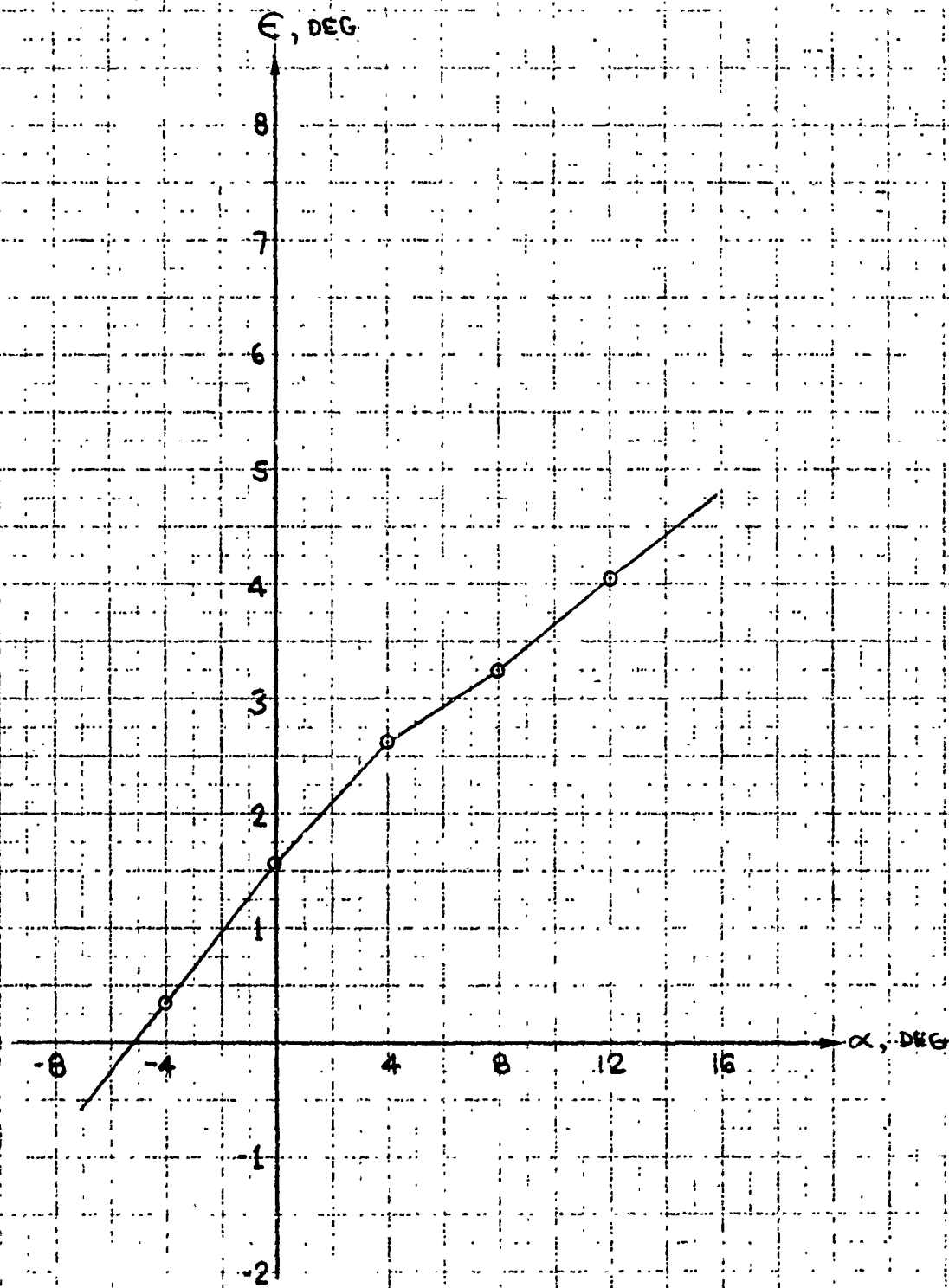


Figure V-41. Basic Airframe Effects, Model Clean.

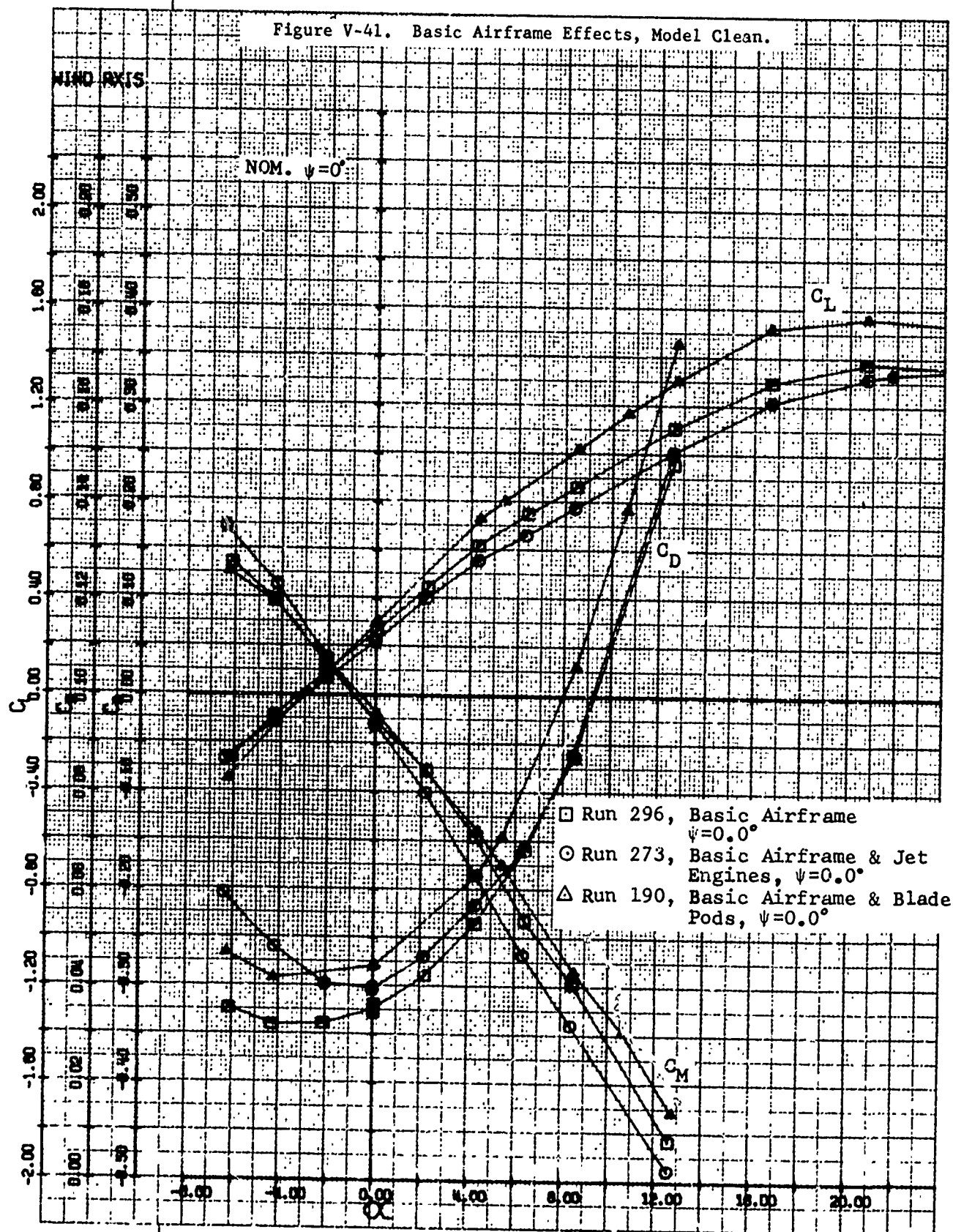


Figure V-42. Basic Airframe Effects.

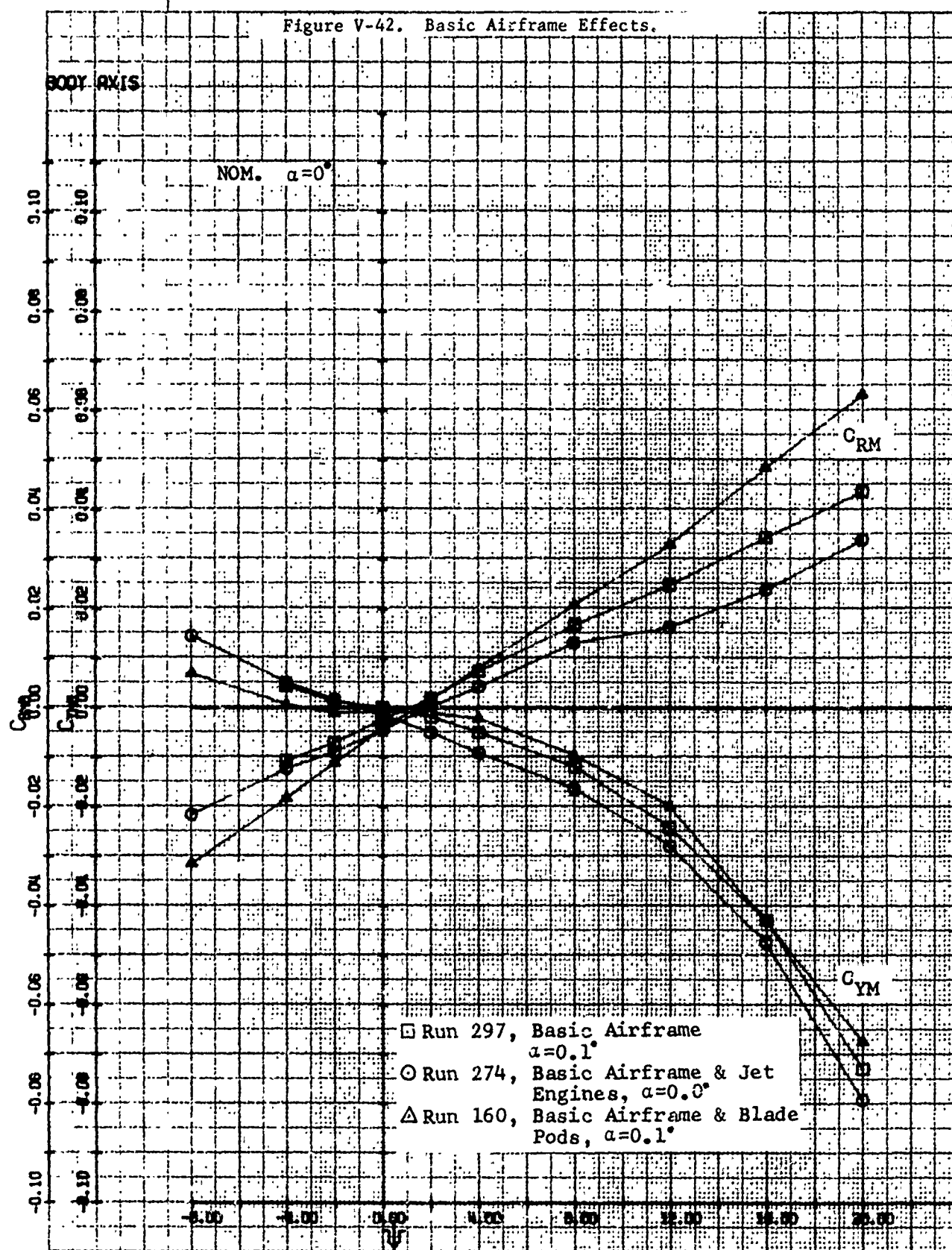


Figure V-43. Effect of Vortex Generators on Wing Contribution to $C_{l\beta}$.

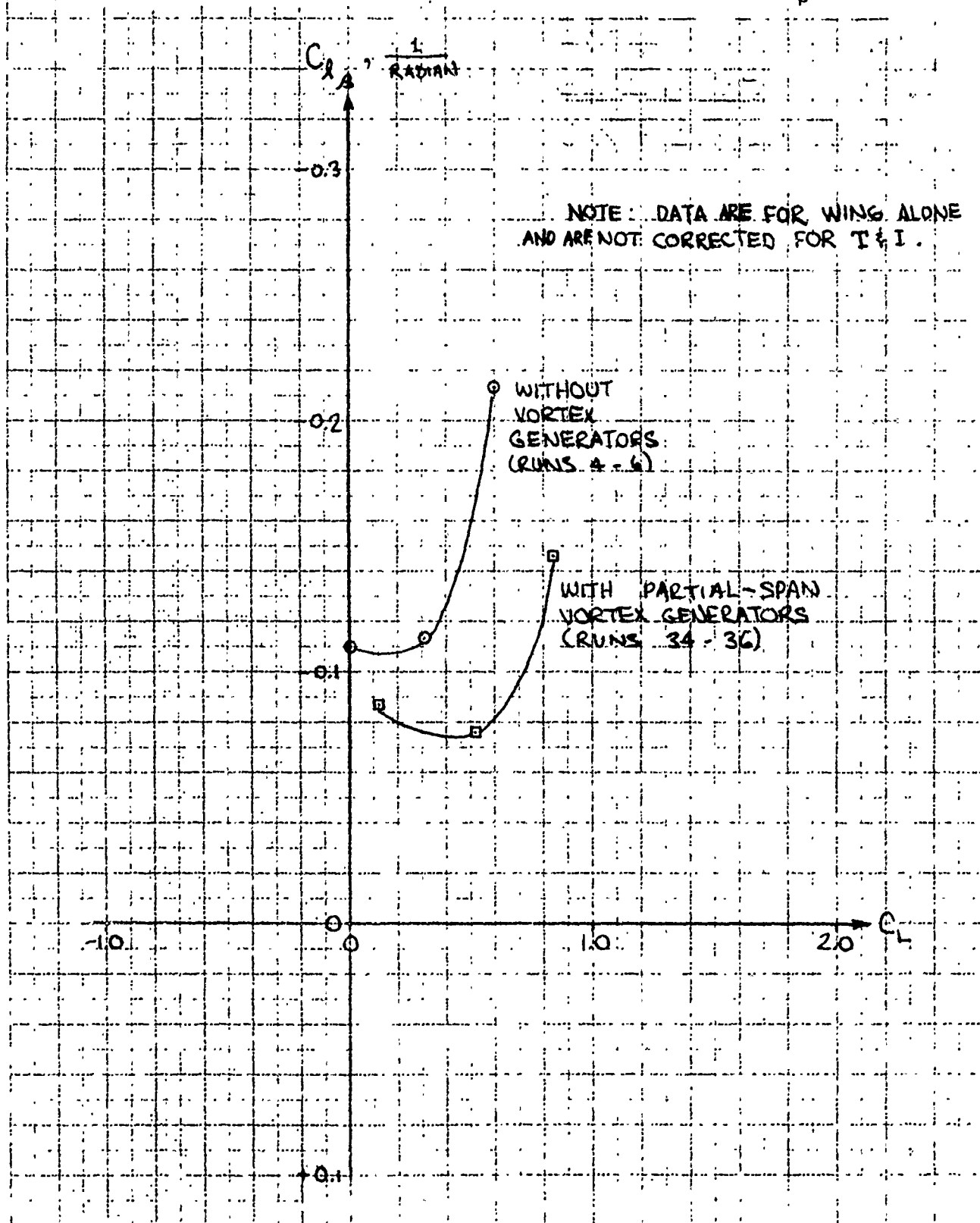


Figure V-44. Effect of Blade Pods on Aircraft Dihedral Stability.

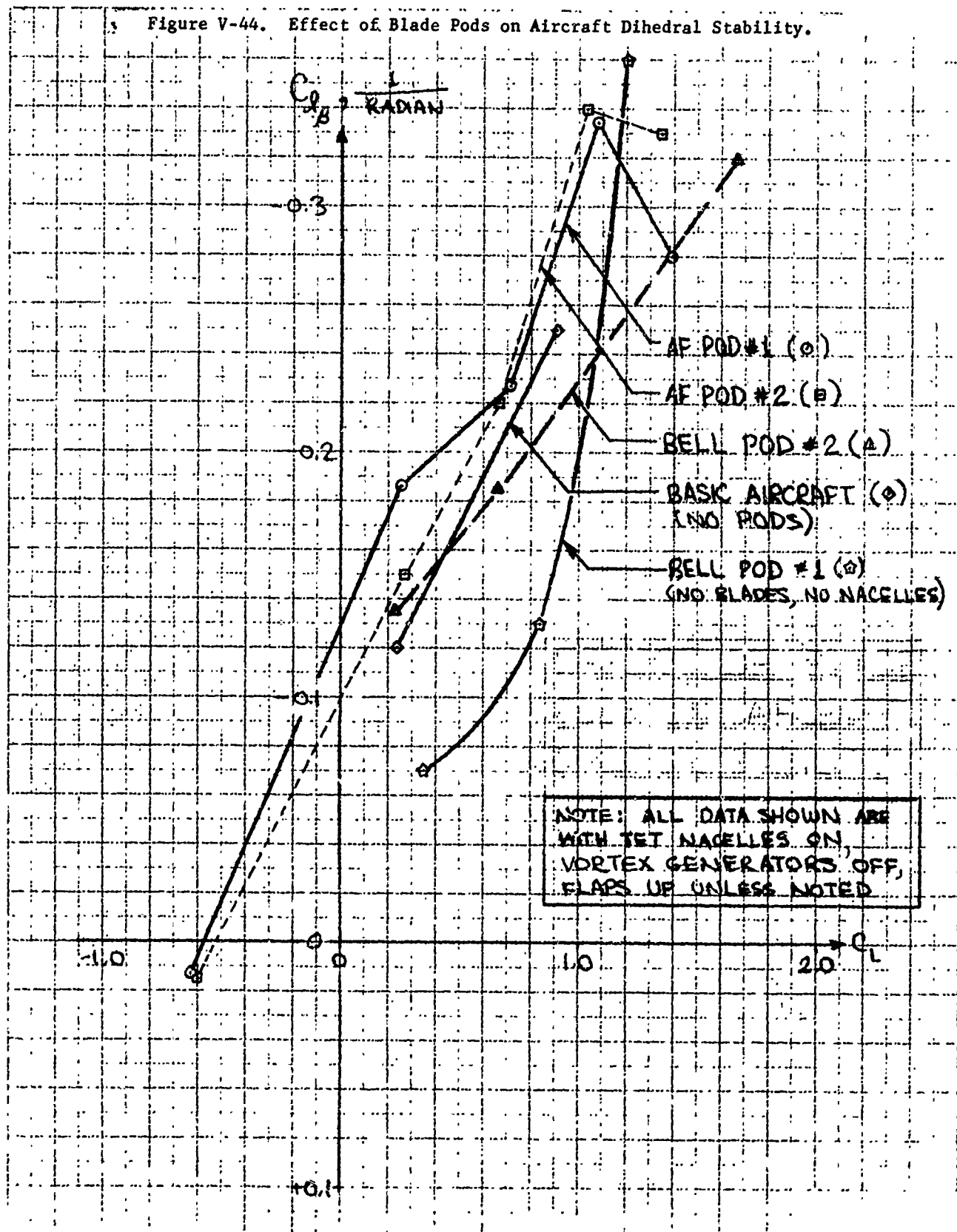


Figure V-45. Aircraft Dihedral Stability - Vortex Generators On.

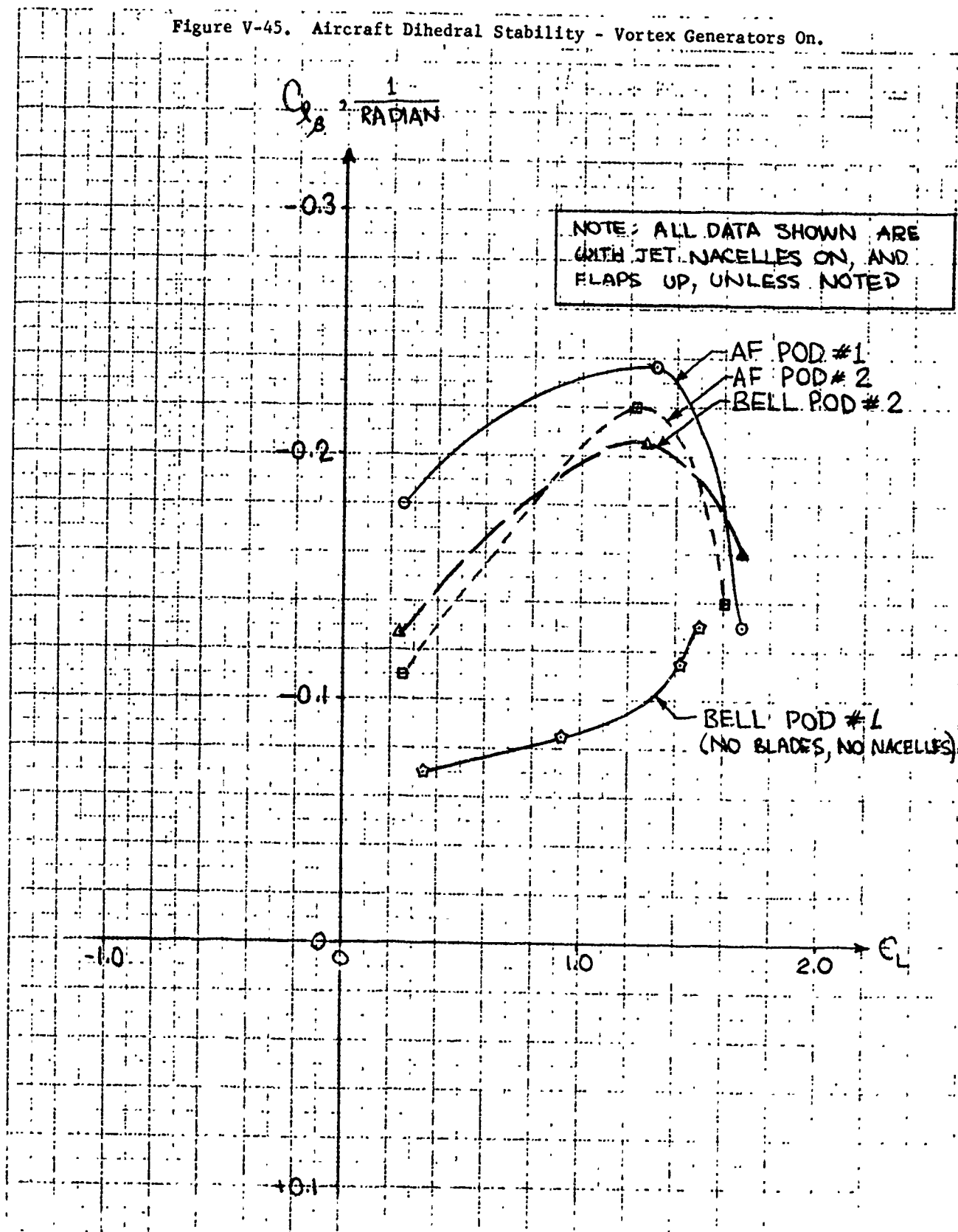


Figure V-46. Aircraft Dihedral Stability, Vortex Generators On.

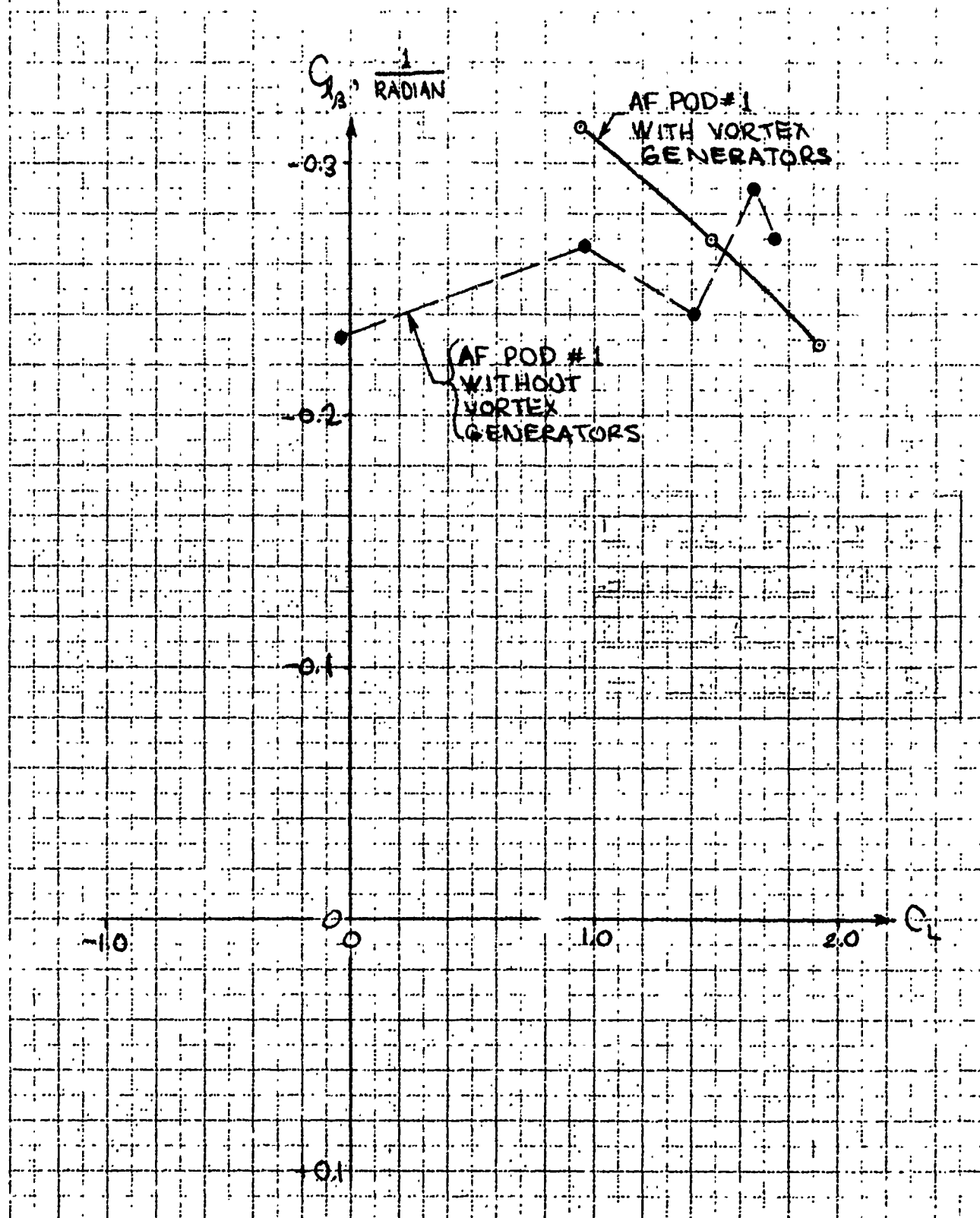


Figure V-47. Blade Opening Effects, Air Force Pod No. 1 Flaps Down,
Vortex Generators On

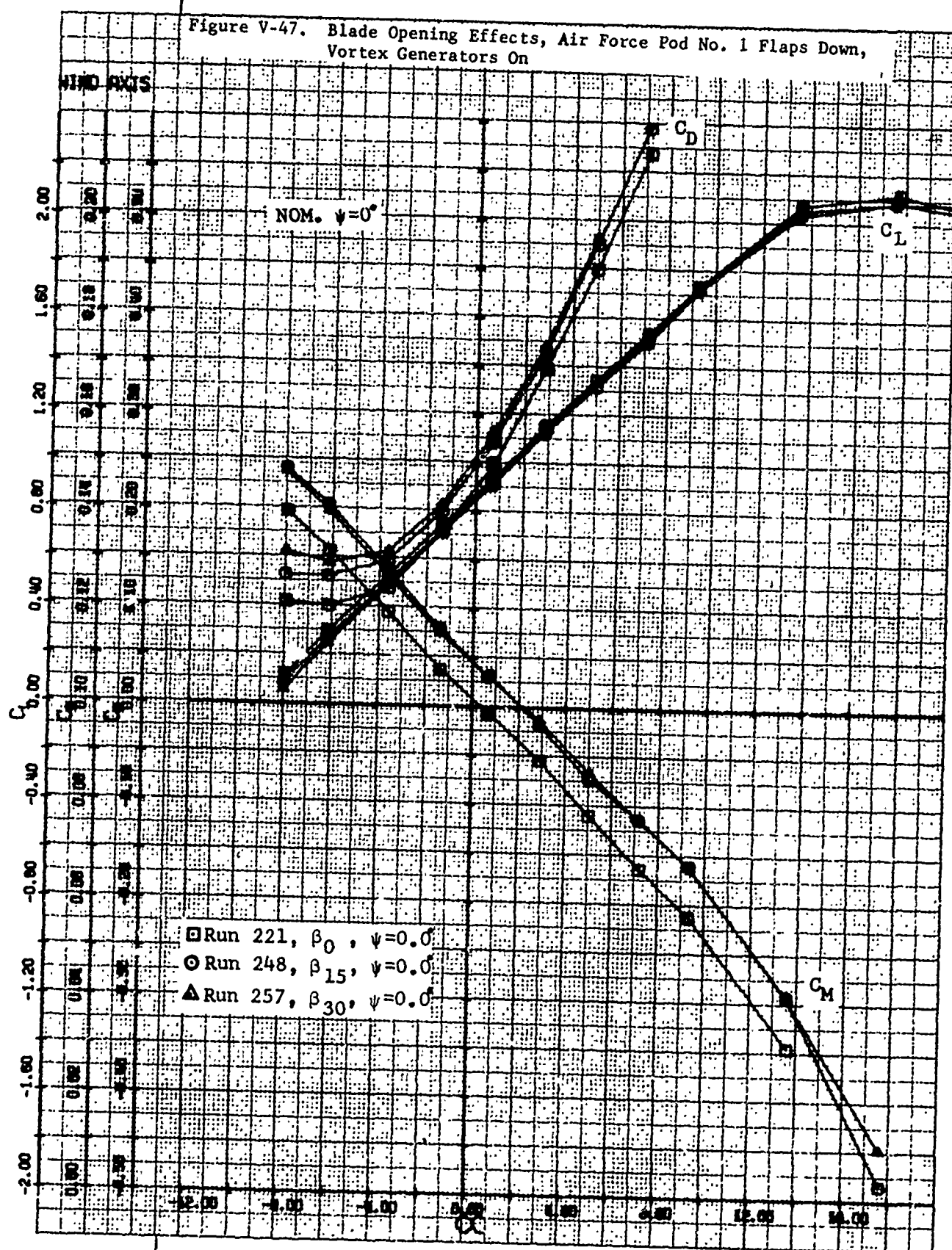


Figure V-48. Blade Opening Effects, Air Force Pod No. 1, Flaps Down, Vortex Generators On.

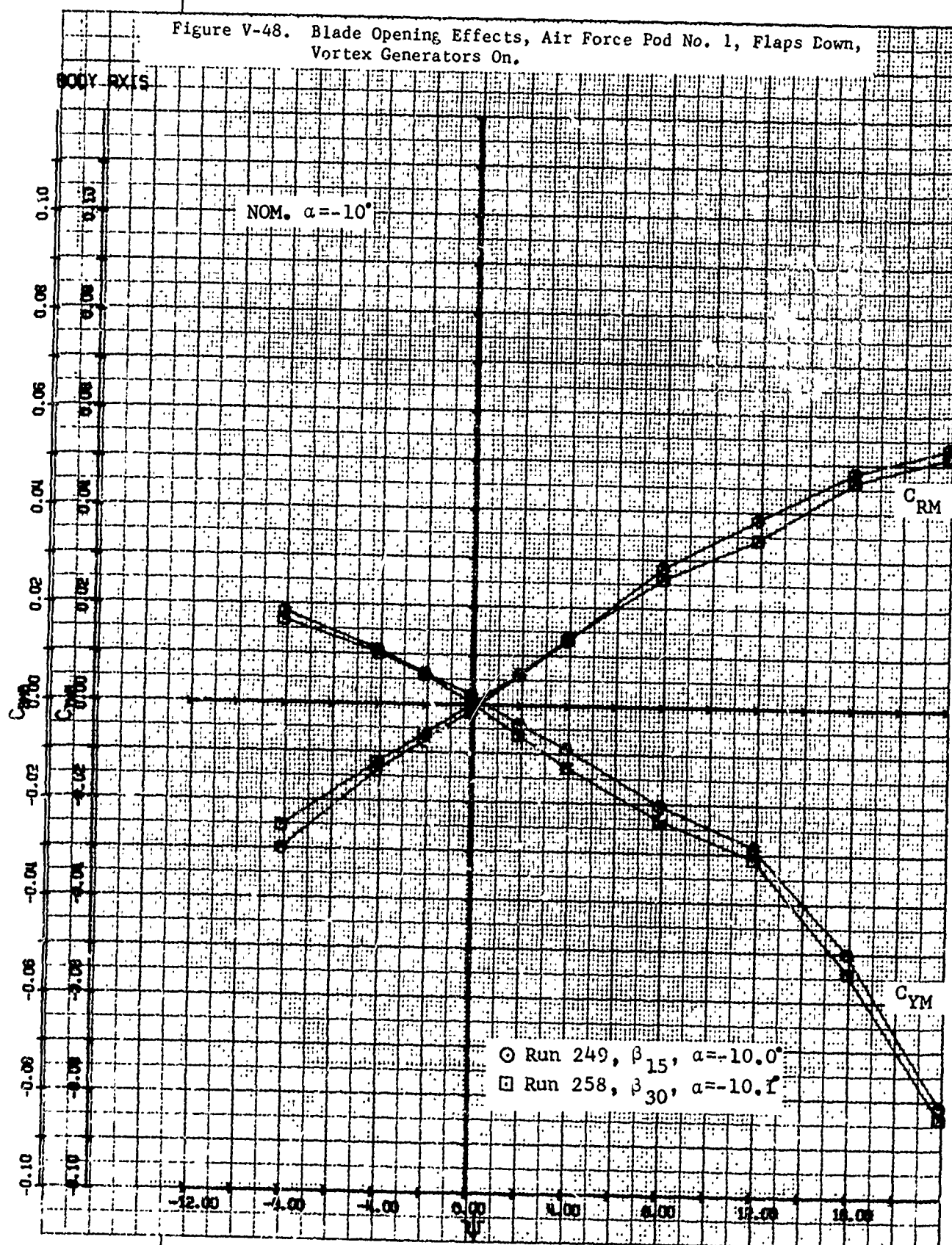


Figure V-49. Blade Opening Effects, Air Force Pod No. 1, Flaps Down,
Vortex Generators On.

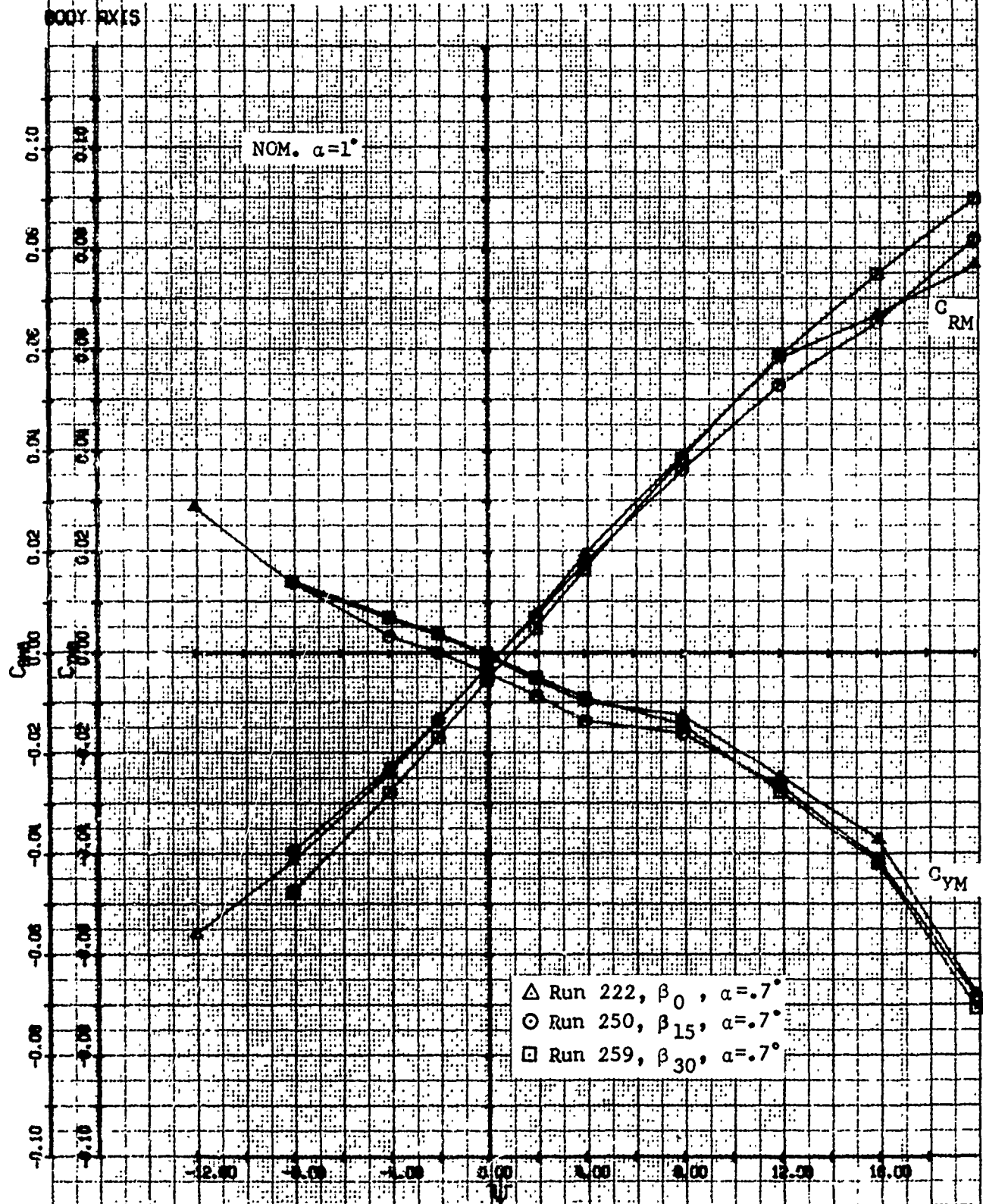


Figure V-50. Blade Opening Effects, Air Force Pod No. 1, Flaps Down, Vortex Generators On.

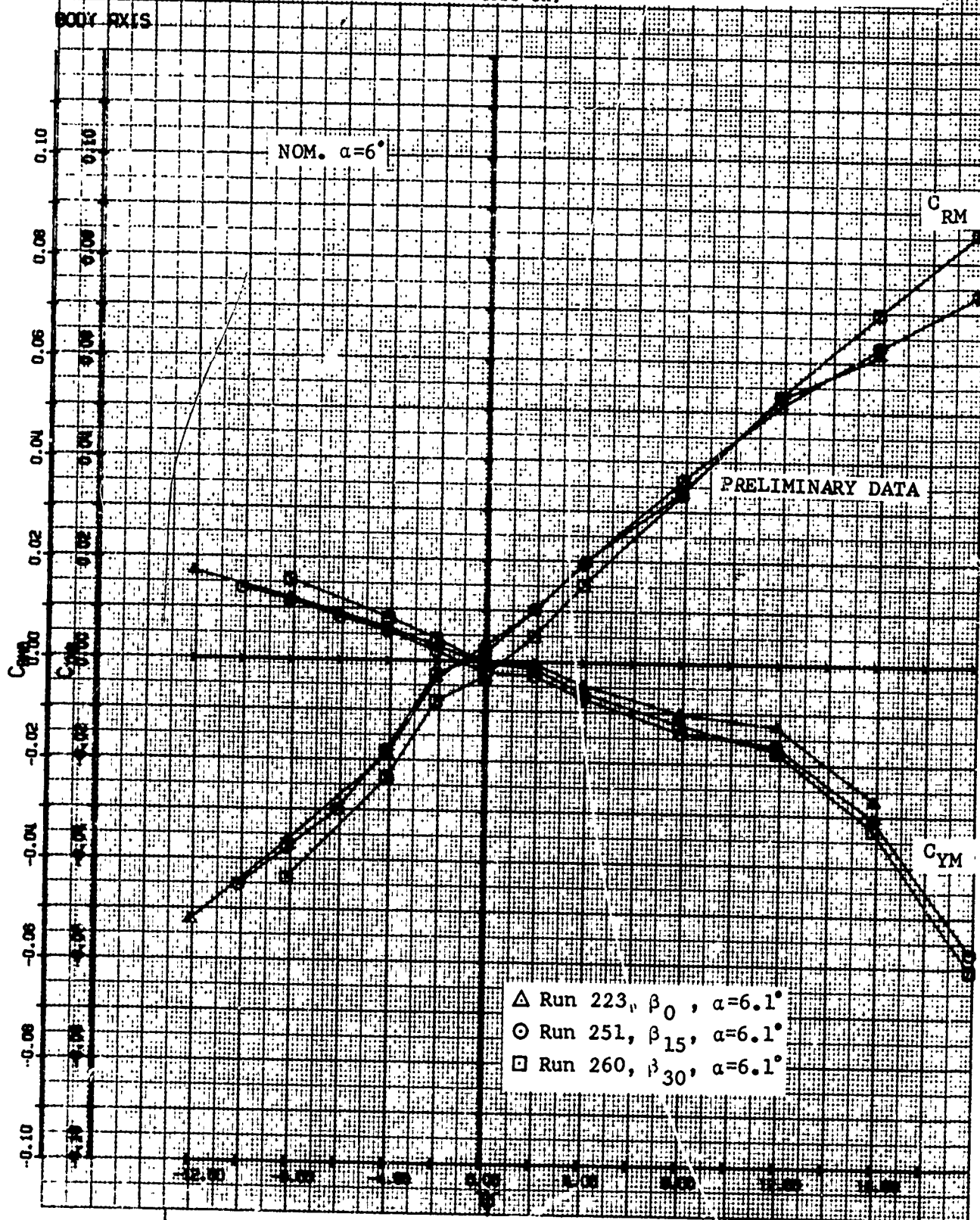


Figure V-51. Blade Opening Effects, Air Force Pod No. 1, Flaps Down, Vortex Generators On.

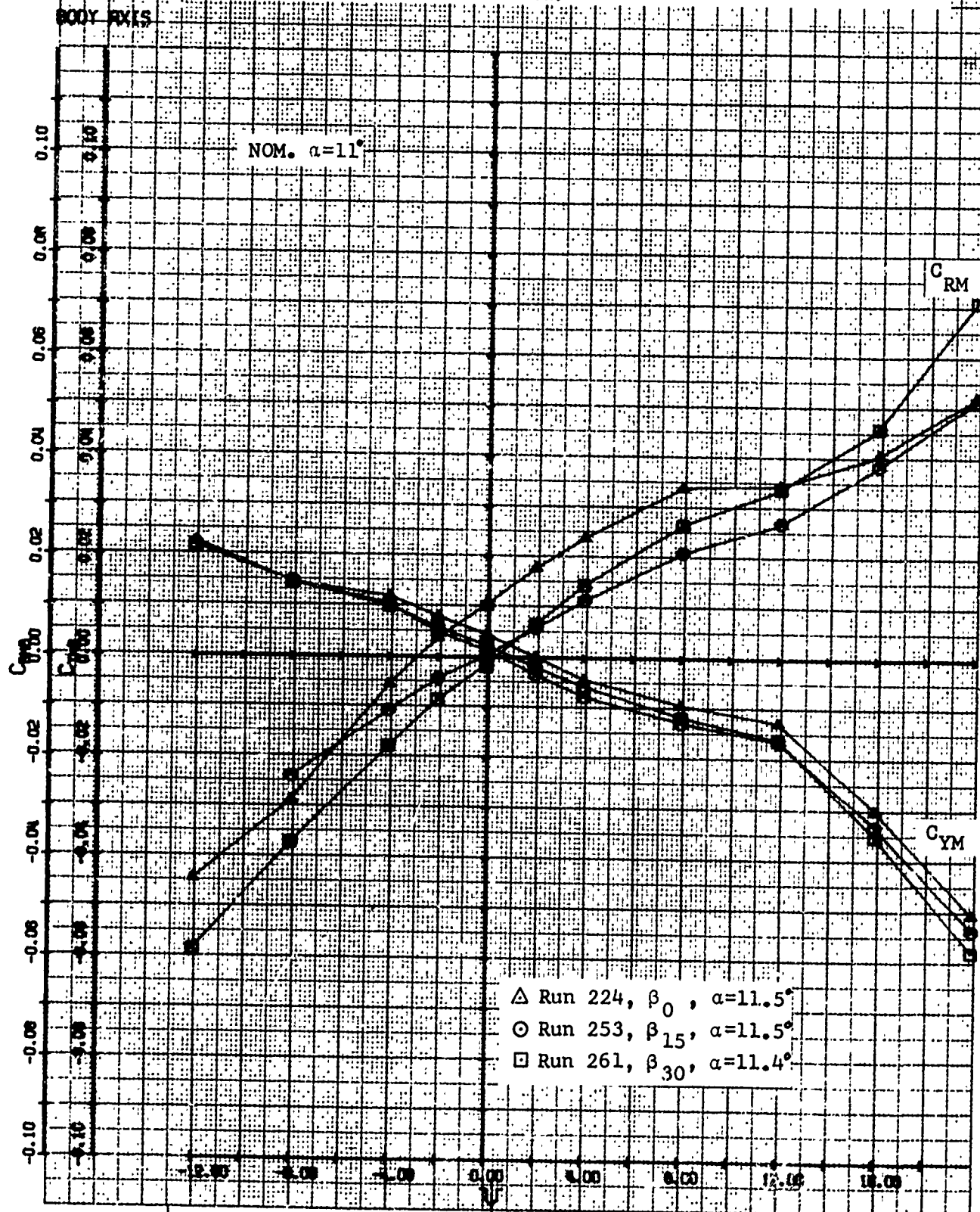


Figure V-52. Blade Opening Effects, Air Force Pod No. 1, Flaps Down,
Vortex Generators On.

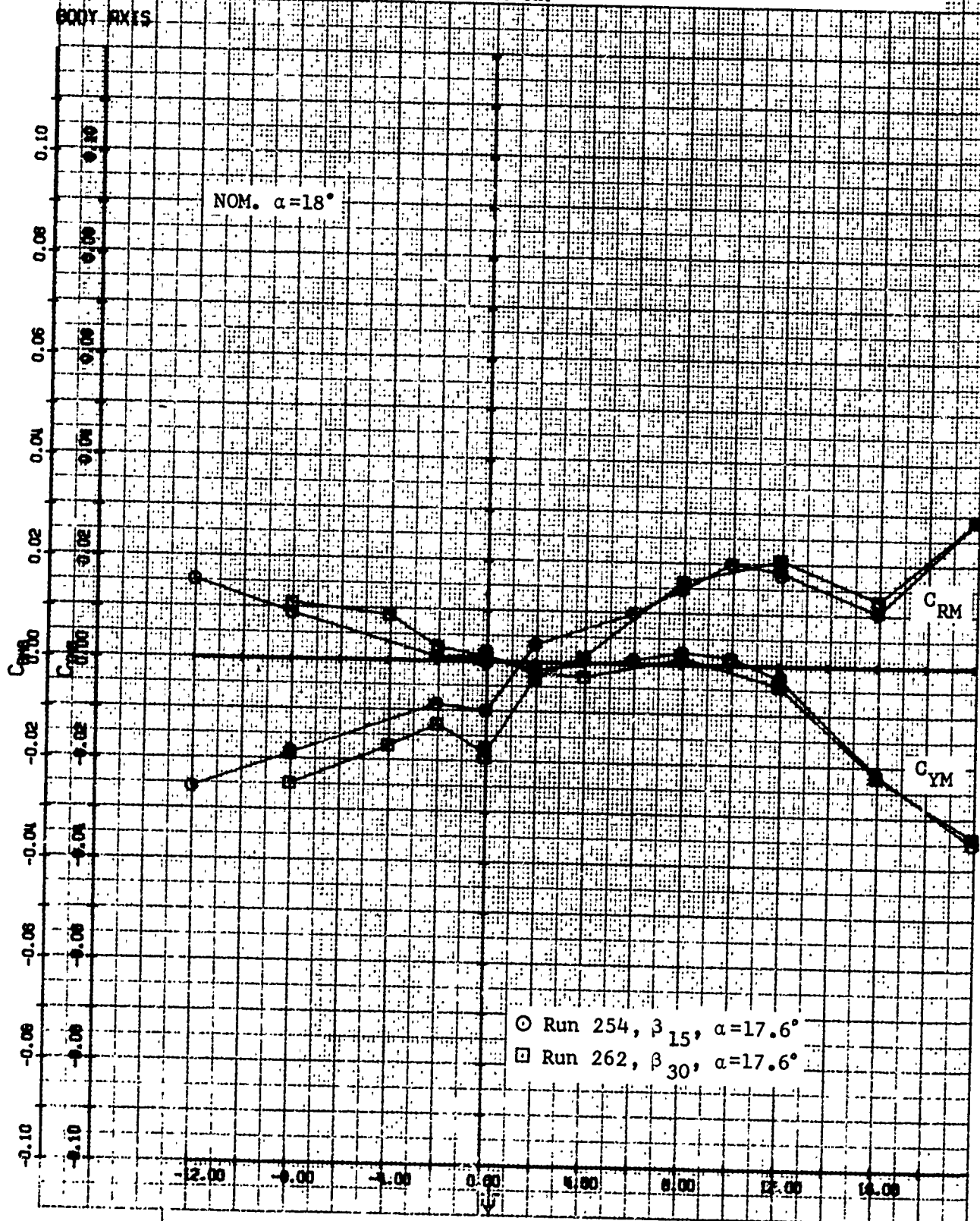


Figure V-53. Aileron Effectiveness, Flaps and Ailerons Up.

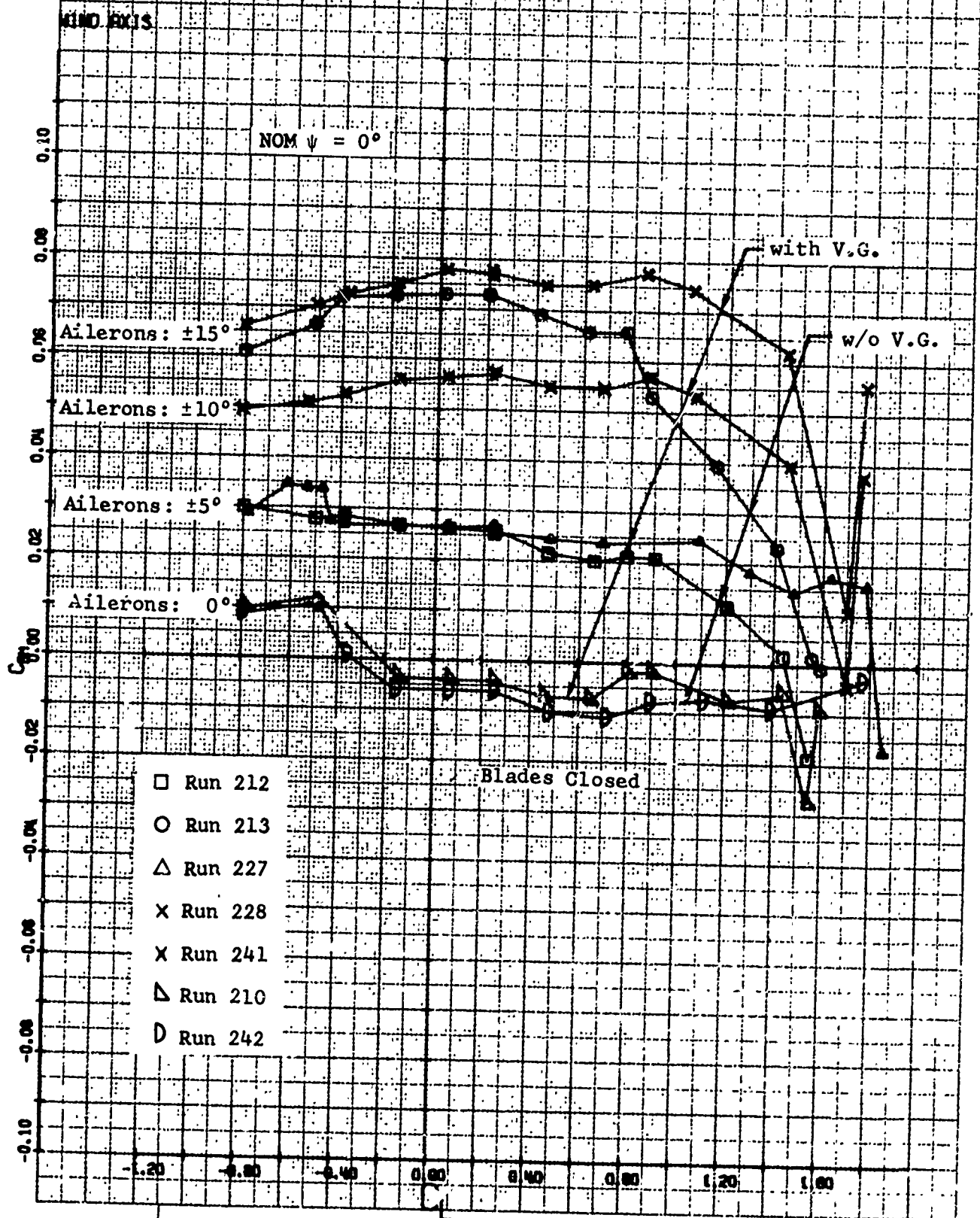


Figure V-54. Aileron Effectiveness, Flaps and Ailerons Down.

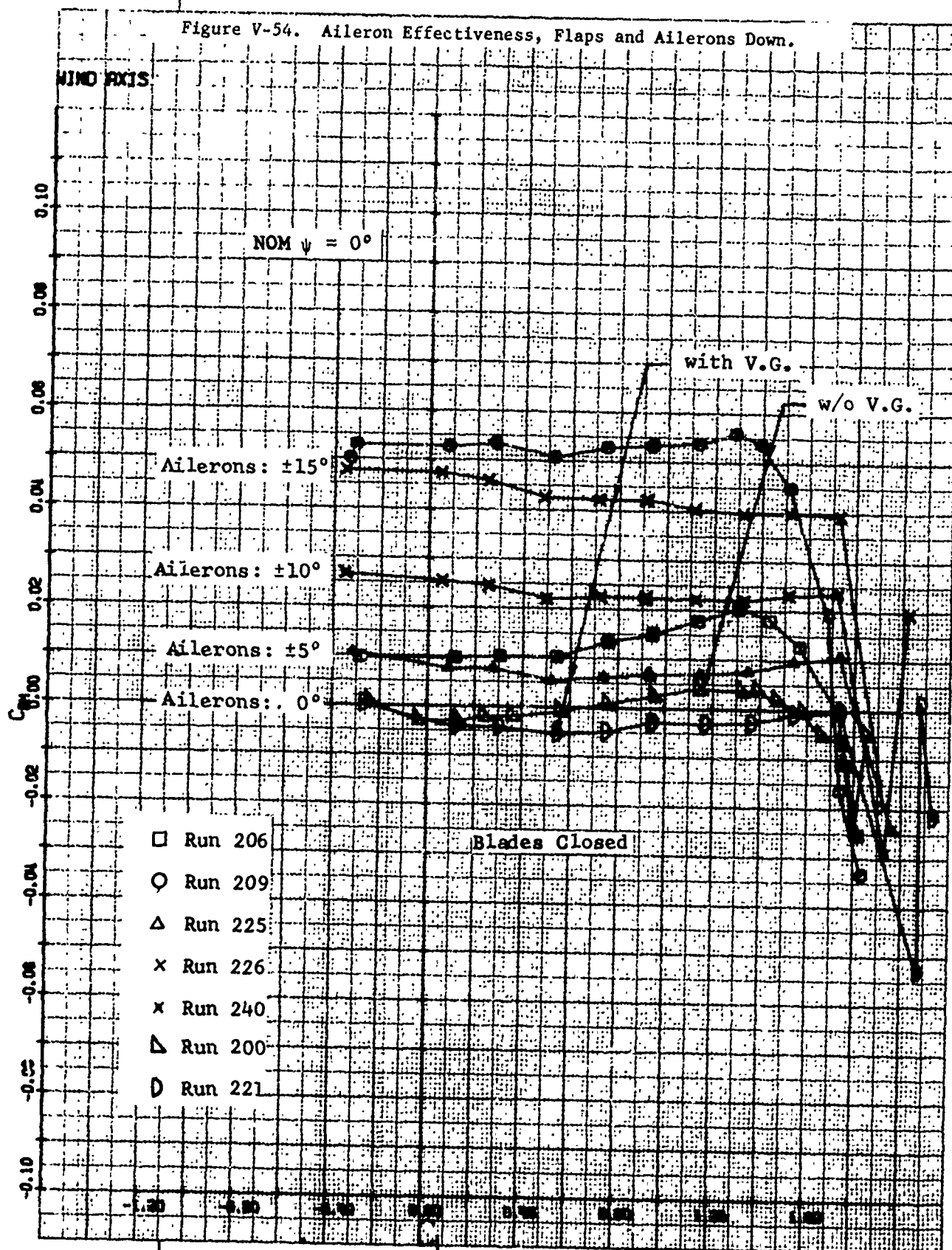


Figure V-55. Effect of Opening Blades 15 Degrees on Aileron Effectiveness, Flaps and Ailerons Up.

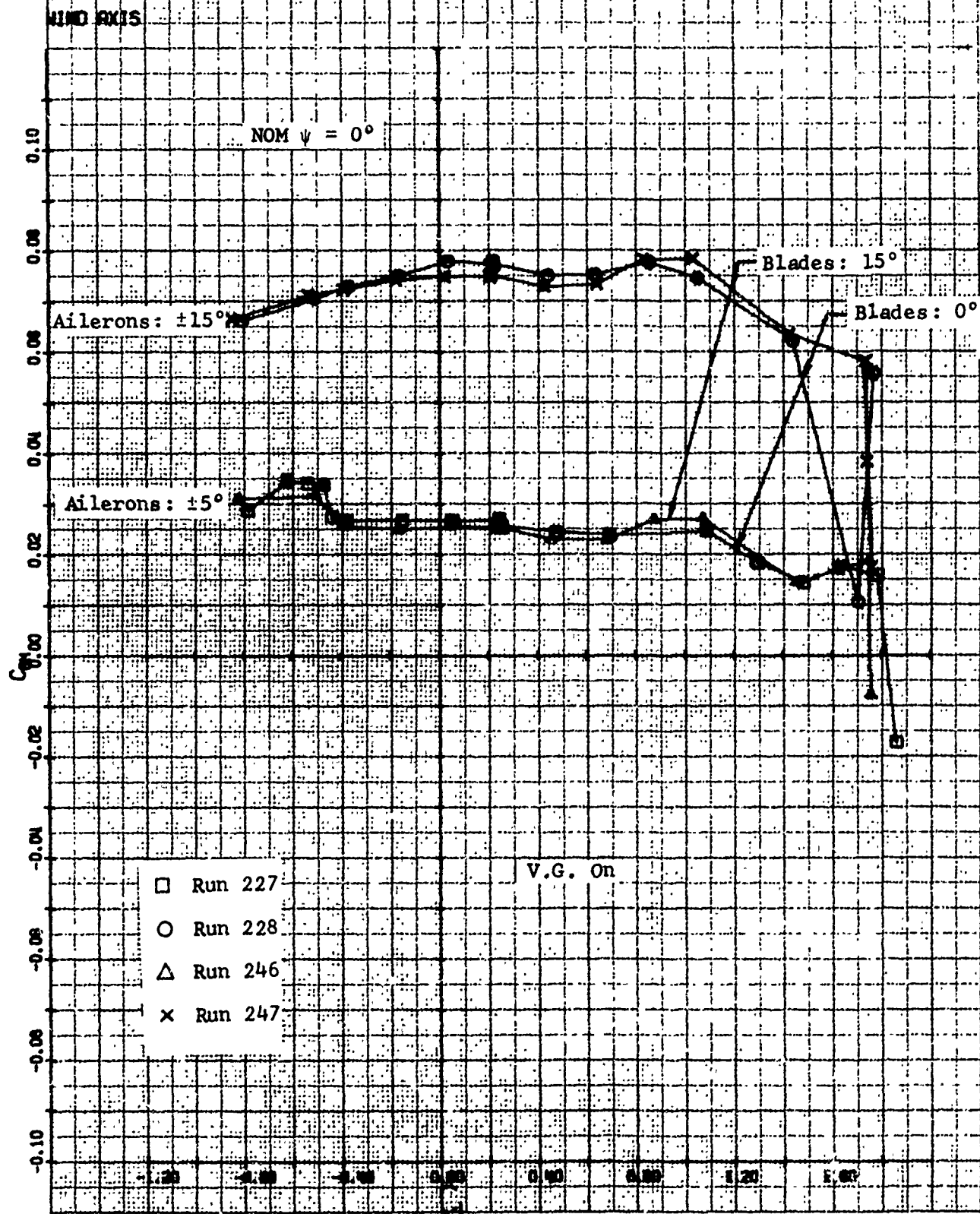


Figure V-56. Effect of Opening Blades 15 Degrees on Aileron Effectiveness, Flaps and Ailerons Down.

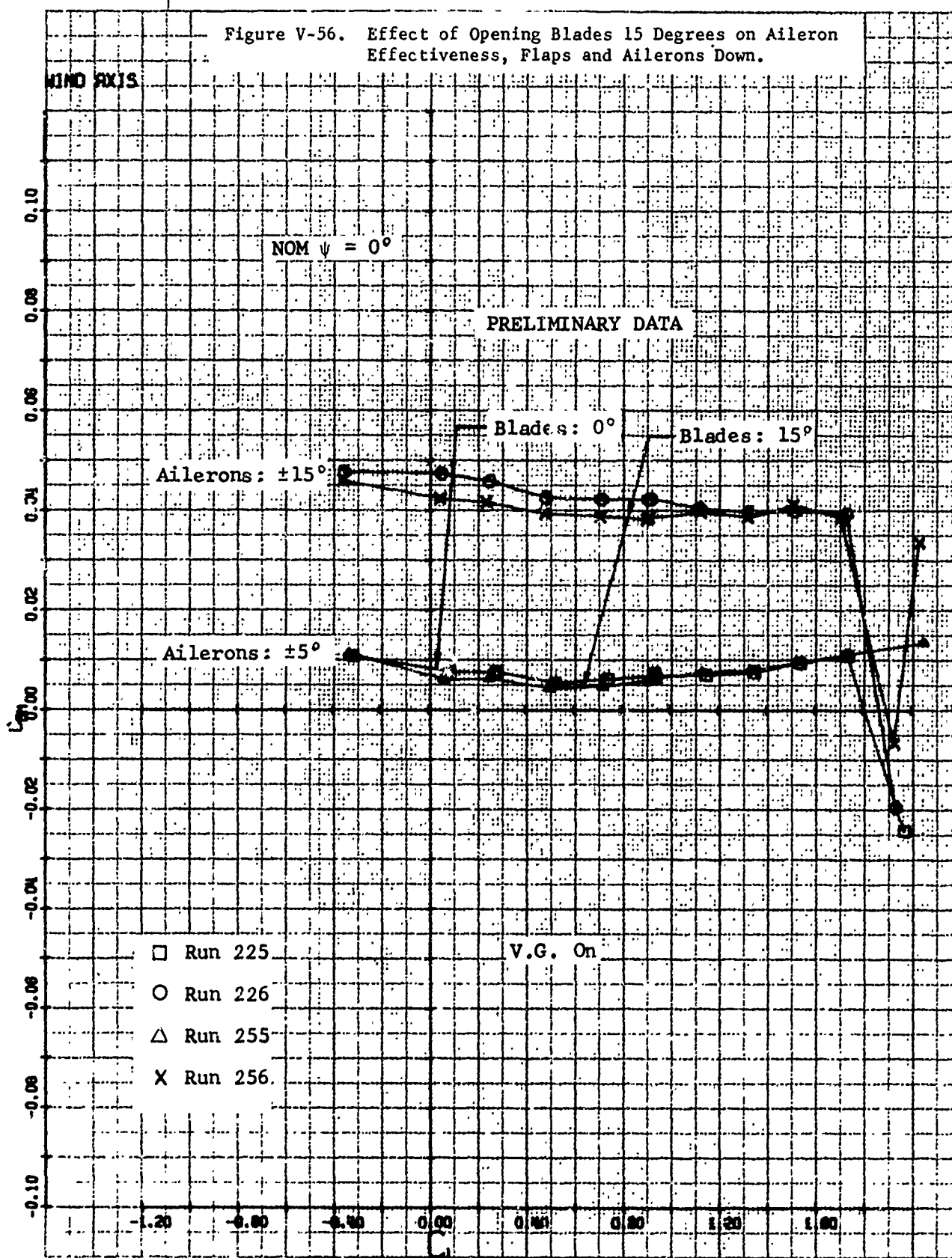


Figure V-57. Effect of Roughness on Aileron Effectiveness.

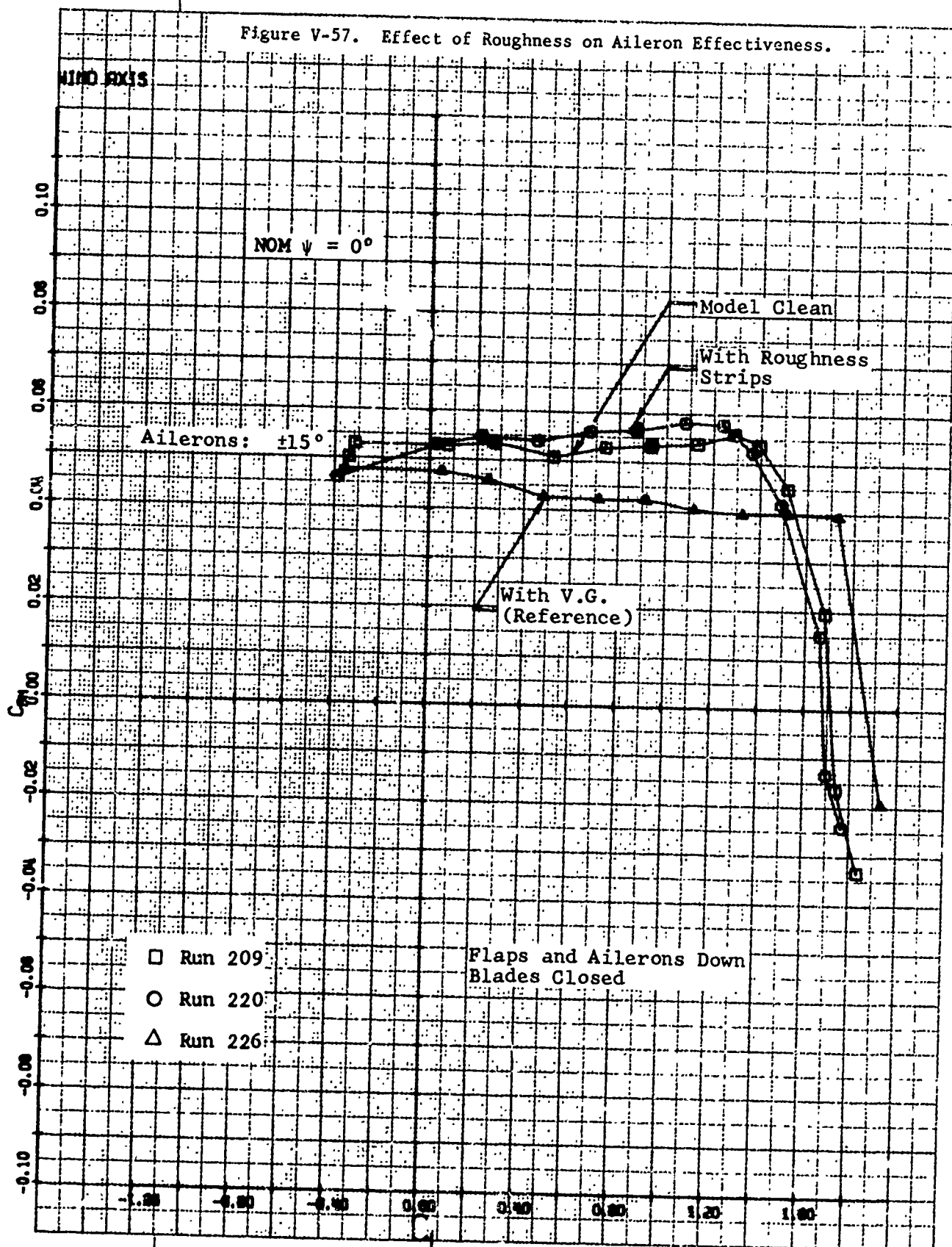


Figure V-58. Effect of Wingtip Pod and Blade Configuration on Aileron Effectiveness with Blades Folded, Flaps Up.

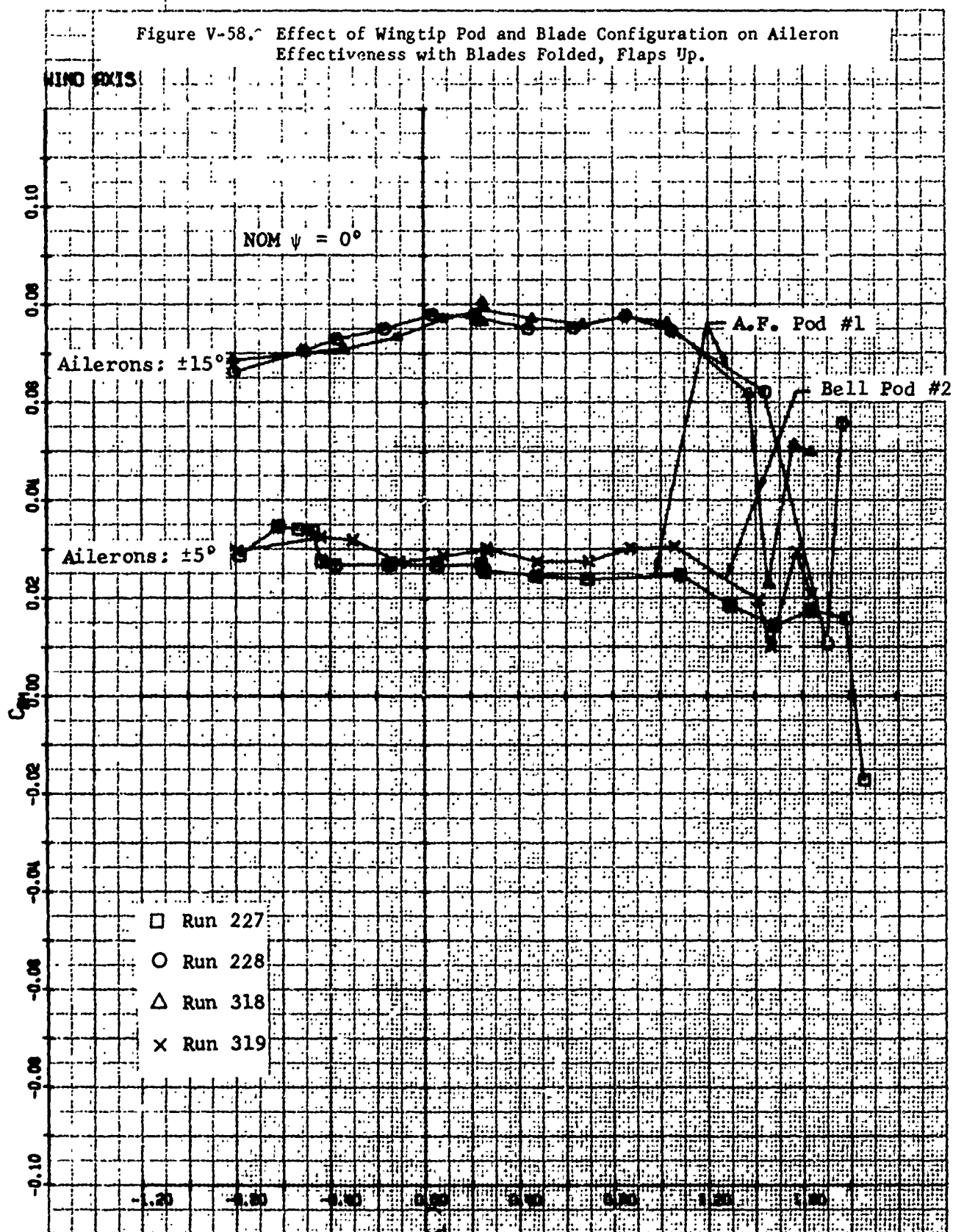


Figure V-59. Effect of Wingtip Pod and Blade Configuration on Aileron Effectiveness with Blades Folded, Flaps Down.

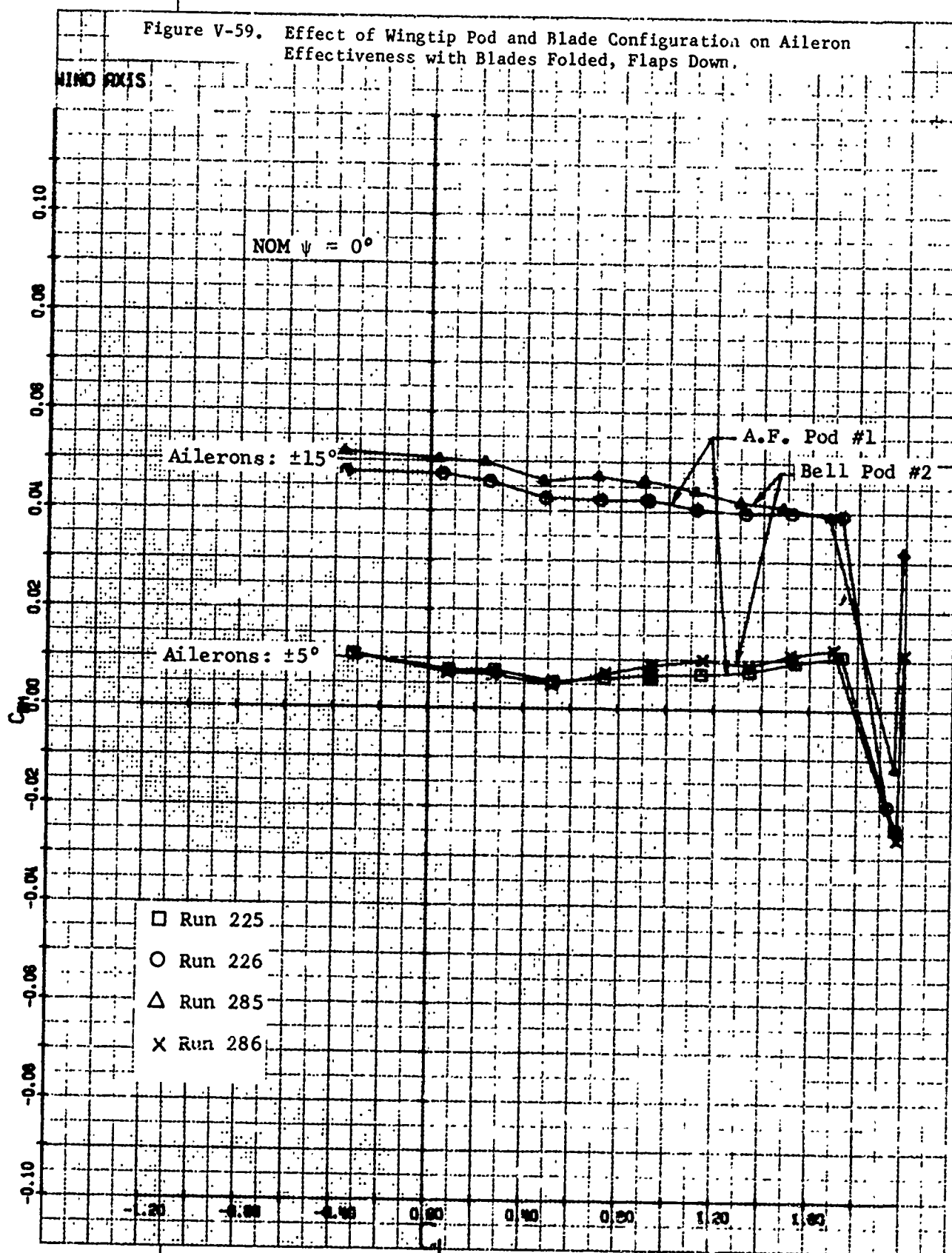


Figure V-60. Effect of Wingtip Pod and Blade Configuration on Aileron Effectiveness with Blades Open 15 Degrees, Flaps Down.

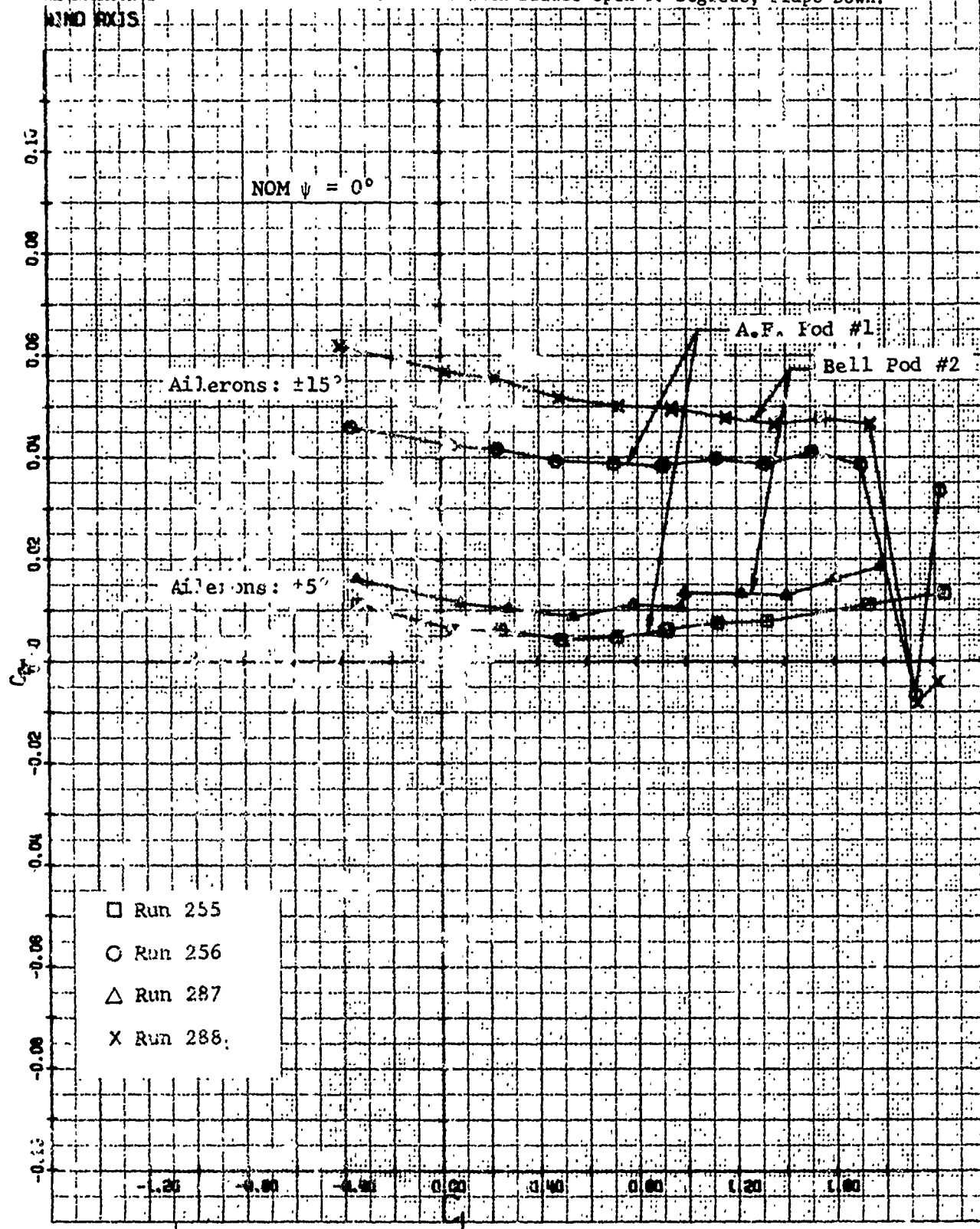
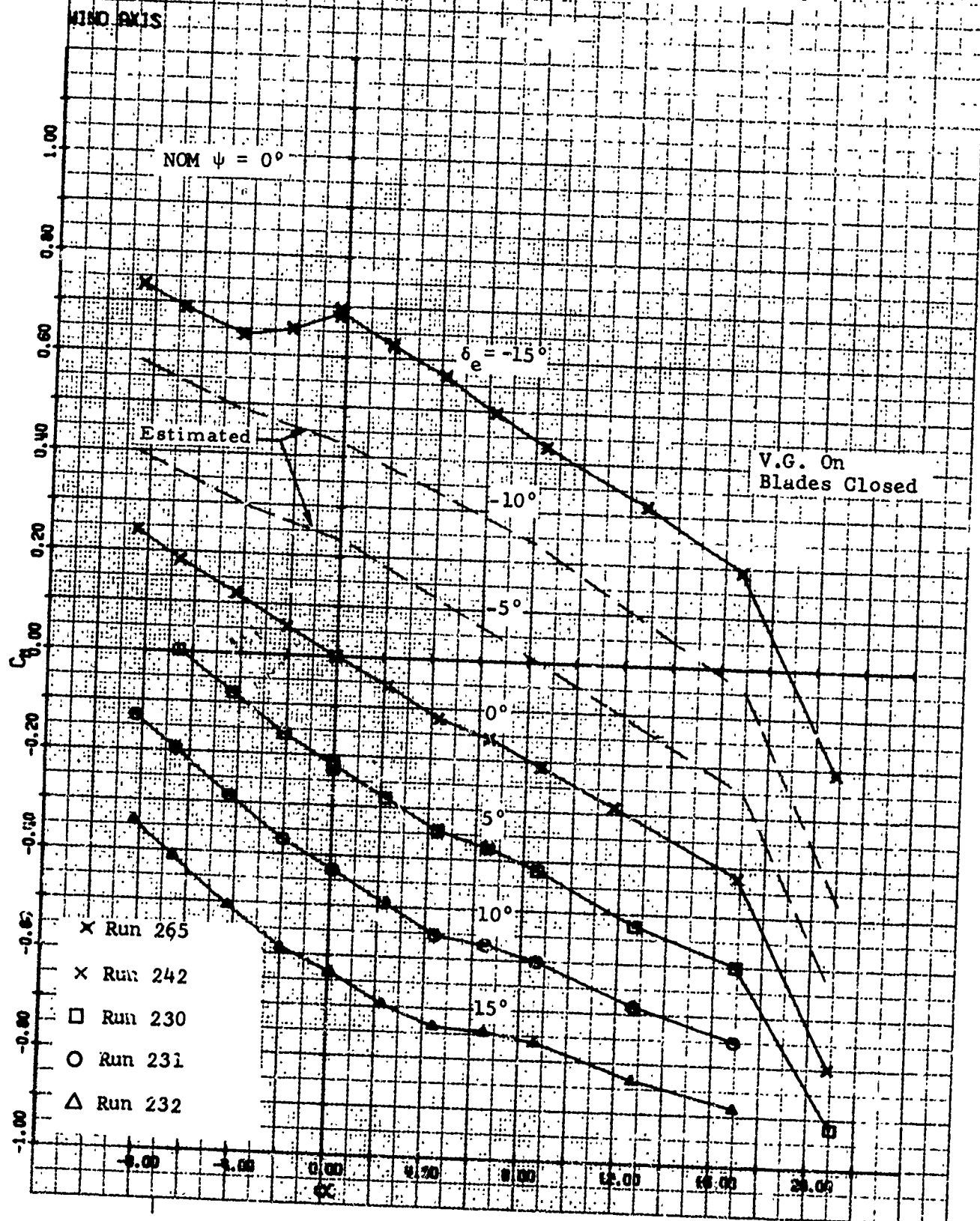


Figure V-61. Elevator Effectiveness, Flaps and Ailerons Up.



D270-099-003

Figure V-62. Elevator Effectiveness, Flaps and Ailerons Down.

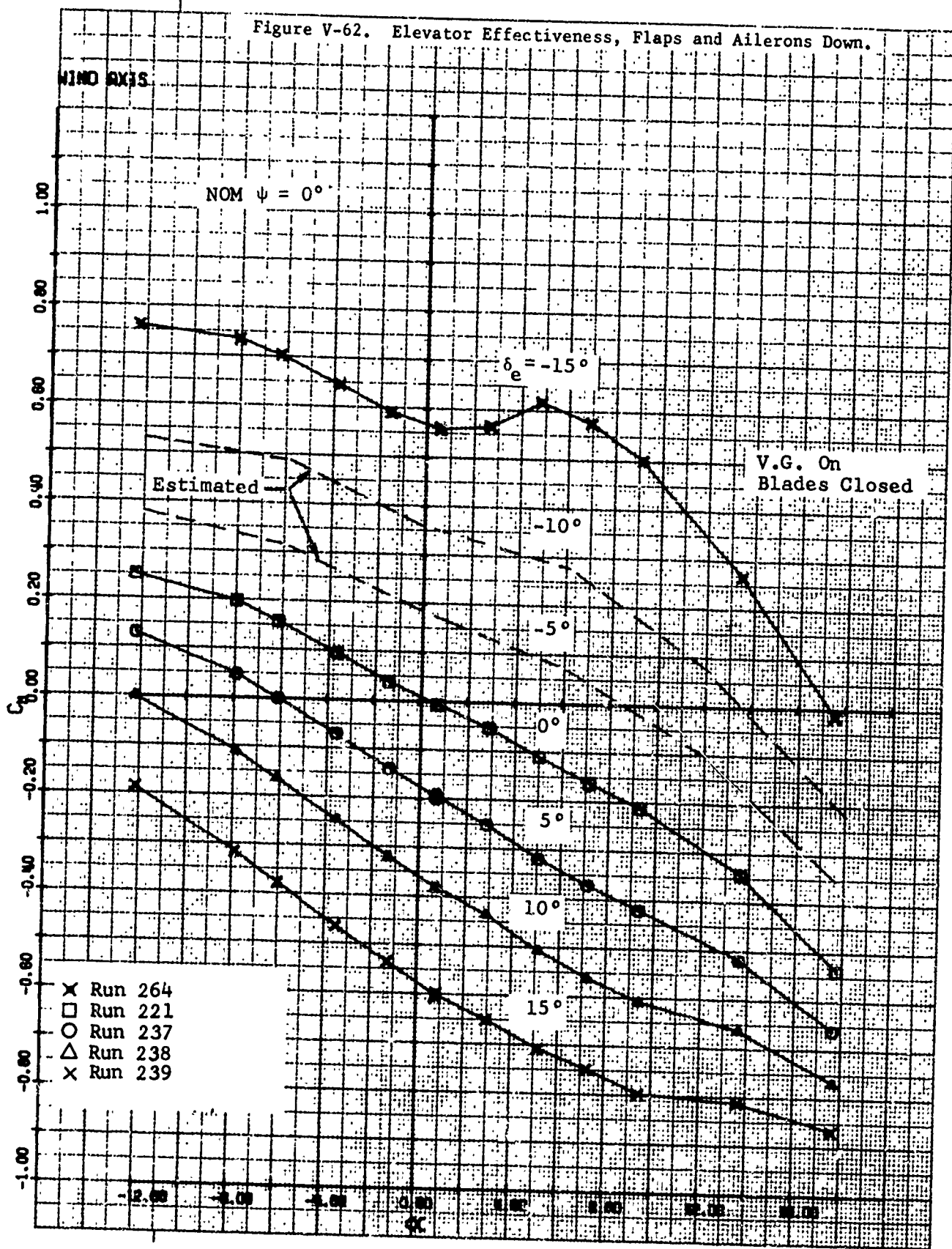


Figure V-63. Rudder Effectiveness, Angle of Attack Equal Zero Degrees.

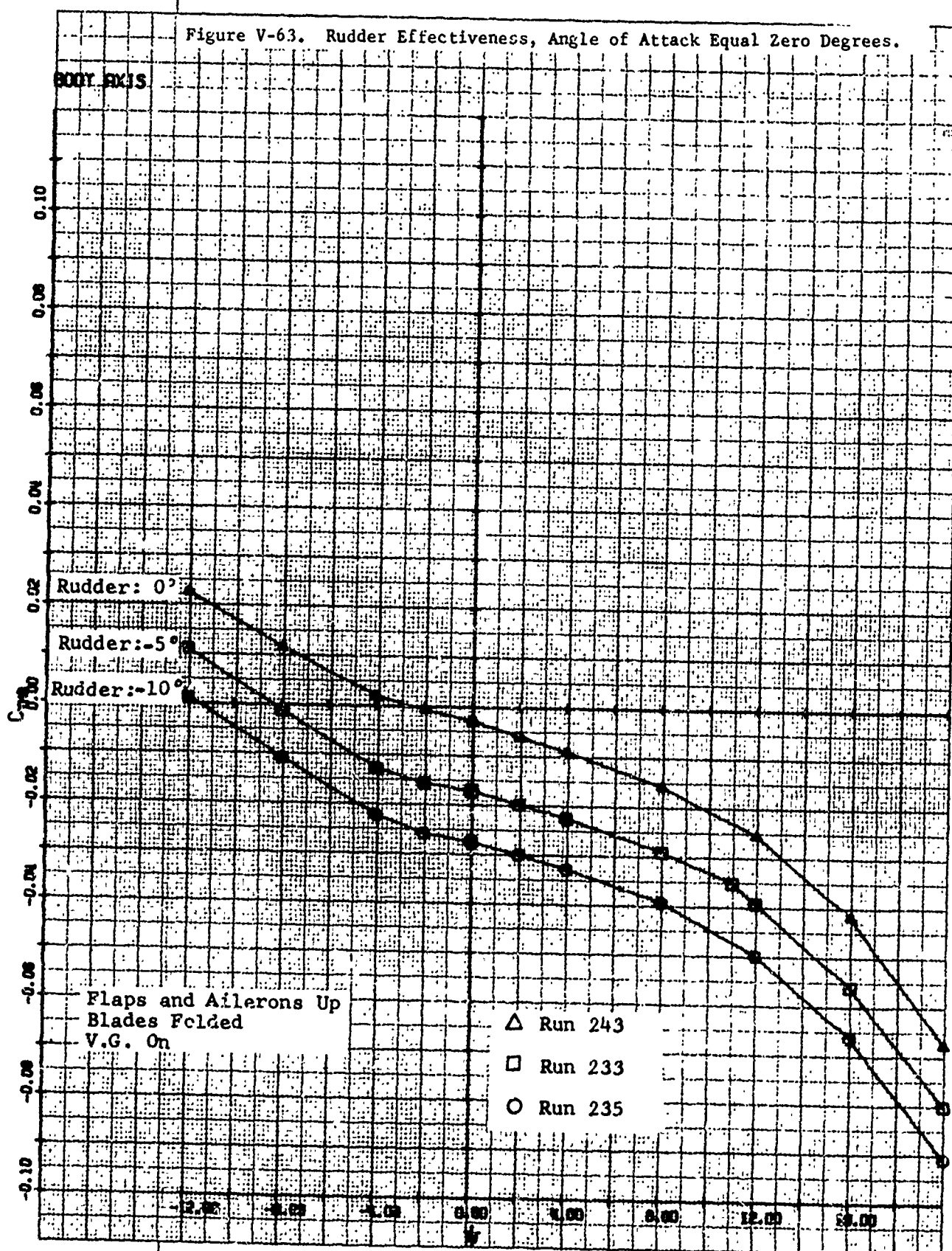


Figure V-64. Rudder Effectiveness, Angle of Attack Equal 11 Degrees.

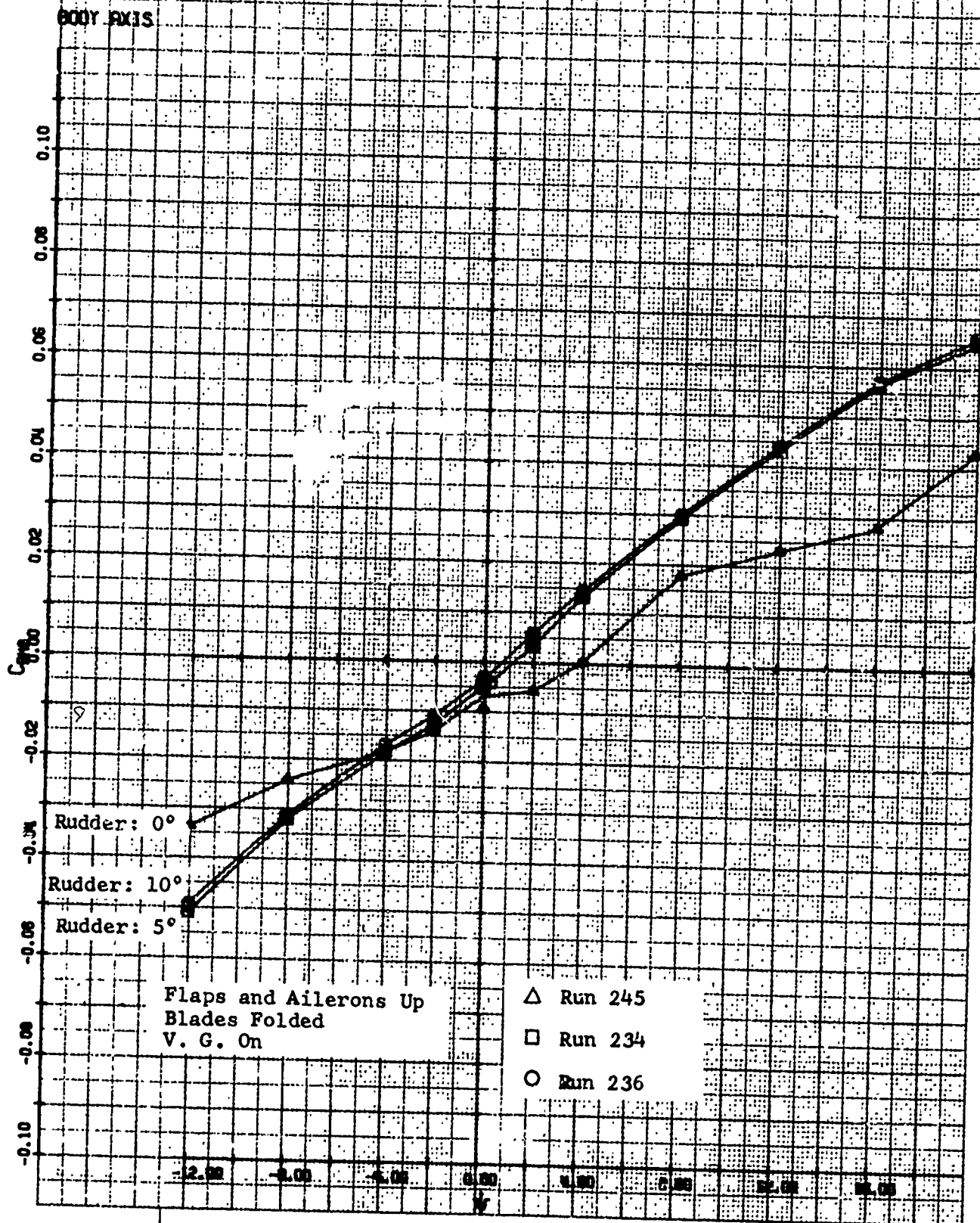


Figure V-65. Rolling Effectiveness of Rudder, Angle of Attack Equal Zero Degrees.

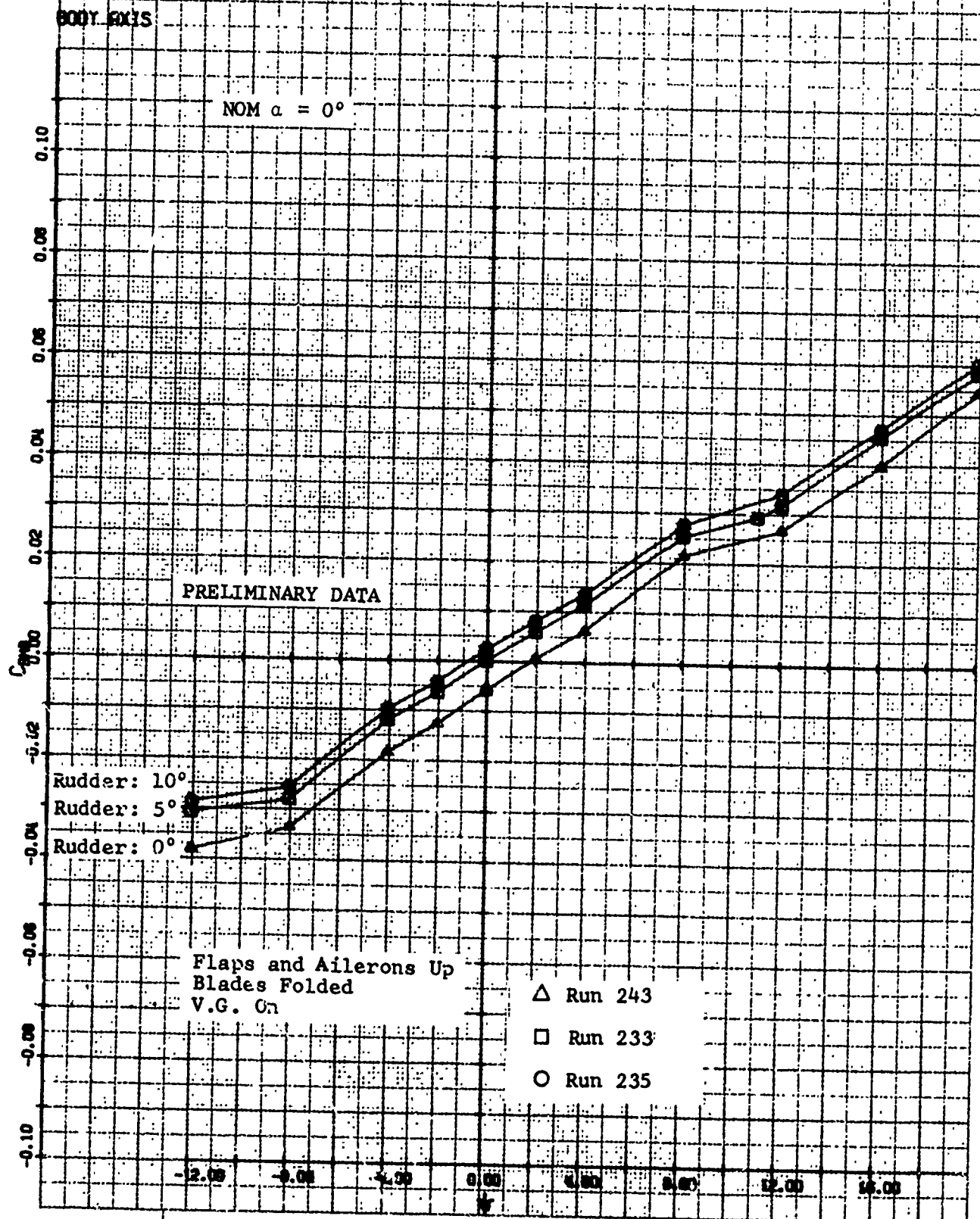
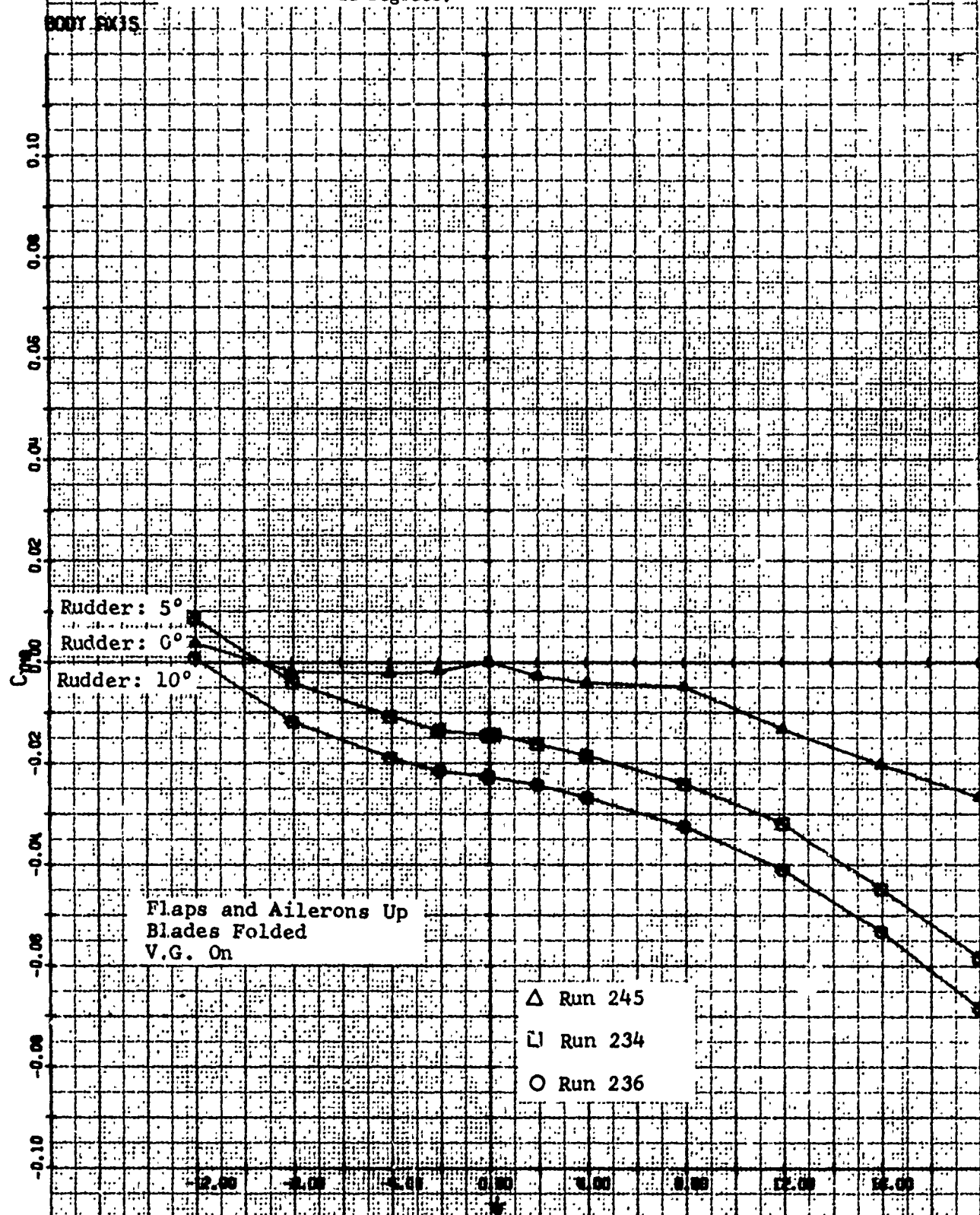


Figure V-66. Rolling Effectiveness of Rudder, Angle of Attack Equal 11 Degrees.



VI. POWERED FULL-SPAN FORCE MODEL

A. OBJECTIVES

A full-span powered force model of the D270A point design was designed and fabricated as part of the Phase II effort. This comprised the larger part of the Phase II contracted effort, and therefore a description of the model is included in this report. The model has subsequently completed initial tests in the NASA V/STOL Wind Tunnel at Langley, Virginia under a separate contract.

The objectives of tests with this model were:

- To perform aerodynamic tests of the low-speed/transition-flight range from helicopter mode through low-speed proprotor mode to investigate baseline trim characteristics, forces and moments, and stability and control derivatives.
- To identify and explore potential problem areas.
- To provide an experimental base for the validation of analytical methods of deriving stability and control characteristics.

B. GENERAL

The capabilities of the model can best be summarized in terms of typical stages in the testing of the tilt-rotor aircraft. The model can be used to investigate at least the following areas:

- Net hover performance - derived from measuring total model lift, input torque at each rotor, and rotor rpm. In addition, the gross rotor thrust required to offset net airframe download may be determined by measuring the thrust of each rotor by means of balances in each pylon.
- Differences in net hover performance - as influenced by changing flap settings and ground proximity.
- Hovering downwash patterns and flow recirculation effects - under and around the model at various heights as determined by flow visualization or measuring techniques.
- Hovering acoustic signature distributions
- Hover control power assessment - by measuring net model pitch, roll, and yaw moments as a function of remotely controlled mean longitudinal cyclic pitch, differential collective pitch, and differential longitudinal cyclic pitch. Rotor moment contributions can be determined by the pylon balances and flapping measurements. In addition, net pitching moment contributions due to the effects of wake recirculation on horizontal tail loads, in and out of ground effect, may be determined by removing the horizontal tail and measuring differences with the sting balance.
- Variations in hover roll stability due to changes in ground proximity - as caused by cross-flow effects under the wing.

- Performance and stability and control derivative variations - in very low-speed helicopter flight (backside of the power curve). In addition, the influence of the rotor wake on the net tail contribution to the pitching moment may be determined by removing the tail. This flight speed range would be investigated with tunnel test section walls open.
- Helicopter mode climb and descents/autorotation - this area can be investigated with tunnel walls open or closed depending on speed and model power.
- Transition/conversion - in this higher speed range, tunnel walls will be closed and pylon tilt angle would be changed between runs. Various flight conditions would be encompassed by changes in model angles of attack and remotely-controlled settings of collective and cyclic rotor pitch and elevator to determine stability and controllability derivatives.
- Proprotor mode - performance and stability and control derivatives can be obtained in proprotor mode representative of the speeds where pylon tilting takes place and to higher speeds if desired.

Additional areas can be investigated which would be representative of later stages of testing in a tilt-rotor test program. Typical of such investigations would be:

- Maneuver envelope expansion - conditions near the limits of model/balance capability would simulate maneuver conditions in pitch, roll, and yaw (static effects only).
- STOL characteristics - in ground effect, high gross weight takeoff runs could be simulated with moving-belt ground plane operation and with walls open and closed.

Additional areas of investigation with the model, or its rotor and pylon components, may be defined. Obviously, not all can be addressed in a single test program. The maximum value of this model will be obtained by a safe progression in testing from previous areas of operation into new areas with excursions of a minimum number of control and operating condition parameters.

C. MODEL DESCRIPTION

The subject model, designated the Bell C100-F1B, is a one-tenth-scale powered full-span force model of the Bell D270A defined in Phase I.

The model's one-tenth-scale size and length scale factor were selected such that the diameter of its proprotors are the same as that of aeroelastic models from which prior blade and rotor fabrication experience was available. The proprotors are five feet in diameter. The blades are scaled to have a Lock number of one in air, scale spanwise and chordwise mass distributions, and scale beam and chord inertias for the length, mass, and time scale factors selected. A principal design objective was development of the highest possible model thrust and power while maintaining scale wingtip-pod dimensions. This resulted after design iterations in a velocity scale factor of 0.6.

A four-component balance system is incorporated in each pylon assembly for measurement of rotor lift and torque and the complete model is supported on a fuselage-mounted six-component balance for total aircraft forces and moments. The proprotors are mechanically interconnected and are driven by two variable-frequency motors mounted in the fuselage and having a continuous-operating temperature rating of 34 horsepower total. Flaps, ailerons, horizontal stabilizer, and mast angle are adjustable to fixed angle settings, and cyclic and collective pitch are remotely controllable on each proprotor.

Model parameters are shown in Table VI-I and photographs of the model during functional checkout are shown in Figure VI-1.

1. Model Installation

Testing is planned for the NASA V/STOL wind tunnel. By use of either fixed variable or remotely variable sting knuckles, sufficient pitch range is available to test steep descent or climb angles or to operate in ground effect above the moving-belt ground plane. The sting enters the lower aft portion of the fuselage. A balance block is furnished with the model for mounting to the tunnel-furnished six-component balance. Possible test speed range is from zero to maximum tunnel speed.

2. Fuselage

The center transmission of the drive system is made an integral part of the fuselage center structure in order to provide the necessary interconnect shaft placement and gear sizing for design powers. Wing spars are bolted to the top of the gearbox and integral bulkheads pick up sting loads and loads from the forward and aft fuselage structure.

The basic fuselage backbone from the gearbox and wing aft to the tail is a square steel tube with aluminum plate bulkheads to support removable fiberglass fairing shells. Forward of the wing bulkhead, four aluminum longerons extend forward to support motor and center gearbox mounting bulkheads and the nose section aft bulkhead. The cylindrical fuselage section at and ahead of the wing is formed by two removable shells of curved aluminum plate. Forward of the nose section bulkhead, a V-shaped brace extends to the inside of the nose of the fiberglass forward section. A level plate is built into the nose section for internal mounting of the remote-reading angle of attack indicator. Double-curvature windshield area lines were accepted for test purposes.

3. Empennage

The vertical tail is conventional construction, having a steel spar attached to the aft portion of the fuselage backbone. Near the root end of the vertical tail spar is the drive motor and potentiometer for remote control and readout of elevator setting. The horizontal tail aluminum spar is mounted midway up the vertical. No rudder is provided, but the elevator is remotely adjustable over a range of ± 20 degrees. Horizontal stabilizer incidence may be varied ± 5 degrees by changing fillet blocks which attack the horizontal tail spars to the vertical tail spar. The aerodynamic shape for the horizontal and vertical tail is formed from wood panels.

Both vertical and horizontal stabilizers have a change in airfoil section percent thickness between root and tip. To avoid development time for modifications required for wrapped skins, the surfaces are developed to have straight lines between points at the root and tip at the same percent chord. Root and tip airfoil section were changed to the A series for easier fabrication. Conflicting information was found on the effect of this on elevator and rudder effectiveness but it was indicated to be small. Dorsal cross sections were developed. The objective here was a sharp-edge dorsal for improved directional stability at small angles.

4. Wing

The basic wing structure is an aluminum channel section which is closed to form a torque box by means of bolted-on, lower-surface aluminum plates. At the root end of each wing box, a forked-shaped steel root fitting is attached which straddles the upper part of the center gearbox. The rotor interconnect power shaft is thereby introduced into the wing box for powering the tip-mounted rotors. The wing is mounted to the model at the center gearbox case. The wing has ailerons and flaps which can be set at fixed incidences by angle brackets. Available flap angle brackets are 0 or 50 degrees, and ailerons are 0 or 20 degrees. The aerodynamic contours are provided on wing and control surfaces by shaped wood panels attached to the metal spars. Wing and pylon coupled frequencies are not scale, but are planned to avoid resonance with principal exciting frequencies. Wing airfoil selection and incidence definition during Phase I was minimal. This was reviewed briefly for the model, and a 64-318 (a equals 0.8) section was used, set at an NACA airfoil section chord line to fuselage waterline incidence of 2 degrees.

5. Drive System

The proprotor drive system consists of two TASK motors (TASK Part Number 13390-1) mounted in the fuselage driving aft through flexible couplings (LOVEJOY Part Number U-62) into a gearbox which reduces motor speed by three at its output. The outputs of the gearbox are coupled to the interconnect shafts with universal joints (LOVEJOY NB-8B). The center gearbox-to-interconnect shaft angle is equal to the angle between the interconnect shaft and the wingtip gearboxes. The U-joint fittings are aligned to minimize torsional oscillations of the wingtip gearbox input. The angle is created due to wing dihedral. The wingtip gearboxes provide a further reduction of shaft speed by a ratio of two to one. The wingtip gearboxes are modified Bell Model 47 helicopter, 90-degree, tail rotor gearboxes. The rotor pylon conversion axis is concentric with the input drive quill to allow for adjusting pylon tilt angles. Pylon tilt struts are provided for pylon angles of 90 (helicopter), 75, 60, 45, and 30 degrees, and the pylon bolts to the wing for an angle of 0 degrees (airplane).

The output of the 90-degree box is aligned with the rotor shaft axis and is coupled to the rotor shaft with a special coupling. The coupling is designed to minimize the transmittal of longitudinal elastic or friction forces into the rotor assembly which is mounted on a three-component balance. The last link in the model drive system is the rotor shaft. Each rotor shaft is strain gaged to sense rotor torque with dual, temperature-compensated bridges. An extension of the wingtip gearbox output shaft opposite to the rotor coupling

carries an instrumentation slip ring (for rotor blade loads, flapping, etc.) and a tachometer/azimuth wheel for driving a magnetic pulse pickup. The drive motors and center gearbox are water cooled and have water flow rates of three gallons per minute for each motor and 2.5 gallons per minute for the center gearbox.

6. Proprotors and Controls

Each five-foot-diameter proprotor has three blades, mounted to a gimbal hub to permit rotor flapping. The gimbal flapping is restrained by springs located in the rotating system. The blade grips are provided with needle bearings to accommodate changes in blade pitch while the rotor is operating. Blade centrifugal force is reacted with tension-torsion wire belts which accommodate oscillatory and steady pitch change motions due to flapping or cyclic and collective pitch motions. Flapping of the gimbal, as defined by flapping about the reference blade, is sensed with a strain gaged flexure referenced to the rotor shaft. On the left rotor, flapping is measured about an axis in line with the white blade and on the right rotor, the yellow blade. The rotor blades are dynamically scaled in stiffness and mass distribution based on a model tip speed 0.6 times full-scale tip speed. The model rotors have been operated at 1884 rpm, representative of a full-scale hover tip speed of 822 feet per second, a thrust of 340 pounds, representative of 133 percent of full-scale design gross weight (assuming 7 percent wing download), and a cyclic pitch of ± 8 degrees. The model blades are provided with strain gages for monitoring beam, chord, and torsion loads. A temporary set of allowable loads have been used for functional check runs of the model at the contractor's facility.

The proprotors have remotely-controlled collective pitch and longitudinal monocyclic pitch control for each rotor. The cyclic pitch range provided at the blade is about ± 12 degrees. The collective range of the blade at the 3/4R station is continuously variable from -5 to +39 degrees. Cyclic and collective control angle positions are instrumented on both rotors. During adjustments of blade pitch, the maximum cyclic rate is approximately 1.6 degrees per second and the maximum collective rate is approximately 4.0 degrees per second. Provisions are made to command the collective actuator motors together, or the right motor independently for trim. Loads generated in the model collective and cyclic pitch control systems do not cross the rotor three-component balances and are monitored by an instrumented pitch link on each rotor.

TABLE VI-I. FULL-SCALE AND MODEL PARAMETERS

<u>Scale Factors (Model/Full Scale)</u>	
Length	0.10
Velocity	0.60
Force	0.36×10^{-2}
Moment	0.36×10^{-3}
Power	0.216×10^{-2}
Time	0.1667
Air density	1.000
Blade Lock number	1.00
Blade mass	0.001

TABLE VI-I. Continued

Blade stiffness		0.36 x 10 ⁻⁴	
Blade elastic modulus		0.36	
Blade stress		0.36	
Area		0.010	
Volume		0.001	
Frequency		6.0	
Acceleration		3.6	
Angular velocity		6.0	
Reynolds number		0.06	
Froude number		0.036	
<u>Parameters</u>		<u>Full Scale</u>	<u>Model</u>
Aircraft and model designation		D270A	C100-F1B
<u>Design Gross Weight and Model Lift</u>			
Gross weight/ σ' at SLS	lb	66000	238
Gross weight/ σ' at design conditions (3000 ft, 95°F)	lb	68659	284
<u>Rotor</u>			
Diameter	ft	50	5
Number of blades per rotor		3	3
Disc area per rotor	ft ²	1964	19.64
Disc loading			
Design gross weight/ σ' at SLS	lb/ft ²	16.8	6.1
Design gross weight/ σ' at 3000 ft, 95°F	lb/ft ²	20.0	7.3
Solidity		0.1275	0.1275
Blade chord	in.	40	4.0
Blade twist	deg	25	25
Airfoil section			
Tip		64-208, a = 0.3	64-208, a = 0.3
30 percent R		64-217.3, a = 0.3	64-217.3, a = 0.3
Tip speed			
Helicopter, takeoff	ft/sec	822	493
Transition	ft/sec	700	420
Rotational speed			
Helicopter, takeoff	rpm	314	1884
Transition	rpm	268	1604
Distance between rotor centerlines	ft	64.25	6.425
Distance, conversion axis to rotor hub	ft	10.19	1.02
Pylon angles	deg	0-90	0, 15, 30, 45, 60, 90
Hub spring rate (each rotor)	ft-lb/deg	1500	0.54

TABLE VI-I. Continued

<u>Wing</u>	<u>Units</u>	<u>Full Scale</u>	<u>Model</u>
Airfoil			
Root		64 x 18	64-318, a = 0.8
Tip		64 x 15	64-318, a = 0.8
Span	ft	64.25	6.425
Area	ft ²	706	7.06
Loading at gross weight/ σ' at SLS	lb/ft ²	93.5	33.7
Aspect ratio		5.85	5.85
Root chord (centerline fuselage)	in.	157.0	15.7
Tip chord (centerline pod)	in.	107.0	10.7
Mean aerodynamic chord	in.	133.4	13.34
Leading edge sweep	deg	6	6
Dihedral	deg	2	2
Flap area per side	ft ²	34.94	0.397
Aileron area per side	ft ²	23.3	0.296
Aileron settings			
Hover	deg	60	60
Transition	deg	20	20
Flap settings			
Hover	deg	60	60
Transition	deg	50	50
<u>Horizontal Stabilizer</u>			
Airfoil			
Root		64012	64A012
Tip		64008	64A008
Span	ft	33.33	3.33
Area	ft ²	250	2.50
Aspect ratio		4.5	4.5
Mean aerodynamic chord	ft	7.56	0.756
Elevator area	ft ²	51	0.51
<u>Vertical Stabilizer</u>			
Airfoil			
Root		64015	64A015
Tip		64008	64A008
Area	ft ²	205	2.05
Aspect ratio		1.6	1.6
Mean aerodynamic chord	in.	139	13.9
Rudder area	ft ²	43.9	none

TABLE VI-I. Concluded

<u>Power</u>		<u>Full Scale</u>	<u>Model</u>
Installed, MRP, SLS (4) Lycoming LTC4V-1 der.	shp	17680	(38.2)
Full-scale transmission power limits			
Helicopter, takeoff	shp	16000	(34.6)
Transition	shp	13500	(29.16)
Model transmission gear ratio, motor:rotor			6:1
Model drive motor speed			
Helicopter, takeoff	rpm	-	11303
Transition	rpm	-	9625
Model drive motor design power at operating rpm, total (2 motors)			
Helicopter, takeoff	shp	-	57
Transition	shp	-	50
Model drive motor, one hour power rating (73.5 percent) total (2 motors)			
Helicopter, takeoff	shp	-	42
Model drive motor power at continuous operating temperature during calibra- tion	shp	-	34
() Required scale installed power			

7. Instrumentation and Wiring Items

a. Parameters Measured

The model instrumentation permits measuring the following parameters:

- Blade beamwise loads (27.3% R)
- Blade chordwise loads (27.3% R)
- Blade torsion loads (27.3% R)
- Blade (gimbal) flapping
- Pitch link load
- Rotor torque
- Rotor speed and azimuth
- Collective pitch actuator position
- Cyclic pitch actuator position
- Rotor axial force (three-component balance)
- Rotor pitching moment (three-component balance)
- Rotor yawing moment (three-component balance)
- Wiring provisions for pylon-mounted accelerometers

- Wing driveshaft bearing temperature (3 per wing)
- Wingtip gearbox temperatures
- Center gearbox temperature
- Drive motor forward bearing temperature
- Drive motor aft bearing temperature

8. Rotor Balances

A three-component rotor load cell is installed in each pylon. The balances are one-piece construction with two concentric cylinders welded together, and with eight flexures. The primary measurement is rotor axial force for rotor-wing lift-distribution data. Longitudinal and lateral moments are measured and included in balance equations to obtain the specified accuracy of rotor axial force and to provide additional rotor data. The balances are temperature and modulus compensated, and they are stiff longitudinally and laterally for frequency control. Bell Specification 85-643 gives loads, stiffnesses, accuracies, and temperature ranges, and Vought Aeronautics Report 2-59720/1R-50809 presents a structural analysis and four component equations derived from six-component calibration of the load cell alone.

An integral part of the balance assembly, although not structurally a part of the balance, is the dual metal-bellows coupling that transmits rotor torque across the balance. The balance is axially stiff and the coupling soft. Balance stiffness in this direction is 1200 times that of the coupling to minimize the coupling effect on balance thrust slope. The bellows provide a symmetrical load path for transmittal of torque, low torque interactions on thrust, and are loaded to one half of their rated infinite-life torque for linearity of the remaining torque interaction. Dual bellows permit misalignments, if any, and safety stops are incorporated, if a bellows fails, to restrain the coupling parts and to continue transmittal of torque to the proprotor.

Dual thrust bridges are incorporated in each balance to permit the tunnel test to continue if signal from one bridge is lost, and as found during calibration, to cancel interaction of residual torque acting on the upper balance flange due to upper mast bearing friction. Dual torque bridges are included on each rotor shaft to permit the test to continue if a signal is lost, and as found during calibration, to cancel static-calibration hysteresis traceable to the calibration-fixture attachment joint at the mast, which is close to the torque bridges. Each bridge is recorded separately during calibration and test and included in the equation for thrust.

The three-component rotor load cells and mast torque as assembled make up a four-component system. Measurement of rotor flapping of the gimbaled hub and hub/spinner tares will give additional rotor data for analysis of selected points.

D. TEST PROGRAM

The following paragraphs discuss specific aspects which can be investigated during initial wind-tunnel testing.

1. Hover Flight

Tests in this mode, as well as in helicopter forward flight, would investigate differences in performance and control between the tilt-proprotor aircraft

and the conventional helicopter for which theory and prediction methods are largely developed and verified. The differences are due to the side-by-side rotors, the wing, the ability to tilt the masts, large blade twist, and the large horizontal tail.

Wing download in hover causes an increase in prop rotor thrust required to hover. The download is a significant function of ratio of disc area to wing area, wing geometry including flaps, blade geometry including solidity (disc loading), and blade twist. The model is equipped with rotor balances to measure lift at each rotor and it has a sting balance to measure total aircraft lift, for measurement of this lift distribution. With variable collective pitch and rotary sting, a range of thrust levels and rotor height-to-diameter ratios (H/D), can easily be tested during operational checkout of the model prior to tunnel entry.

With the ability to roll the model using the rotary sting, roll static stability can be determined in ground effect where unique aerodynamic interference effects exist due to proximity of wing and fuselage to the ground plane. With the remote cyclic, and differential collective and cyclic pitch, tests can easily include pitch, roll, and yaw control power test in hover, in and out of ground effect.

The hover tests can include the following, shown in the order of priority:

- Definition of wing download, hover power, and rotor thrust over a range of collective pitch settings, out of ground effect.
- Definition of hover control gradients out of ground effect in pitch, roll and yaw at one thrust level.
- Definition of wing download, hover power required versus ground effect height.
- Definition of roll stability in ground effect.
- Definition of roll control gradients in ground effect while rolled.

2. Helicopter Flight

Interference between the wing, prop rotor, and empennage occurs in all flight modes. The effects are both static and dynamic. With respect to static effects, there are uncertainties in the helicopter mode, particularly in regard to representation of prop rotor wakes at the horizontal tail. It is important to conduct tests in this area with tail-on and tail-off for data than can be used to validate theory used in calculation of control positions. These tests should encompass level flight, climb, and steep-descent/autorotation flight conditions.

The side-by-side rotors mounted at wing tips result in a large overall span of the prop rotor-wing lifting system. One effect of this is an increase in aspect ratio of the side-by-side rotors relative to that of a single rotor having the same equivalent total disc area. Induced power should be reduced considerably, particularly at low to moderate speeds. The magnitude of this reduction, however, is unknown due in part to the gap between inboard edges of the rotor discs and due to bi-plane interference between rotor and wing. Tests for these effects

should include measurements of power and lift from minimum tunnel speeds for meaningful data up to helicopter-mode high speed. Results will be compared with theoretical predictions.

Another characteristic of the tilt proprotor in this mode is the ability to tilt the masts and to share lift between the rotors and wing beginning at moderate speeds. It is desirable to reduce wing download from its hover value as soon as possible and to develop positive wing lift at moderate to high advance ratios to unload the proprotors. The test should encompass two mast angles.

Proprotor blade twist rate is more than three times that used on helicopter blades. During forward flight, in this mode, this produces a high amount of inboard blade stall with subsequent power losses, which could restrict flight ranges for steep descents or autorotative flight. The high twist also causes the advancing blade to operate at large negative angles of attack in high-speed flight. This may be more of a limitation to helicopter-mode flight boundaries than retreating blade stall. Tests of these operating conditions should be included to verify or adjust the theory and determine blade dynamic loading.

A preliminary test matrix for the helicopter mode is given below. (Velocities are typical full-scale values.)

MAST ANGLE 90 DEGREES

Velocity, knots	<u>40</u>	<u>80</u>	<u>120</u>
α_{Fuselage} (level flight)	-1	-5	-10
α_{Fuselage} (climb)	-10	-15	-

MAST ANGLE 75 DEGREES

Velocity, knots	<u>40</u>	<u>80</u>	<u>120</u>
α_{Fuselage} (level flight)	15	10	5
α_{Fuselage} (climb)	5	0	0

MAST ANGLE 90 DEGREES

Velocity, knots	<u>60</u>	<u>80</u>	<u>100</u>
α_{Fuselage}	15	15	15

The initial run at each point in the matrix is a collective pitch sweep to encompass one g lift conditions, near trim. Angle of attack, tunnel speed,

mast angle, and rpm are constant. Cyclic pitch is adjusted to zero longitudinal flapping at each collective pitch setting. The procedure is similar to that used in other tests and at the NASA-Langley 30- by 60-foot wind tunnel during recent rotor tests.

At the collective pitch nearest one g flight (and cyclic pitch from the prior run), angle of attack is varied ± 4 degrees for longitudinal stability derivatives and aerodynamic characteristics. Tunnel speed, mast angle, collective pitch, and cyclic pitch are constant. Similarly, yaw angle is varied ± 5 and ± 10 degrees for lateral characteristics.

The above runs are repeated with the horizontal stabilizer removed. Angle of attack and yaw runs are made with collective and cyclic pitch settings used during tail-on runs.

3. Helicopter Slow-Speed Flight

The calculation of tilt-proprotor control and aerodynamic characteristics in the transition range from hover to 40 knots involves uncertainties. It is in this range where the XV-3 initially experienced a substantial stick reversal due to upwash on the tail during in-ground-effect takeoffs. It is in this range where wake angles are changing rapidly and the side-by-side rotors make a transition from single rotor to side-by-side rotor-wake characteristics. Calculation of power required both in and out of ground effect is uncertain due to unknown variations of wing download in the complex rotor wake. It is considered important that data be obtained in these areas.

The following test matrix is proposed:

Yaw Angle degrees	V knots (full scale)					
		0	10	20	30	40
0	H/D	.5	—————→			
0	H/D	.67	—————→			
0	OGE		—————→			

10	H/D	.5	—————→			
10	H/D	.67	—————→			
10	OGE		—————→			

Tests at each point in the matrix should be conducted with tail on and tail off. Collective pitch, cyclic pitch, and fuselage angle are constant, and collective pitch is near that for one g lift as determined from hover tests.

4. Conversion Flight

A tentative test matrix for conversion flight mode tests is shown below.

<u>MAST ANGLE</u> (degrees)	<u>FUSELAGE ANGLE</u> (degrees)
60	5
60	10
45	10
30	10
0	10

Tests at each point are conducted at one tunnel speed corresponding to a full-scale speed of 120 knots. At each point, collective pitch sweeps are made encompassing one g lift and cyclic pitch is set for zero flapping. Airframe pitch and yaw sweeps are made during subsequent runs with constant control settings for stability characteristics. At a selected collective pitch setting, rotor moment gradients generated by a cyclic pitch sweep of ± 2 degrees may be obtained.

5. Airplane Flight

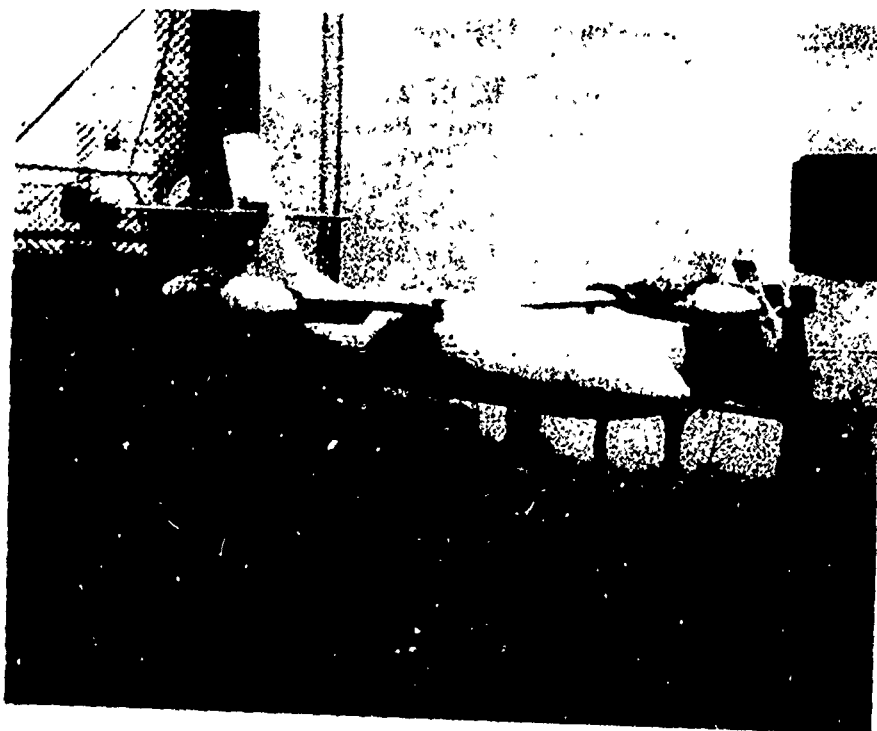
In airplane mode, it is proposed to test at maximum tunnel speed. At that speed, collective pitch sweeps are made at two tip speeds to measure propulsive efficiency. Perturbations of angle of attack and yaw angle are made at one tip speed and two collective pitch settings.

6. Rotor-Off Data

Conventional rotor-off airframe data, tail on and tail off, are obtained for selected tunnel speeds to complete the data needed for analysis of test results.



a. Helicopter Mode



b. Airplane Mode

Figure VI-1. C100 Model During Functional Check Runs.

VII. REFERENCES

1. Deckert, W. H. and Ferry, R. G., "Limited Flight Evaluation of the XV-3 Aircraft," Air Force Flight Test Center Report TR-60-4, May 1960.
2. Contract between USAAVLABS and Bell Helicopter Company, Contract DAAJ02-67-C-0044, "Composite Aircraft Program," 24 March 1967.
3. "Exploratory Definition Final Report, Model 266 Composite Aircraft Program," Bell Helicopter Company Technical Volume, Reports 266-099-201 and 266-099-223.
4. Edenborough, H. K., "Investigation of Tilt-Rotor VTOL Aircraft Rotor-Pylon Stability," Journal of Aircraft, March-April 1968.
5. Gaffey, T. M., "The Effect of Positive Pitch-Flap Coupling (Negative δ_3) on Rotor Blade Motion Stability and Flapping," Journal of the American Helicopter Society, April 1969.
6. Wernicke, K. G., "Tilt-Proprotor Composite Aircraft, Design State of the Art," Journal of the American Helicopter Society, April 1969.
7. "Advancement of Proprotor Technology Task I - Design Study Summary," NASA Contractor Report CR114363, September 1968, Contract NAS2-5386.
8. "Advancement of Proprotor Technology Task II - Wind-Tunnel Test Results," NASA Contractor Report CR114363, September 1971, Contract NAS2-5386.
9. Wernicke, K. G. and Edenborough, H. K., "Full-Scale Proprotor Development," presented at the 27th Annual National V/STOL Forum of the American Helicopter Society, May 1971.
10. Brown, E. L. and Red, J. A., "Results of the Wind-Tunnel Tests of the Quarter-Scale Semispan Model of the Bell XV-3 Tilting-Rotor Convertiplane," Report 200-094-270, 18 August 1958.
11. DeTore, J. A. and Sambell, K. W., "Preliminary Investigation of the Folding-Proprotor V/STOL Aircraft," Bell Helicopter Company Report 599-189-900, November 1968, Confidential.
12. DeTore, J. A. and Gaffey, T. M., "The Stopped-Rotor Variant of the Proprotor VTOL Aircraft," Journal of the American Helicopter Society, July 1970.
13. Livingston, C. L., "A Stability and Control Prediction Method for Helicopters and Stoppable Rotor Aircraft," Technical Report AFFDL-TR-69-123, February 1970, Contract AF 33615-69-C-1121.
14. Yen, Dr. Jing G., Weber, G. E., and Gaffey, T. M., "A Study of Folding Proprotor VTOL Aircraft Dynamics," Technical Report AFFDL-TR-71-7, September 1971, Contract AF 33615-69-C-1339.

REFERENCES - Concluded

15. Matthys, C. G., Joglekar, M. M., and Hsieh, P. Y., "An Analysis of Fixed Wing-Proprotor Interference for Folding Proprotor Aircraft," Bell Helicopter Company Report 299-099-556, to be published, Contract AF 33615-70-C-1133.
16. "Summary Report - Task I Preliminary Design Studies NASA Folding Proprotor Program," Bell Helicopter Company Report D272-099-001, April 1970, Contract NAS2-5461.
17. "Large-Scale Wind-Tunnel Investigation of a Folding Tilt Rotor," Final Report D272-099-002, May 1972, NASA Contract NAS2-5461.
18. "Design Studies of Folding-Proprotor VTOL Aircraft," Bell Report D270-099-001, October 1968, Air Force Contract F33615-69-C-1578.
19. DeTore, J. A., "Lift/Propulsion System Size Selection Considerations for Stoppable Rotor VTOL Aircraft," presented at the USAF V/STOL Technology and Planning Conference, Las Vegas, Nevada, September 23-25, 1969.
20. Odenbuttal, R. H., "A Low-Speed Wind-Tunnel Test of the Bell Helicopter 0.200-Scale Semispan Aeroelastic C300-A1C Model," Vought Aeronautics Report LSWT 367, October 1971.
21. Etkin, Bernard, "Dynamics of Flight," John Wiley and Sons, Incorporated, New York, London, 1959.
22. Young, A. D., "The Aerodynamic Characteristics of Flaps," R&M 2622, 1947, R.A.E. Report Aero 2185, 1947.
23. Foster, R. D., Unpublished Calculations, Bell Helicopter Company, 1968.
24. Kemp, L. D., Unpublished Calculations, Bell Helicopter Company 1968.
25. Tiller, F. E., "Choice of Vertical Stabilizer for the Model 300," Bell Helicopter Company Inter-Office Memo 87:FET:jb/bm-295, 7 May 1969.
26. Pope, A., Wind Tunnel Testing, Second Edition, John Wiley and Sons, New York, 1954.
27. Vaughan, J. B. "A Low-Speed Wind-Tunnel Force Test of the 0.20 Scale Bell Helicopter Model 300," Vought Aeronautics Division Report LSWT333, May 1970.